

Justus Liebig University Giessen

Inaugural Dissertation

**Fibroblast Growth Factor 10 Reverses Cigarette Smoke- and
Elastase-induced Emphysema and Pulmonary Hypertension in Mice**

to obtain the academic degree of

doctor of natural sciences

- Dr. rer. nat. -

Submitted to the Faculty of Biology and Chemistry

at the Justus Liebig University Giessen

by

Stefan Hadzic, MSc

of Budva, Montenegro

Giessen 2022

First Supervisor and Committee Member:

Prof. Dr. Reinhard Lakes-Harlan

Institute for Animal Physiology, FB 08
Justus Liebig University Giessen
Heinrich-Buff-Ring 38
35392 Giessen, Germany

Second Supervisor and Committee Member:

Prof. Dr. Norbert Weißmann

Excellence Cluster Cardio-Pulmonary Institute
(CPI), Department of Internal Medicine, FB 11
Justus Liebig University Giessen
Aulweg 130
35392 Giessen, Germany

Committee Member:

Prof. Dr. Saverio Bellusci

Excellence Cluster Cardio-Pulmonary Institute
(CPI), Department of Internal Medicine, FB 11
Justus Liebig University Giessen
Aulweg 130
35392 Giessen, Germany

Committee Member:

Prof. Dr. Ivan Manzini

Institute for Animal Physiology, FB 08
Justus Liebig University Giessen
Heinrich-Buff-Ring 38
35392 Giessen, Germany

Date of Doctoral Defence: 14. 07. 2022

Velika, duga i teška putovanja imaju bar jednu dobru stranu, pored tolikih rđavih: da nas spasavaju od površnih sudova i jevtinih refleksija, upravo tom svojom dužinom i težinom. Gledajući širinu i raznovrsnost sveta oko sebe, čovek postaje obazriv u zaključcima i izbirljiv u izrazu.

Ivo Andrić, Znakovi pored puta

TABLE OF CONTENTS

1	INTRODUCTION	1
1.1	Respiratory system anatomy and gas exchange	1
1.1.1	Conductive airways	1
1.1.2	Lung circulation	3
1.1.3	Respiratory surface	5
1.2	Chronic obstructive pulmonary disease (COPD)	6
1.2.1	COPD diagnosis	7
1.2.2	COPD therapy	8
1.2.3	Chronic obstructive bronchitis and small airway remodelling in COPD	10
1.2.4	Pulmonary emphysema	12
1.2.5	COPD-associated pulmonary hypertension (PH)	14
1.2.6	Animal models of COPD	15
1.2.7	Mechanisms of COPD pathology	18
1.2.7.1	Protease-anti-protease disbalance	19
1.2.7.2	Augmented inflammation in COPD pathology	19
1.2.7.3	Oxidative and nitrosative stress in COPD pathology	22
1.2.7.4	Cell death and senescence in COPD pathology	24
1.2.7.5	Developmental pathways in COPD pathology	25
1.2.8	Growth factors and impaired lung repair in COPD	28
1.2.9	Fibroblast growth factor (FGF) signalling	29
1.2.10	FGF receptors	30
1.2.11	FGF7 subfamily	33
1.2.12	FGF10 in development, homeostasis and disease	34
1.2.13	Aims of this work	36
2	MATERIAL AND METHODS	39

2.1	Material	39
2.1.1	Equipment.....	39
2.1.2	Chemicals and consumables.....	42
2.1.3	Software.....	52
2.1.4	Experimental animals.....	53
2.1.5	Antibodies.....	54
2.1.6	Primer sequences.....	56
2.2	Methods	58
2.2.1	Human lung samples.....	58
2.2.2	Animal studies and experimental design.....	58
2.2.2.1	Therapeutic setup with inducible nitric oxide (iNOS) inhibition	59
2.2.2.2	FGF10 loss-of-function setup.....	59
2.2.2.3	Therapeutic approach with FGF10 overexpression.....	61
2.2.2.3.1	FGF10 overexpression after cigarette smoke (CS)-induced emphysema and PH.....	61
2.2.2.3.2	FGF10 overexpression after elastase-induced pulmonary emphysema and PH.....	62
2.2.3	Cigarette smoke exposure	63
2.2.4	Intratracheal elastase instillation	64
2.2.5	<i>In vivo</i> fluorescence molecular tomography (FMT) and micro-computed tomography (μCT)	66
2.2.6	Non-invasive echocardiography	67
2.2.7	<i>In vivo</i> lung function and hemodynamic measurement.....	67
2.2.8	Lung fixation and organ harvest	69
2.2.9	Lung vasculature casting and <i>ex vivo</i> μCT imaging.....	69
2.2.10	Histology	70
2.2.10.1	Tissue section preparation.....	70
2.2.10.2	Haematoxylin & Eosin (H&E) staining.....	71
2.2.10.3	Weigert's elastin staining protocol	72
2.2.10.4	Picrosirius red staining protocol and collagen quantification	72
2.2.10.5	Alveolar morphometry analysis.....	73

2.2.10.6	Design-based stereology.....	73
2.2.10.7	Immunohistochemistry staining and quantification	73
2.2.10.8	Immunofluorescence staining and confocal microscopy	74
2.2.11	<i>In vitro</i> cell culture experiments.....	75
2.2.11.1	Cigarette smoke extract (CSE) preparation	75
2.2.11.2	Interstitial lung fibroblasts from human patients.....	75
2.2.11.3	Precision cut lung slices (PCLS)	76
2.2.11.4	Mouse alveolar type 2 (ATII) cell isolation.....	78
2.2.11.5	Cell apoptosis and cell viability assays.....	79
2.2.12	Molecular biology experiments	79
2.2.12.1	Ribonucleic acid (RNA) isolation and purification	79
2.2.12.2	Complementary deoxyribonucleic acid (cDNA) synthesis	79
2.2.12.3	Message RNA (mRNA) expression analysis by quantitative polymerase chain reaction (qPCR)	80
2.2.12.4	Laser-assisted microdissection	81
2.2.12.5	Transcriptome analysis via microarray technology	82
2.2.12.6	Protein expression analysis by Western-blot	83
2.2.12.7	3-nitrotyrosine quantification via enzyme-linked immunoassay (ELISA)	84
2.2.13	Data processing.....	85
2.2.14	Statistical analysis	85
3	RESULTS.....	87
3.1	FGF10 expression in lungs from CS-exposed and L-NIL treated mice.....	87
3.1.1	FGF signalling in human COPD lungs	88
3.1.2	CS-induced emphysema in mice with impaired FGF10 signalling	98
3.1.3	CS-induced PH in mice with impaired FGF10 signalling	106
3.1.4	COPD traits in mice with impaired FGF10 signalling	110
3.1.5	Gene expression regulation during emphysema and PH development in CS-exposed wild-type (Wt) mice and in FGF10-haploinsufficient mice	116

3.1.6	The effect of doxycycline on CS-induced emphysema and PH.....	123
3.1.7	The effect of FGF10 overexpression on CS-induced emphysema and PH.....	125
3.1.8	Signalling pathways underlying emphysema and PH reversal upon FGF10 overexpression.....	132
3.1.9	Effect of the <i>in vitro</i> FGF10 treatment on human COPD PCLS	137
3.1.10	FGF10 overexpression after elastase-induced emphysema and PH	139
4	DISCUSSION.....	148
4.1	FGF10 signalling is impaired in lungs of CS-exposed mice and COPD patients	149
4.2	Mice with impaired FGF10 signalling spontaneously develop emphysema and PH	153
4.3	Signalling pathways of FGF10 and CS-induced emphysema and PH development	156
4.4	Doxycycline alone does not affect CS-induced emphysema and PH.....	160
4.5	FGF10 overexpression reverses CS-induced emphysema and PH.....	162
4.6	FGF10 overexpression ameliorates elastase-induced emphysema and PH.....	165
5	CONCLUSIONS.....	169
6	SUMMARY	171
7	ZUSAMMENFASSUNG	173
8	INDEX OF FIGURES	176
9	INDEX OF TABLES	181
10	DECLARATION	183

11	REFERENCES.....	185
12	ACKNOWLEDGEMENTS.....	228
13	ATTACHMENT.....	230
13.1	Publications.....	230
13.2	Oral presentations	234
13.3	Poster presentations.....	235
13.4	Awards	236
13.5	Courses and workshops	237
13.6	Curriculum vitae.....	238

1 Introduction

1.1 Respiratory system anatomy and gas exchange

The respiratory system is one of the earliest and most recently evolved adaptations to terrestrial life. The primary function of the respiratory system is gas exchange – blood oxygenation and CO₂ release (Weibel 1984; West *et al.* 2016; Zepp *et al.* 2019). Lungs are the central organ of the respiratory system, found in most terrestrial animals, including amphibians, birds, reptiles and mammals. The anatomy and physiology of the mammalian respiratory system are very complex. To enable gas exchange, the respiratory system is tightly interconnected with the cardiovascular system (Weibel 1984; West *et al.* 2016; Zepp *et al.* 2019).

In humans, the respiratory system is anatomically divided into the upper and lower respiratory tract. Nose, nasal cavity, sinuses, and pharynx belong to the upper respiratory tract (Weibel 1984; West *et al.* 2016; Zepp *et al.* 2019; Rehfeld *et al.* 2017). Based on the structural and functional differences, the lower respiratory tract is divided into two compartments: the conducting airways (trachea, bronchus system, and conductive bronchiole) and the respiratory zone. The respiratory zone corresponds to the lung parenchyma and includes respiratory bronchiole, alveolar ducts, alveolar sacs and alveoli (Weibel 1984; West *et al.* 2016; Zepp *et al.* 2019; Huang *et al.* 2015; Suarez *et al.* 2012). Anatomically, the left lung in humans is divided in the upper and lower lobe by a single interlobar fissure – the oblique fissure. Two interlobar fissures – the oblique and the horizontal fissures divide the right lung in the upper, middle and lower lobes (Suarez *et al.* 2012).

1.1.1 Conductive airways

The primary function of the airways is to conduct and distribute the inhaled air towards the distal respiratory surface (Huang *et al.* 2015; Suarez *et al.* 2012; West *et al.* 2016). Airway branching is shown in **Table 1**. The lumen of the conductive airways is covered with a thin mucus layer that moistens the air and captures small inhaled particles (De Rose *et al.* 2018; Wittekindt 2017). The cellular composition of the conductive airway epithelium differs greatly

along proximal-distal axes. Namely, pseudostratified epithelium, present in the trachea, is gradually substituted with bronchial epithelium that mainly consists of basal, ciliated and secretory cells (Wittekindt 2017; Zepp *et al.* 2019).

Table 1: Airway branching in the human respiratory system from the conductive towards the respiratory zone. Modified from Huang *et al.* 2015.

Airway generation		Function
0	Trachea	Conductive zone
1	Main bronchi	
2	Lobar bronchi	
3-4	Segmental bronchi	
5-11	Sub-segmental bronchi	
12-15	Bronchioles	
16	Terminal bronchioles	
17-19	Respiratory bronchioles	Respiratory zone
20-22	Alveolar ducts	
23	Alveolar sacs	

Basal cells are relatively small cells, which adhere to the basal lamina. They do not reach the lumen of the airways and serve as progenitors for the other cell types in the airway epithelium (Rock *et al.* 2010). In humans, basal cells are distributed all the way from the pseudostratified tracheal epithelium to the terminal bronchioles (Nakajima *et al.* 1998; Rock *et al.* 2010). Ciliated and secretory cells are column-shaped and elongated towards the lumen of the airways. Near the apical membrane, these cells are interconnected via tight junctions forming a selectively permeable barrier (Rawlins *et al.* 2008; Wittekindt 2017). Ciliated cells with synchronised movements of their cilia move mucus towards the upper airways and thereby have a crucial function in mucus clearance (Khelloufi *et al.* 2018). Two main classes of secretory cells are goblet and Club cells (Hovenberg *et al.* 1996). Club cells mainly synthesise secretoglobins, stored in dense apical granules and released in the lumen (Davies *et al.* 2002). Club cells also have progenitor cell properties and could give rise to the other cell types during

homeostasis or repair process (Rawlins *et al.* 2008). Goblet cells synthesise mucins, which are highly glycosylated proteins. Intracellularly, mucins are stored in large distinct vesicles and released into the airway lumen (Hovenberg *et al.* 1996). In pathological conditions, goblet cells play a significant role in the airway mucus plugging and remodelling process (Ghosh *et al.* 2018).

1.1.2 Lung circulation

The lung is the only organ with two distinct circulations – the bronchial and the pulmonary circulation. The bronchial circulation belongs to the systemic circulation and supplies the thick walls of the large bronchi and pulmonary vessels (as *vasa vasorum*) with oxygenated blood (Grippi *et al.* 1996; Suarez *et al.* 2012; Huang *et al.* 2015). In humans, several systemic arteries, originating mainly from anterior branches of the aorta or upper intercostal arteries, supply the bronchial circulation. Only about 1% of the left ventricular cardiac output is allocated to the bronchial circulation (Suresh *et al.* 2016; Baile 1996).

The bronchial arteries enter the lungs at the hilum and follow the entire length of the bronchial tree up to the level of the bronchiole (Baile 1996; Huang *et al.* 2015; Suarez *et al.* 2012; Grippi *et al.* 2015). A unique feature of bronchial circulation is a dual venous drainage system. At the extra-parenchymal level, the bronchial arteries that supply the lower trachea down to the lobar bronchi drain through bronchial veins into the azygous vein and further in the right atrium (Suresh *et al.* 2016; Baile 1996). At the intra-parenchymal level, the bronchial vessels anastomose with the pulmonary circulation at the precapillary, capillary, and post-capillary level and drain through the pulmonary vein into the left atrium (Baile 1996; Grippi *et al.* 2015). Of interest, the bronchial circulation plays a vital role in the primary defence mechanism of the lung by maintaining the bronchial mucus membrane humidity (Alving *et al.* 1993). Furthermore, in response to inhaled particles such as air pollutants and cigarette smoke, bronchial vessels respond with local vasodilation that can contribute to the inflammatory response (Alving *et al.* 1993).

In contrast to the bronchial circulation, representing only a part of the systemic circuit, the pulmonary circulation accommodates the entire cardiac output from the right ventricle. The main pulmonary artery divides into two branches that supply the left or right lung. The arteries then branch again at the level of lung lobes and further, following the bronchial tree (Murillo *et al.* 2012; Suresh *et al.* 2016; Suarez *et al.* 2012; Huang *et al.* 2015). The primary function of the pulmonary circulation is gas exchange (Suresh *et al.* 2016; Baile 1996; Suarez *et al.* 2012). One of the unique features of the pulmonary circulation is the fact that pulmonary arteries carry deoxygenated blood, whereas oxygenated blood drains in pulmonary veins upon gas exchange. Another unique feature of the pulmonary vasculature is hypoxic pulmonary vasoconstriction (HPV) (Sommer *et al.* 2016; Suresh *et al.* 2016). In contrast to the systemic circulation, hypoxia causes vasoconstriction of the pulmonary arteries (Sommer *et al.* 2016; Suresh *et al.* 2016). Hypoxic pulmonary vasoconstriction (HPV), also known as the von Euler-Liljestrand mechanism, is an intrinsic mechanism in pulmonary vessels triggered by a response to hypoxia from the alveoli (von Euler *et al.* 1946; Sommer *et al.* 2016). Almost all vertebrates, including humans, depend on such mechanism to divert the blood flow from poorly ventilated towards the well ventilated alveolar regions. It is an important mechanism leading to ventilation-perfusion matching and therefore optimising the gas exchange process (Weissmann *et al.* 1995; Weissmann *et al.* 2004; Sommer *et al.* 2016). Although beneficial, prolonged HPV can underlay the pulmonary vascular remodelling process leading to an increase in pulmonary vascular resistance (PVR) and pulmonary hypertension (PH) (Weissmann *et al.* 1995; Weissmann *et al.* 2004; Sommer *et al.* 2016). This may occur at a high altitude or upon several respiratory diseases, including chronic obstructive pulmonary disease (COPD), sleep apnoea and pulmonary fibrosis that cause hypoxia (Sommer *et al.* 2016; Collum *et al.* 2017; Chaouat *et al.* 2008; Klinger 2016). Increased PVR over time causes changes in right ventricle of the heart. In an adaptive phase, right ventricular wall hypertrophies. Long-term PH can lead to right ventricular decompensation and cor pulmonale (Collum *et al.* 2017; Behnke *et al.* 1970; Niederman *et al.* 1986; Gredic *et al.* 2021; Gredic *et al.* 2020; Pichl *et al.* 2019; Seimetz *et al.* 2020).

1.1.3 Respiratory surface

Efficient gas exchange depends on the very thin barrier of a very large surface between the air and the blood. Massive branching occurs at the level of terminal bronchioli, resulting in an exponential increase of cross-sectional area (Huang *et al.* 2015) (**Figure 1**). With this, epithelium transitions towards a thin respiratory surface.

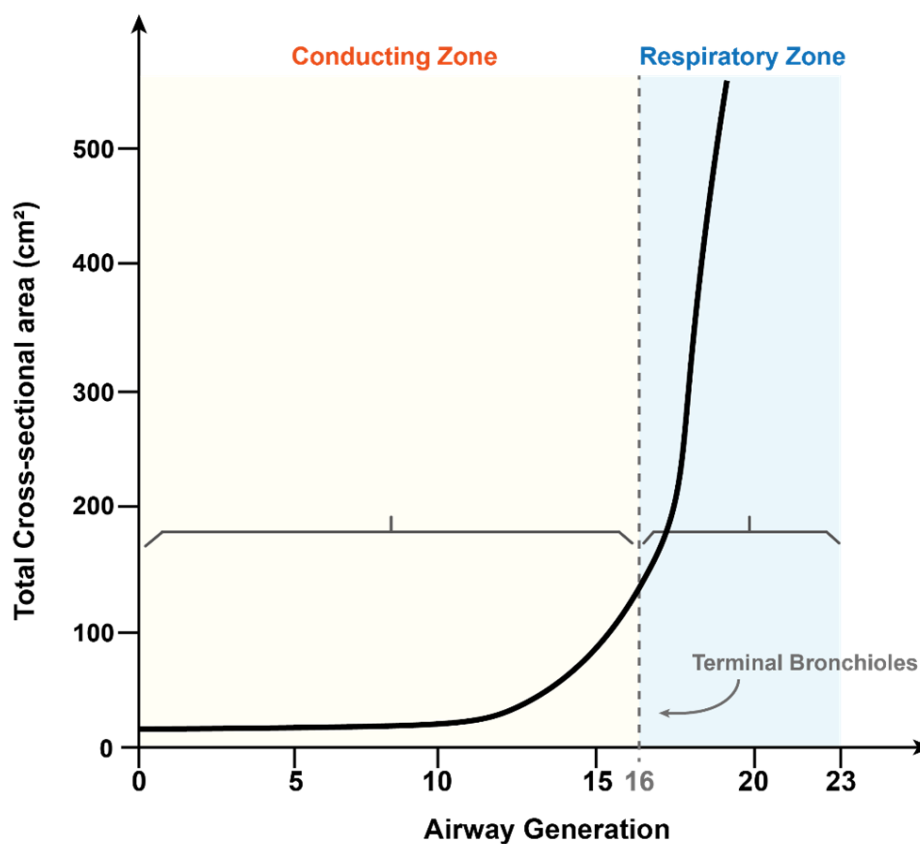


Figure 1: Airway branching and cross-sectional area in adult human lung. The graph illustrates the massive expansion in the cross-sectional area with each airway branching. In the respiratory zone, after airway generation 16 (terminal bronchioles), the increase in the cross-sectional area is exponential. Such a feature of the respiratory system enables aeration of the large gas-exchange surface. Modified from Huang *et al.* 2015.

The respiratory surface is primarily covered by alveolar epithelial type I (AT I) cells. Together with capillary endothelial cells and a basal membrane layer located between them, AT I cells create a thin barrier that enables gas diffusion (Huang *et al.* 2015; Suarez *et al.* 2012; Suresh

et al. 2016). The large surface of the respiratory epithelium is covered with a thin layer of surfactant. This reduces the surface tension and prevents from the collapse of the alveolar structure. Alveolar type II epithelial cells (AT II) secrete most surfactant components and serve as progenitors for AT I. In contrast to AT I, which are terminally differentiated cells, AT II repeatedly re-enter the cell cycle to self-propagate and give rise to the AT I (Barkauskas *et al.* 2013; Gouveia *et al.* 2020; Huang *et al.* 2015). In the case of a substantial injury, Club cells from terminal bronchioles can serve as progenitors and give rise to alveolar epithelial cells. Interestingly, a sub-population of Club cells found at bronchioalveolar duct junction - bronchioalveolar stem cells (BASCs) (**Figure 2**) appear to be very resistant to injury and are very potent in the alveolar repair process (Giangreco *et al.* 2002). The lung is continuously flushed with the inhaled air and is thus exposed to various environmental stimuli. Therefore, homeostasis in the adult lung is crucial for maintaining the function throughout a lifetime (Kim *et al.* 2018). In the recent past, chronic lung diseases increased in prevalence, most likely due to population ageing and increased air pollution (Viegi *et al.* 2001; Ito *et al.* 2009). Frequent chronic respiratory diseases are asthma, chronic obstructive pulmonary disease, fibrosis, and lung cancer (Shukla *et al.* 2020).

1.2 Chronic obstructive pulmonary disease (COPD)

Chronic obstructive pulmonary disease (COPD) is a severe and still incurable disease (Lozano *et al.* 2012; Pauwels *et al.* 2001; Gouveia *et al.* 2020; Grippi 2015). COPD pathology comprises chronic obstructive bronchitis, emphysema and is often associated with at least mild pulmonary hypertension (PH) (Black *et al.* 2008; Gouveia *et al.* 2020; Gredic *et al.* 2020). Chronic obstructive bronchitis, emphysema and PH are described later in greater detail. The most common symptoms are shortness of breath, chronic cough, mucus hypersecretion, and wheezing. In COPD, persistent airflow limitation is not fully reversible but rather progressive (Graham *et al.* 2017; Pauwels *et al.* 2001). Together with malignant and cardiovascular diseases, COPD is among the top causes of death in the developed world (Berry *et al.* 2010; Hansell *et al.* 2003). In addition to the respiratory-related symptoms, COPD is frequently accompanied by comorbidities such as cardiovascular diseases, lung cancer, osteoporosis,

muscle weakness, and cachexia (Decramer *et al.* 2013). These comorbidities contribute greatly to morbidity and mortality rate in COPD patients (Berry *et al.* 2010; Hansell *et al.* 2003).

The main risk factor for COPD development is chronic inhalation of noxious gases and/or fine particulate matter, mainly coming from cigarette smoking, but also air pollution or other sources (Barnes *et al.* 2004; Grippi *et al.* 2015). Besides the exogenous risk factors, COPD patients often have a genetic susceptibility for disease development. Therefore, only a portion of cigarette smokers suffers from COPD, and many COPD patients were not in contact with smoke (Zhai *et al.* 2007). Air pollution is a well-known risk factor contributing to poor health worldwide (Cohen *et al.* 2017). Long-term exposure to air pollutants was associated with increasing emphysema and worsening in lung function (Wang *et al.* 2019). Furthermore, COPD patients suffer from frequent exacerbations caused mainly by viral or bacterial infections (Wu *et al.* 2014; Cukic 2013), which accelerate the disease progression (Baker *et al.* 2013).

1.2.1 COPD diagnosis

In patients who present typical respiratory symptoms, COPD is finally diagnosed by a routine spirometry test. The best diagnostic parameters are forced total vital capacity (FVC) and forced expiratory volume in the first second (FEV₁), measured after pharmacological bronchodilation (Pauwels *et al.* 2001; Singh *et al.* 2019; Virani *et al.* 2021). COPD is diagnosed if the FEV₁/FVC ratio (also called the Tiffeneau-Pinelli index) is lower than 0.7 (Tiffeneau *et al.* 1948). According to the Global Initiative for Chronic Obstructive Lung Disease (GOLD), airflow limitation severity in patients is categorised on a scale from 1-4 (**Table 2**). This GOLD classification mainly relies on the ratio between measured and predicted FEV₁ (Pauwels *et al.* 2001; Singh *et al.* 2019; Virani *et al.* 2021).

Table 2: COPD classification based on airflow limitation severity in patients.
Abbreviations - FEV₁: forced expiratory volume in the first second; FVC: forced vital capacity. Modified from Pauwels *et al.* 2001.

GOLD class:	Severity:	Spirometry results:
1	Mild	FEV ₁ /FVC <0.7; FEV ₁ ≥ 80% predicted
2	Moderate	FEV ₁ /FVC <0.7; 50% ≤ FEV ₁ < 80% predicted
3	Severe	FEV ₁ /FVC <0.7; 30% ≤ FEV ₁ < 50% predicted
4	Very severe	FEV ₁ /FVC <0.7; FEV ₁ < 30% predicted

1.2.2 COPD therapy

Medical treatment for COPD includes smoking cessation, bronchodilators and oxygen administration (Lahzami *et al.* 2010). However, these treatment strategies are ineffective in patients with advanced COPD when surgical procedures are needed. Surgical options include lung volume reduction surgery, bullectomy and lung transplantation (Lahzami *et al.* 2010; Martinez *et al.* 2005; De Giacomo *et al.* 2002).

Oxygen supplementation is therapy with clear evidence for benefit in patients with COPD with resting hypoxemia, defined as partial arterial pressure of oxygen (PaO₂) ≤ 55 mmHg (Stoller *et al.* 2010). Continuous oxygen supplementation therapy increased survival in COPD patients (Stoller *et al.* 2010).

Most currently available medication for COPD treatment belong to one of the 3 main categories: beta-2 agonists (short-acting beta-2 agonists – SABA and long-acting beta-2 agonists – LABA), anti-muscarinic agents (short-acting anti-muscarinic agent – SAMA and long-acting anti-muscarinic agent – LAMA) and inhaled corticosteroids – ICS (Singh *et al.* 2019). Beta-2 agonists and anti-muscarinic agents act as bronchodilators and partially ameliorate the airflow limitation in COPD patients. Nevertheless, no available treatments have been shown to slow the COPD progression or suppress the inflammation in small airways and lung parenchyma (Barnes *et al.* 2004). However, currently available anti-inflammatory drugs,

combined with antibiotics, were shown to reduce exacerbation frequency (Barnes 2007; Barnes 2016; Rabe 2010; Fabbri *et al.* 2009).

Despite the effects observed in mouse models, anti-inflammatory drugs, such as tumour necrosis factor-alpha (TNF- α) receptor antagonists, do not seem to influence the disease progression in COPD patients (Barnes 2007). In addition, corticosteroids are ineffective in suppressing inflammation, including cytokines and proteases (Barnes 2016). In COPD patients, roflumilast, a phosphodiesterase 4 inhibitor, has a modest effect on clinical symptoms or pulmonary function (Rabe 2010). On the other hand, roflumilast provided some protection against acute exacerbations in patients with moderate-to-severe COPD (Rabe 2010; Fabbri *et al.* 2009).

The GOLD 2019 strategy document sheds light on precision medicine in COPD by recommending an assessment (ABCD group) for initial treatment and follow-up treatment guidelines depending on the symptoms and exacerbation of individuals (Singh *et al.* 2019).

In addition, new treatments are repeatedly proposed and tested in clinical trials. According to the clinical trial (ClinicalTrials.gov) database, 615 out of 2,500 interventional studies regarding COPD have reached phase 3 or phase 4 completion (Gouveia *et al.* 2020). Most of them are the β 2-agonists, the anti-muscarinic agents, the inhaled corticosteroids (ICS) or the combined therapy such as PT010 (Budesonide/glycopyrronium/formoterol fumarate) to attenuate bronchoconstriction and inflammation similarly to asthma patients (Gouveia *et al.* 2020). However, none of these treatments can cure the disease. Only some studies in early phase 1 to phase 3, which have not yet been completed, demonstrated different aspects of COPD treatments to cure the disease instead of only alleviating the symptoms, for instance, mesenchymal stem cells-based regenerative medicine (Gouveia *et al.* 2020).

Bullectomy and lung volume reduction are surgical options for patients with severe emphysema (Martinez *et al.* 2005; De Giacomo *et al.* 2002). Bullectomy is the surgical removal of a bulla, defined as localised dilated airspace in the lung parenchyma (Petro *et al.* 1983). Lung volume reduction represents a surgical procedure where small wedges of the emphysematous

lung tissue are removed. Both procedures improve breathing mechanics, ventilation/perfusion matching and better function of the residual lung tissue (De Giacomo *et al.* 2002; Petro *et al.* 1983).

Lung transplantation is a treatment option for several end-stage lung diseases, such as severe cystic fibrosis, COPD, PH or pulmonary fibrosis (van der Mark *et al.* 2020; Lahzami *et al.* 2010; Martinez *et al.* 2005). Lung transplantation is an option for a very limited number of patients (Martinez *et al.* 2005). Candidates for lung transplantation have advanced lung disease with projected shortened life expectancy and impaired life quality (van der Mark *et al.* 2020). COPD patients can be considered for lung transplantation when the FEV1 is < 25% predicted and/or the partial pressure of carbon dioxide (PaCO₂) is ≥ 55 mmHg at rest (Martinez *et al.* 2005). However, the survival benefit of lung transplantation in COPD is still under debate (Lahzami *et al.* 2010). Therefore, the BODE score (Body mass index, airflow Obstruction, Dyspnoea and Exercise capacity) is used for listing COPD patients for lung transplantation based on survival data obtained from the original BODE cohort (Pirard *et al.* 2018). The current worldwide median survival upon lung transplantation is 6.2 years. If the recipient survives the first year, the median survival expectancy increases to 8.3 years (van der Mark *et al.* 2020; Khush *et al.* 2018).

1.2.3 Chronic obstructive bronchitis and small airway remodelling in COPD

Healthy airway epithelium consists of a single layer of basal cells that lie on the basal lamina and give rise to ciliated, goblet and club cells (**Figure 2**). Upon epithelial injury caused by, e.g. cigarette smoking or virus infection, cells in the basal layer are stimulated to proliferate and differentiate (Gouveia *et al.* 2020). That way, injury is repaired, and homeostasis is maintained. Sometimes, depending on the circumstances, duration or magnitude of the damage, this results in bronchitis. Bronchitis is characterised by goblet cell hyperplasia and mucus hypersecretion. However, if the stimuli persist, it results in chronic bronchitis accompanied by airway remodelling (Maestrelli *et al.* 2001; Saetta *et al.* 2000; Gouveia *et al.* 2020). **Figure 2** depicts the main features of chronic bronchitis and airway remodelling in lungs from COPD patients.

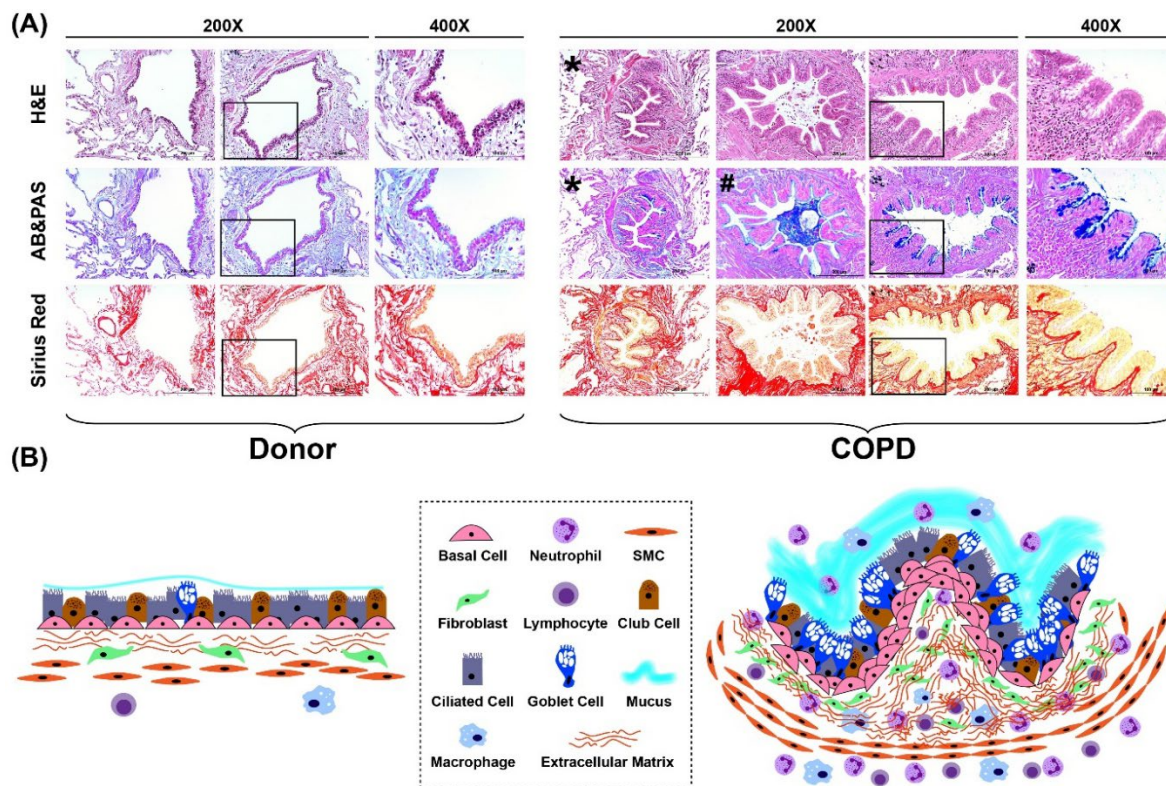


Figure 2. Airway wall of small bronchi in healthy and COPD lungs. (A) Representative images depicting small airways (< 2 mm in diameter) in lung sections from healthy donors or individuals with end-stage COPD (200x-400x magnification). The upper panel line shows the staining with Haematoxylin & Eosin (H&E; cytoplasm – orange; nuclei – blue). The Middle panel line shows the staining with Alcian blue & Periodic acid/Schiff reagent (AB&PAS; acidic glycoproteins – blue; neutral glycoproteins – magenta; nuclei – red). The lower panel line shows Picro-Sirius red staining (collagen – red; cytoplasm – yellow). **(B)** Schematic drawing of the healthy (left) and remodelled (right) airway wall. *bronchoconstriction; #mucus plugging. Abbreviations - SMC: Smooth muscle cell. Scale bars = 200 μm (for 200x magnification); 100 μm (for 400x magnification). Modified from Hadzic *et al.* 2020.

Chronic bronchitis in COPD is characterised by hyper-responsiveness towards inhaled particles. Furthermore, it self-propagates and progresses, even in the absence of the initial stimuli. Airway remodelling is a process of structural changes. Besides goblet cell hyperplasia, airway remodelling comprises thickening of the basement membrane, peribronchial collagen deposition, and bronchial smooth muscle cell proliferation (**Figure 2**) (Hirota *et al.* 2013) (Gouveia *et al.* 2020). Some studies point out a positive correlation between COPD progression

and thickening of airway epithelium, *lamina propria* or *adventitia* (Hogg *et al.* 2004; Koo *et al.* 2018).

In healthy lungs, goblet cells are sporadic in airways with a diameter less than 2 mm. In COPD patient lungs, the number of goblet cells dramatically increases in small airways, which subsequently causes mucus hypersecretion (Saetta *et al.* 2000). Altogether, this narrows the inner airway lumen and contributes significantly to poorly reversible airflow limitation in COPD patients (**Figure 2**). The degree of mucus plugging and peribronchial accumulation of immune cells were also associated with the disease progression (Hogg *et al.* 2004).

1.2.4 Pulmonary emphysema

Emphysema is defined as abnormal, permanent enlargement of the distal airspace, accompanied by the destruction of alveolar septal walls, without apparent signs of fibrosis (Snider *et al.* 1985). The main pathological event behind the emphysema development is the destruction of the typical elastic architecture in the distal respiratory compartments of the lung, leading to enlargement of the airspaces (Black *et al.* 2008), as shown in **Figure 3**. Loss of respiratory surface is mainly attributed to proteases derived from immune cells (Churg *et al.* 2005). Once proteases destroy the alveolar architecture, progenitor cells in COPD lungs cannot repair the lung structure (Barnes 2016). Furthermore, apoptosis and senescence of progenitor cells also contribute to the impaired lung regeneration in COPD (Mercado *et al.* 2015).

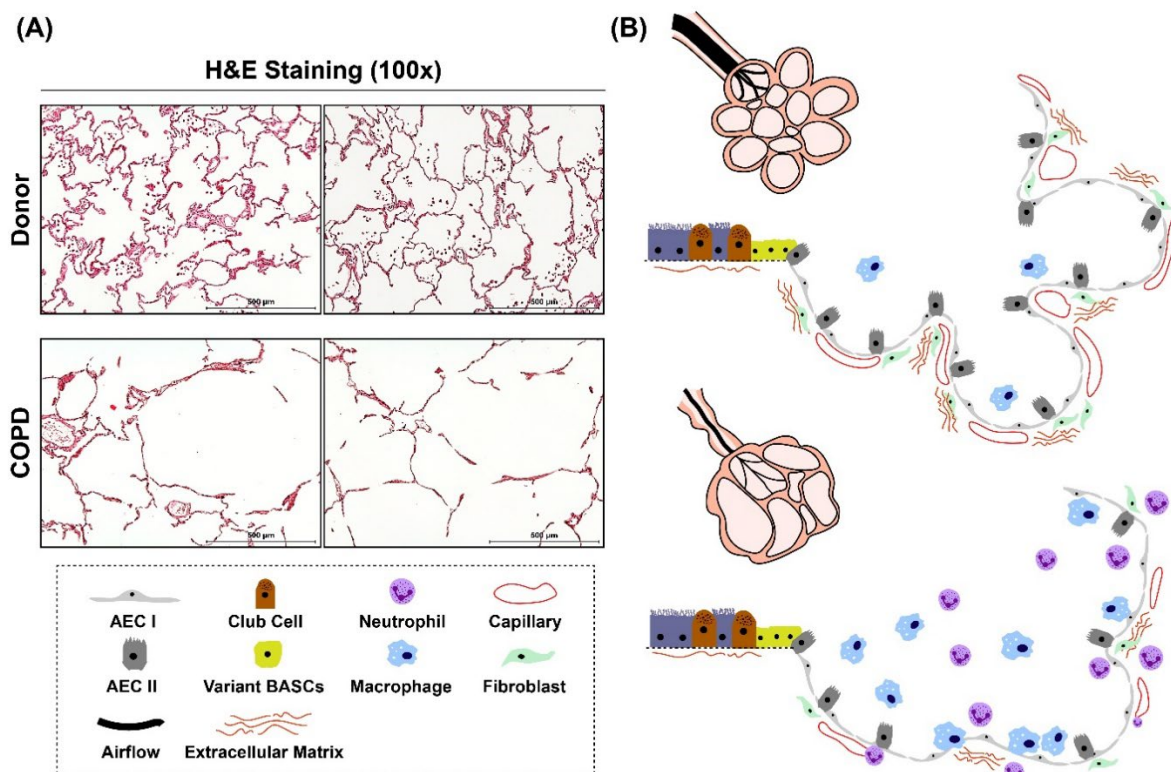


Figure 3. Alveolar septal wall in healthy and COPD lungs. (A) Representative images depicting distal lung parenchyma in a healthy donor (upper panel) and COPD (lower panel) lung tissue sections (100x magnification). H&E staining was performed (cytoplasm – pink; nuclei – blue). Scale bars = 500 μ m. (B) A schematic drawing of the healthy (upper panel) and emphysematous (lower panel) lung parenchyma. AT I: Alveolar epithelial cell type 1; AT II: Alveolar epithelial cell type 2; BASCs: Broncho-alveolar stem cells. Modified from Hadzic *et al.* 2020.

Several different patho-morphological emphysema types have been described in COPD patients (Smith *et al.* 2014; Kim *et al.* 1991). Centrilobular emphysema is the most common type. It is characterised by centrally positioned parenchymal destruction, mainly affecting the area around the bronchiole. Centrilobular emphysema is associated with severe airflow limitation and airway remodelling. Patients with centrilobular emphysema do not have increased lung compliance (Kim *et al.* 1991; Smith *et al.* 2014). Panlobular emphysema is a very severe form of emphysema with a phenotype similar to that observed in α 1-antitrypsin deficient patients (Smith *et al.* 2014; Kim *et al.* 1991). Paraseptal (also called distal acinar) emphysema type primarily affects the peripheral regions near the pleura, and it is not

associated with airflow obstruction (Smith *et al.* 2014). In some COPD patients, emphysema is characterised as irregular, where different emphysema types overlap. Irregular emphysema might also be associated with scars from prior inflammatory processes (e.g. tuberculosis) (Im *et al.* 1995).

Chronic bronchitis and emphysema coexist in many COPD patients, but one phenotype is usually predominant over the other (Hersh *et al.* 2014; Miravittles *et al.* 2013). The reason behind this phenomenon is still not well understood (Hersh *et al.* 2014; Miravittles *et al.* 2013). Recent studies demonstrated genetic associations with either emphysema or an airway disease phenotype in COPD (Ragland *et al.* 2019). This suggests that different mechanisms may be involved in the development of emphysema and chronic bronchitis. Also, emphysema and chronic bronchitis in COPD may even occur independently (Ragland *et al.* 2019; Castaldi *et al.* 2014). Furthermore, genetic associations were also found in patients with different pathomorphological emphysema types (Castaldi *et al.* 2014).

1.2.5 COPD-associated pulmonary hypertension (PH)

Pulmonary hypertension (PH) is a serious disease affecting pulmonary circulation. It is defined as an increase in mean pulmonary arterial pressure (mPAP) ≥ 20 mmHg and a pulmonary artery wedge pressure (PAWP) of ≤ 15 mmHg and elevated pulmonary vascular resistance (PVR) > 3 wood units (Simonneau *et al.* 2019; Collum *et al.* 2017; Hoeper *et al.* 2013; Hoeper *et al.* 2019). PH is accompanied by right ventricular wall hypertrophy and, eventually, right heart failure. Due to significant structural remodelling of the pulmonary vasculature, COPD is often associated with at least mild PH (Gredic *et al.* 2020). Up to 90% of COPD patients have mPAP higher than 20 mmHg at rest (Gredic *et al.* 2020). According to the classification (6th World Symposium on Pulmonary Hypertension held in Nice in 2018), COPD associated PH is categorised in group 3 – PH due to lung disease and/or hypoxia (Simonneau *et al.* 2019; Gredic *et al.* 2020; Collum *et al.* 2017). Even though HPV is an important factor contributing to the increase in PVR, the aetiology of COPD-associated PH may differ from the PH due to hypoxia (Seimetz *et al.* 2011; Gredic *et al.* 2020). On the contrary, HPV might be a beneficial mechanism in COPD lungs, ensuring ventilation-perfusion matching and near-normal blood oxygen

saturation despite the damaged lung parenchyma. Therefore, treatment with vasodilators could impair oxygen saturation in COPD patients (Gredic *et al.* 2020).

Pulmonary vascular remodelling, seen as increased muscularization or pruning of small blood vessels, was observed in COPD patients (Bunel *et al.* 2019; Gredic *et al.* 2020; Estépar *et al.* 2013). Furthermore, pulmonary vascular remodelling was observed in smokers without COPD (Santos *et al.* 2002). In animal models of long-term chronic CS exposure, pulmonary vascular remodelling precedes emphysema development (Weissmann *et al.* 2014; Seimetz *et al.* 2020; Seimetz *et al.* 2011; Ferrer *et al.* 2009; Wright *et al.* 1991). Hence, it is suggested that alterations in the pulmonary vascular compartment precede lung parenchymal changes during COPD development. PH in COPD is associated with increased exacerbations rates and decreased survival (Gredic *et al.* 2020). Therefore, PH in COPD can contribute to disease development and progression.

1.2.6 Animal models of COPD

Several animal models have been developed and utilised to study COPD (Shapiro 2000; Wright *et al.* 2008; Tanner *et al.* 2020; Groneberg *et al.* 2004). Rodents are primarily used in animal experiments, and species differences should be considered when designing studies and interpreting results. Most of the transgenic animals created for research purposes are mice. Therefore, mice models are widely used in studies that require transgenic animals. Recent technological advances, such as the development of the adeno virus-associated (AAV) vectors, may allow easier genetic manipulation regardless of the animal species and thus give more freedom when choosing animal species for experimental studies (Martino *et al.* 2020; Zhao *et al.* 2019). The general anatomic organization of mice and human lungs is similar. However, there are significant differences in the architectural organization of the lung, airway branching, and cellular composition along the conductive airways (Pan *et al.* 2019). Mouse lung consists of one left (*l. sinister*) and four right (*l. cranialis*, *l. medius*, *l. caudalis* and *l. cardialis*) lung lobes (Hoang *et al.* 2018; Pan *et al.* 2019). Airway branching in mice is more asymmetric compared to human lungs and gives 13-17 generations of airways (Irvin *et al.* 2003; Pan *et al.* 2019). In the mouse, a single central bronchiole spans each lobe and branches giving multiple

bronchioles along its length. Each of these bronchioles branches 3 to 4 times before ending in the terminal bronchioles (Pan *et al.* 2019; Irvin *et al.* 2003). The other significant characteristic of the mouse lung is a relatively large airway lumen. It is speculated that these features increase breathing efficacy in mice and reduce flow resistance resulting from a high breathing frequency of 250 – 350 breaths per minute. (Pan *et al.* 2019; Irvin *et al.* 2003). The cellular composition of the airway epithelium and its proximal-distal distribution differs significantly between the species, limiting studies of airway remodelling and chronic bronchitis. For example, human basal and goblet cells are distributed more distally towards the smaller airways, in contrast to mice (Yang *et al.* 2018; Irvin *et al.* 2003; Pan *et al.* 2019; Plopper *et al.* 2015). In the small airways, these cells contribute greatly to the airflow limitation, an important pathological feature of COPD.

Chronic exposure to cigarette exposure (CS) appears to be a model of choice since cigarette smoking is indeed the leading risk factor for COPD development in humans. In mice, this model mimics most of the COPD hallmarks (Wright *et al.* 2008; Churg *et al.* 2008). Long-term CS exposure leads to the development of emphysema and PH in mice (Weissmann *et al.* 2014; Pichl *et al.* 2019; Seimetz *et al.* 2020; Seimetz *et al.* 2011; Seimetz *et al.* 2015; Hadzic *et al.* 2021). Data from animal studies and human patients indicate that structural and/or molecular alterations in the pulmonary vasculature can precede emphysema development in COPD (Santos *et al.* 2002; Weissmann *et al.* 2014; Seimetz *et al.* 2020; Seimetz *et al.* 2011; Gredic *et al.* 2020). However, CS-exposed mice develop very mild alterations in the airway compartment. Hence, only a slight increase in bronchial wall thickness is reported in mice after chronic CS exposure (Wright *et al.* 2008). On the other hand, studies of CS-induced airway disease can be performed in guinea pigs (Wright *et al.* 2007). Unlike mice, guinea pigs have a distribution of airway epithelial cells along proximal-distal axes that resembles the human situation (Wright *et al.* 2007). A major disadvantage of the CS exposure models is the long exposure duration of the experiment; 6 – 8 months are required for stable emphysema and PH development (Wright *et al.* 2008; Hadzic *et al.* 2021; Pichl *et al.* 2019). The required duration of CS exposure can depend on the animal model (e.g. different species or animal strain), daily exposure duration and particulate matter properties (concentration or physical/chemical properties).

Another model often used in COPD research is intratracheal elastase application. The mouse model of elastase-induced pulmonary emphysema is characterised by a sudden onset of severe emphysema (Antunes *et al.* 2011; Limjunyawong *et al.* 2015; Wright *et al.* 2008; Kneidinger *et al.* 2011; Fysikopoulos *et al.* 2020; Takahashi *et al.* 2008; Ishizawa *et al.* 2004; Tanner *et al.* 2020). Depending on the application protocol and enzyme selection, elastase-induced emphysema can be progressive what is comparable to the situation in COPD patients (Limjunyawong *et al.* 2015; Wright *et al.* 2008; Lüthje *et al.* 2009). Elastase derived from porcine pancreas or neutrophils has been used, and both types give similar results (Antunes *et al.* 2011; Fysikopoulos *et al.* 2020). Different protocols exist, but a single intratracheal administration of elastase was shown to be sufficient. Analysis or treatment usually starts 3 – 4 weeks after the elastase instillation, ensuring that the acute signs of lung injury vanished (Ishizawa *et al.* 2004; Fysikopoulos *et al.* 2020; Takahashi *et al.* 2008). Even though this short-term model does not mimic all the complex traits observed upon CS exposure, it is often used in animal models studying therapeutic approaches (Kneidinger *et al.* 2011; Wright *et al.* 2008; Fysikopoulos *et al.* 2020; Takahashi *et al.* 2008; Ishizawa *et al.* 2004). Besides pulmonary emphysema, mice develop increased airway resistance and PH upon elastase instillation (Fysikopoulos *et al.* 2020; Toumpanakis *et al.* 2020; Antunes *et al.* 2011; Fukuzaki *et al.* 2018; Hantos *et al.* 2008; Padilha *et al.* 2015; Cruz *et al.* 2012). It is speculated that airway resistance in the elastase model appears due to destroyed alveolar attachments (Hantos *et al.* 2008). Interestingly there are indications that spontaneous breathing upon increased airway resistance induces pulmonary inflammation and injury in previously healthy animals (Glynos *et al.* 2015; Toumpanakis *et al.* 2010). Remodelling of the pulmonary vasculature, that can contribute to PH development, has been described in the elastase model (Fysikopoulos *et al.* 2020; Lüthje *et al.* 2009; Oliveira *et al.* 2016). In addition, the effect of hypoxemia or vascular pruning due to the significant parenchymal injury should be taken into account (Icochea *et al.* 1982; Oliveira *et al.* 2016; Lüthje *et al.* 2009).

Several other, more specific, animal models of COPD are described in the literature (Shapiro 2000; Wright *et al.* 2008; Tanner *et al.* 2020; Groneberg *et al.* 2004; Ghorani *et al.* 2017). Inhalation exposure to nitrogen dioxide, sulphur dioxide, ozone, cadmium chloride, or other

oxidant stimuli or particulates has been used to induce inflammation and emphysematous changes in animals (Groneberg *et al.* 2004; Hutchinson *et al.* 2018; Shapiro 2000). Intratracheal lipopolysaccharide (LPS) instillation is used to model massive lung inflammation, mainly utilised to study exacerbations (Tanner *et al.* 2020; Lee *et al.* 2018; Ghorani *et al.* 2017). However, it remains unclear whether inflammatory infiltrates observed in this model recapitulate the phenotype found with CS exposure. Furthermore, emphysema in animal models could be induced by severe starvation or vascular endothelial growth factor (VEGF) receptor inhibition (Harkema *et al.* 1984; Kojonazarov *et al.* 2019; Sahebajami *et al.* 1981; Kasahara *et al.* 2000).

The usefulness of results obtained from animal experiments is directly related to the similarities between the animal model of choice and human pathology. As mentioned above, COPD in humans consists of emphysema, small airway remodelling, chronic bronchitis and PH. A given patient may develop only some or all of these hallmarks. Similarly, animal models only partially mimic the situation observed in patients with COPD (Wright *et al.* 2008; Tanner *et al.* 2020; Groneberg *et al.* 2004). Such facts should be considered when interpreting the data obtained from pre-clinical studies.

1.2.7 Mechanisms of COPD pathology

COPD is a heterogeneous lung pathology. Most of the underlying signalling pathways studied in the context of COPD are related to protease/anti-protease disbalance, augmented inflammatory response, increased oxidative/nitrosative stress, cellular senescence and cell death (Gouveia *et al.* 2020; Barnes *et al.* 2015). In COPD, many developmental pathways are dysregulated, resulting in a lack of or even aberrant lung repair after injury (Gouveia *et al.* 2020; Barnes *et al.* 2015). Furthermore, these mechanisms may differ between different patients and during the disease progression (Churg *et al.* 2011). Despite continuous research and substantial progress, mechanisms underlying COPD are still poorly understood.

1.2.7.1 Protease-anti-protease disbalance

Protease-anti-protease disbalance was among the first molecular mechanisms studied in the pathology of COPD. Elastase, a neutrophil-derived protease, and its inhibitor α 1-antitrypsin were described in patients with severe COPD (Henaio *et al.* 2016; Brode *et al.* 2012; Perciaccante *et al.* 2018). Neutrophil-derived elastase causes severe panlobular emphysema in patients lacking functional α 1-antitrypsin. In physiological conditions, α 1-antitrypsin is produced by macrophages, epithelial cells, or diffuses in the lung parenchyma from the circulation (Henaio *et al.* 2016; Brode *et al.* 2012). The protease-anti-protease disbalance was then also described in the context of CS-induced emphysema, where besides elastase, inflammatory cells secrete various other proteases. Impaired anti-protease defence in this model may be caused by oxidative stress (Evans *et al.* 1994).

In cigarette smoke exposure animal models of COPD, it has been shown that neutrophil elastase deficient mice or treatment with neutrophil elastase inhibitors exhibited protective effects towards emphysema development (Shapiro 2003; Wright *et al.* 2002; Churg *et al.* 2003). Apart from the neutrophil-derived elastase, other proteases have been investigated. In acute CS-induced connective tissue breakdown in mice, it appears that both neutrophil- and macrophage-derived metalloelastases are required for emphysema development (Churg *et al.* 2002; Hautamaki *et al.* 1997). Furthermore, mice treated with matrix metalloprotease (MMP) inhibitors and MMP 12 deficient mice are, to a significant extent, protected against emphysema in the CS exposure COPD model (Churg *et al.* 2005; Shapiro 2003; Churg, Wang, Wang, Onnervik, *et al.* 2007; Churg, Wang, Wang, Meixner, *et al.* 2007). Neutrophil elastase and other proteases have also been described in PH (Taylor *et al.* 2018; Cowan *et al.* 2000; Chelladurai *et al.* 2012). Furthermore, serine elastase inhibition could completely reverse monocrotaline-induced PH in rats (Cowan *et al.* 2000).

1.2.7.2 Augmented inflammation in COPD pathology

One of the main COPD hallmarks is the hyper-responsiveness of the lungs towards inhaled noxious agents, leading to an altered immune response and massive inflammation (Wang *et al.* 2018) (**Figure 4**). Innate and adaptive immunity, with related cytokine signalling pathways,

have been extensively studied in the context of COPD pathology. Even though CS has been associated with foremost neutrophilic inflammation, the studies examining histologic sections of the lungs have failed to correlate neutrophil number with lung parenchymal destruction (Eidelman *et al.* 1990; Finkelstein *et al.* 1995).

Furthermore, mast cells have been reported to increase in number and activation in the lungs of COPD patients (Kosanovic *et al.* 2014). These findings are in line with increased protease activity in COPD since mast cell-derived mediators (especially chymase) are known to activate pro-matrix metalloproteinases. Surprisingly, the number of mast cells in lung sections from smokers with COPD positively correlated with FEV₁/FVC ratio, suggesting the potential beneficiary effect on lung function (Kosanovic *et al.* 2014). These findings may suggest the difference in airway obstruction mechanisms in COPD compared to asthma.

Besides the innate immunity cells, lymphocytes were also described in the context of COPD. A subpopulation of cytotoxic CD8⁺ T-lymphocytes appears to be involved in CS-induced emphysema development in mice (Maeno *et al.* 2007). CD8⁺ T lymphocytes in COPD have a complex pro-inflammatory function rather than just inducing epithelial cell death through their cytotoxicity (McKendry *et al.* 2016). This fact brings a novel insight into explaining the relationship between the higher susceptibility towards viral infections and the excessive inflammation associated with exacerbations in COPD patients (McKendry *et al.* 2016). There is increasing evidence about the role of B cells and autoantibodies against proteins damaged in oxidative stress conditions in the context of COPD (Kirkham *et al.* 2011). Autoimmunity in COPD patients is enhanced by the interleukin (IL)-33. IL-33 is an alarmin mainly released from epithelial or endothelial cells in response to inhaled environmental insults such as CS (Li *et al.* 2019). Autoantibodies trigger a humoral autoimmune response that could be responsible for the disease progression even after smoking cessation (Li *et al.* 2019). Furthermore, IL-33 affects bronchial epithelium and it is associated with goblet cell hyperplasia and increased mucus secretion (Liew *et al.* 2016).

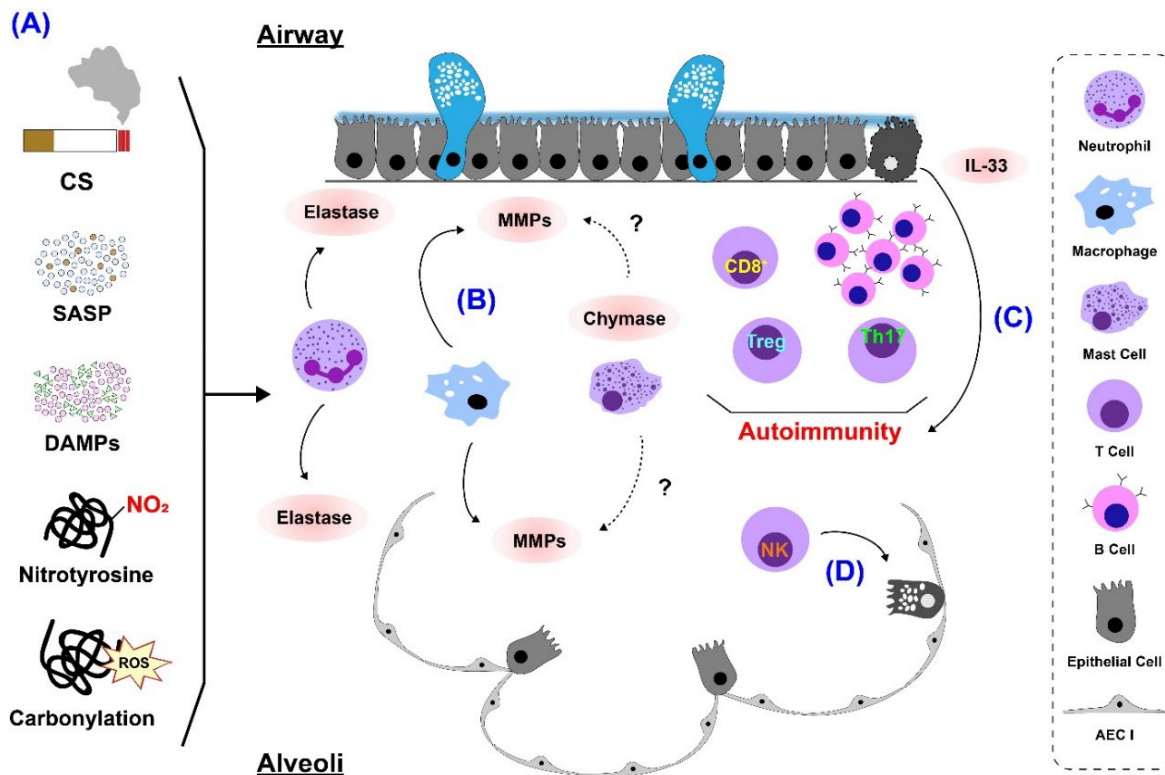


Figure 4. Augmented inflammatory response in COPD. (A) Noxious agents and inflammatory stimuli trigger inflammation in COPD. **(B)** Proteases such as neutrophils-derived elastase, macrophages-derived MMPs and mast cells-derived chymase. **(C)** IL-33 facilitates the initial steps in triggering an autoimmune response in COPD. **(D)** NK cells directly induce cell death. Abbreviations - MMPs: Matrix metalloproteases; Treg: Regulatory T cell; Th17: T helper cell 17; NK: Natural killer; CS: Cigarette smoke; ROS: Reactive oxygen species; DAMPs: Damage associated molecular patterns; AT II: Alveolar epithelial cell type 2; AT I: Alveolar epithelial cell type 1; SASP: Senescence-associated secretory phenotype. Modified from Hadzic *et al.* 2020.

Various animal models have been employed to decipher the role of different inflammatory pathways in airway remodelling and emphysema. For example, knockout mice for tumour necrosis factor α (TNF- α) or IL-1 receptors are shown to be partially protected against CS-induced emphysema (Churg *et al.* 2004; Churg *et al.* 2009). Mice lacking CC chemokine receptor (CCR) 5 are protected against emphysema but interestingly show no protection against airway remodelling in the CS-induced emphysema model (Leberl *et al.* 2013). CCR 6 deficient mice appear to be protected against TNF- α induced and CS-induced emphysema (Bracke *et al.* 2006).

Interestingly, in COPD patients, the inflammatory pattern seems similar but augmented compared to the smokers without COPD (Barnes 2016). As an underlying mechanism for the amplified inflammatory signal, the reduction of histone deacetylase-2 (HDAC2) has been proposed. HDAC2 has a vital role in switching off activated inflammatory genes, and its expression is markedly reduced in COPD pathology (Barnes 2009; Ito *et al.* 2005).

1.2.7.3 Oxidative and nitrosative stress in COPD pathology

Oxidative and nitrosative stress are elevated in COPD and positively correlate with the disease severity (Seimetz *et al.* 2020; Seimetz *et al.* 2011; Osoata *et al.* 2009; Brindicci *et al.* 2009) (**Figure 5**). When overcoming the intrinsic antioxidant defences, reactive oxygen species (ROS) can trigger the immune response via various mechanisms (Seimetz *et al.* 2020; Seimetz *et al.* 2011; Foronjy *et al.* 2006). Abated oxidative stress via activation of nuclear factor erythroid 2-related factor 2 (Nrf2) (Sussan *et al.* 2009), overexpression of superoxide dismutase isoforms or treatment with the antioxidants have a protective effect against inflammation and emphysema development in the CS-induced emphysema model (Churg *et al.* 2011).

Superoxide (O_2^-) in COPD pathology is thought to be generated primarily by mitochondrial metabolism, molybdenum hydroxylase, arachidonic acid metabolism, and nicotinamide adenine dinucleotide phosphate (NADPH) oxidase-dependent processes (Repine *et al.* 1997; Seimetz *et al.* 2020; Seimetz *et al.* 2011). NOX1-NOX5, dual oxidases (DUOX) 1 and 2 are identified as membrane-bound ROS-producing subunits of NADPH multi-protein complexes (Seimetz *et al.* 2020; Lambeth *et al.* 2007). NOX2 is a subunit of phagocytic, whereas NOX1, NOX3-5 DUOX1 and 2 are subunits in non-phagocytic NADPH complexes (Seimetz *et al.* 2020). NOX4 and DUOX1 and 2 directly generate hydrogen peroxide (H_2O_2), while other subunits release superoxide (Brandes *et al.* 2014). The function of NOX1-NOX4 depends on interaction with an integral protein p22^{phox} (Ambasta *et al.* 2004; Seimetz *et al.* 2020). Furthermore, NOX1-NOX3 activity also depends on interaction with cytosolic regulatory subunits (Brandes *et al.* 2014; Seimetz *et al.* 2020). NOX1 activity requires NADPH oxidase organizer 1 (NOXO1) and NADPH oxidase activator 1 (NOXA1), whereas NOX3 seems to depend only on NOXO1 (Schröder *et al.* 2017; Brandes *et al.* 2014; Seimetz *et al.* 2020). Recent evidence points out

that non-phagocytic NOX1 is an essential driver of CS-induced emphysema and PH (Seimetz *et al.* 2020). NOX1 was upregulated in COPD lungs and in animals upon CS exposure. NOX1 potentiates the superoxide-generating activity of non-phagocytic NADPH oxidases NOX1 and NOX3 (Seimetz *et al.* 2020; Brandes *et al.* 2014). Knock-out mice for *Nox1* are protected against CS-induced emphysema and PH (Seimetz *et al.* 2020). ROS can directly modify the proteins (for example, via carbonylation), and such proteins may act as autoantigens to induce autoimmunity (**Figure 5**). Autoantibodies to carbonylated proteins are detectable in the plasma and lungs of patients with COPD (Kirkham *et al.* 2011; Gouveia *et al.* 2020).

Furthermore, superoxide can react with nitric oxide (NO) to create peroxynitrite (ONOO⁻) (Szabo *et al.* 2007; Lomonosova *et al.* 1998; Seimetz *et al.* 2020), a potent oxidant that preferably reacts with tyrosine residues in the proteins when 3-nitrotyrosine (3-NT) is formed (Ricciardolo *et al.* 2004; Tsumakidou *et al.* 2005; Seimetz *et al.* 2011). Those modified proteins can further alter cell signalling, triggering inflammatory response and apoptosis. Importantly, levels of 3-nitrotyrosine in sputum proteins have been found to negatively correlate with FEV1 in COPD patients (Tsumakidou *et al.* 2005; Ricciardolo *et al.* 2004; Ichinose *et al.* 2000; Sugiura *et al.* 2004). Nitration of tyrosine residues above a certain threshold can alter the cellular signalling, suggesting that 3-nitrotyrosine is not only a marker of nitrosative stress in COPD but also has a functional relationship with the pathophysiology of inflammatory airway diseases (Sugiura *et al.* 2004; Murata *et al.* 2004; Davis *et al.* 2002). In line with this view, it has been proposed that 3-nitrotyrosine contributes to airway hyper-responsiveness and epithelial damage (Tsumakidou *et al.* 2005) and plays a significant role in the development of airway remodelling (Ichinose *et al.* 2000). Dysregulation of inducible nitric oxide synthase (iNOS), a leading source of NO in COPD, has been proposed as an underlying mechanism of COPD pathology (Brindicci *et al.* 2009; Seimetz *et al.* 2011). Mice deficient in iNOS are protected against emphysema development and show less inflammation when exposed to CS (Seimetz *et al.* 2011). Additionally, the data obtained from the same animal model suggest that emphysema development can be independent of iNOS in bone marrow-derived cells (Seimetz *et al.* 2011). For peroxynitrite to be formed, NO and superoxide need to be produced in close proximity (Wink *et al.* 1998). Furthermore, peroxynitrite as an extremely unstable free radical

can modify the tyrosine residues in a very short range from the formation site (Szabo *et al.* 2007). Furthermore, L-N6-(1-Iminoethyl) lysine (L-NIL), a selective iNOS inhibitor, has been found to successfully reverse CS-induced emphysema and PH in mice (Seimetz *et al.* 2011). L-NIL reversed the CS-induced upregulation of MMP 9, restored tissue inhibitor of MMP 3 (TIMP3) expression and reduced inflammatory cell count in the lung parenchyma (Seimetz *et al.* 2011).

From the antioxidant defence proteins, strong upregulation of heme oxygenase 1 (HO-1) has been observed in the lungs of healthy smokers, which was not the case in COPD patients. This suggests a pivotal role of HO-1 in defence against CS-induced lung damage. HO-1 protects against oxidative stress through antioxidant, anti-apoptotic, and anti-inflammatory actions (Fredenburgh *et al.* 2007). Moreover, HO-1 is interconnected with the iNOS pathway, and NO in physiological conditions is a potent inducer of HO-1 expression (Sarady *et al.* 2004).

1.2.7.4 Cell death and senescence in COPD pathology

Some studies demonstrate the importance of cell death of bronchial and alveolar epithelial cells in the pathogenesis of COPD (Kirkham *et al.* 2011; Louhelainen *et al.* 2010; Faiz *et al.* 2018) and suggest oxidative stress as a critical pathological driver of cell death (Rahman 2012; Yao *et al.* 2011) (**Figure 4, 5**).

In the context of lung injury and emphysema development, apoptosis is mainly linked to AT II cells, which further causes impaired lung regeneration. On the other hand, in the context of bronchitis and airway remodelling, necroptosis is described in bronchial epithelial cells (Faiz *et al.* 2018). Unlike apoptosis, which is thought to be a weak inducer of inflammation with little release of damage-associated molecular patterns (DAMPs) from dying cells, necroptosis and ferroptosis are considered as potent inducers of inflammation by releasing massive amounts of DAMPs (Yoshida *et al.* 2019).

Accelerated ageing and cellular senescence have been observed in both animal models of COPD as well as in COPD patients (Adnot *et al.* 2015). A popular theory proposes oxidative stress to be a key driver of accelerated ageing (Chung *et al.* 2006; Hekimi *et al.* 2011). Several

features of cellular senescence, including telomere shortening, mitochondrial dysfunction, defective DNA repair and stem cell exhaustion, have been identified in COPD patients (Mercado *et al.* 2015; Meiners *et al.* 2015).

Impaired lung repair is associated with the depletion of stem cells, which is a feature of lung ageing (Barnes 2016; Lopez-Otin *et al.* 2013; Barnes 2017). AT II cells show evidence of cellular senescence in COPD (Tsuji *et al.* 2006), but also, senescence of mesenchymal cells may be a mechanism of emphysema development and impaired repair of lung injury (Adnot *et al.* 2015). Furthermore, the senescence of endothelial cells, coupled with endothelial dysfunction, has been observed in the context of COPD (Green *et al.* 2017).

Additionally, senescent cells, rather than being removed by programmed cell death, remain metabolically active and exhibit what is termed as a senescence-associated secretory phenotype (SASP) (**Figure 4, 5**). Unlike apoptotic cells, they alter their environment as long as they persist by secreting, among others, pro-inflammatory cytokines and MMPs (Lopez-Otin *et al.* 2013).

1.2.7.5 Developmental pathways in COPD pathology

Developmental pathways that control lung development are often reactivated in the adult lung during regeneration. Many developmental pathways are dysregulated in COPD, which jeopardises lung homeostasis and repair processes (Boucherat *et al.* 2016). These pathways include Wnt/ β -catenin, Notch, bone morphogenic protein (BMP), hedgehog and retinoic acid (RA) signalling pathways (Ng-Blichfeldt *et al.* 2019).

Genome-wide association (GWA) studies pinpointed several COPD-associated loci. Most of the identified loci indeed encode for genes that play a role in lung development (Huang *et al.* 2019). These genes include MMPs (MMP 1-3, 7, 9, 12, 14, 21), their inhibitors TIMPs (TIMP 1-3) and several developmental regulators, such as SRY-Box 5 (SOX 5), NK2 homeobox 1 (NKX2-1), hedgehog interacting protein (HHIP), pathway patched homolog 1 (PTCH1) and retinoic acid receptor (RAR) beta (Huang *et al.* 2019).

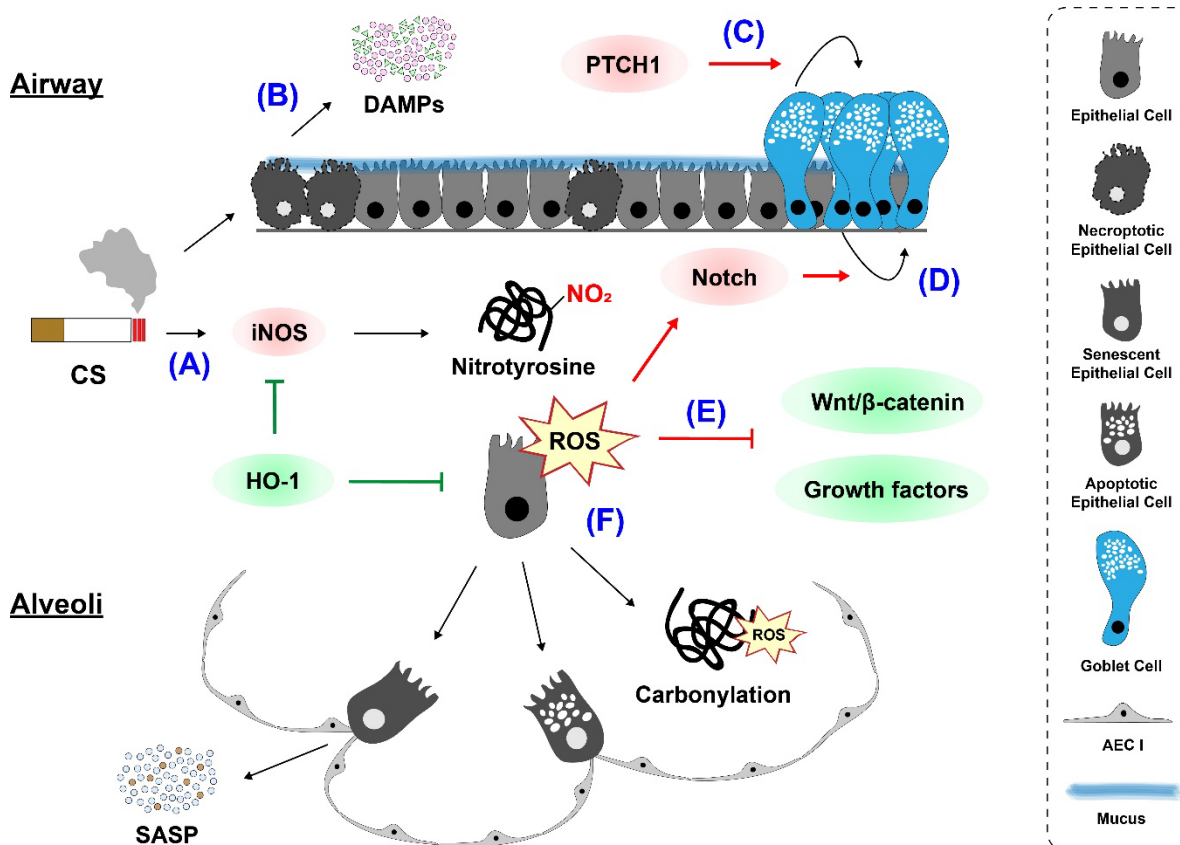


Figure 5. Cellular and molecular pathways in COPD. (A) Cigarette smoke-induced iNOS is responsible for excessive NO production, which in the context of COPD results in nitration of tyrosine residues. This can be prevented by HO-1. **(B)** Cigarette smoke in small airways causes cell death and subsequent DAMPs release. **(C)** PTCH1 upregulation is associated with goblet cell hyperplasia in COPD. **(D)** Alteration of Notch signalling pathways can contribute to airway remodelling and including goblet cells hyperplasia/metaplasia. **(E)** ROS in COPD hampers the canonical Wnt/β-catenin pathway and growth factor-mediated cell repair. **(F)** Excessive ROS lead to protein carbonylation, AT II cell apoptosis and cellular senescence, further triggering inflammation. **Abbreviations** - CS: Cigarette smoke; iNOS: Inducible nitric oxide synthase; ROS: Reactive oxygen species; DAMPs: Damage associated molecular patterns; HO-1: Heme oxygenase 1; AT II: Alveolar epithelial cell type 2; AT I: Alveolar epithelial cell type 1; SASP: Senescence-associated secretory phenotype; PTCH1: Protein patched homolog 1. Modified from Hadzic *et al.* 2020.

Wnt/β-catenin dependent repair could be a victim of increased ROS production in the context of COPD. A decrease in nuclear β-catenin was found in AT II cells in the COPD lungs. Furthermore, activation of the canonical Wnt/β-catenin pathway could attenuate emphysema in mice (Kneidinger *et al.* 2011). Finally, downregulation of this pathway was also found in the

airways of smokers and COPD patients (Wang *et al.* 2011) (**Figure 5**). In contrast to the canonical Wnt/ β -catenin pathway, activation of the non-canonical Wnt/ β -catenin pathway via Wnt5a impairs lung repair in COPD (Baarsma *et al.* 2017).

Downregulation of the Notch pathway in human airway epithelium is indeed associated with smoking and COPD (Tilley *et al.* 2009). Altered Notch signalling was found to lead to secretory cell differentiation in the airway epithelium and was coupled with goblet cell metaplasia in chronic bronchitis phenotype (Shaykhiev 2019) (**Figure 5**).

Furthermore, BMP-6 protein expression was observed in airway smooth muscle cells, endothelial cells, and pulmonary macrophages (Verhamme *et al.* 2019). Interestingly, its expression was decreased in the lungs of COPD patients and levels inversely correlated with disease severity (Verhamme *et al.* 2019).

Hedgehog (Hh) signalling was indeed confirmed to play an essential role in the airway epithelium of patients with COPD via maintaining the balance between proliferation and quiescence during homeostasis and regeneration (Tam *et al.* 2019; Peng *et al.* 2015). Disruption of this balance in epithelial cells upon injury leads to changes in the mesenchyme, which in return may disrupt epithelial regeneration after injury (Peng *et al.* 2015). Activation of hedgehog signalling during epithelial injury attenuates the expansion of the lung mesenchyme, whereas inactivation of hedgehog signalling prevents the restoration of quiescence during injury resolution (Peng *et al.* 2015). PTCH1, a receptor for the secreted hedgehog ligands, is upregulated in COPD and associated with airway cell proliferation, goblet cell hyperplasia and elevated mucus secretion (**Figure 5**) (Tam *et al.* 2019).

RARs, retinoid x receptor (RXR), and the associated ligands that play critical roles in the generation of the lungs were also confirmed to play an important role in COPD. Activation of retinoid X receptor, a RAR partner protein, was shown to attenuate pulmonary emphysema and airway inflammation in mice (Morichika *et al.* 2019). Furthermore, retinoic acid treatment in mice could induce alveolar regeneration (Hind *et al.* 2004). Interestingly, despite promising results obtained in animal models, palovarotene, a selective RAR gamma agonist, failed to

induce beneficial clinical effects in patients with moderate to severe COPD (Stolk *et al.* 2012). These data suggest that the RAR pathway alone may not have sufficient therapeutic potential for treating COPD in patients (Gouveia *et al.* 2020).

1.2.8 Growth factors and impaired lung repair in COPD

Preventive approaches are commonly investigated in animal models of COPD and give a valuable insight into signalling pathways involved in disease initiation and progression. However, in the case when therapeutic strategies are explored, the potential treatment intervention (e.g. drug application or knockout induction) is performed after the disease is established. This approach better mimics the situation in COPD patients. The treatment follows a successful diagnosis, which is usually postulated when the disease is in advanced stages. In contrast to the preventive models, in therapeutic approaches, much fewer targets showed promising effects (Gouveia *et al.* 2020).

Growth factors, such as vascular endothelial growth factor (VEGF), hepatocyte growth factor (HGF), fibroblast growth factors (FGF), and transforming growth factor β (TGF- β), are shown to be essential for alveolar epithelium formation during development and homeostasis later in life (Yildirim *et al.* 2010). Interactions between the epithelium and the endothelium are crucial for normal lung development. The signalling is mainly conducted through VEGF, secreted by epithelial cells and VEGF receptor 2, localised on epithelial and endothelial cells (Boucherat *et al.* 2016). Moreover, blocking VEGF signalling in adult mice and rats results in emphysema (Petrache *et al.* 2005; Kasahara *et al.* 2000; Kojonazarov *et al.* 2019). Poor cell survival, which occurs in the context of a VEGF-deprived environment, could be a contributing mechanism of emphysema development in the adult lung (Schweitzer *et al.* 2011). Interestingly, it appears that VEGF is upregulated in patients with predominant chronic bronchitis phenotype and downregulated in patients with emphysema (Green *et al.* 2017).

Palifermin, which is a truncated recombinant form of human FGF7 (Δ N23-KGF/ Δ N23-FGF7), was able to partially reverse elastase-induced emphysema in mice (Yildirim *et al.* 2010). The proposed mechanisms were the proliferation of AT II and locally induced TGF- β expression in

epithelial cells (Yildirim *et al.* 2010). The potential role of adult stem cells has also been explored in the context of lung regeneration after injury. Stem cells derived from either bone marrow or adipose tissue contributed to lung regeneration after elastase-induced pulmonary emphysema (Ishizawa *et al.* 2004; Shigemura *et al.* 2006). Adipose-derived stem cells can secrete factors such as VEGF or HGF in a paracrine fashion (Schweitzer *et al.* 2011). Additionally, these effects may be combined with a direct cellular interaction in cases when the stem cells integrate into the lung parenchyma (Schweitzer *et al.* 2011). Taken together, it seems that lung repair is weakened in COPD. This could be due to dysregulated developmental pathways and impaired growth factor stimulation.

1.2.9 Fibroblast growth factor (FGF) signalling

The fibroblast growth factor (FGF) family comprises several secreted protein ligands and intracellular non-signalling proteins. Members of the FGF family are found in vertebrates and invertebrates and have a conserved core sequence and structure. In mammals, eighteen FGFs are characterised as secreted, while four (FGF11, FGF12, FGF13 and FGF14) act as intracellular cofactors (Ornitz *et al.* 2015; Powers *et al.* 2000). Intracellular FGFs mainly serve as cofactors for voltage-gated sodium channels, while secreted FGFs act in either paracrine or endocrine fashion to initiate signalling cascades via binding to receptors with intrinsic tyrosine kinase activity (Ornitz *et al.* 2015; Powers *et al.* 2000). Secreted FGFs are expressed in almost all tissues, and they play essential roles in early development, organogenesis, and in the adult tissues. In adults, secreted FGFs are homeostatic factors that are essential for tissue maintenance, repair and regeneration (Ornitz *et al.* 2015; Lanner *et al.* 2010; Bellusci *et al.* 1997; Gupte *et al.* 2009; Ahmadvand *et al.* 2021; Volckaert *et al.* 2011; Volckaert *et al.* 2017; Yuan *et al.* 2019). In general, secreted FGFs signal in an autocrine or paracrine fashion and thus are called canonical or paracrine FGFs. Secreted FGFs control cell proliferation, differentiation and survival. However, through evolution, three members (FGF15/19, FGF21 and FGF23) have gained an endocrine function. FGF15 is a rodent orthologue of human FGF19, and these two proteins share only 52% of the amino acid sequence (Jackson *et al.* 2018). The endocrine FGFs

regulate bile acid, calcium and phosphate homeostasis, and carbohydrate and lipid metabolism (Ornitz *et al.* 2015; Powers *et al.* 2000).

According to the current consensus, based on structural similarities, twenty-two ligands are divided into seven FGF subfamilies (**Table 3**): five paracrine (FGF1, 2, 7, 8 and 9 subfamilies), one endocrine (FGF15/19 subfamily) and one intracellular (FGF11 subfamily) (Ornitz *et al.* 2015).

1.2.10 FGF receptors

Secreted FGFs interact with four FGF receptors (FGFRs) with intrinsic tyrosine kinase domains and subsequently regulate fundamental cellular processes. Downstream signalling cascades regulate proliferation, survival, migration, differentiation, and metabolism (Ornitz *et al.* 2015; MacKenzie *et al.* 2015; Yuan *et al.* 2019; Bellusci *et al.* 1997; El Agha *et al.* 2018; Gupte *et al.* 2009; El Agha *et al.* 2016; Jones *et al.* 2021).

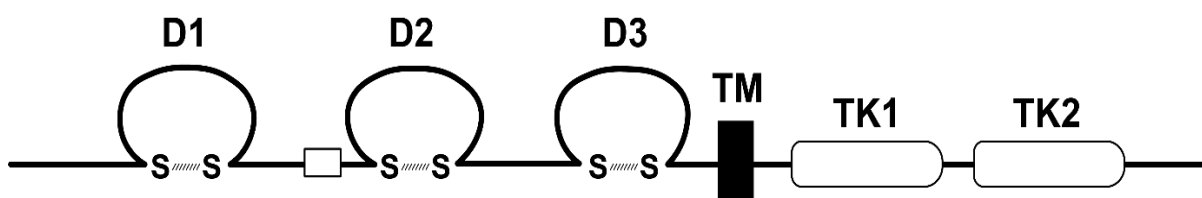


Figure 6. Schematic drawing of FGFR structure. FGF receptors contain three extracellular immunoglobulin-like (IGL) domains (D1-D3), transmembrane domain (TM) and two tyrosine kinase domains. Modified from Ornitz *et al.* 2015.

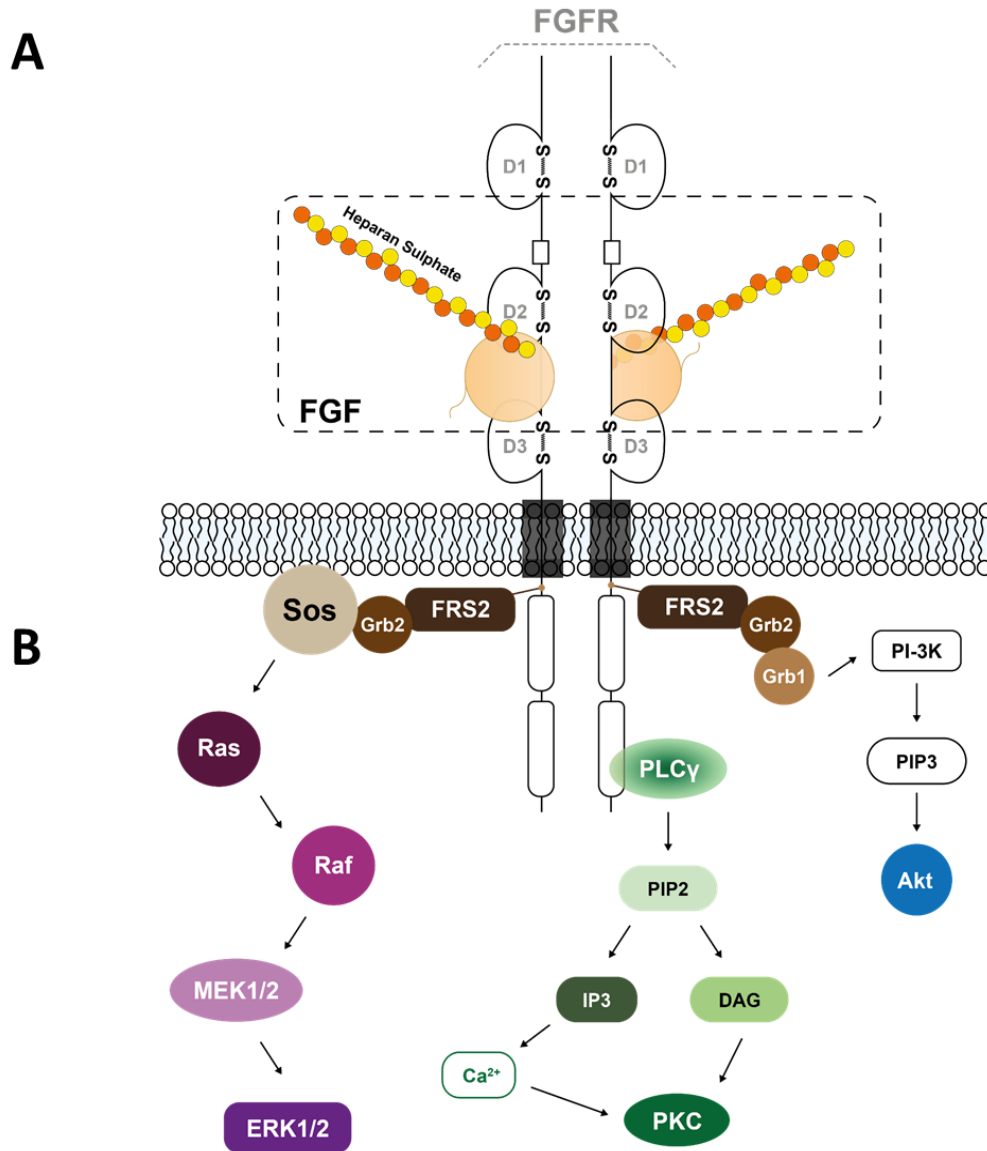


Figure 7. FGF receptor activation and downstream signalling. (A) Two FGF ligands interact with two FGF receptors in the presence of heparan sulphate. **(B)** Receptor dimerization subsequently triggers intracellular signalling cascades, mediated by intrinsic tyrosine kinase domains. Depending on the cell type and the cell status, downstream signalling can be carried out via activation of Ras, PLC γ or PI-3K pathways. Abbreviations - FRS2: Fibroblast growth factor receptor substrate 2; Grb1/2: Growth factor receptor-bound protein 1/2; Sos: Son of Sevenless; Ras: Rat sarcoma; Raf: Rapidly accelerated fibrosarcoma; MEK1/2: Mitogen-activated protein kinase kinase 1/2; ERK1/2: Extracellular signal-regulated kinase 1/2; PLC γ : Phospholipase C gamma; PIP2: Phosphatidylinositol 4,5-bisphosphate; IP3: Inositol-1,4,5-trisphosphate; DAG: Diacylglycerol; PKC: Protein kinase C; PI-3K: Phosphatidylinositol-3-kinase; PIP3: Phosphatidylinositol-3,4,5-trisphosphate; Akt: Ak strain transforming. Modified from Kovacevic *et al.* 2015.

FGFRs are encoded by four genes: *FGFR1* – in humans located on chromosome 8 (Kornmann *et al.* 2013); *FGFR2* – on chromosome 10 (Houssaint *et al.* 1990; Dionne *et al.* 1990); *FGFR3* – on chromosome 4 (Wang *et al.* 2013); *FGFR4* – on chromosome 5 (Dai *et al.* 2020). The structure of FGFRs is depicted in **Figure 6**. In the extracellular region, FGFRs contain three immunoglobulin-like (IGL) domains (labelled as I, II, III). These domains are responsible for interaction with the different FGF ligands. Ligands bind in the region of IGL domains II and III. FGFRs contain one transmembrane domain and two tyrosine kinase domains in the intracellular region (Ornitz *et al.* 2015; MacKenzie *et al.* 2015; Jones *et al.* 2021).

For successful interaction between ligand and receptor, an additional cofactor is needed (listed in **Table 3**). For paracrine FGFs, this is heparin or heparan sulphate. Endocrine FGF ligands require the Klotho protein as a cofactor. In the presence of a cofactor, the ligand binds to the corresponding receptor, leading to receptor dimerization and subsequent downstream signalling activation (**Figure 7**) (Ornitz *et al.* 2015; Ornitz 2000; Matsuo *et al.* 2013; Rapraeger *et al.* 1991).

Alternative splicing in the IGL III region of *FGFR1-FGFR3* mRNA leads to the formation of two isoforms, IIIb and IIIc. Among FGFRs, alternative splicing of *FGFR2* is functionally the most relevant (Ornitz *et al.* 2015). Different isoforms have differential expression patterns and interact with different ligands. The FGFR2IIIb (FGFR2b) isoform is expressed on the cell membrane of epithelial and endothelial cells. FGFR2b preferably binds ligands from the FGF7 subfamily, which are mainly secreted by mesenchymal cells. Isoform IIIc (FGFR2c) is predominantly expressed on mesenchymal cells and binds ligands from FGF4 or FGF8 subfamilies (Ornitz *et al.* 2015). Preferential ligand-receptor interactions are listed in **Table 3**.

Table 3. FGF subfamilies and their receptor specificity. Modified from Ornitz and Itoh 2015.

FGF subfamily	FGF ligand	Cofactor	Receptor specificity
FGF1 subfamily	FGF1 FGF2	Heparin or Heparan sulphate	Binds to all FGFRs with high affinity
FGF4 subfamily	FGF4 FGF5 FGF6		FGFR 1c, 2c >3c, 4Δ
FGF7 Subfamily	FGF3 FGF7 FGF10 FGF22		FGFR 2b >1b
FGF8 subfamily	FGF8 FGF17 FGF18		FGFR 3c >4Δ >2c >1c >>3b
FGF9 subfamily	FGF9 FGF16 FGF20		FGFR 3c >2c >1c, 3b >>4Δ
FGF11 Subfamily (intracellular)	FGF11 FGF12 FGF13 FGF14	- (intracellular FGFs)	- (intracellular FGFs)
FGF15/19 Subfamily (endocrine)	FGF15/19 FGF21 FGF23	Klotho proteins	FGFR 1c, 2c, 3c, 4Δ FGFR 1c, 2c FGFR 1c, 2c, 4

1.2.11 FGF7 subfamily

The FGF7 subfamily comprises FGF3, FGF7, FGF10 and FGF22 (Ornitz *et al.* 2015; Powers *et al.* 2000). Even though FGFs that are members of this family activate signalling through the same receptors, there are makeable differences in their expression profiles and downstream signalling cascade. FGF3 is mainly expressed in the neuronal tissue, while FGF22 is expressed in neuronal tissue and skin (Uhlén *et al.* 2015). Haploinsufficiency of FGF3 or missense mutations in the gene region led to abnormalities in the inner ear. FGF22 plays a role in the nervous system by supporting the formation of synapses – synaptogenesis (Ornitz *et al.* 2015).

FGF 7 and FGF10, also known as keratinocyte growth factor (KGF) 1 and 2, respectively, are mainly expressed in mesenchymal cells (Ye *et al.* 2005; Wu *et al.* 2018). FGF7 and FGF10 have been shown to play an important role in wound healing and in lung development and homeostasis (Ornitz *et al.* 2015; Yin and Ornitz. 2020; Yuan *et al.* 2019; Gupte *et al.* 2009; Ahmadvand *et al.* 2021; Volckaert *et al.* 2011; Volckaert *et al.* 2017; Moiseenko *et al.* 2020). Initially, FGF10 (KGF2) was identified in the skin shortly after the discovery of FGF7 (KGF1). Both FGF10 and FGF7 have a high affinity to bind receptors FGFR2b (epithelium) and FGFR1b (mesenchyme) (Shimbori *et al.* 2020; Ornitz *et al.* 2015) and redundantly contribute to the wound healing process in the skin (El Agha *et al.* 2016). Interestingly, FGF10 signalling is critical for lung development in mice, whereas FGF7 is dispensable (MacKenzie *et al.* 2015; Bellusci *et al.* 1997; Ohuchi *et al.* 2000; Izvolsky *et al.* 2003). Loss of *Fgf10* leads to lung agenesis, whereas loss of *Fgf7* during development does not cause any lung phenotype in mice (MacKenzie *et al.* 2015; Bellusci *et al.* 1997; Ohuchi *et al.* 2000; Izvolsky *et al.* 2003). FGF7 and FGF10 could trigger different signalling cascades downstream of the Fgfr2b receptor (MacKenzie *et al.* 2015; Francavilla *et al.* 2013). In an *in vitro* model, FGF7 was a potent inducer of cell proliferation, whereas FGF10 specifically promoted cell migration. It has been proposed that FGF10 stimulation enables the recycling of the FGFR2b at the cell membrane, whereas FGF7 results in transient signalling (Francavilla *et al.* 2013; MacKenzie *et al.* 2015). Furthermore, FGF7, but not FGF10, promoted sustained Erk phosphorylation. The different dynamics of Erk phosphorylation could result in the opposite cellular response induced by FGF7 compared to FGF10 (Francavilla *et al.* 2013; MacKenzie *et al.* 2015). As FGF10 is essential for lung development and repair, in the current study, I focused on investigating the role of FGF10 in COPD.

1.2.12 FGF10 in development, homeostasis and disease

In humans, the *FGF10* gene is located on chromosome 5 (Emoto *et al.* 1997). FGF10 protein is a 215 amino acids-long polypeptide expressed mainly in mesenchymal cells (Wu *et al.* 2018; Watson *et al.* 2018). FGF10 acts as an autocrine or paracrine growth factor (Watson *et al.* 2018; Ornitz *et al.* 2015). Like the other canonical FGFs, FGF10, when secreted, is tightly bound to

the heparin/heparan sulfate (Ornitz 2000; Ornitz *et al.* 2015; Rapraeger *et al.* 1991; Matsuo *et al.* 2013). On the one hand, such interactions increase protein stability and promote binding to the receptors (Buchtova *et al.* 2015). On the other hand, this interaction with the extracellular matrix (ECM) limits the diffusion of the FGFs (Ornitz 2000; Ornitz *et al.* 2015; Rapraeger *et al.* 1991; Matsuo *et al.* 2013; Buchtova *et al.* 2015).

During lung development, FGF10 is crucial for branching morphogenesis (Bellusci *et al.* 1997; Prince 2018). *Fgf10* knock-out (*Fgf10*^{-/-}) mice die at birth due to undeveloped lungs (Chao *et al.* 2017), while mice with *Fgf10* haploinsufficiency (*Fgf10*^{+/-}) are born with the broncho-pulmonary dysplasia-like phenotype (Chao *et al.* 2017). FGF10 is crucial not only during development but also in adult tissue homeostasis (El Agha *et al.* 2016; Shimbori *et al.* 2020; Prince 2018). Postnatally, FGF10/FGFR2b signalling regulates various aspects of stem/progenitor cell homeostasis. Activation of this signalling cascade in the lung promotes wound healing and prevents oxidant- and stretch-induced DNA damage in alveolar epithelial cells (Yuan *et al.* 2019; Gupte *et al.* 2009; Ahmadvand *et al.* 2021; Volckaert *et al.* 2011; Volckaert *et al.* 2017; Moiseenko *et al.* 2020). FGF10 overexpression, during the inflammatory or fibrotic phase of bleomycin-induced lung injury, significantly reduced the extent of pulmonary fibrosis (Gupte *et al.* 2009; Yuan *et al.* 2019). Furthermore, in the lungs of PH patients, FGF10 immuno-reactivity (staining score) was increased compared to the donors. However, the staining score negatively correlated with the disease severity assessed by mPAP (El Agha *et al.* 2018).

Of interest, *FGF10* haploinsufficiency in humans has been linked with impaired lung function, and single nuclear polymorphisms in the region of the *FGF10* locus were identified in COPD patients (Jackson *et al.* 2018; Smith *et al.* 2018; Klar *et al.* 2011). The rs1448044 SNP near the *FGF10* gene has been linked with reduced pulmonary function (Jackson *et al.* 2018; Prince 2018). Furthermore, single nuclear polymorphisms in the region of the *FGF10* locus were associated with airway branching variations in COPD patients (Jackson *et al.* 2018; Smith *et al.* 2018). However, the exact role of FGF10 in COPD remains unknown.

1.2.13 Aims of this work

Despite the intensive research in the field of chronic obstructive pulmonary disease (COPD), mechanisms of the disease development and progression remain poorly understood. Hence, COPD is still an incurable disease with limited treatment options.

As already mentioned, Seimetz *et al.* previously identified inducible nitric oxide synthase (iNOS) as an important player in COPD pathology (Seimetz *et al.* 2011). Briefly, they reported that selective iNOS inhibition with L-N6-(1-Iminoethyl) lysine (L-NIL) treatment successfully reversed cigarette smoke (CS)-induced emphysema and pulmonary hypertension (PH) in mice (Seimetz *et al.* 2011). Interestingly, in lungs from L-NIL-treated animals, *fibroblast growth factor 10 (Fgf10)* mRNA expression positively correlated with the septal wall repair and reverse remodelling of the pulmonary vasculature. FGF10 is an indispensable growth factor in lung development. Moreover, FGF10 has been shown to control the survival and proliferation of endogenous distal alveolar epithelial progenitor cells during lung development. Also, polymorphisms in the human *FGF10* gene correlate with an increased susceptibility to develop COPD.

Following this line, I hypothesised that impaired FGF10 signalling is involved in the pathogenesis of CS-induced emphysema and PH and that restoring such a signalling pathway could reverse the disease.

To test this hypothesis, the following aspects were closely investigated:

1. FGF10 signalling was examined in the relevant lung structures, such as the pulmonary vasculature and alveolar septa in human lungs from healthy donors and smokers without and with COPD and in mouse lungs after room air (RA) or CS exposure.
2. FGF10 expression was analysed in the primary culture of interstitial fibroblasts isolated from lungs explanted from healthy donors or COPD patients. Furthermore, I explored the connection between peroxynitrite stress and FGF10 expression in interstitial lung fibroblasts.

-
3. The contribution of FGF10 signalling in the pathogenesis of CS-induced emphysema and PH was investigated in a mouse model of chronic CS exposure. Hence, FGF10 or FGFR2b haploinsufficient mice and corresponding wild-type (Wt) littermates were exposed to CS for 3 or 8 months, as depicted in **Figure 8A**.
 4. I employed mice with inducible FGF10 overexpression to study the possible therapeutic effects of FGF10. These transgenic mice were exposed to CS for 8 months. Afterwards, CS exposure was discontinued, and animals were fed with a doxycycline-containing chow to induce FGF10 overexpression. Treatment lasted 1, 5 or 12 weeks, as depicted in **Figure 8B**.
 5. The therapeutic effect of FGF10 overexpression was further examined in a mouse model of end-stage elastase-induced pulmonary emphysema and PH.
 6. Using microarray technology, I investigated gene expression profiles in laser-assisted microdissected alveolar septa and pulmonary vessels of the experimental animals. I analysed the signalling pathways in *Fgf10* haploinsufficient mice and in CS-exposed Wt mice, compared to the RA-exposed Wt control animals. Furthermore, I explored signalling pathways underlying FGF10-mediated reversion of CS-induced emphysema and PH.

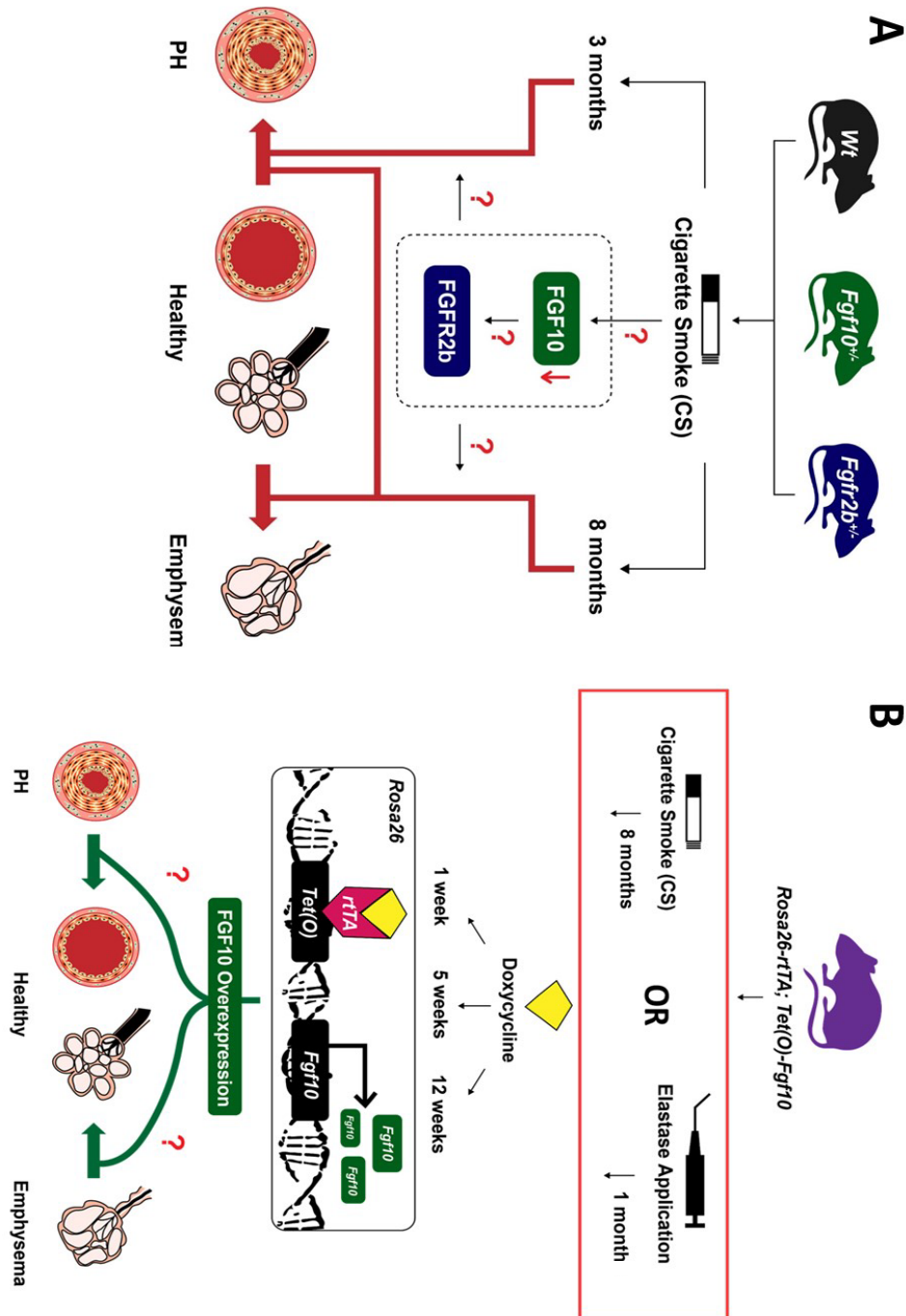


Figure 8. Schematic drawing of the experimental design and hypothesis. (A) To elucidate the contribution of impaired FGF10 signalling in cigarette smoke (CS)-induced emphysema and pulmonary hypertension (PH), *Fgf10*^{+/-} and *Fgfr2b*^{+/-} mice, together with wild-type (Wt) littermate controls, were exposed to CS or room air (RA) for 3 or 8 months. **(B)** Mice with inducible FGF10 expression were used to elucidate whether restoring FGF10 signalling can reverse CS- or elastase-induced emphysema and PH. After the lung injury, FGF10 overexpression was induced in these transgenic animals by feeding mice with doxycycline-containing chow. Animals were sacrificed after 1, 5 or 12 weeks of treatment. Animals fed with regular food were used as controls.

2 Material and methods

2.1 Material

2.1.1 Equipment

Equipment	Company
Automated microtome (Leica RM 2165)	<i>Leica Microsystems GmbH, Wetzlar, Germany</i>
Balance for substances (Mettler Toledo PB303 Delta Range®)	<i>Mettler Toledo GmbH, Greifensee, Switzerland</i>
Cell incubator HERAcell 150	<i>Thermo Fisher Scientific Inc. Waltham, MA, USA</i>
Centrifuge Mikro 200R	<i>Andreas Hettich GmbH & Co. KG, Tuttlingen, Germany</i>
ChemiDoc™ Touch Imaging System	<i>Bio-Rad Laboratories GmbH, Hercules, CA, USA</i>
ChemiDoc™ XRS+	<i>Bio-Rad Laboratories GmbH, Hercules, CA, USA</i>
Cigarette smoke exposure chambers	<i>Burghart GmbH, Wedel, Germany</i>
Cigarette smoke generator	<i>Burghart GmbH, Wedel, Germany</i>
Computer tomography	<i>PerkinElmer Inc., Waltham, MA, USA</i>
Confocal microscope SP8	<i>Leica Microsystems GmbH, Wetzlar, Germany</i>
Cooling Plate EG 1150C	<i>Leica Microsystems GmbH, Wetzlar, Germany</i>
Culture Hood	<i>Heraeus GmbH, Hanau, Germany</i>
Flattening bath for paraffin sections (Leica HI 1210)	<i>Leica Microsystems GmbH, Wetzlar, Germany</i>

FlexiVent mechanical ventilator equipped with FX2 module and data-acquisition system	<i>SCIREQ Scientific Respiratory Equipment Inc., Montreal, Canada</i>
Fluorescence molecular tomography (FMT) imaging system	<i>VisEn Medical, Bedford, USA</i>
Heating Block	<i>VWR, Bruchsal, Germany</i>
Heating chamber	<i>Memmert, Schwabach, Germany</i>
Heating Plate Hi 1220	<i>Leica Microsystems GmbH, Wetzlar, Germany</i>
High-pressure syringe (Model FMJ-250)	<i>Penn-Century Inc., Wyndmoor, PA, USA</i>
Hotplate/Stirrer (371)	<i>VWR International GmbH, Bruchsal, Germany</i>
Ice flake machine (Icematic F100 Compact)	<i>Castelmac SPA, Castelfranco, Italy</i>
IncuCyte ZOOM	<i>Essen BioScience Ltd., Ann Arbor, MI, USA</i>
InnoScan is900	<i>Innopsys Inc., Chicago, IL, USA</i>
Ismatec® roller-pump	<i>Cole-Parmer GmbH, Wertheim Germany</i>
Laser microdissection system (LMD6000)	<i>Leica Microsystems GmbH, Wetzlar, Germany</i>
Light microscope (DMLA)	<i>Leica Microsystems GmbH, Wetzlar, Germany</i>
Low Voltage Power Supplies Power pack P25T	<i>Biometra GmbH, Jena, Germany</i>
Microplate reader Infinite M200	<i>Tecan Trading AG, Männedorf, Switzerland</i>
MicroSprayer® Aerosolizer (Model IA-1C)	<i>Penn-Century Inc., Wyndmoor, PA, USA</i>
Mini-PROTEAN® electrophoresis cells	<i>Bio-Rad Laboratories GmbH, Hercules, CA, USA</i>
MiniVent type 845 Hugo Sachs	<i>Hugo Sachs Elektronik, a division of Harvard Bioscience Inc., March-Hugstetten, Germany</i>

Multimode microplate reader Infinite 200 PRO	<i>Tecan Trading AG, Männedorf, Switzerland</i>
Multimode microplate reader Spark®	<i>Tecan Trading AG, Männedorf, Switzerland</i>
NanoDrop (ND-1000)	<i>Kisker-Biotech, Steinfurt, Germany</i>
Paraffin cooling station Leica EG 1150C	<i>Leica Microsystems GmbH, Wetzlar, Germany</i>
Paraffin embedding station Leica EG 1140H	<i>Leica Microsystems GmbH, Wetzlar, Germany</i>
PCR Plate sealer PX1	<i>Bio-Rad Laboratories GmbH, Hercules, CA, USA</i>
pH meter-766 Calimatic	<i>Knick Elektronische Messgeraete GmbH & Co. KG, Berlin, Germany</i>
PowerLab system	<i>AD Instruments GmbH, Spechbach, Germany</i>
Precellys® 24 bead beating Tissue Homogenizer	<i>Thermo Fisher Scientific Inc. Waltham, MA, USA</i>
QIAxcel Advanced System	<i>Qiagen GmbH, Hilden, Germany</i>
Quantum GX µCT scanner	<i>PerkinElmer Inc., Waltham, MA, USA</i>
Real-Time polymerase chain reaction (PCR) Detection System (CFX Connect™)	<i>Bio-Rad Laboratories GmbH, Hercules, CA, USA</i>
Rectal thermometer	<i>Indus Instruments, Houston, TX, USA</i>
Roller mixer LLG-uniROLLER 10	<i>Lab Logistics Group GmbH, Meckenheim, Germany</i>
Rotary microtome cryostat (CM1520)	<i>Leica Microsystems GmbH, Wetzlar, Germany</i>
Shaking table Swip	<i>Edmund Bühler GmbH, Bodelshausen, Germany</i>

SPR-671 Mikro-Tip® mouse pressure catheter, REF 8406719	<i>Millar Instruments Inc., Houston, TX, USA</i>
Table Centrifuge Mikro 200R	<i>Andreas Hettich GmbH & Co. KG, Tuttlingen, Germany</i>
Thermocycler, T3000	<i>Biometra GmbH, Jena, Germany</i>
Thermoregulation plate TCAT-2LV controller	<i>Physitemp Instruments Inc., Clifton, NJ, USA</i>
Trans-Blot® SD Semi-dry Cell	<i>Bio-Rad Laboratories GmbH, Hercules, CA, USA</i>
Trans-Blot® Turbo Semi-dry Cell	<i>Bio-Rad Laboratories GmbH, Hercules, CA, USA</i>
Ultrapure Milli-Q®	<i>Merck KGaA, Darmstadt, Germany</i>
Vevo® 2100 high-resolution Imaging System	<i>FUJIFILM VisualSonics Inc., Toronto, Canada</i>
Vibratome (Microm HM650V)	<i>Thermo Fisher Scientific Inc. Waltham, MA, USA</i>
Vortexer MS1 Minishaker	<i>IKA GmbH, Staufen, Germany</i>
Water bath	<i>Memmert GmbH + Co.KG, Schwabach, Germany</i>

2.1.2 Chemicals and consumables

Chemicals and consumables	Company
Acetone (32201)	<i>Merck KGaA, Darmstadt, Germany</i>
Adenosine (A9251)	<i>Merck KGaA, Darmstadt, Germany</i>
Agarose (11406)	<i>SERVA Electrophoresis GmbH, Heidelberg, Germany</i>

Agarose, low-gelling temperature (6351)	<i>Carl Roth GmbH + Co. KG, Karlsruhe, Germany</i>
AlamarBlue cell viability reagent (A50101)	<i>Thermo Fisher Scientific Inc. Waltham, MA, USA</i>
Alkaline Phosphatase (AP) Polymer System (POLAP-100)	<i>Zytomed Systems GmbH, Berlin, Germany</i>
Amersham ECL Plus Western Blotting Detections System (29018903)	<i>GE Healthcare, Munich, Germany</i>
Ammonium persulfate (APS, A3678)	<i>Promega GmbH, Madison, WI, USA</i>
Ampuwa® water (3478.1)	<i>Carl Roth GmbH + Co. KG, Karlsruhe, Germany</i>
Annexin Vivo 750 (NEV11053)	<i>PerkinElmer Inc., Waltham, MA, USA</i>
Antibody Diluent (ZUC025-100)	<i>Zytomed Systems GmbH, Berlin, Germany</i>
Apoptosis kinetic assay (ab129817)	<i>Abcam plc., Cambridge, UK</i>
Automatic pipettes (100-1000 µl, 10-100 µl, 1-10 µl)	<i>Eppendorf AG, Hamburg, Germany</i>
Background punisher (BP974)	<i>Biocare Medical LLC, Pacheco, CA, USA</i>
Bovine serum albumin (BSA, A7030)	<i>Merck KGaA, Darmstadt, Germany</i>
Bradford assay (5000114)	<i>Bio-Rad Laboratories GmbH, Hercules, CA, USA</i>
Cannulas (16G, 18G)	<i>BD Microlance, Franklin Lakes, NJ, USA</i>
CAT Hematoxylin (CATHE-M)	<i>Biocare Medical LLC, Pacheco, CA, USA</i>
Cell culture dishes (35er, 60er)	<i>Sarstedt AG & Co. KG, Nümbrecht, Germany</i>
Cell culture plates (6, 12, 24, 96 well)	<i>Greiner Bio-One GmbH, Frickenhausen, Germany</i>

Cell lysis buffer (9803S)	<i>Cell Signaling Technology Inc., Danvers, MA, USA</i>
Cell proliferation ELISA kit, Bromodeoxyuridine (BrdU, colorimetric, 11 647 229 001)	<i>Roche Diagnostics GmbH, Mannheim, Germany</i>
Cell scrapers	<i>Greiner Bio-One GmbH, Frickenhausen, Germany</i>
Cell strainers (40 µl, 100 µm)	<i>Greiner Bio-One GmbH, Frickenhausen, Germany</i>
Cellulose swabs Pur-Zellin®	<i>Paul Hartmann AG, Heidenheim, Germany</i>
Cigarettes 3R4F	<i>Kentucky Tobacco Research & Development Center, Lexington, KY, USA</i>
Combtips advanced (5 ml, 10 ml, 25 ml)	<i>Eppendorf AG, Hamburg, Germany</i>
Comp-Beads	<i>BD Biosciences, San Jose, CA, USA</i>
Conical centrifuge tubes (15 ml, 50 ml)	<i>Greiner Bio-One GmbH, Frickenhausen, Germany</i>
Coverslips 24x36 mm	<i>Menzel GmbH&Co.KG, Braunschweig, Germany</i>
Cryo Tubes	<i>Sarstedt AG & Co. KG, Nümbrecht, Germany</i>
DAPI (4',6-Diamidino-2-phenyl-indol – dihydrochloride; D9542)	<i>Merck KGaA, Darmstadt, Germany</i>
Dimethylsulfoxide (DMSO, D4540)	<i>Merck KGaA, Darmstadt, Germany</i>
Disodiumhydrogenphosphate dihydrate (Na ₂ HPO ₄ ,106580)	<i>Merck KGaA, Darmstadt, Germany</i>
Distilled Water (3478.1)	<i>Carl Roth GmbH + Co. KG, Karlsruhe, Germany</i>

Distilled Water (dH ₂ O, DNase-/RNase-free, 10977023)	<i>Invitrogen™, Thermo Fisher Scientific Inc. Waltham, MA, USA</i>
DIVA Decloaker (DV2004MX)	<i>Biocare Medical LLC, Pacheco, CA, USA</i>
DMEM-F12 (11320-033)	<i>GIBCO™, Thermo Fisher Scientific Inc. Waltham, MA, USA</i>
DNase (04536282001)	<i>Roche Diagnostics GmbH, Mannheim, Germany</i>
Doxycycline hyclate (D9891)	<i>Merck KGaA, Darmstadt, Germany</i>
Dulbecco's Modified Eagle Medium (DMEM, 31885023)	<i>GIBCO™, Thermo Fisher Scientific Inc. Waltham, MA, USA</i>
Elastase from porcine pancreas (E7885)	<i>Merck KGaA, Darmstadt, Germany</i>
Electronic animal identification reusable implanter needles (mini)	<i>Planet-ID GmbH, Essen, Germany</i>
Embedding cassettes	<i>Leica Microsystems GmbH, Wetzlar, Germany</i>
Eosin Y, alcoholic (6766007)	<i>Thermo Fisher Scientific Inc. Waltham, MA, USA</i>
Ethanol (pure) for molecular biology (108543)	<i>Merck KGaA, Darmstadt, Germany</i>
Ethanol 100% (27694)	<i>Otto Fischar GmbH, Saarbrücken, Germany</i>
Ethanol 70% (ETO-5000-70-1)	<i>SAV Liquid Production GmbH, Flintsbach a. Inn, Germany</i>
Ethanol 96% (27695)	<i>Otto Fischar GmbH, Saarbrücken, Germany</i>
Ethylenediaminetetraacetic acid (EDTA, 8043)	<i>Carl Roth GmbH + Co. KG, Karlsruhe, Germany</i>
Fetal bovine serum (FBS, F0804)	<i>Merck KGaA, Darmstadt, Germany</i>

FGF10, recombinant human (345-FG)	<i>R&D Systems Inc., Minneapolis, MN, USA</i>
FGF10, recombinant mouse (6224-FG)	<i>R&D Systems Inc., Minneapolis, MN, USA</i>
Fibronectin (F1141)	<i>Merck KGaA, Darmstadt, Germany</i>
Filtered tips (10 µl, 100 µl, 1000 µl)	<i>Nerbe plus GmbH & Co. KG, Winsen, Germany</i>
Filtopur S 0.2 µm (83.1826.001)	<i>Sarstedt AG & Co. KG, Nümbrecht, Germany</i>
Fluoro Care Anti-Fade Mountant (FP 001 G10)	<i>Biocare Medical LLC, Pacheco, CA, USA</i>
Formaldehyde (3,5 – 3,7 %, stabilized with methanol, 27244)	<i>Otto Fischar GmbH, Saarbrücken, Germany</i>
GeneRuler™ 100 bp DNA Ladder (SM0313)	<i>Thermo Fisher Scientific Inc. Waltham, MA, USA</i>
Glass bottles, beakers, cylinders	<i>DURAN Group Holding GmbH, Wertheim, Germany</i>
Glass bottles, beakers, cylinders	<i>VWR International LLC, Bruchsal, Germany</i>
Glass bottles, beakers, cylinders	<i>Fisher Scientific GmbH, Schwerte, Germany</i>
Glass slides with polyethylene naphthalate membrane (11505158)	<i>Leica Microsystems GmbH, Wetzlar, Germany</i>
Gloves (Nitra-Tex®)	<i>Ansell Ltd., Tamworth, UK</i>
Glycine (A1067)	<i>AppliChem GmbH, Darmstadt, Germany</i>
Hand towels	<i>Essity Hygiene and Health, Stockholm, Sweden</i>
Hank's Balanced Salt Solution (HBSS, 14025050)	<i>GIBCO™, Thermo Fisher Scientific Inc. Waltham, MA, USA</i>
Heparin (Heparin-Natrium 5000 I.U.)	<i>Ratiopharm GmbH, Ulm, Germany</i>

Histological glass slides 25x75x1 mm (SuperFrost UltraPlus®)	<i>R. Langenbrinck GmbH, Emmendingen, Germany</i>
Human serum (Seraclot; P40-3011)	<i>PAN-Biotech GmbH, Aidenbach, Germany</i>
Hydrochloride (HCl, 37%, 4625.1)	<i>Carl Roth GmbH + Co. KG, Karlsruhe, Germany</i>
Hydrogen-peroxide (30%, 107209)	<i>Merck KGaA, Darmstadt, Germany</i>
iScript complementary DNA (cDNA) Synthesis Kit (1708890)	<i>Bio-Rad Laboratories GmbH, Hercules, CA, USA</i>
Isoflurane (HDG9623)	<i>Baxter Deutschland GmbH, Unterschleissheim, Germany</i>
Isopropyl-alcohol (99.8%, 190764)	<i>Merck KGaA, Darmstadt, Germany</i>
iTaq Universal SYBR® Green Supermix (1725124)	<i>Bio-Rad Laboratories GmbH, Hercules, CA, USA</i>
Ketamine (Ursotamin®)	<i>Serumwerk Bernburg AG, Bernburg, Germany</i>
Laemmli protein sample buffer (4x) for SDS-PAGE (4x, 1610747)	<i>Bio-Rad Laboratories GmbH, Hercules, CA, USA</i>
L-Glutamine (P04-80100)	<i>GIBCO™, Thermo Fisher Scientific Inc., Waltham, MA, USA</i>
lumox® multiwell, 96-well	<i>Sarstedt AG & Co. KG, Nümbrecht, Germany</i>
Medical adhesive bands	<i>3M Health Care, St.Paul, MN, USA</i>
Medium 199 (M199, 31150022)	<i>GIBCO™, Thermo Fisher Scientific Inc. Waltham, MA, USA</i>
Methanol (99.8%, 32213)	<i>Merck KGaA, Darmstadt, Germany</i>
Micro tubes (0.5 ml, 1.5 ml, 2.0 ml)	<i>Sarstedt AG & Co. KG, Nümbrecht, Germany</i>

Microfil® (MV122 Yellow)	<i>Flow Tech Inc., Carver, MA, USA</i>
Microtome blades (MX35 Premier)	<i>Thermo Fisher Scientific Inc. Waltham, MA, USA</i>
MMPsense 750 FAST (NEV10168)	<i>PerkinElmer Inc., Waltham, MA, USA</i>
Mounting medium (Pertex®, 41-4012-00)	<i>Medite GmbH, Burgdorf, Germany</i>
Multipette E3x	<i>Eppendorf AG, Hamburg, Germany</i>
Multiplate™ PCR Plate 96-Well, clear	<i>Bio-Rad Laboratories GmbH, Hercules, CA, USA</i>
N6-(1-Iminoethyl)-L-lysine (L-NIL, 80310)	<i>Cayman Chemical Co., Ann Arbor, MI, USA</i>
Needles (BD Microlance 3®) (18 G /1.2 mm x 40 mm, 20 G /0.9 mm x 40 mm, 26G /0.45 mm x 13 mm)	<i>Becton Dickinson GmbH, Heidelberg, Germany</i>
Neubauer counting chamber	<i>Paul Marienfeld GmbH & Co. KG, Lauda-Königshofen, Germany</i>
Nile red (N3013)	<i>Merck KGaA, Darmstadt, Germany</i>
Nitrotyrosine ELISA kit (17-376)	<i>Merck KGaA, Darmstadt, Germany</i>
Non-treated culture Petri dishes	<i>Sarstedt AG & Co. KG, Nümbrecht, Germany</i>
Normocin (ant-nr-1)	<i>InvivoGen, Toulouse, France</i>
Nuclear Fast Red (Kernechtrot Aluminiumsulfat, 2E-012)	<i>Waldeck GmbH & Co.KG, Münster, Germany</i>
Oligonucleotide spotted microarray slides 8 × 60 K 60-mer (Design ID 028005)	<i>Agilent Technologies Inc., Santa Clara, CA, USA</i>
Ovation PicoSL WTA System V2 kit (3312-24)	<i>NuGEN Technologies Inc., San Carlos, CA, USA</i>
Parafilm®	<i>Merck KGaA, Darmstadt, Germany</i>

Paraformaldehyde (PFA, sc-281692)	<i>Santa Cruz Biotechnology Inc., Dallas, TX, USA</i>
Paraplast Plus® for tissue embedding (P3683)	<i>Merck KGaA, Darmstadt, Germany</i>
Paveron N (A03AD01)	<i>Linden Arzneimittel GmbH, Heuchelheim, Germany</i>
Penicillin/Streptomycin (15070-063)	<i>GIBCO™, Thermo Fisher Scientific Inc., Waltham, MA, USA</i>
Phenylmethansulfonylfluorid (PMSF, P7626)	<i>Merck KGaA, Darmstadt, Germany</i>
Phenylmethylsulfonyl Fluoride (PVDF)-membrane	<i>Pall Deutschland Holding GmbH & Co. KG, Dreieich, Germany</i>
Phosphate-buffered saline (D-PBS, P04-53500)	<i>PAN-Biotech GmbH, Aidenbach, Germany</i>
Picrosirius red staining kit (ab150681)	<i>Abcam, Cambridge, United Kingdom</i>
Polystyrene round-bottom tubes with cell strainer cap (5 ml)	<i>Greiner Bio-One GmbH, Frickenhausen, Germany</i>
Potassium chloride (KCl, 6781.1)	<i>Merck KGaA, Darmstadt, Germany</i>
Potassiumdihydrogenphosphate (KH ₂ PO ₄ , 104873)	<i>Merck KGaA, Darmstadt, Germany</i>
Povidone-iodine solution (Braunoderm®)	<i>B.Braun Melsungen AG, Melsungen, Germany</i>
Precision Plus Protein Dual Color Standards (1610374)	<i>Bio-Rad Laboratories GmbH, Hercules, CA, USA</i>
Primers (listed below)	<i>Metabion International AG, Planegg, Germany</i>
Protease-Inhibitor-Cocktail cOmplete™ Mini EDTA-free	<i>Roche Diagnostics GmbH, Mannheim, Germany</i>
Proteinase K Novocastra™ (RE7160-K)	<i>Leica Microsystems GmbH, Wetzlar, Germany</i>

Red blood cell (RBC) lysis buffer (BD Pharm Lyse™, 555899)	<i>BD Biosciences, Heidelberg, Germany</i>
Resorcin-Fuchsin (2E-030)	<i>Waldeck GmbH & Co.KG, Münster, Germany</i>
RNeasy Micro Kit (74004)	<i>Qiagen GmbH, Hilden, Germany</i>
RNeasy®Mini Kit (74106)	<i>Qiagen GmbH, Hilden, Germany</i>
Rodent Decloaker 10X (RD913)	<i>Biocare Medical LLC, Pacheco, CA, USA</i>
RPMI medium 1640 (P04-16500)	<i>PAN-Biotech GmbH, Aidenbach, Germany</i>
Saline solution (0,9% NaCl; 3570160)	<i>B.Braun Melsungen AG, Melsungen, Germany</i>
Serological pipette (5 ml, 10 ml, 25 ml, 50 ml)	<i>BD Falcon, Heidelberg, Germany</i>
Skimmed milk powder (T145.3)	<i>Carl Roth GmbH + Co. KG, Karlsruhe, Germany</i>
Smooth Muscle Cell Basal Medium 2 (C-22262)	<i>Promo Cell GmbH, Heidelberg, Germany</i>
Smooth Muscle Cell Growth Medium 2 (C-22062)	<i>Promo Cell GmbH, Heidelberg, Germany</i>
Smooth Muscle Supplement 2 mix (C-39267)	<i>Promo Cell GmbH, Heidelberg, Germany</i>
Sodium dodecyl sulfate (SDS, AM9820)	<i>Invitrogen, by Thermo Fisher Scientific Inc. Waltham, MA, USA</i>
SureTag DNA Labelling Kit (5190-3400)	<i>Agilent Technologies Inc. Santa Clara, CA, USA</i>
Surgical instruments	<i>Fine Science Tools GmbH, Heidelberg, Germany</i>
SYBR® Safe DNA gel stain (S33102)	<i>Invitrogen, by Thermo Fisher Scientific Inc. Waltham, MA, USA</i>

Syringes (Injekt®-F) (1 ml, 2 ml, 5 ml, 20 ml)	<i>Carl Roth GmbH + Co. KG, Karlsruhe, Germany</i>
Tetramethylethylenediamine (TEMED, 2367.3)	<i>Carl Roth GmbH + Co. KG, Karlsruhe, Germany</i>
TGX FastCast Kit (12% gels, 1610185)	<i>Bio-Rad Laboratories GmbH, Hercules, CA, USA</i>
Thread, black no.16	<i>Coats GmbH, Kenzingen, Germany</i>
Tips for automatic pipettes (200 µl, 1000 µl, 10 µl)	<i>Sarstedt AG & Co. KG, Nümbrecht, Germany</i>
Tissue-Tek® O.C.T.™	<i>Sakura Finetek Germany GmbH, Staufen im Breisgau, Germany</i>
TRIS (4855.2)	<i>Carl Roth GmbH + Co. KG, Karlsruhe, Germany</i>
Tris-buffered saline 20x (TBS, ZUC052-500)	<i>Zytomed Systems GmbH, Berlin, Germany</i>
TRIS-HCl (9090.2)	<i>Carl Roth GmbH + Co. KG, Karlsruhe, Germany</i>
TritonX-100 (X100)	<i>Merck KGaA, Darmstadt, Germany</i>
Trypsin/EDTA (10x, P10-024100)	<i>PAN-Biotech GmbH, Aidenbach, Germany</i>
Tween® 20 (P1379)	<i>Merck KGaA, Darmstadt, Germany</i>
Warp Red Chromogen Kit (WR 806)	<i>Biocare Medical LLC, Pacheco, CA, USA</i>
Water, sterile (00088992)	<i>B.Braun Melsungen AG, Melsungen, Germany</i>
Whatman Gel Blotting Paper	<i>GE Healthcare, Marlborough, MA, USA</i>
Xylazine 20 mg/ml	<i>Serumwerk, Bernburg, Germany</i>
Xylol (9713.2)	<i>Carl Roth GmbH + Co. KG, Karlsruhe, Germany</i>

β -Mercaptoethanol (4227.3) *Carl Roth GmbH + Co. KG, Karlsruhe, Germany*

2.1.3 Software

Software	Company
Analyze Pro software	<i>Analyze Direct, Mayo Clinic, Rochester MI, USA</i>
Adobe Illustrator	<i>Adobe Inc., San José, CA, USA</i>
AutoQuant X2 software	<i>Bitplane AG, Zurich, Switzerland</i>
CFX Manager™ Software	<i>Bio-Rad Laboratories GmbH, Hercules, CA, USA</i>
FlexiVent software	<i>SCIREQ Scientific Respiratory Equipment Inc., Montreal, Canada</i>
GraphPad Prism Version 8	<i>GraphPad Software, Inc., La Jolla, CA, USA</i>
Image Lab Version 4.1	<i>Bio-Rad Laboratories GmbH, Hercules, CA, USA</i>
LabChart 7	<i>AD Instruments GmbH, Spechbach, Germany</i>
Mapix 6.5.0 software	<i>Innopsys Inc., Chicago, IL, USA</i>
Tecan i-control™ Microplate Reader Software	<i>Tecan Trading AG, Männedorf, Switzerland</i>
Microsoft Office 2016	<i>Microsoft Corporation, Redmond, WA, USA</i>
PowerLab data acquisition system (MPVS-Ultra Single Segment Foundation System)	<i>AD Instruments GmbH, Spechbach, Germany</i>

Qwin software	<i>Leica Microsystems GmbH, Wetzlar, Germany</i>
R software	<i>The R Foundation, Iowa City, IA, USA</i>
Stereology software	<i>Visiopharm, Hørsholm, Denmark</i>
VisualSonics	<i>FUJIFILM VISUALSONICS INC., Toronto, Canada</i>

2.1.4 Experimental animals

Animal line	Breeding
C57BL/6NCrl	<i>Charles River Laboratories, Sulzfeld, Germany</i>
B6;Cg-Fgf10 ^{tm1.3Sbel} /Sbel	<i>Bred in house; obtained by crossing Fgf10^{tm1.2Sms}/J (Jackson lab reference 023729) with CMV-Cre mice</i>
B6;Cg-Fgfr2b ^{tm1.2Sbel} /Sbel	<i>Bred in house; obtained by crossing Fgfr2b^{flox/flox} from Clive Dickson with CMV-Cre mice</i>
B6-Gt(ROSA)26Sor ^{tm1.1(rtTA,EGFP)Nagy} Tg(TetO-Fgf10)1Jaw/Sbel	<i>Bred in house; (Jackson lab reference 025671)</i>
B6-Gt(ROSA)26Sor ^{tm1.1(rtTA,EGFP)Nagy}	<i>Bred in house; (Jackson lab reference 005572)</i>

2.1.5 Antibodies

Antibody	Host species	Ordering No. / RRID	Company	Verification / References
Anti-Akt antibody	Rabbit	9272 / AB_329827	<i>Cell Signaling Technology Inc., Danvers, MA, USA</i>	(Keen <i>et al.</i> 2022; Zhu, Shukla, <i>et al.</i> 2019; Caffa <i>et al.</i> 2020)
Anti-Bek/FGFR2 antibody	Rabbit	sc-6930 / AB_669015	<i>Santa Cruz Biotechnology Inc., Dallas, TX, USA</i>	(Kim <i>et al.</i> 2019; Seymour <i>et al.</i> 2012; Volckaert <i>et al.</i> 2017; Kolobaric <i>et al.</i> 2021)
Anti-beta-actin antibody	Mouse	ab8226 / AB_306371	<i>Abcam, Cambridge, UK</i>	(Chen <i>et al.</i> 2021; Morgan <i>et al.</i> 2013; Hadzic <i>et al.</i> 2021)
Anti-beta-catenin antibody	Rabbit	8480 / AB_11127855	<i>Cell Signaling Technology Inc., Danvers, MA, USA</i>	(Zou <i>et al.</i> 2021; El Zein <i>et al.</i> 2019; Hsu <i>et al.</i> 2018)
Anti-BrdU antibody (Bu20a)	Mouse	339808 / AB_10895898	<i>Biolegend Inc., San Diego, CA, USA</i>	(Grinstein <i>et al.</i> 2019; Sundaravinayagam <i>et al.</i> 2019; Jimenez <i>et al.</i> 2019)
Anti-CD16/CD32 antibody (Mouse BD Fc Block™)	Rat	553142/ AB_394656	<i>BD Biosciences, San Jose, CA, USA</i>	(Seimetz <i>et al.</i> 2020; Lee <i>et al.</i> 2014; Römer <i>et al.</i> 2015; Basrai <i>et al.</i> 2016)
Anti-CD31 antibody	Rat	550274/ AB_393571	<i>BD Biosciences, San Jose, CA, USA</i>	(Seimetz <i>et al.</i> 2020; Li, Li, <i>et al.</i> 2021; Koyanagi <i>et al.</i> 2021)

Anti-CD45 antibody	Rat	550539/ AB_396376	<i>BD Biosciences, San Jose, CA, USA</i>	(Seimetz <i>et al.</i> 2020; Hill <i>et al.</i> 2017; Ng <i>et al.</i> 2018; Sim <i>et al.</i> 2018)
Anti-FGF10 antibody (for human IHC)	Rabbit	ABIN360398/ AB_2715513	<i>Antibodies-online GmbH, Achen, Germany</i>	(El Agha, Moiseenko, <i>et al.</i> 2017; El Agha <i>et al.</i> 2018; Chao <i>et al.</i> 2019)
Anti-FGF10 antibody (for human WB)	Rabbit	ABN44 / AB_11204345	<i>Merck KGaA, Darmstadt, Germany</i>	(Fischer <i>et al.</i> 2017; Li, Zhu, <i>et al.</i> 2021a; Volckaert <i>et al.</i> 2017)
Anti-FGF10 antibody (for mouse WB and IHC)	Rabbit	AP14882PU- N / AB_1752406	<i>Acris Antibodies GmbH, Herford, Germany</i>	(Volckaert <i>et al.</i> 2017)
Anti-Mouse IgG, horseradish-peroxidase-labelled (secondary) antibody	Goat	W4011 / AB_430833	<i>Promega GmbH, Madison, WI, USA</i>	(Hesse <i>et al.</i> 2010; Massaad <i>et al.</i> 2009; Hu <i>et al.</i> 2012)
Anti-p-Akt antibody	Rabbit	9271 / AB_329825	<i>Cell Signaling Technology Inc., Danvers, MA, USA</i>	(Dummler <i>et al.</i> 2006; Castets <i>et al.</i> 2019; Luu <i>et al.</i> 2019)
Anti-Rabbit IgG, Alexa Fluor 488 labelled (secondary) antibody	Goat	A32731 / AB_2633280	<i>Thermo Fisher Scientific Inc., Waltham, MA, USA</i>	(Benderradji <i>et al.</i> 2022; Pretorius <i>et al.</i> 2022)
Anti-Rabbit IgG, horseradish-peroxidase-labelled (secondary) antibody	Goat	W4021 / AB_430834	<i>Promega GmbH, Madison, WI, USA</i>	(Hesse <i>et al.</i> 2010; Massaad <i>et al.</i> 2009; Hu <i>et al.</i> 2012)

Anti-Sp1 antibody	Rabbit	9389 / AB_11220235	<i>Cell Signaling Technology Inc., Danvers, MA, USA</i>	(Xu <i>et al.</i> 2016; Chen, Cai, <i>et al.</i> 2018; Hoesel <i>et al.</i> 2018)
Anti-von Willebrand factor (vWF) antibody	Rabbit	A0082 / AB_2315602	<i>Dako Deutschland GmbH, Hamburg, Germany</i>	(Ono <i>et al.</i> 2019; Thomson <i>et al.</i> 2017; Campreciós <i>et al.</i> 2021)

2.1.6 Primer sequences

Gene abbreviation	Sequence
Human <i>B2M</i>	Forward: 5' GCCGTGTGAACCATGTGACT 3' Reverse: 5' GCAAGCAAGCAGAATTTGGA 3'
Human <i>FGF1</i>	Forward: 5' GCCGGGCTACTCTGAGAAGAA 3' Reverse: 5' CTGCTTGTGCGCTTTCAAGA 3'
Human <i>FGF2</i>	Forward: 5' ACTGCAAAAACGGGGGCTTC 3' Reverse: 5' GGTAACGGTTAGCACACTCC 3'
Human <i>FGF7</i>	Forward: 5' CTGTGCAACACAGTGGTACCTGA 3' Reverse: 5' TTCCACCCCTTTGATTGCCAC 3'
Human <i>FGF9</i>	Forward: 5' TCAGGCGGAGGCAGCTATAC 3' Reverse: 5' CTGACCAGGCCCACTGCTAT 3'
Human <i>FGF10</i>	Forward: 5' AGAAGAACGGGAAGGTCAGCG 3' Reverse: 5' ATGGCTTTGACGGCAACAAC 3'
Human <i>FGFR1B</i>	Forward: 5' GCATTCGGGGATTAATAGCTC 3'

	Reverse: 5' CCACAGGTCTGGTGACAGTG 3'
Human <i>FGFR2B</i>	Forward: 5' GATAAATAGTTCCAATGCAGAAGTGCT 3'
	Reverse: 5' TGCCCTATATAATTGGAGACCTTACA 3'
Human <i>FGFR1C</i>	Forward: 5' ACCACCGACAAAGAGATGGA 3'
	Reverse: 5' GCAGAGTGATGGGAGAGTCC 3'
Human <i>FGFR2C</i>	Forward: 5' TTCTCTCCAGGCGCTGG 3'
	Reverse: 5' CTCTGCGTGGCTGGTGGTGC 3'
Human <i>FGFR3</i>	Forward: 5' CAAGTTTGGCAGCATCCGGCAGAC 3'
	Reverse: 5' CACCACCAGCCACGCAGAGTGATG 3'
Mouse <i>Fgf10</i>	Forward: 5' CGGGACCAAGAATGAAGACT 3'
	Reverse: 5' GCAACAACCTCCGATTTCCAC 3'
Mouse <i>B2m</i>	Forward: 5' AGCCCAAGACCGTCTACTGG 3'
	Reverse: 5' AGCCCAAGACCGTCTACTGG 3'
Mouse <i>Fgf10</i> (genotyping)	Forward: 5' GCAGAGATTGCAAAGGAAGC 3'
	Reverse: 5' GTCTTTTTGACTGAAACCTCAC 3'
Mouse <i>Fgfr2b</i> (genotyping)	Forward: 5' GACCAGTCCAACCTTCTCTGTTCCAC 3'
	Reverse: 5' CTCAACAGGCATGCAAATGCAAGGTC 3'
Mouse <i>rtTA</i> (genotyping)	Forward: 5' GAGTTCTCTGCTGCCTCCTG 3'
	Reverse: 5' GAGTTCTCTGCTGCCTCCTG 3'
Mouse <i>tetO-Fgf10</i> (genotyping)	Forward: 5' GACGCCATCCACGCTGTTTTGACC 3'
	Reverse: 5' ATTTGCCTGCCATTGTGCTGCCAG 3'

2.2 Methods

2.2.1 Human lung samples

Human lung tissue samples were obtained from the DZL Biobank, from individuals with COPD who had undergone lung transplantation or from healthy lung-transplantation donors. The human lung tissue was snap-frozen directly after explantation for mRNA and protein extraction or fixed with formalin and embedded in paraffin for histological analysis. For cell isolation and precision-cut lung slices, only fresh lung tissue was used. The pathologist examined all the lungs and determined the smoking status of the donors. The Ethics Committee of the Justus-Liebig-University School of Medicine approved all the studies involving human lung samples (AZ 58/15).

2.2.2 Animal studies and experimental design

A maximum of 5 mice were kept in a single cage placed in an individually ventilated cage (IVC) system. The cages were supplemented with bedding (wood shavings), nesting material and a house. Mice were housed under controlled conditions with 12 hours dark/light cycle with water and food supply *ad libitum*. The ambient air temperature was kept at 22 °C and humidity at 40-70%. Adult mice not younger than 12 weeks, weighing at least 20 g, were used for experiments. An approximately equal portion of male and female mice was randomly allocated to the experimental groups. All animal experiments were approved by the local governmental authorities (Regierungspräsidium Gießen) and performed in accordance with the German animal welfare law and the European legislation for the protection of animals used for scientific purposes (2010/63/EU). Ethical approvals for the animal experiments performed in the scope of my thesis are stated in **Table 4**.

Table 4. Ethical approvals for animal experiments approved by Regierungspräsidium Gießen.

Animal approval number	Experimental setup
115 / 2014	Organ harvest and cell isolation
70 / 2015	Cigarette smoke exposure and elastase application
G6 / 2018	Doxycycline controls

2.2.2.1 Therapeutic setup with inducible nitric oxide (iNOS) inhibition

L-NIL treatment experiments were performed earlier in the research group where I did my thesis. Briefly, adult Wt C57BL/6J mice were obtained from Charles River Laboratories, Sulzfeld, Germany and exposed to RA or CS for 8 months. The CS exposure was then discontinued, and animals were treated with either L-NIL (Biotium, Hayward, CA, USA; 2.68mM dissolved in drinking water) or a placebo for the following 3 months, as previously described (Seimetz *et al.* 2011). The drinking water for the placebo was adjusted to the same pH as the L-NIL solution. Each day, freshly prepared L-NIL and placebo solutions were supplied to the animals. I used the paraffin-embedded lung samples from these animals.

2.2.2.2 FGF10 loss-of-function setup

In order to evaluate the effect of impaired FGF10 signalling on emphysema and PH development, I used *Fgf10* or *Fgfr2b* heterozygous mice. Both animal lines were crossbred for at least 10 generations on B57BL/6J genetic background. Mice that lack one functional copy of the *Fgf10* gene (B6;Cg-*Fgf10*^{tm1.3Sbel}/Sbel; obtained by crossing *Fgf10*^{tm1.2Sms/J} (Jackson lab reference 023729) with CMV-Cre mice) are abbreviated *Fgf10*^{+/-} and mice that lack one functional copy of the receptor *Fgfr2b* gene (B6;Cg-*Fgfr2b*^{tm1.2Sbel}/Sbel; obtained by crossing *Fgfr2b*^{flox/flox} mice from Clive Dickson with CMV-Cre mice) are abbreviated *Fgfr2b*^{+/-}. Since the complete knock-out mice for each one of the genes die at birth due to undeveloped lungs (Sekine *et al.* 1999; Bellusci *et al.* 1997; Watson *et al.* 2018; Wu *et al.* 2018), for breeding always one parent was wild type (Wt) and the other heterozygous (either *Fgf10*^{+/-} or *Fgfr2b*^{+/-}). The

genotype of each mouse used in the experiment was determined via PCR reaction followed by agarose gel electrophoresis. All animals were bred in-house and genotyped by the working group of Prof. Dr. Saverio Bellusci at the Justus Liebig University, Department of Internal Medicine, Excellence Cluster Cardio-Pulmonary Institute, Giessen, Germany. After genotyping, animals were randomly allocated to the experimental groups, as shown in **Table 5**; each group contained 12 animals.

Table 5. Experimental groups for the loss-of-function experimental setup. Abbreviations - RA: Room air; CS: Cigarette smoke.

3-months time-point						8-months time-point					
Wt		<i>Fgf10</i> ^{+/-}		<i>Fgfr2b</i> ^{+/-}		Wt		<i>Fgf10</i> ^{+/-}		<i>Fgfr2b</i> ^{+/-}	
RA	CS	RA	CS	RA	CS	RA	CS	RA	CS	RA	CS

At the age of 12-16 weeks, Wt (littermates), *Fgf10*^{+/-} and *Fgfr2b*^{+/-} mice were exposed to cigarette smoke (CS) or room air (RA) for the following 3 or 8 months (**Figure 9**).

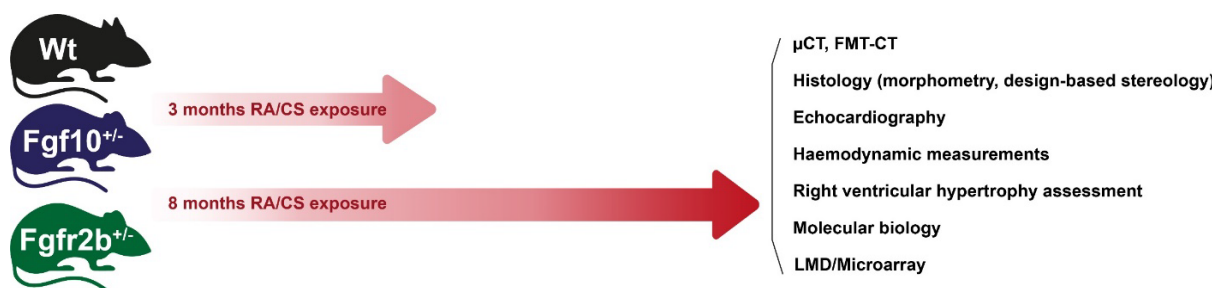


Figure 9. Experimental design for the loss-of-function setup. *Fgf10*^{+/-} and *Fgfr2b*^{+/-} animals, together with the Wt littermates, were exposed to room air (RA) or cigarette smoke (CS) for 3 or 8 months. Afterwards, emphysema and PH phenotypes were characterised. Abbreviations – μCT: Mico computed tomography; FMT-CT: Fluorescence molecular tomography – computed tomography; LMD: Laser-assisted microdissection.

2.2.2.3 Therapeutic approach with FGF10 overexpression

For the therapeutic approach, B6-Gt(*ROSA*)26Sor^{tm1.1(rtTA,EGFP)*Nagy*} Tg(*tetO-Fgf10*)1Jaw/SpdII (Jackson lab reference 025671) transgenic mice were used. Such mice express the reverse tetracycline transactivator (rtTA) under the global *ROSA26* (Reverse Oriented Splice Acceptor, Clone 26) promoter. Additionally, the *Tet(O)* operator sequence is inserted in the promoter region of the *Fgf10* gene. In the presence of doxycycline, rtTA binds to the *Tet(O)* operator sequence and initiates the gene transcription (Kistner *et al.* 1996).

Hereby, emphysema and PH in mice were induced either by 8 months of CS exposure or by a single intratracheal instillation of elastase solution. *Fgf10* was then globally overexpressed by feeding mice with doxycycline-containing chow. After established emphysema and PH, animals were fed *ad libitum* with chow containing doxycycline (600 mg/kg supplemented with 2% saccharose; Altromin Spezialfutter GmbH & Co, Lage, Germany) or regular chow (Altromin Spezialfutter GmbH & Co, Lage, Germany) for an 1, 5 or 12 weeks (**Figure 10, 11**). Animals were fed with doxycycline-containing food in a specific regimen, as previously described (Gupte *et al.* 2009; Redelsperger *et al.* 2016; Hadzic *et al.* 2021). I fed mice with doxycycline-containing chow for 7 days, followed by 7 days of regular chow feeding. This weekly scheme of doxycycline feeding I repeated during the entire treatment period. Such a feeding regime allowed the animals to ingest high dosages of doxycycline with minimizing common side effects of long-term antibiotic treatment.

2.2.2.3.1 FGF10 overexpression after cigarette smoke (CS)-induced emphysema and PH

In this experimental setup, animals were exposed to CS or RA for 8 months. The exposure was then interrupted, and animals were fed with a doxycycline-containing chow in RA conditions for additional 1, 5 or 12 weeks (**Figure 10**).

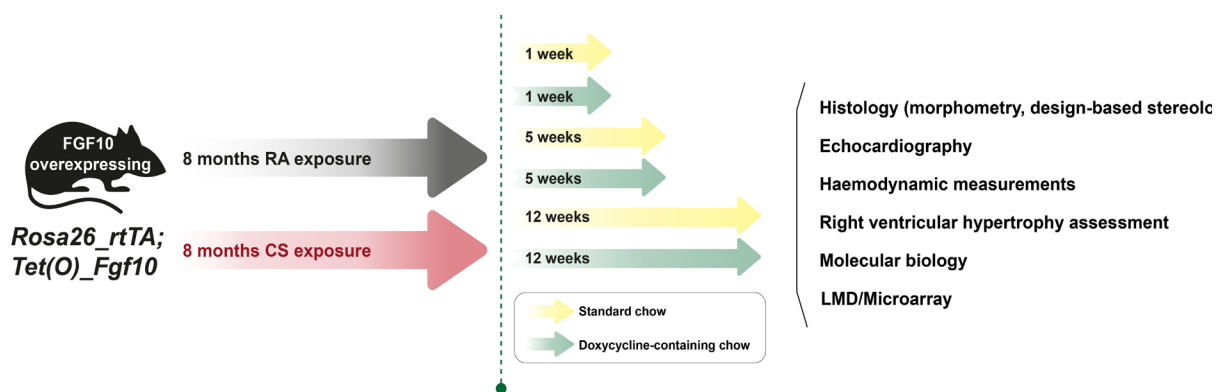


Figure 10. Experimental design for therapeutic approach after CS-induced emphysema and PH. FGF10 overexpression was induced by doxycycline treatment for 1, 5 or 12 weeks after 8 months of CS exposure. Afterwards, emphysema and PH phenotype were characterised. Abbreviations –LMD: Laser-assisted microdissection; RA: Room air; CS: Cigarette smoke.

Animals were randomly allocated to 4 groups, for each one of the 3 therapeutic time-points as shown (**Table 6**): room air-exposed control group (RA); room air exposure with doxycycline treatment (RA + DOXY); cigarette smoke-exposed control group (CS); cigarette smoke exposure with doxycycline treatment (CS + DOXY).

Table 6. Experimental groups for therapeutic approach after CS-induced emphysema and PH. Abbreviations - RA: Room air; CS: Cigarette smoke; DOXY: Doxycycline.

1 week treatment				5 weeks treatment				12 weeks treatment			
RA		CS		RA		CS		RA		CS	
-	DOXY	-	DOXY	-	DOXY	-	DOXY	-	DOXY	-	DOXY

2.2.2.3.2 FGF10 overexpression after elastase-induced pulmonary emphysema and PH

In the case of the elastase model, animals were allocated to groups similarly like in the CS exposure setup, as shown in **Table 7**. The experimental timeline is depicted in **Figure 11**. Based on my previous experience, treatment (feeding with doxycycline-containing chow) started 4 weeks after the elastase or saline instillation and was conducted in the same manner as described earlier.

Table 7. Experimental groups for therapeutic approach after elastase-induced emphysema and PH. Abbreviations - DOXY: Doxycycline.

1 week treatment				5 weeks treatment				12 weeks treatment			
Saline		Elastase		Saline		Elastase		Saline		Elastase	
-	DOXY	-	DOXY	-	DOXY	-	DOXY	-	DOXY	-	DOXY

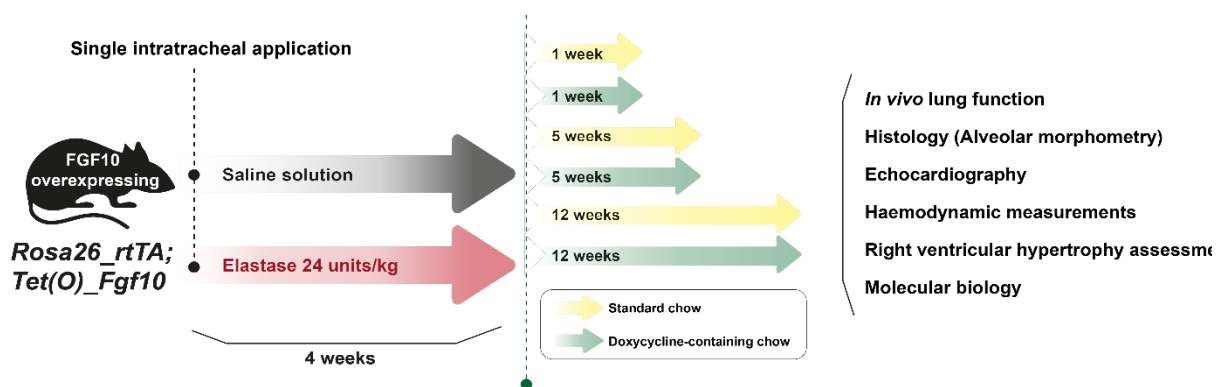


Figure 11. Experimental design for therapeutic approach after elastase-induced emphysema and PH. A single dose of saline or elastase (24 activity units/Kg body weight) solution was applied intratracheally. Four weeks later, FGF10 overexpression was induced by doxycycline treatment for 1, 5 or 12 weeks. Mice fed with regular chow were used as controls. Afterwards, emphysema and PH phenotype were characterised.

2.2.3 Cigarette smoke exposure

Animals were (whole-body) exposed to the mainstream smoke from 3R4F cigarettes (Lexington, KY, USA) for 3 or 8 months (5 days/week, 6 hours/day). Cigarette smoke was produced by a semi-automatic generator (Burghart GmbH, Wedel, Germany) as previously described (Seimetz *et al.* 2011; Pichl *et al.* 2019; Hadzic *et al.* 2021). A cigarette smoke generator with an exposure chamber is depicted in **Figure 12A**. CS concentration in the exposure chamber was measured gravimetrically and adjusted at 200 mg particulate matter per m³. Age-matched controls were kept under identical conditions but without CS exposure.

Macroscopically visible difference in mice formalin-fixed left lung lobes upon 8 months of RA or CS exposure is shown in **Figure 12B**.

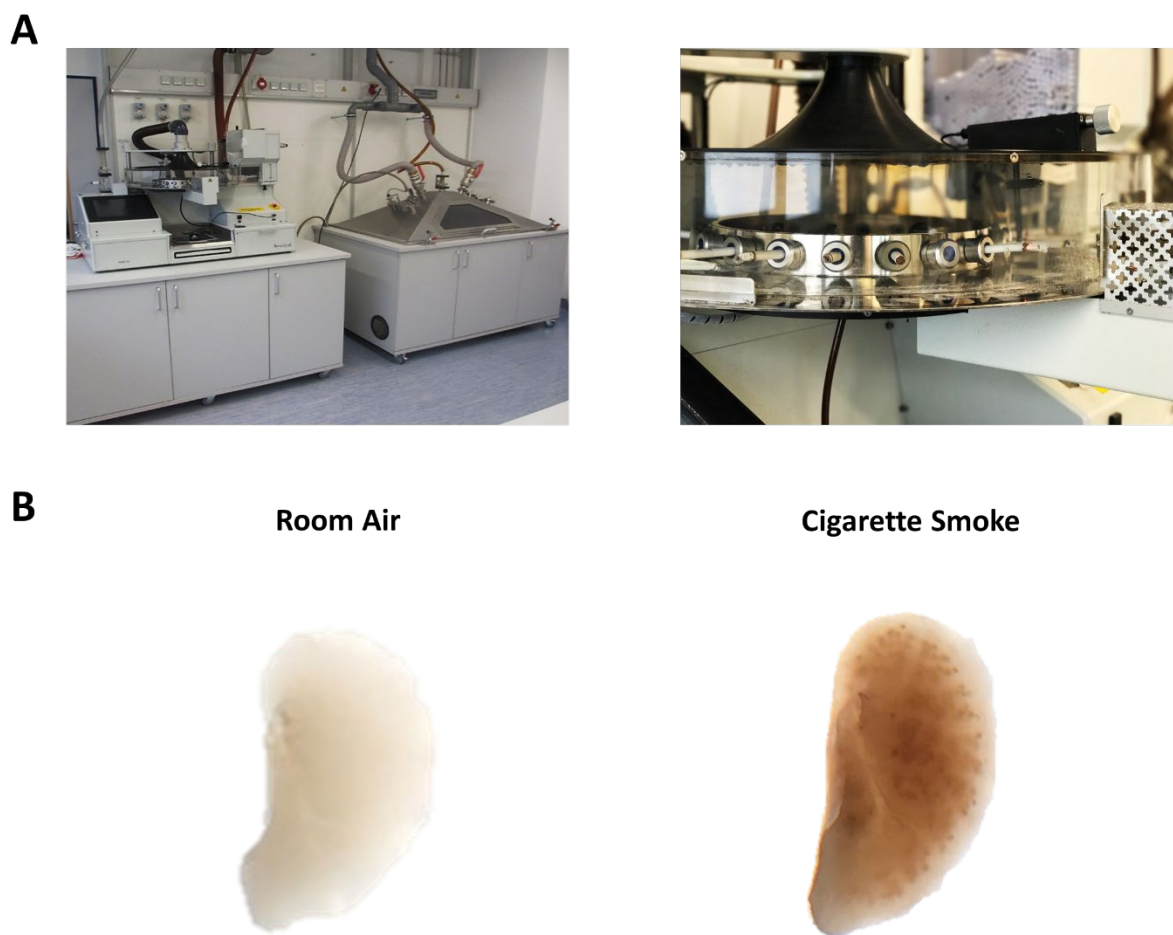
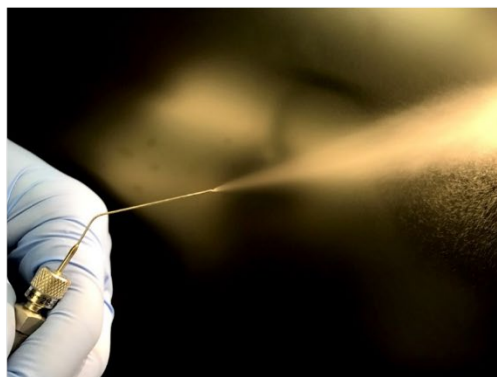


Figure 12. Mouse model of long-term cigarette smoke exposure. (A) Left: Semi-automatic cigarette smoke generator (Burghart GmbH, Wedel, Germany) with the exposure chamber; right: carousel with burning cigarettes. **(B)** Formalin-fixed left lung lobes from mice exposed for 8 months either to room air or cigarette smoke.

2.2.4 Intratracheal elastase instillation

Anaesthesia in mice was induced in a chamber with 4% isoflurane (Baxter Deutschland GmbH, Unterschleissheim, Germany) in 100% O₂. The animal was further fixed by the upper teeth on a thin horizontal bar and anaesthesia was maintained with 2% isoflurane in 100% O₂ through a nose-only mask. The lower jaw and the tongue were gently held with forceps to open the mouth so that the epiglottis could be clearly seen through the binoculars. A plastic 20 G tubus

(B.Braun Melsungen AG, Melsungen, Germany) was placed through the epiglottis in the trachea. To ensure that the mouse is intubated properly, breathing through the tubus was confirmed using a small mirror, where a trace of condensate from the exhaled air could be seen.

A**B**

Saline



Elastase



Figure 13. Mouse model of elastase-induced pulmonary emphysema. (A) High-pressure syringe and MicroSprayer® Aerosolizer (Penn-Century, Inc., Wyndmoor, PA, USA) used for inrta-tracheal application of elastase or saline. **(B)** Formalin-fixed left lung lobes from mice 16 weeks after a single application of saline or elastase (24 activity units/Kg body weight) solution.

In order to reach equal distribution, a MicroSprayer® Aerosolizer (Model IA-1C; Penn-Century, Inc., Wyndmoor, PA, USA) with a high-pressure syringe (Model FMJ-250; Penn-Century, Inc., Wyndmoor, PA, USA) was used for application (**Figure 13A**). The tip of the MicroSprayer® Aerosolizer was placed through the tubus, and elastase or saline solution was sprayed directly

in the lung. Immediately after the elastase or saline application, 200 μ l of air was applied through the tubus, mimicking deep inflation, ensuring that the liquid reaches distal areas of the lung. The tube was then removed, and the mouse returned to the cage to recover from anaesthesia.

Elastase from porcine pancreas (E7885; Merck KGaA, Darmstadt, Germany) was always freshly diluted in sterile saline solution (B.Braun Melsungen AG, Melsungen, Germany) and kept on ice prior to the application; 100 μ l of the solution was applied per mouse. The elastase concentration was adjusted for each mouse, so that an amount of 24 activity units per kg of body weight (U/Kg bw) was applied in a constant volume of 100 μ l. In the control mice, 100 μ l of pure saline solution saline was applied. The macroscopically visible difference in mouse lungs upon saline or elastase application is depicted in **Figure 13B**.

2.2.5 *In vivo* fluorescence molecular tomography (FMT) and micro-computed tomography (μ CT)

In vivo fluorescence molecular tomography (FMT) and micro-computed tomography (μ CT) were performed by Dr. Baktybek Kojonazarov at the Justus Liebig University, Department of Internal Medicine, Institute for Lung Health, Giessen, Germany. FMT imaging was performed using an FMT 2500 system (VisEn Medical, Bedford, MA, USA) as previously described (Seimetz *et al.* 2020). FMT scanning was performed 6 hours after tail vein injection of 2 nmol matrix metalloproteinase probe (MMPSense 750 FAST; PerkinElmer Inc., Waltham, MA, USA) or 2 hours after the injection of 2 nmol of Annexin Vivo 750 (Perkin Elmer, Waltham, USA). Anaesthesia was induced with 3% isoflurane (Baxter Deutschland GmbH, Unterschleißheim, Germany) in 100% O₂ and maintained with 1.5-2.0% isoflurane during imaging with a gas-delivery system integrated into the multimodal-imaging cassette that holds the mouse during FMT and μ CT imaging. Micro CT (μ CT) was performed using a Quantum GX μ CT scanner (PerkinElmer Inc., Waltham, MA, USA) as previously described (Hadzic *et al.* 2021). Reconstructed volumes were processed with the Analyze Pro software (Analyze Direct, Mayo Clinic, Minnesota, USA). Lung segmentation and quantitative analysis were performed as

previously described (Hadzic *et al.* 2021; Seimetz *et al.* 2020). Scans were loaded into Analyze 12 software (Analyze Direct, Mayo Clinic), where FMT and μ CT images were merged.

2.2.6 Non-invasive echocardiography

Non-invasive *in vivo* transthoracic echocardiography was performed by Dr. Simone Kraut and Cheng-Yu Wu at the Justus Liebig University, Department of Internal Medicine, Excellence Cluster Cardio Pulmonary Institute, Giessen, Germany. Echocardiography was performed under isoflurane inhalation anaesthesia as previously described (Pichl *et al.* 2019; Hadzic *et al.* 2021; Seimetz *et al.* 2020). Briefly, imaging was done using a Vevo[®] 2100 high-resolution Imaging System (FUJIFILM VisualSonics Inc., Toronto, Canada) equipped with the high-frequency M550D transducer (22-55 MHz). Mice were initially anaesthetized with 3% isoflurane, and anaesthesia was maintained with 1-2% isoflurane supplemented in 100% O₂. The chest hair was removed before the imaging, and the body temperature was monitored using a rectal thermometer (Indus Instruments, Houston, TX, USA). Tricuspid annular plane systolic excursion (TAPSE) was obtained under RV-focused apical 4-chamber view and analysed using anatomical M-mode as previously described (Pichl *et al.* 2019; Hadzic *et al.* 2021; Seimetz *et al.* 2020).

2.2.7 *In vivo* lung function and hemodynamic measurement

Measurements of *in vivo* lung function and hemodynamic measurements I performed as previously described with slight modifications (Pichl *et al.* 2019; Seimetz *et al.* 2020; Hadzic *et al.* 2021). Briefly, anaesthesia was induced by putting a mouse in a chamber with 3% isoflurane in 100% O₂. The mouse was then restrained on a thermoregulation plate with constant anaesthesia supply via a nose-only mask. Electrocardiogram (ECG) electrodes and a rectal thermometer (Indus Instruments, Houston, TX, USA) were placed for monitoring the heart beating frequency and body temperature. After tracheotomy, the animals were intubated with 18 G metal tubus (SCIREQ Scientific Respiratory Equipment Inc., Montreal, Canada). The trachea was fixed with a thread and ventilated, using a FlexiVent system, equipped with an FX2 module (SCIREQ Scientific Respiratory Equipment Inc., Montreal, Canada), at a frequency of 150 breaths/minute and a tidal volume of 5 ml/kg.

Lung function tests were performed as previously described (Hadzic *et al.* 2021; Gouveia *et al.* 2020), using the FlexiVent predetermined script at positive end-expiratory pressure (PEEP) of 3 cmH₂O, with a consistent perturbation order, following the manufacturer's recommendations. Briefly, prior to the lung function measurement, deep inflation was performed as a recruitment manoeuvre. The deep inflation consisted of inflating the lung with air pressure from 3 to 40 cmH₂O over 3 seconds and then holding at 40 cmH₂O for additional 3 seconds (Boucher *et al.* 2021). That way, closed lung areas were recruited, and lung volume history was standardized (McGovern *et al.* 2013; Boucher *et al.* 2021; Zosky *et al.* 2008). The overall resistance of the respiratory system, a single compartment model perimeter, was measured using a single frequency forced oscillation (SnapShot-150) perturbation (McGovern *et al.* 2013). Broadband frequency forced oscillation (Qick Prime-3) perturbation was used to measure constant phase model parameters (Newtonian resistance and tissue damping) (McGovern *et al.* 2013). Static compliance measurement was obtained from a respiratory pressure-volume (P-V) loop (Bates 2009; McGovern *et al.* 2013). The P-V manoeuvre included stepwise lung inflation through 8 steps of increasing pressure from 3 to 40 cmH₂O with a 1-second hold at each step. It was then followed by stepwise deflation in a similar manner back to PEEP pressure of 3 cmH₂O. The whole manoeuvre lasted 16 seconds. The P-V loop was created by recording volume changes and plotting it with pressure values at each holding step (Bates 2009; McGovern *et al.* 2013). The results were presented as an average of at least three repeated measurements with the coefficient of determination (COD) above 0.95.

I performed hemodynamic measurements as previously described (Hadzic *et al.* 2021; Pichl *et al.* 2019; Seimetz *et al.* 2020; Gouveia *et al.* 2020). Briefly, for right ventricular systolic pressure (RVSP) measurements, the jugular vein was catheterized by a micro-tip catheter (SPR 671 REF 8406719; Millar Instruments Inc., Houston, TX, USA) that was then forwarded into the right ventricle. Systemic arterial and left ventricular systolic pressures were measured by a catheter inserted through the carotid artery into the aorta and then in the left ventricle. The animals were afterwards sacrificed by exsanguination through the carotid artery. Measurements were recorded and analysed using the PowerLab system and LabChart 7.0 software (AD Instruments GmbH, Spechbach, Germany).

2.2.8 Lung fixation and organ harvest

After the hemodynamic measurement, the thoracic cavity was opened, and the lungs were perfused through the pulmonary artery with the saline solution under 22 cmH₂O pressure during continuous ventilation (Minivent, Hugo Sachs Electronic, March-Hugstetten, Germany). Right lung lobes were collected and snap-frozen in liquid nitrogen for further analysis. The left lung lobe was either fixed with formalin (Otto Fischar GmbH, Saarbrücken, Germany) or inflated with Tissue-Tek® O.C.T.™ (Sakura Finetek Germany GmbH, Staufen im Breisgau, Germany) and snap-frozen in liquid nitrogen. Fixation was performed under simultaneous vascular perfusion (22 cmH₂O) and inflation (12 cmH₂O) with formalin for 20 minutes before removing from the thoracic cavity. The left lung lobe was then incubated in formalin overnight at room temperature. Afterwards, I washed the lungs in phosphate-buffered saline (PBS) for 24 h at 4 °C. Formalin-fixed lung lobes are shown in **Figures 12 and 13**. In order that histological analysis is performed at all depths through the left lung lobe, the fixed tissue was placed in an agarose block, cut in 3 mm thick sections and dehydrated following routine protocol and as previously described (Hadzic *et al.* 2021; Gredic *et al.* 2021). For right-heart hypertrophy measurement, the right ventricle (RV) was separated from the left ventricle and septum (LV+S), and the weight was measured as previously described (Hadzic *et al.* 2021; Gouveia *et al.* 2020; Gredic *et al.* 2021; Pichl *et al.* 2019).

2.2.9 Lung vasculature casting and *ex vivo* μ CT imaging

Prior to the experiments, vasodilation buffer was prepared – PBS containing 4 mg/l papaverine (Linden Arzneimittel GmbH, Heuchelheim, Germany), 1 g/l adenosine (Merck KGaA, Darmstadt, Germany) and 1000 IU/l heparin (Ratiopharm GmbH, Ulm, Germany). I perfused the lungs for 5 minutes with a vasodilation buffer using an Ismatec® roller-pump (Cole-Parmer GmbH, Wertheim Germany) at the flow rate of 5 ml/min. Subsequently, the lung was perfused with freshly prepared Microfil® (MV122 YELLOW; Flow Tech Inc., Carver, MA, USA) solution, at the rate of 1 ml/min for 2 minutes according to the manufacturer's recommendations. Subsequently, the lung was inflated via the trachea with formalin solution (Otto Fischar GmbH,

Saarbrücken, Germany) under a pressure of 20 cmH₂O. After 30 minutes, the fixed lung was gently removed from the chest cavity and kept in formalin solution until further processing.

The lungs were then embedded in an agarose block, and images were acquired using a Quantum GX μ CT scanner (PerkinElmer Inc., Waltham, MA, USA) with the help of Dr. Baktybek Kojonazarov at the Justus Liebig University, Department of Internal Medicine, Institute for Lung Health, Giessen, Germany. The scanner's complementary metal-oxide-semiconductor X-ray flat-panel detector was set to allow image acquisition with an X-ray tube voltage of 90 kV and current of 80 μ A. μ CT data were collected in list-mode over a single complete gantry rotation with a total rotation time of 57 minutes. Raw projection images were reconstructed using Analyze 12.0 software (Analyze Direct, Mayo Clinic).

2.2.10 Histology

2.2.10.1 Tissue section preparation

For histological analysis, paraffin blocks were cooled down, cut in 3 μ m thick sections using microtome (Leica RM 2165; Leica Microsystems GmbH, Wetzlar, Germany), placed on microscope glass (R. Langenbrinck GmbH, Emmendingen, Germany) and dried for at least 2 hours on a warm plate (Heating Plate Hi 1220; Leica Microsystems GmbH, Wetzlar, Germany) at 40 °C. Prior to any type of histological staining, paraffin-cut tissue sections on the microscope glass were first deparaffinized and rehydrated following the protocol shown in the **Table 8**.

Table 8. Deparaffinization and rehydration protocol performed on paraffin cut tissue sections.

Incubation time (minutes)	Reagent or condition	Procedure
60	59°C	Deparaffinization
3 x 10	Xylene	
2 x 5	Ethanol 99.6%	Rehydration
5	Ethanol 96%	
5	Ethanol 70%	
2 x 3	Distilled water	

2.2.10.2 Haematoxylin & Eosin (H&E) staining

Rehydrated lung sections on a microscope slide were stained following a routine Haematoxylin & Eosin (H&E) staining protocol, as described in **Table 9**. After staining and final dehydration in xylene, slides were mounted with Pertex (Medite GmbH, Burgdorf, Germany) and a thin covering glass (Menzel GmbH&Co.KG, Braunschweig, Germany) was placed over the specimen. As a result, nuclei were stained blue by haematoxylin and cytoplasm orange by eosin.

Table 9. Haematoxylin & Eosin (H&E) staining protocol.

Incubation time	Reagent or condition	Procedure
20 minutes	Acidic haematoxylin (Mayer)	Staining
5 minutes	Running lukewarm tap water	
1 minute	Ethanol 96%	
4 minutes	Eosin Y	
2 x 5 minutes	Ethanol 96%	
5 minutes	Ethanol 99.6%	Dehydration
5 minutes	Isopropanol	
3 x 5 minutes	Xylene	

2.2.10.3 Weigert's elastin staining protocol

Rehydrated lung sections were stained following a routine Wiegert's elastin staining protocol, as described in **Table 10**. After staining and final dehydration in xylene, slides were mounted with Pertex and a thin covering glass was placed over the specimen. The colour complex with resorcin-fuchsin (Waldeck GmbH & Co.KG, Münster, Germany), binds to the elastic fibres, resulting in purple-black staining. Nuclei were stained red by Nuclear Fast Red solution (Waldeck GmbH & Co.KG, Münster, Germany).

Table 10. Wiegert's elastin staining protocol.

Incubation time	Reagent or condition	Procedure
16 hours	Resorcin – fuchsin solution	Staining
15 minutes	Tap water	
10 minutes	Nuclear Fast Red solution	
2 x 5 minutes	Ethanol 96%	
5 minutes	Ethanol 99.6%	Dehydration
5 minutes	Isopropanol	
3 x 5 minutes	Xylene	

2.2.10.4 Picrosirius red staining protocol and collagen quantification

For collagen quantification, rehydrated lung sections were stained with the commercially available Picrosirius red staining kit (ab150681, Abcam, Cambridge, United Kingdom) following the manufacturer's recommendation and as described in **Table 11**. After staining and final dehydration in xylene, slides were mounted with Pertex and a thin covering glass was placed over the specimen. Red stained collagen fibres were quantified under a light microscope (CTR6000; Leica Microsystems GmbH, Wetzlar, Germany) using Qwin software (Leica Microsystems GmbH, Wetzlar, Germany). Collagen stained area was always normalised to the stained tissue area in the quantified area to avoid the effects of alveolar septal wall loss (emphysema).

Table 11. Picrosirius red staining protocol.

Incubation time	Reagent or condition	Procedure
1 hour	Picrosirius red solution	Staining
2 x 15 seconds	0.5% acetic acid solution	
2 x 1 minute	Ethanol 99.6%	Dehydration
3 x 2 minutes	Xylene	

2.2.10.5 Alveolar morphometry analysis

For alveolar morphometry, paraffin-cut lung sections were stained with H&E following routine protocol and as described above. Mean linear intercept (MLI) and airspace percentage I assessed under a light microscope (CTR6000; Leica Microsystems GmbH, Wetzlar, Germany) using uniform random sampling and Qwin alveolar morphometry software (Leica Microsystems GmbH, Wetzlar, Germany) as previously described (Pichl *et al.* 2019; Seimetz *et al.* 2011; Hadzic *et al.* 2021). Only the alveolar compartment was considered for the measurements; all visible vessels or airways were excluded from each analysed image.

2.2.10.6 Design-based stereology

The density of alveoli I estimated using a physical dissector method, as previously described (Seimetz *et al.* 2020; Hadzic *et al.* 2021). Briefly, two alternate 3 µm thick sections, with a 3 µm distance from each other, were placed on the same slide and stained according to Weigert's elastin staining protocol (**Table 10**). Slides were then scanned and analysed using a light microscope (CTR6000; Leica Microsystems GmbH, Wetzlar, Germany) equipped with newCast software for stereology (Visiopharm, Hørsholm, Denmark). Respective counts were then related to the left lung volume, and the total alveoli number was calculated.

2.2.10.7 Immunohistochemistry staining and quantification

Paraffin-embedded mouse or human lungs were cut in 2 µm thick sections, deparaffinised and rehydrated following routine protocols. Antigen retrieval was then performed by cooking

slides in decloaking solution. Rodent Decloaker (RD913; Biocare Medical LLC, Pacheco, CA, USA) solution was used for mice and Diva Decloaker (Biocare Medical LLC, Pacheco, CA, USA) for human lung sections. The slides were washed in TBS buffer (ZUC052; Zytomed Systems GmbH, Berlin, Germany), and unspecific binding was blocked using 10% Bovine Serum Albumin (BSA; A7030; Merck KGaA, Darmstadt, Germany) solution. The slides were incubated with primary antibody solution diluted in antibody diluent (ZUC025; Zytomed Systems GmbH, Berlin, Germany) overnight at 4 °C. Following primary antibodies were used: Anti-FGF10 (1:200; ABIN360398; Antibodies-online GmbH, Aachen, Germany; RRID: AB_2715513) – for human tissue; Anti-FGF10 (1:200; ABN44; Merck KGaA, Darmstadt, Germany; RRID: AB_11204345) – for mouse tissue; Anti-Bek/FGFR2 (1:200; sc-6930; Santa Cruz Biotechnology Inc., Dallas, TX, USA; RRID: AB_669015); Anti-BrdU (1:100; Bu20a; #339808; Biolegend Inc., San Diego, CA, USA; RRID: AB_10895898). ZytoChem Plus phosphatase polymer kit (POLAP-100; Zytomed Systems GmbH, Berlin, Germany) and Warp Red Chromogen substrate kit (WR 806; Biocare Medical LLC, Pacheco, CA, USA) were used, following the manufacturer's protocol, to visualise staining. Counterstaining was performed using CAT Haematoxylin solution (CATHE-M; Biocare Medical LLC, Pacheco, CA, USA). The stained area or number of cells was quantified in randomly selected fields using Qwin software (Leica Microsystems GmbH, Wetzlar, Germany). Quantification was performed separately in alveolar septa and pulmonary vessels. To avoid effects of the septal wall loss or vascular remodelling, the stained area was always standardized to the overall tissue area in each given picture.

2.2.10.8 Immunofluorescence staining and confocal microscopy

Paraffin-embedded mice or human lungs were cut into 3 µm thick sections, deparaffinised and rehydrated following the above-described protocol (**Table 8**). Antigen retrieval was performed by cooking slides in Rodent Decloaker (RD913; Biocare Medical LLC, Pacheco, CA, USA). Unspecific binding was blocked using 10% BSA solution. The slides were incubated with Rabbit Anti- von Willebrand factor antibody (1:500; A0082; Dako Deutschland GmbH, Hamburg, Germany; RRID: AB_2315602) overnight at 4 °C. The next day slides were washed in PBS and incubated with Goat anti-Rabbit Alexa Fluor Plus 488 (1:400; A32731; Thermo Fisher Scientific

Inc. Waltham, MA, USA; RRID: AB_2633280) for 3 hours at room temperature. After washing and staining with 0.1 µg/ml DAPI (D9542; Merck KGaA, Darmstadt, Germany), slides were covered using an anti-fade mounting medium (FP001G10; Biocare Medical LLC, Pacheco, CA, USA). The slides were sealed with nail polish and stored in the dark at 4 °C until imaging.

Tissue sections were examined by laser scanning confocal microscopy (TCS SP5; Leica Microsystems GmbH, Wetzlar, Germany) as previously described (Seimetz *et al.* 2020). Series of confocal optic sections were taken using a Leica Plan Apo ×63/1.32 objective lens (Leica Microsystems GmbH, Wetzlar, Germany). Each recorded image was taken using multichannel scanning and consisted of 1.024 × 1.024 pixels. To improve image quality and to obtain a high signal/noise ratio, each image from the series was signal-averaged and was deconvoluted using AutoQuant X2 software (Bitplane AG, Zurich, Switzerland). Quantification for each animal was based on the average fluorescence intensity in five randomly selected fields.

2.2.11 *In vitro* cell culture experiments

2.2.11.1 Cigarette smoke extract (CSE) preparation

Cigarette smoke extract (CSE) I always prepared fresh by burning one 3R4F cigarette in one minute. The smoke was bubbled in 10 ml of basal cell culture medium as previously described with slight modifications (Seimetz *et al.* 2020; Gredic *et al.* 2021). The medium was then sterile-filtered through a syringe filter with 0.2 µm pore diameter (#83.1826.001; Sarstedt AG & Co. KG, Nümbrecht, Germany). The resulting CSE was considered 100% and was further diluted with the adequate cell culture medium for treatments.

2.2.11.2 Interstitial lung fibroblasts from human patients

Interstitial lung fibroblasts were obtained from the DZL Biobank, isolated, following routine protocols. Briefly, cells were isolated from fresh tissue – lungs explanted either from healthy donors or subjects with end-stage COPD. The distal lung tissue (cleared from pleura and distinguishable bronchi and vessels) was first placed in a falcon tube with PBS (P04-36503, PAN-Biotech, Aidenbach, Germany) containing 2% penicillin-streptomycin (15070-063; GIBCO™, Thermo Fisher Scientific Inc., Waltham, MA, USA). Using the 3-scissors technique, the

tissue was cut into small pieces and washed thoroughly with PBS containing 2% penicillin-streptomycin. The pieces were then centrifuged at 240 g for 5 minutes, resuspended in Dulbecco's Modified Eagle Medium (DMEM, #41965039, Gibco, Thermo Fisher Scientific Inc. Waltham, MA, USA) containing 10% FBS (F4135, Sigma-Aldrich, Germany) and 1% penicillin-streptomycin and plated in a T75 flask. The fibroblasts were left to outgrow for 1-2 weeks, changing medium every 3 days. Cells were then amplified and after the first passage cryopreserved until further use.

For the treatments, cells were recovered and, in the following passage, seeded in 6-well plates. After reaching 80% confluence, cells were treated for 6 hours with either 1% CSE, 20 μ M SIN-1 (3-morpholinosydnonimine N-ethylcarbamide, #82220, Cayman Chemical Co., Ann Arbor, MI, USA) or 10 μ M L-NIL (N6-(1-iminoethyl)-L-lysine, dihydrochloride, #80310, Cayman Chemical Co., Ann Arbor, MI, USA) + 1% CSE. Protein samples were collected by scraping cells in the presence of commercially available Cell Lysis Buffer (#9803, Cell Signaling Technology Inc., Danvers, MA, USA) containing 1 mM protease inhibitor - phenylmethylsulfonyl fluoride (PMSF; Cell Signaling Technology Inc., Danvers, MA, USA) and stored at -20 °C until further processing.

2.2.11.3 Precision cut lung slices (PCLS)

Low melt agarose (4%; 6351, Carl Roth GmbH + Co. KG, Karlsruhe, Germany) was prepared in PBS and boiled in the microwave until the agarose liquefied. The agarose was then mixed with an equal volume of 1640 medium (P04-16500; PAN-Biotech GmbH, Aidenbach, Germany) containing 20% FBS (F4135; Merck KGaA, Darmstadt, Germany) and 2% penicillin-streptomycin (15070-063; GIBCO™, Thermo Fisher Scientific Inc., Waltham, MA, USA); final concentration: 2% low-melt agarose, 10% FBS and 1% penicillin-streptomycin.

A piece of the human lung was inflated with agarose solution through bronchi and left in ice-cold PBS until the agarose solidified (**Figure 14A**). The PCLS were cut 400 μ m thick using a vibratome (Microm HM650V, Thermo Fisher Scientific Inc., Waltham, MA, USA) and cultured in RPMI 1640 medium (**Figure 14C, 14D**) containing 10% human serum (Seraclot; P40-3011;

PAN-Biotech GmbH, Aidenbach, Germany), 1% penicillin-streptomycin, 100 $\mu\text{g}/\text{ml}$ Normocin™ (ant-nt-1; InvivoGen, Toulouse, France). The medium was changed hourly in the first 6 hours to remove the dead cells. The PCLS were incubated in a medium containing bromodeoxyuridine (BrdU, #11647229001; Roche Diagnostics GmbH, Mannheim, Germany) with or without 250 ng/ml recombinant human FGF10 (rhFGF10; #345-FG-250; R&D Systems Inc., Minneapolis, MN, USA). After 24 h, the PCLS were washed in cold PBS, fixed with 4% paraformaldehyde (sc-281692; Santa Cruz Biotechnology Inc., Dallas, TX, USA) for 2 hours at room temperature, dehydrated and embedded in paraffin following routine protocols.

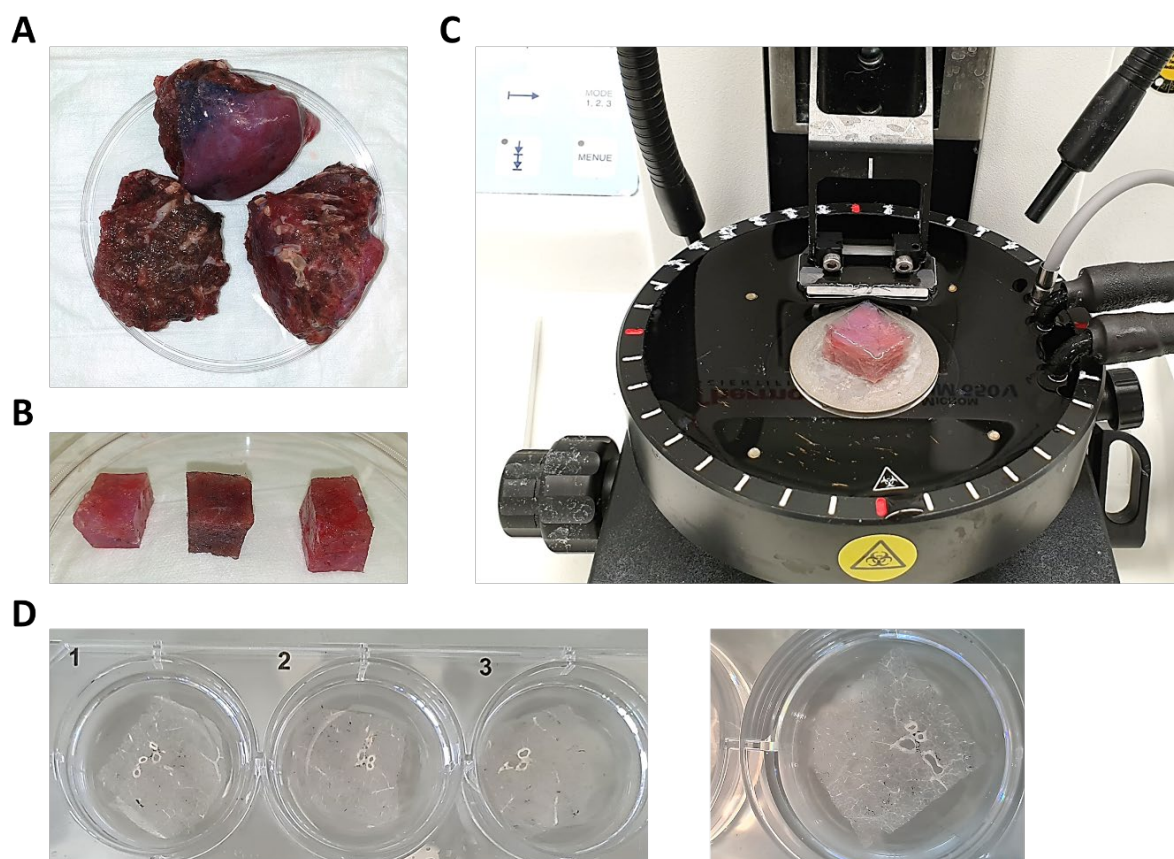


Figure 14. Human precision cut lung slices (PCLS) preparation. (A) COPD lung segments after the low-melting agarose solidified. **(B)** The tissue pieces were cleared of large vessels and bronchi and shaped into cubes for slicing by vibratome. **(C)** Agarose cube containing lung tissue was placed in cold phosphate-buffered saline (PBS) and sliced into 400 μm thick PCLS using a vibratome. **(D)** Paraformaldehyde fixed PCLS and prepared for dehydration.

2.2.11.4 Mouse alveolar type 2 (ATII) cell isolation

Mouse alveolar type 2 (ATII) cells were isolated as previously described (Seimetz *et al.* 2020). Briefly, I anaesthetised mice by intraperitoneal injection containing xylazine (20 mg/kg body weight; Serumwerk, Bernburg, Germany), ketamine (100 mg/kg body weight; Ursotamin®; Serumwerk Bernburg AG, Bernburg, Germany) and heparin (50000 IU heparin/kg body weight; Ratiopharm GmbH, Ulm, Germany). The mice were subsequently sacrificed by exsanguination, and lungs were perfused through the pulmonary artery with saline solution (B.Braun Melsungen AG, Melsungen, Germany), inflated through the trachea with 1 ml dispase (#354235; Corning Inc., New York, NY, USA) and put in a tube containing dispase. After 45 minutes of incubation at 37 °C, I separated the lung lobes and chopped them using two scalpels. The fine suspension was then washed with DMEM and filtered through 70 µm and 40 µm strainers (#83.3945.070; #83.3945.040; Sarstedt AG & Co. KG, Nümbrecht, Germany). Following a centrifugation at 300 g for 10 minutes, cell pellets were re-suspended in DMEM medium, and plated on a 10-cm dish which was pre-coated with rat anti-mouse CD31 (1:1000; #550274; BD Biosciences, San Jose, CA, USA; RRID: AB_393571) rat anti-mouse CD45 (1:1000; #550539; BD Biosciences, San Jose, CA, USA; RRID: AB_396376) and rat anti-mouse CD16/CD32 (Mouse BD Fc Block™; 1:1000; #553142; BD Biosciences, San Jose, CA, USA; RRID: AB_394656) antibodies. After 30-minute incubation at 37 °C, non-adherent cells were gently washed out and plated on cell culture dishes to negatively select fibroblasts. Following 1-hour incubation at 37 °C, the remaining cells were collected and centrifuged. The number of ATII cells was determined by the Nile red staining (Merck KGaA, Darmstadt, Germany) staining and counting in a Neubauer chamber (#0640010; Paul Marienfeld GmbH & Co. KG, Lauda-Königshofen, Germany). ATII cells were further cultured on fibronectin-coated (F1141; Merck KGaA, Darmstadt, Germany) 96-well plates in DMEM medium containing 10mM glutamine (GIBCO™, Thermo Fisher Scientific Inc., Waltham, MA, USA) 10% FBS and 1% penicillin-streptomycin (15070-063; GIBCO™, Thermo Fisher Scientific Inc., Waltham, MA, USA).

2.2.11.5 Cell apoptosis and cell viability assays

For each well in a 96-well plate, 35000 ATII cells were seeded. Cells were incubated with or without 250 ng/ml recombinant human FGF10 (rhFGF10; R&D Systems Inc., Minneapolis, MN, USA) for 24 hours. Afterwards, CSE was added in the medium and 6 hours after apoptosis or cell viability was measured. For the assessment of apoptosis, a fluorescently labelled annexin V-based probe from the kinetic apoptosis kit (ab129817; Abcam, Cambridge, UK) was used according to the manufacturer's instructions. The images were obtained using an IncuCyte ZOOM (Essen BioScience Ltd., Ann Arbor, MI, USA) live-cell imaging system. Results are presented as a ratio between the green fluorescence signal from the annexin V probe and cell confluence assessed in a bright field. The viability of ATII cells was measured using AlamarBlue[®] assay (DAL1100; Thermo Fisher Scientific Inc., Waltham, MA, USA), following the manufacturer's protocol. Briefly, AlamarBlue[®] reagent was added to the cell culture medium (dilution ratio 1:10) and the fluorescence signal at 590 nm wave length was measured 4 hours later using a Spark[®] multimode microplate reader (Tecan Trading AG, Männedorf, Switzerland).

2.2.12 Molecular biology experiments

2.2.12.1 Ribonucleic acid (RNA) isolation and purification

Human or mouse lungs were homogenised in the presence of commercially available RLT RNA lysis buffer (#79216; Qiagen GmbH, Hilden, Germany) containing 1% 2-Mercaptoethanol (M3148; Merck KGaA, Darmstadt, Germany), using Precellys[®] 24 bead beating tissue homogenizer (Bertin Corp; Thermo Fisher Scientific Inc., Waltham, MA, USA). Total RNA was further purified using the RNeasy Mini Kit (#74106, Qiagen GmbH, Hilden, Germany) following the manufacturer's recommendations.

2.2.12.2 Complementary deoxyribonucleic acid (cDNA) synthesis

The concentration of the isolated total RNA was measured by a NanoDrop device (ND-1000; Kisker Biotech, Steinfurt, Germany). 1 µg of the total RNA was reverse-transcribed using the iScript[™] cDNA Synthesis Kit (#1708891; Bio-Rad Laboratories GmbH, Hercules, CA, USA)

following manufacturer's recommendation and as described in **Table 12 and 13**. Synthesized cDNA was kept at -20 °C until further processing.

Table 12. Sample preparation for reverse transcription – cDNA synthesis.

Component	Volume per reaction (µl)
5x iScript Reaction Mix	4
iScript Reverse Transcriptase	1
Total RNA diluted in nuclease-free water	15 (containing 1 µg RNA)
Total volume (µl):	20

Table 13. Thermal reaction for reverse transcription – cDNA synthesis.

Process	Conditions
Priming	5 minutes at 25 °C
Reverse transcription	20 minutes at 46 °C
Reverse transcriptase inactivation	1 minute at 95 °C

2.2.12.3 Message RNA (mRNA) expression analysis by quantitative polymerase chain reaction (qPCR)

Synthesized cDNA was mixed with the iQ™ SYBR® Green Supermix (#1708885; Bio-Rad Laboratories GmbH, Hercules, CA, USA) and respective primers for the target gene as described in **Table 14** and plated on the Hard-Shell® 96-Well PCR Plate (HSP9601; Bio-Rad Laboratories GmbH, Hercules, CA, USA).

Table 14. Sample preparation for quantitative polymerase chain reaction (qPCR).

Component	Volume per reaction (μ l)
iQ™ SYBR® Green Supermix	5
Nuclease-free water	3.5
A mixture of forward (10 μ M) and reverse (10 μ M) primers	0.5
cDNA diluted in nuclease-free water (200 ng/ μ l)	1
Total volume (μl):	10

Gene expression levels were assessed by a CFX Connect Real-Time PCR Detection System (Bio-Rad Laboratories GmbH, Hercules, CA, USA) as previously described (Seimetz *et al.* 2020; Veith *et al.* 2022) using a thermal cycling program as listed in **Table 15**.

Table 15. Thermal reaction program for quantitative polymerase chain reaction (qPCR).

Process	Temperature	Duration	Number of cycles
Initial denaturation	95 °C	10 minutes	1
Denaturation	95 °C	10 seconds	40 (sequentially repeated)
Annealing	59 °C	10 seconds	
Elongation	72 °C	10 seconds	

2.2.12.4 Laser-assisted microdissection

Laser microdissection was done as described previously with subtle modifications (Pichl *et al.* 2019; Seimetz *et al.* 2020; Veith *et al.* 2022). Cryopreserved mouse lungs embedded in Tissue-Tek® O.C.T.™ (Sakura Finetek Germany GmbH, Staufen im Breisgau, Germany) were cut in 12 μ m thick sections using a cryotome (CM1850; Leica Microsystems GmbH, Wetzlar, Germany) and placed on a glass slide that was covered with polyethene naphthalate (PEN) membrane (#11505158; Leica Microsystems GmbH, Wetzlar, Germany). Slides were immediately stained in haematoxylin solution for 30 seconds and then washed in 100% ethanol. Microdissection was performed using an LMD 6000 system (Leica Microsystems GmbH, Wetzlar, Germany)

equipped with a laser. Around 60 pulmonary vessels and 50 frames containing only alveolar septa were dissected from each mouse lung and collected separately in tubes containing RLT RNA lysis buffer (#79216; Qiagen GmbH, Hilden, Germany) supplemented with 1% 2-Mercaptoethanol (M3148; Merck KGaA, Darmstadt, Germany). Collected samples were stored at -80 °C until further processing.

2.2.12.5 Transcriptome analysis via microarray technology

Total RNA from microdissected pulmonary vessels and alveolar septa was purified using RNeasy Micro Kit (#74004; Qiagen GmbH, Hilden, Germany) following the manufacturer's recommendations. Transcriptome analysis was performed by Dr. Jochen Wilhem at the Justus Liebig University, Department of Internal Medicine, Institute for Lung Health, Giessen, Germany. Purified total RNA was amplified using an Ovation PicoSL WTA System V2 kit (#3312-24; NuGEN Technologies, San Carlos, CA, USA) following the manufacturer's recommendations. For each sample, 2 µg of amplified cDNA was cyanine-labelled using a SureTag DNA Labelling Kit (#5190-3400; Agilent Technologies Inc., Santa Clara, CA, USA) following the manufacturer's recommendations. Hybridisation to oligonucleotide spotted microarray slides (mouse genome 8 × 60 K, Design ID 028005; Agilent Technologies Inc., Santa Clara, CA, US) and subsequent washing and drying of the slides were performed following the Agilent hybridisation protocol in Agilent hybridisation chambers, with the following modifications: 2 µg labelled cDNA was hybridised for 22 hours at 65 °C, and the cDNA was not fragmented before hybridisation. The dried slides were scanned at 2 µm per pixel resolution using an InnoScan is900 device (Innopsys, Chicago, IL, USA). Image analysis was performed with Mapix 6.5.0 software (Innopsys, Chicago, IL, USA; RRID: SCR_002723), and calculated values for all spots were saved as GenePix result files. Stored data were evaluated using R software (The R Foundation, Iowa City, IA, USA; RRID: SCR_001905) and the limma package from BioConductor (RRID: SCR_010943). log₂ mean spot signals were calculated for further analysis. Data were background-corrected using the NormExp procedure on the negative control spots and quantile-normalised before averaging. log₂ signals of replicate spots were averaged, and of several different probes addressing the same gene, only the probe with the

highest average signal was used. Genes with the $-\log p \geq 1.30$ (2.00 for the pulmonary vasculature) for the analysed comparison were considered as regulated. Interactions between genes and pathway analysis I performed using STRING Database (STRING-DB; Search Tool for the Retrieval of Interacting Genes/Proteins) (Szklarczyk *et al.* 2019).

2.2.12.6 Protein expression analysis by Western-blot

Human or mouse lungs were homogenised in commercially available protein lysis buffer (Cell Signaling Technology Inc., Danvers, MA, USA) containing 1 mM PMSF, using a Precellys® 24 bead beating Tissue Homogenizer (Bertin Corp; Thermo Fisher Scientific Inc. Waltham, MA, USA) and following manufacturer's recommendation. To prepare samples for the sodium dodecyl-sulfate polyacrylamide gel electrophoresis (SDS-PAGE), lysates (containing 25 µg protein) were mixed with 4x Laemmli protein sample buffer and 2-mercaptoethanol as described in **Table 16** and incubated at 95 °C for 5 minutes. In such conditions, proteins in the sample are denaturated, and 15 µl of the mixture was loaded per well on the 12% polyacrylamide gel. Proteins were separated by gel electrophoresis (100 Volts, 400 mA, 150 W for 1.5 hours) and then transferred to a polyvinylidene difluoride (PVDF) membrane (Pall Deutschland Holding GmbH & Co. KG, Dreieich, Germany) using a Trans-Blot® Turbo Semi-dry system (Bio-Rad Laboratories GmbH, Hercules, CA, USA) as previously described (Gredic *et al.* 2021; Hadzic *et al.* 2021; Veith *et al.* 2022).

Table 16. Sample preparation for sodium dodecyl-sulphate polyacrylamide gel electrophoresis (SDS-PAGE).

Component	Volume per sample (µl)
4x Laemmli protein sample buffer	5
2-mercaptoethanol	0.5
Protein sample	14.5 (containing 25 µg protein)
Total volume (µl):	20

After blocking, membranes were incubated overnight at 4 °C with a primary antibody and for 1 hour at room temperature with a secondary antibody conjugated with horseradish peroxidase. Antibodies were diluted in blocking buffer, in dilution ratio mentioned below. Protein bands were visualised with the ECL kit (Clarity™, Bio-Rad Laboratories GmbH, Hercules, CA, USA) using ChemiDoc MP Imaging System (Bio-Rad Laboratories GmbH, Hercules, CA, USA). Densitometry was performed in Image Lab™ Software (Bio-Rad Laboratories GmbH, Hercules, CA, USA). Each band was standardized to the intensity of β -actin that was used as a loading control. Expression was shown as a regulation factor, calculated by standardizing each sample to the mean value of the expression in the room air control group.

Following primary antibodies were used: Anti-FGF10 (1:500; AP14882PU-N; Acris Antibodies GmbH, Herford, Germany; RRID: AB_1752406) – for mouse; Anti-FGF10 (1:1000; ABN44; Merck KGaA, Darmstadt, Germany; RRID: AB_11204345) – for human; Anti-p-Akt (1:500; 9271; Cell Signaling Technology Inc., Danvers, MA, USA; RRID: AB_329825); Anti-Bek/FGFR2 (1:1000; sc-6930; Santa Cruz Biotechnology Inc., Dallas, TX, USA; RRID: AB_669015); Anti-Akt (1:1000; 9272; Cell Signaling Technology Inc., Danvers, MA, USA; RRID: AB_329827); Anti-Sp1 (1:1000; 9389; Cell Signaling Technology Inc., Danvers, MA, USA; RRID: AB_11220235); Anti- β -catenin (1:1000; 8480; Cell Signaling Technology Inc., Danvers, MA, USA; RRID: AB_11127855); Anti- β -actin (1:10000; ab8226; Abcam, Cambridge, UK; RRID: AB_306371). Anti-rabbit (1:5000; W4011; Promega GmbH, Madison, WI, USA; RRID: AB_430833) and anti-mouse (1:5000; W4021; Promega GmbH, Madison, WI, USA; RRID: AB_430834) HRP conjugated secondary antibodies were used.

2.2.12.7 3-nitrotyrosine quantification via enzyme-linked immunoassay (ELISA)

Proteins were isolated from lung homogenate as described before (Fysikopoulos *et al.* 2020; Hadzic *et al.* 2021; Pichl *et al.* 2019; Veith *et al.* 2022). Protein concentration in the lysates was determined using Bradford assay (#5000113-5; Bio-Rad Laboratories GmbH, Hercules, CA, USA). For each sample, 50 μ g of protein was loaded per well and 3-nitrotyrosine was quantified using a nitrotyrosine assay kit (#17-376; Merck KGaA, Darmstadt, Germany) following the manufacturer's protocol and as previously described (Pichl *et al.* 2019). Briefly, nitrotyrosine

assay kit is an antibody-based competitive enzyme-linked immunoassay (ELISA) with chemiluminescent detection. Luminescence was measured as relative light units using a Spark® multimode microplate reader (Tecan Trading AG, Männedorf, Switzerland). Results are calculated as the equivalent of nitrated bovine serum albumin (ntBSA), which was used as standard.

2.2.13 Data processing

GraphPad Prism 8 software (GraphPad Software Inc., La Jolla, CA, USA) was used for graph assembly and data analysis. Each value in the graph represents an actual measurement, or a mean value of actual measurements obtained from one individual experimental animal, human individual or technical replicate. All data are shown in scatterplots, and mean values for each group are represented with a horizontal line +/- standard error of the mean (SEM). Data obtained from inappropriate measurements (due to, e.g. inadequate positioning of the echocardiography transducer, mouse dying during measurements or unsuccessful lung fixation) were excluded.

2.2.14 Statistical analysis

Each difference, when $p \leq 0.05$, was considered statistically significant. Statistical tests used to calculate the p value are indicated in figures legend for each individual graph. Briefly, for comparison between two groups, Student's t-test was used. To compare the differences in the same samples under two different scenarios (e.g. untreated *versus* treatment), I used a paired t-test. I performed an unpaired t-test when the difference between the two independent or unrelated groups was compared.

I used unpaired one-way analysis of variance (ANOVA) with Dunnett's corrections to compare differences between the control group and the other two or more analysed groups. A two-way ANOVA was used to compare the influence between two different variables in two or more conditions (e.g. Wt and transgenic animal line upon RA and CS exposure). Normal distribution of residuals was tested and assured visually (using quantile-quantile plot) and formally (using Anderson-Darling, D'Agostino-Pearson, Shapiro-Wilk and Kolmogorov-Smirnov tests).

Interaction, calculated from two-way ANOVA, was considered when interpreting the results. *p* values for each comparison and interaction are noted in the graphs.

3 Results

3.1 FGF10 expression in lungs from CS-exposed and L-NIL treated mice

Using immunohistochemistry (IHC) staining, I could quantify the FGF10 expression *in situ* in experimental mouse lung sections after 8 months of RA or CS exposure treated with either placebo or the iNOS inhibitor L-NIL for additional 3 months in RA conditions (**Figure 15**). FGF10 expression, quantified as stained area, was analysed separately in alveolar septal walls and in pulmonary vessels (**Figure 15**). In order to eliminate the influence of septal wall loss (emphysema) or increase in vessel wall thickness, FGF10 stained area has always been standardized to the overall tissue area in the quantified area. In lungs from CS-exposed placebo-treated animals, FGF10 stained area was decreased in alveolar septal walls (**Figure 15A**). In contrast, it was significantly increased in the pulmonary vasculature (**Figure 15B**) compared to the RA-exposed control mice. The FGF10 stained area was significantly increased in alveolar septa (**Figure 15A**) and pulmonary vessels (**Figure 15B**) upon L-NIL treatment compared to the placebo-treated CS-exposed mice.

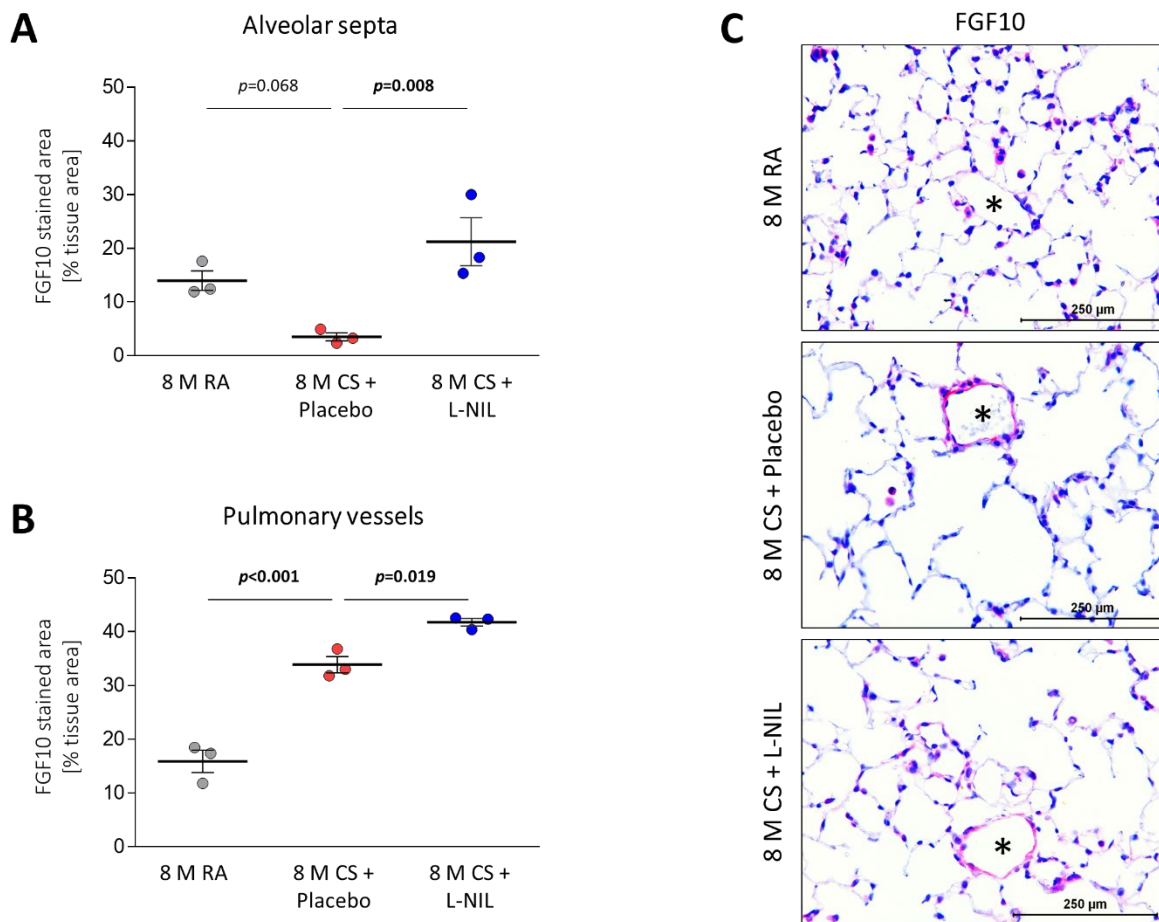


Figure 15. FGF10 expression in lungs from RA- or CS-exposed mice treated with placebo or L-NIL. FGF10 stained area was quantified separately in **(A)** alveolar septa and **(B)** the pulmonary vasculature in lungs from mice that were exposed to cigarette smoke (CS) and subsequently treated with L-NIL for additional 3 months. Room air (RA)-exposed mice and placebo-treated CS-exposed mice were used as controls. **(C)** Representative images showing FGF10 expression in lungs from experimental animals. FGF10 stained area was standardized to the tissue area in the quantified area (alveolar septa or vessel wall area); FGF10 – red, nuclei – blue; 200x magnification; scale bar: 250 μ m. Asterisks (*) points out the pulmonary vessels. Each dot in the graphs represents a value obtained from one experimental animal. The mean value for each group is represented by a horizontal line +/- standard error of the mean (SEM). Statistical analysis – Unpaired One-Way ANOVA with Dunnett’s multiple comparisons corrections; p value for each comparison is noted above.

3.1.1 FGF signalling in human COPD lungs

I further investigated the mRNA expression of FGF ligands (*FGF1*, *FGF2*, *FGF7*, *FGF9*, and *FGF10*) and FGF receptor isoforms (*FGFR1B*, *FGFR1C*, *FGFR2b*, *FGFR2C*, and *FGFR3*) in human lung

homogenates from healthy donors, smokers without and with COPD. Human lung tissues were obtained from people with end-stage COPD who had undergone lung transplantation and from healthy lung transplantation donors. The pathologist examined the lungs and determined the smoking and health status of the lung transplantation donors.

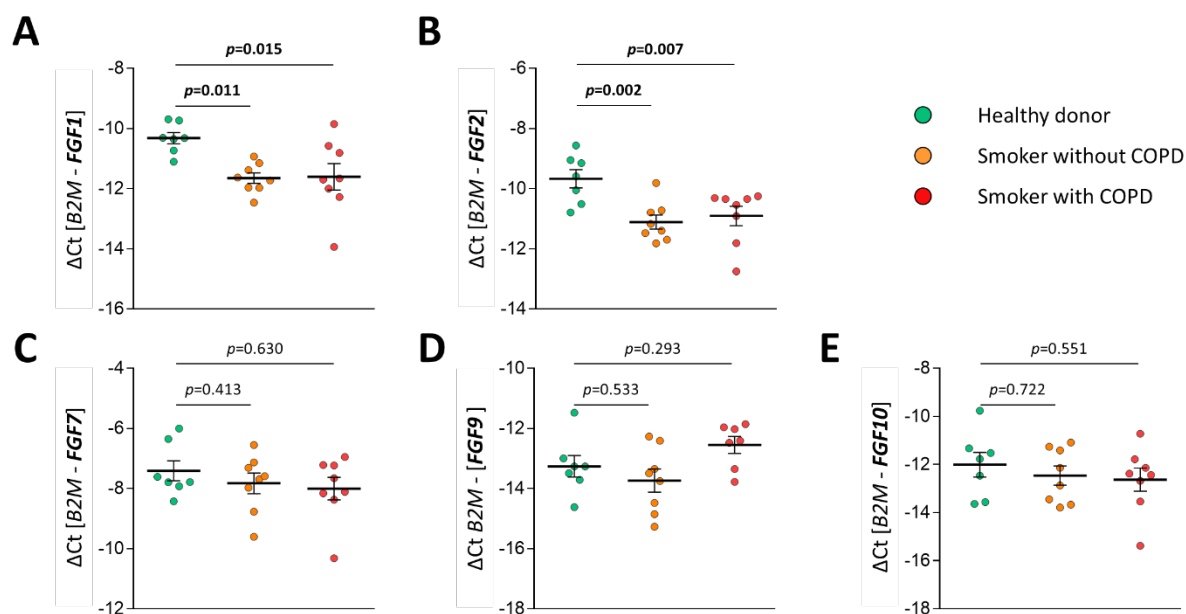


Figure 16. mRNA expression of FGF ligands in lung homogenates from healthy donors, smokers without and with COPD. mRNA expression, analysed using reverse transcription quantitative polymerase chain reaction (RTqPCR), showing ΔCt values for (A) FGF1, (B) FGF2, (C) FGF7, (D) FGF9 and (E) FGF10 in lung homogenates from healthy donors, smokers without COPD and COPD patients. The difference in threshold cycle value (ΔCt) for each given gene was calculated using beta-2-microglobulin (B2M) as a reference (housekeeping) gene. Each dot in the graphs represents a value obtained from one human subject. The mean value for each group is represented by a horizontal line \pm standard error of the mean (SEM). Statistical analysis – Unpaired One-Way ANOVA with Dunnett's multiple comparisons corrections; p value for each comparison is noted above.

FGF1 (Figure 16A) and *FGF2* (Figure 16B) were significantly downregulated on mRNA level in lung homogenates from smokers without and with COPD compared to healthy donors. *FGF7* (Figure 16C), *FGF9* (Figure 16D) and *FGF10* (Figure 16E) mRNA expression was similar in all examined groups. The expression of FGF receptors and their isoforms, *FGFR1B* (Figure 17A),

FGFR1C (Figure 17B), *FGFR2B* (Figure 17C), *FGFR2C* (Figure 17D) and *FGFR3* (Figure 17E) on mRNA level was similar in all three examined groups.

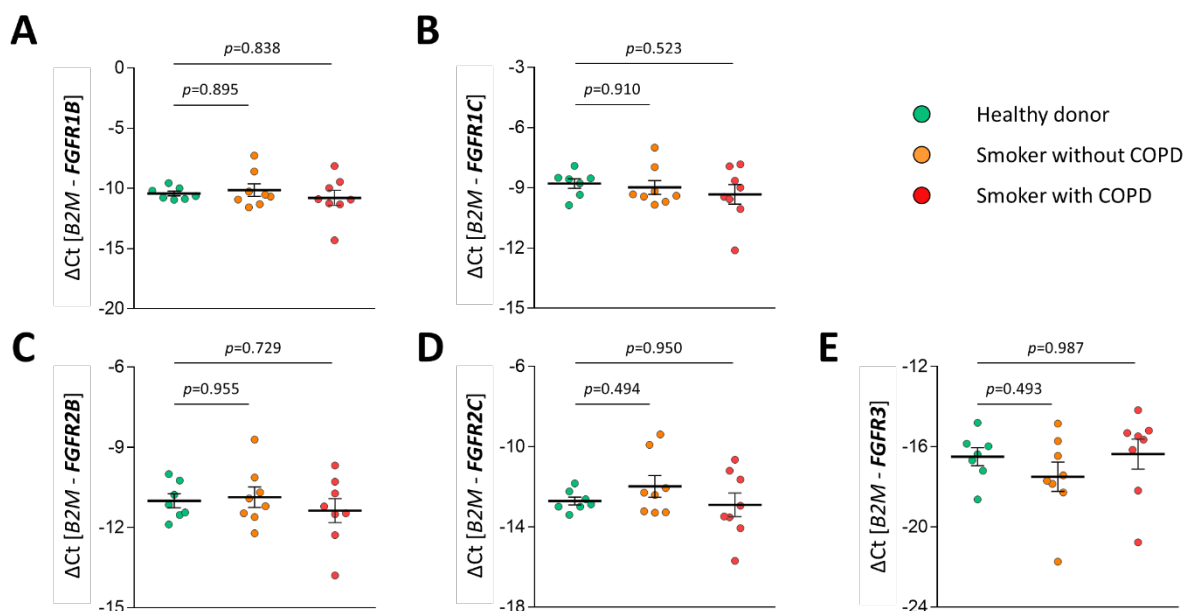


Figure 17. mRNA expression of FGF receptor isoforms in lung homogenates from healthy donors, smokers with and without COPD. mRNA expression analysed using reverse transcription quantitative polymerase chain reaction (RTqPCR), showing ΔCt values for (A) *FGFR1B*, (B) *FGFR1C*, (C) *FGFR2B*, (D) *FGFR2C* and (E) *FGFR3* in lung homogenates from healthy donors, smokers without and with COPD. The difference in threshold cycle value (ΔCt) for each given gene was calculated using beta-2-microglobulin (B2M) as a reference (housekeeping) gene. Each dot in the graphs represents a value obtained from one human subject. The mean value for each group is represented by a horizontal line +/- standard error of the mean (SEM). Statistical analysis – Unpaired One-Way ANOVA with Dunnett’s multiple comparisons corrections; p value for each comparison is noted above.

FGF10 on protein level was slightly decreased in the lung homogenates from smokers without COPD compared to healthy donors (Figure 18A). There was, however, no difference in FGF10 expression between lung homogenates from healthy donors and smokers with COPD. Expression of FGFR2 on protein level was similar in lung homogenates from all examined groups (Figure 18B). However, I could observe a considerable variance in FGF10 and FGFR2 expression in lung homogenates from smokers with COPD. Therefore, I performed IHC staining

for FGF10 and FGFR2 in paraffin-cut lung sections from healthy donors, smokers without and with COPD (**Figure 19 and 20**).

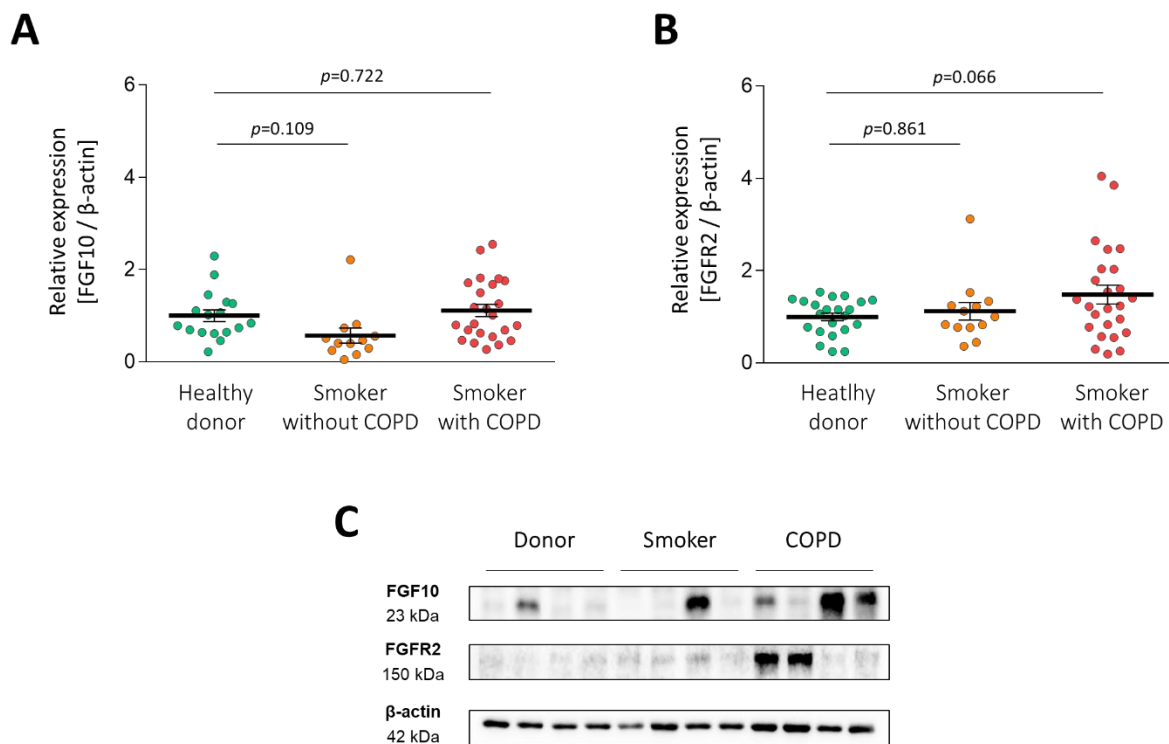


Figure 18. FGF10 and FGFR2 protein expression in lung homogenates from healthy donors, smokers without and with COPD. Relative expression of **(A)** FGF10 and **(B)** FGFR2 assessed by Western blot in lung homogenates from donors, smokers without COPD and COPD patients. Representative blots depict **(C)** FGF10 / β -actin and FGFR2 / β -actin expression in the analysed groups. Protein expression in Western blot was quantified by band densitometry and standardized to β -actin; relative expression was calculated by standardizing each value to the mean value of the donor control group. Each dot in the graphs represents a value obtained from one donor or patient. The mean value for each group is represented by a horizontal line +/- standard error of the mean (SEM). Statistical analysis – Unpaired One-Way ANOVA with Dunnett’s multiple comparisons corrections; p value for each comparison is noted above.

IHC stained lung sections from human patients revealed that FGF10 (**Figure 19A**) and FGFR2 (**Figure 19B**) are expressed in alveolar septa, as well as in pulmonary vasculature. The expression patterns differed between these two compartments in smokers without and with COPD (**Figure 19, 20**).

The FGF10 stained area was significantly decreased in the alveolar septa from smokers without COPD compared to donors (**Figure 20A**). In septa from smokers with COPD, the FGF10 stained area further decreased and was significantly lower compared to smokers without COPD or healthy donors (**Figure 20A**). However, the FGF10 stained area was significantly increased in the pulmonary vasculature of smokers with COPD, compared to healthy donors and smokers without COPD (**Figure 19B**). The FGF10 stained area was not changed in vessels from smokers without COPD compared to donors (**Figure 19B**).

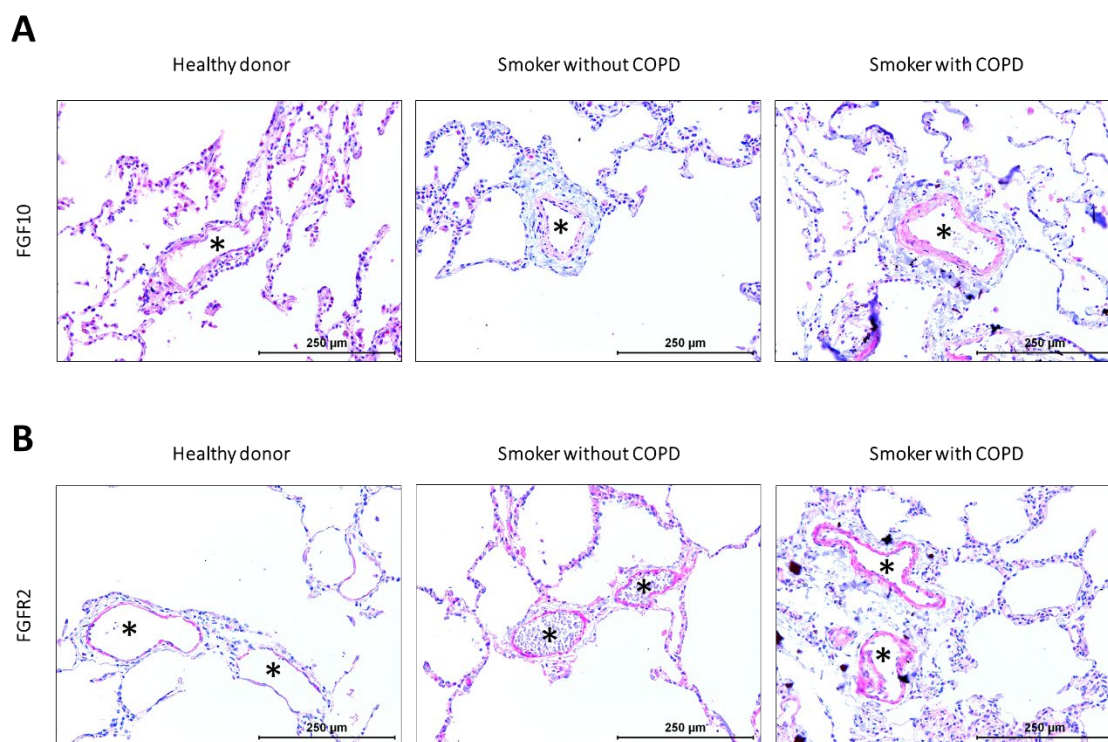


Figure 19. Representative images showing FGF10 and FGFR2 IHC staining in human lungs from healthy donors, smokers without and with COPD. (A) FGF10 and (B) FGFR2 immunohistochemistry (IHC) staining in lung sections from healthy donors, smokers without and with COPD. Asterisks (*) point out pulmonary vessels. FGF10 / FGFR2 – red, nuclei – blue; 200x magnification; scale bar: 250 µm.

In alveolar septa from smokers without COPD compared to healthy donors, I could observe a significant increase in the FGFR2 stained area (**Figure 20C**). However, there was no difference in the FGFR2 stained area between healthy donors and smokers with COPD in alveolar septa

(Figure 20C). In the pulmonary vasculature of smokers with COPD, the FGFR2 stained area was significantly increased compared to healthy donors and smokers without COPD (Figure 20D). Vessels from smokers without COPD had a similar FGFR2 stained area like healthy donors (Figure 20D).

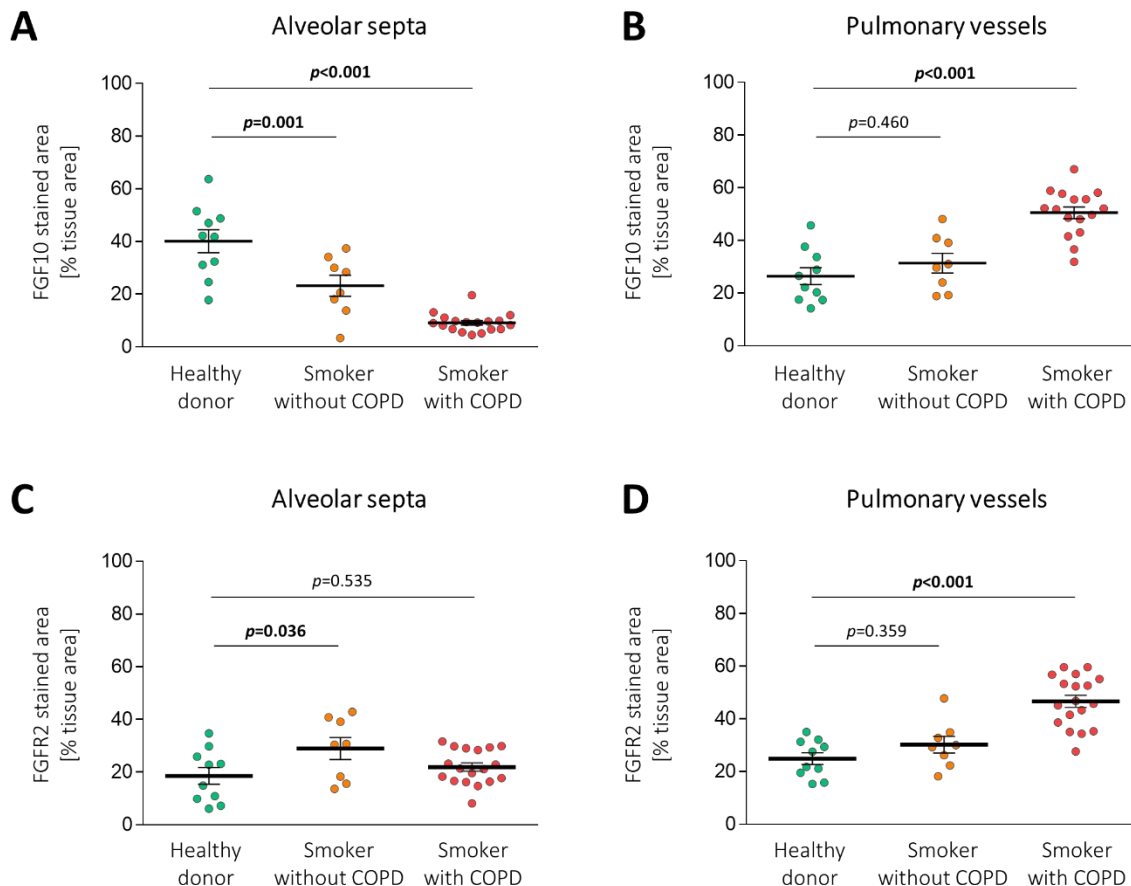


Figure 20. Differential expression of FGF10 and FGFR2 in alveolar septal wall and in pulmonary vessels of healthy donors, smokers without and with COPD. FGF10 expression was quantified separately in (A) alveolar septal walls and (B) pulmonary vessels in human lungs from healthy donors, smokers without and with COPD. Similarly, FGFR2 expression was quantified in (C) alveolar septa and (D) pulmonary vasculature. FGF10 or FGFR2 stained area was always standardized to the tissue area in the quantified area (alveolar septa or vessel wall area). Each dot in the graphs represents a value obtained from one human subject. The mean value for each group is represented by a horizontal line +/- standard error of the mean (SEM). Statistical analysis – Unpaired One-Way ANOVA with Dunnett’s multiple comparisons corrections; p value for each comparison is noted above.

FGF10 is a paracrine factor with a limited diffusion capacity, secreted mainly by mesenchymal cells in the lung (Yuan *et al.* 2018; Bellusci *et al.* 1997). To identify cells responsible for the altered expression of FGF10, I investigated the FGF10 expression in interstitial lung fibroblasts and pulmonary arterial smooth muscle cells (PASMCs) isolated from donor lungs (**Figure 21**). Afterwards, I tested possible cellular mechanisms underlying FGF10 expression regulation in primary culture of isolated interstitial lung fibroblast.

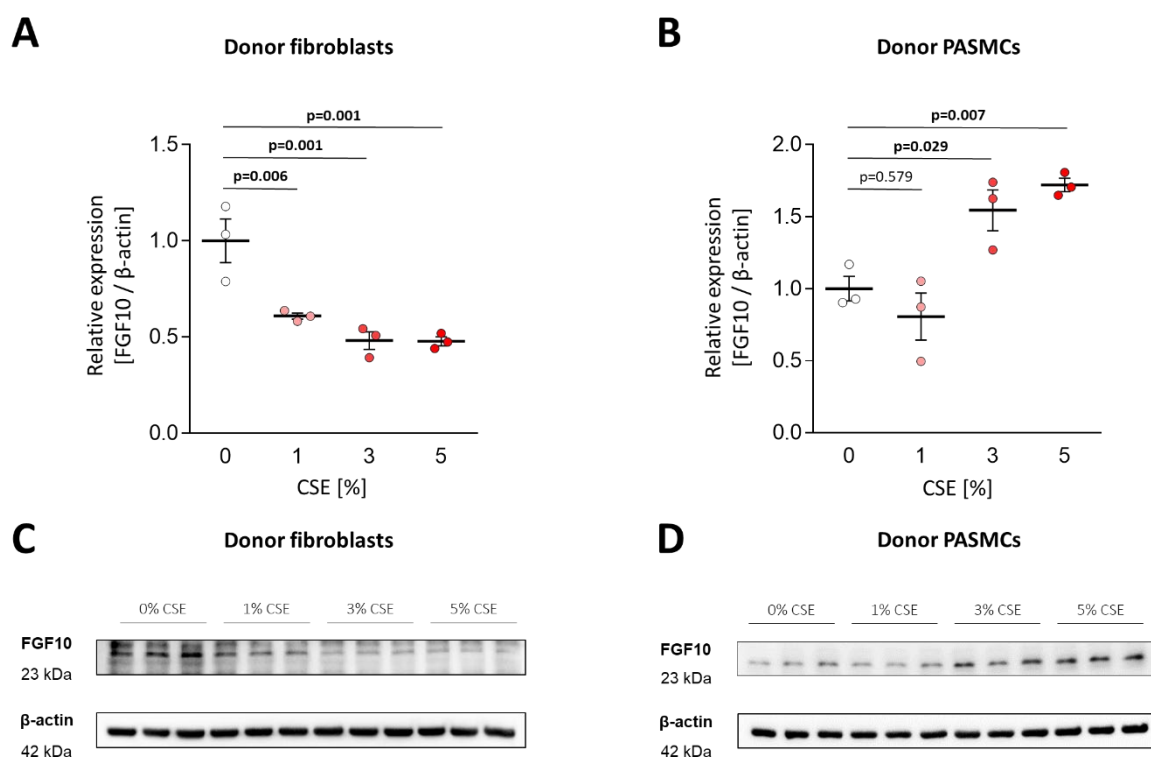


Figure 21. FGF10 expression in CSE-treated donor interstitial lung fibroblasts and PASMCs. Relative expression of FGF10 in **(A)** interstitial lung fibroblasts and **(B)** donor pulmonary arterial smooth muscle cells (PASMCs) isolated from a healthy donor and treated with increasing concentrations of cigarette smoke extract (CSE). Representative blots show FGF10 and β -actin in **(C)** fibroblasts and **(D)** PASMCs. Protein expression in Western blot was quantified by band densitometry and standardized to β -actin; relative expression was calculated by standardizing each value to the mean value of the untreated control group. Interstitial lung fibroblasts or PASMCs are isolated from one human donor; $n=3$ are technical replicates (repeated experiments with cells isolated from one donor). The mean value for each group is represented by a horizontal line \pm standard error of the mean (SEM). Statistical analysis – Unpaired One-Way ANOVA with Dunnett’s multiple comparisons corrections; p value for each comparison is noted above.

As a surrogate of CS exposure, cells were *in vitro* treated with increasing concentrations of cigarette smoke extract (CSE). FGF10 expression on the protein level was significantly decreased in human fibroblasts treated with CSE compared to the untreated cells (**Figure 21A, C**). Already at a low dose – 1% CSE, I observed a significant FGF10 downregulation in fibroblasts (**Figure 21A, C**). PSMCs treated with 3 or 5% CSE had significantly increased FGF10 expression compared to the untreated control cells (**Figure 21B, D**).

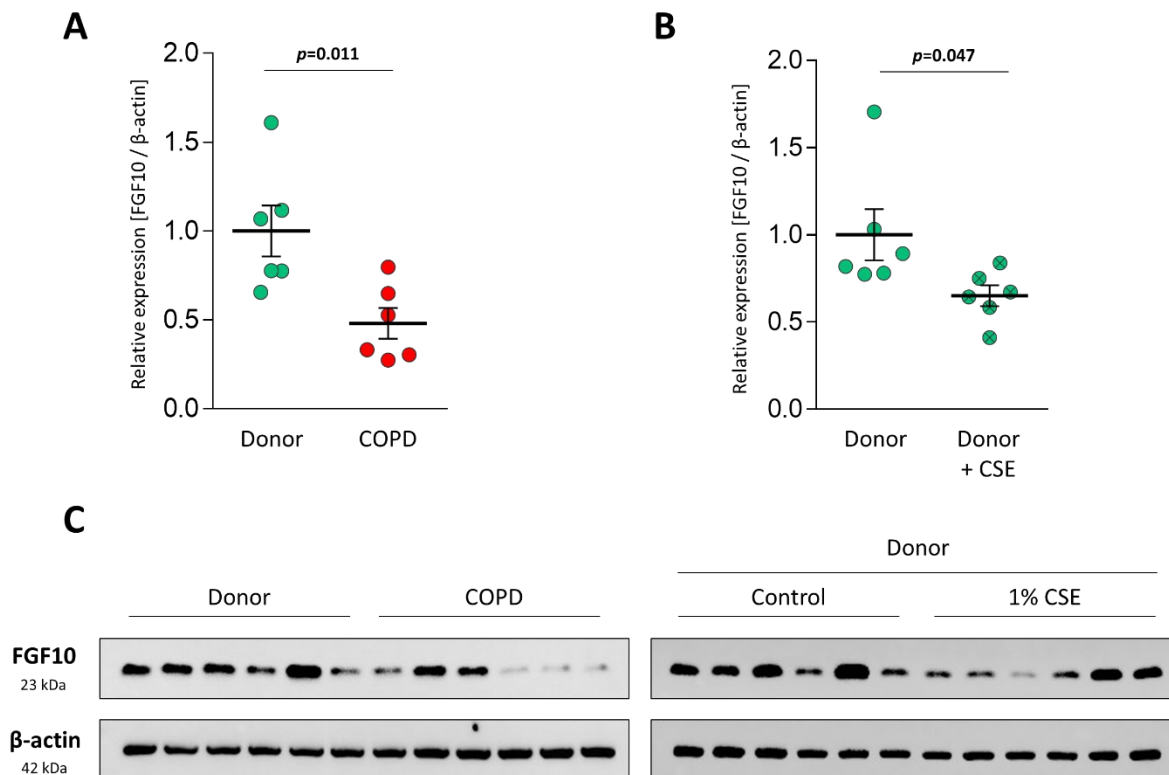


Figure 22. FGF10 expression in interstitial lung fibroblasts isolated from donor and COPD lungs. (A) FGF10 expression quantified by Western blotting in lung interstitial fibroblasts isolated from n=6 donors and n=6 COPD patients. FGF10 expression in human fibroblasts from (B) donors and (C) COPD patients treated with cigarette smoke extract (CSE). (D) Representative blots used for the quantification. The mean value for each group is represented by a horizontal line \pm standard error of the mean (SEM). Protein expression in Western blot was quantified by band densitometry and standardized to β -actin; relative expression was calculated by standardizing each value to the mean value of the control group (donor or untreated control). Statistical analysis – (A) Unpaired t-test or (B) paired t-test; p value for each comparison is noted above.

Following this line, I analysed FGF10 expression in interstitial lung fibroblasts isolated from lungs explanted from 6 donors and 6 individuals with COPD (**Figure 22**). Despite the *in vitro* propagation, interstitial lung fibroblasts from COPD patients had significantly lower FGF10 expression compared to the healthy donors (**Figure 22A**). CSE treatment significantly decreased FGF10 expression in donor fibroblasts (**Figure 22B**).

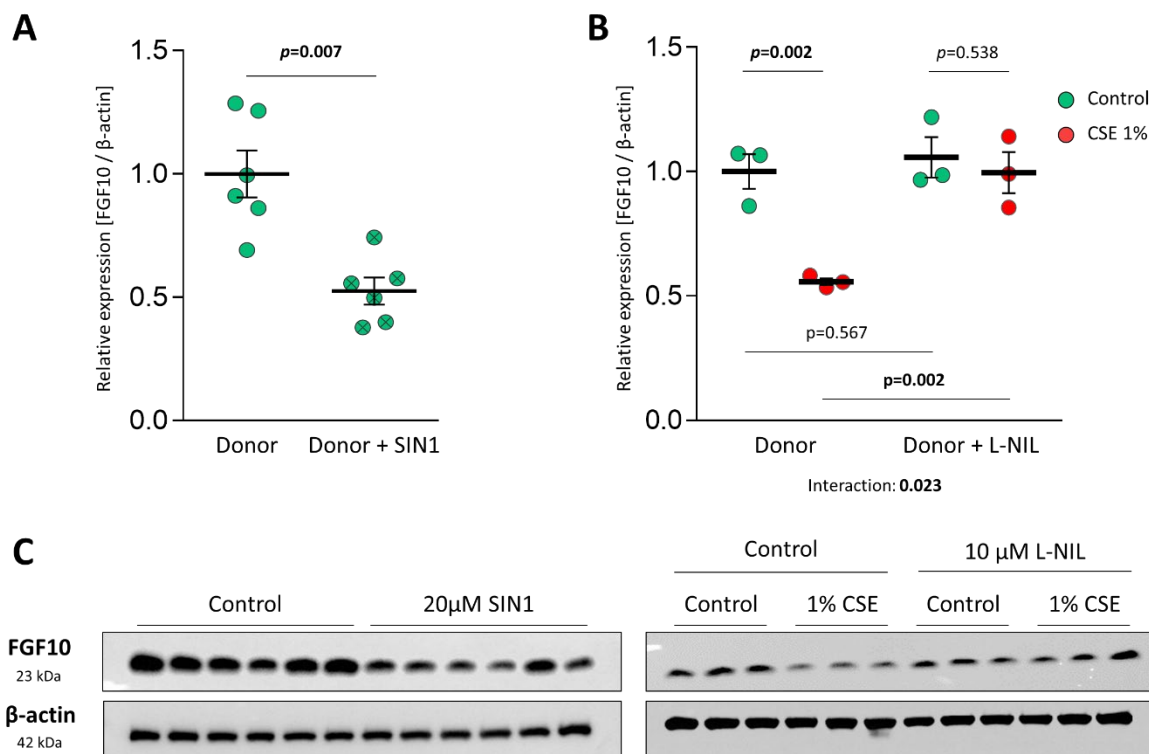


Figure 23. FGF10 expression in interstitial lung fibroblasts upon peroxynitrite stress. (A) FGF10 expression quantified by Western blotting in lung interstitial fibroblasts isolated from $n=6$ donors lungs and treated with the peroxynitrite (ONOO⁻) donor – 3-morpholininosydnonimine N-ethylcarbamide (SIN-1). **(B)** The effect of cigarette smoke extract (CSE) treatment on donor fibroblast with or without pre-treatment with specific iNOS inhibitor N6-(1-iminoethyl)-L-lysine (L-NIL). **(C)** Representative blots used for the quantification. The mean value for each group is represented by a horizontal line \pm standard error of the mean (SEM). Protein expression in Western blot was quantified by band densitometry and standardized to β -actin; relative expression was calculated by standardizing each value to the mean value of the donor untreated control group. Statistical analysis – (A) Paired t-test or (B) Unpaired Two-Way ANOVA; p values for each comparison and interaction are noted in the graphs.

Next, I examined if FGF10 is affected by peroxynitrite. Since peroxynitrite is an unstable reactive peroxide, I treated interstitial lung fibroblasts with peroxynitrite donor – SIN-1 (3-

morpholinosydnonimine N-ethylcarbamide) (Hogg *et al.* 1992). In *in vitro* conditions, in presence of oxygen and absence of HEPES (4-(2-hydroxyethyl)-1-piperazineethanesulfonic acid) buffering, SIN-1 simultaneously releases NO and superoxide, forming peroxynitrite (Lomonosova *et al.* 1998; Hogg *et al.* 1992). FGF10 expression was significantly decreased in donor interstitial lung fibroblasts treated with SIN-1 (**Figure 23A**).

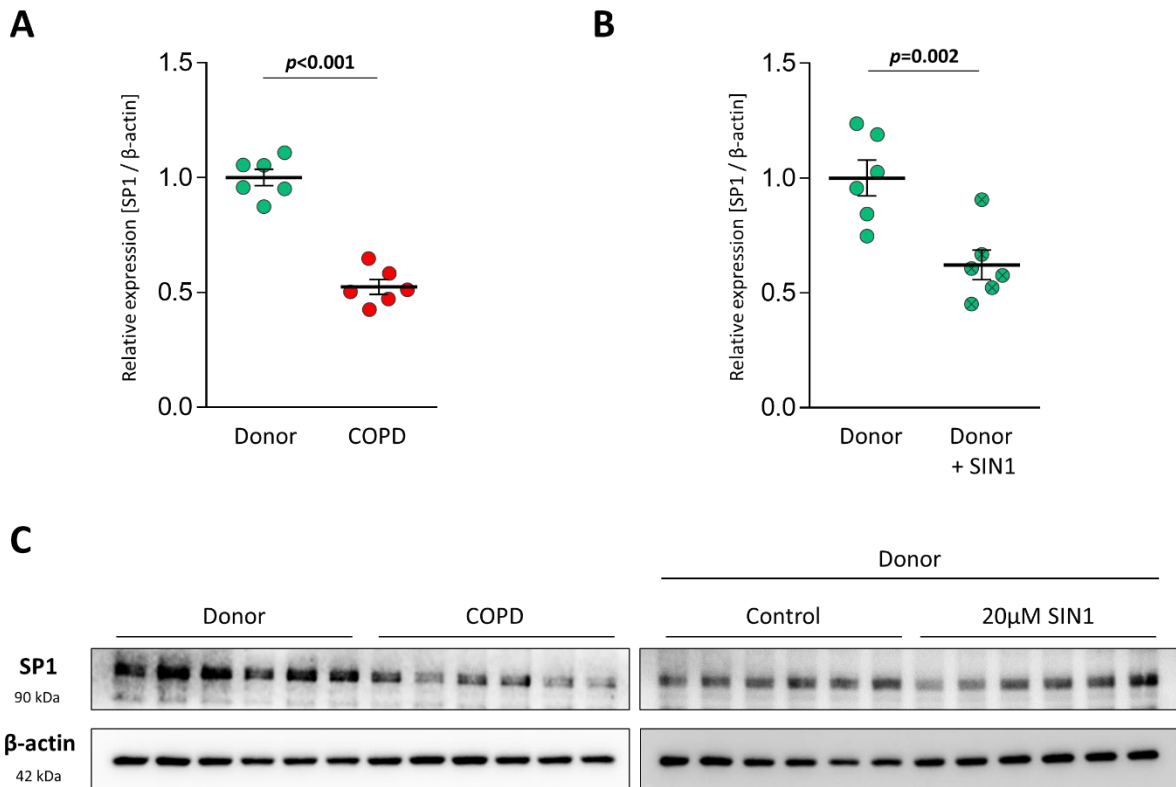


Figure 24. Expression of transcription factor SP1 in interstitial fibroblasts isolated from donor and COPD lungs. Western blot quantification of transcription factor specific protein 1 (SP1) expression in interstitial fibroblasts isolated from **(A)** n=6 donor and n=6 COPD lungs or **(B)** donor fibroblasts treated with peroxynitrite (ONOO-) donor – SIN-1. **(C)** Representative blot scans for SP1 in interstitial lung fibroblasts. The mean value for each group is represented by a horizontal line +/- standard error of the mean (SEM). Protein expression in Western blot was quantified by band densitometry analysis and standardized to β -actin; relative expression was calculated by standardizing each value to the mean value of the control group (donors or untreated controls). Statistical analysis – (A) Unpaired t-test or (B) paired t-test; p value for each comparison is noted above.

As shown above, iNOS inhibition increased FGF10 expression in alveolar septa of mice exposed to CS for 8 months. Correspondingly, L-NIL treatment abolished the decrease of FGF10 expression in interstitial lung fibroblast treated with 1% CSE (**Figure 23B**). Donor fibroblasts pre-treated with 10 μ M L-NIL had significantly higher FGF10 expression upon CSE treatment than CSE-treated cells without L-NIL (**Figure 23B**). At this concentration, L-NIL treatment alone did not have any effect on the FGF10 expression (**Figure 23B**).

Finally, using a hypothesis-driven approach, I investigated the potential role of transcription factor specific protein 1 (SP1) in transcriptional regulation of FGF10 expression in interstitial lung fibroblasts (Benjamin *et al.* 2010; Kelly *et al.* 2014; Prince 2018). SP1 expression was significantly lower in interstitial lung fibroblasts isolated from COPD lungs compared to donors (**Figure 24A**). Furthermore, peroxynitrite stress upon SIN-1 treatment significantly downregulated SP1 expression in donor fibroblasts (**Figure 24B**).

3.1.2 CS-induced emphysema in mice with impaired FGF10 signalling

In order to decipher the role of the FGF10-FGFR2b signalling axis in the development of CS-induced emphysema and PH, I used FGF10 and FGFR2b haploinsufficient (*Fgf10*^{+/-} and *Fgfr2b*^{+/-}) mice. As mentioned earlier, mice with homozygous deletion of *Fgf10* die at birth due to lung aplasia.

Together with their Wt littermates (both functional copies of *Fgf10* and *Fgfr2b* alleles), transgenic mice were exposed to CS for 3 or 8 months. Control animals (further referred as RA controls) were kept under similar conditions but without CS exposure. Simplification of the distal lung parenchyma of experimental mice was quantified histologically in H&E stained lung sections using random uniform sampling and alveolar morphometry software (**Figure 25**). At the 3-month time-point, airspace percentage remained unchanged in *Fgf10*^{+/-} and *Fgfr2b*^{+/-} mice that were not exposed to CS, compared to corresponding Wt littermates (**Figure 25A**). In the RA-exposed *Fgf10*^{+/-} mice at the 3-months time-point, I observed a slight but significant increase in mean linear intercept (MLI; **Figure 25C**) and micro-computed tomography (μ CT)-measured air-to-tissue volume ratio (**Figure 26A**). This could be due to impaired airway branching during development.

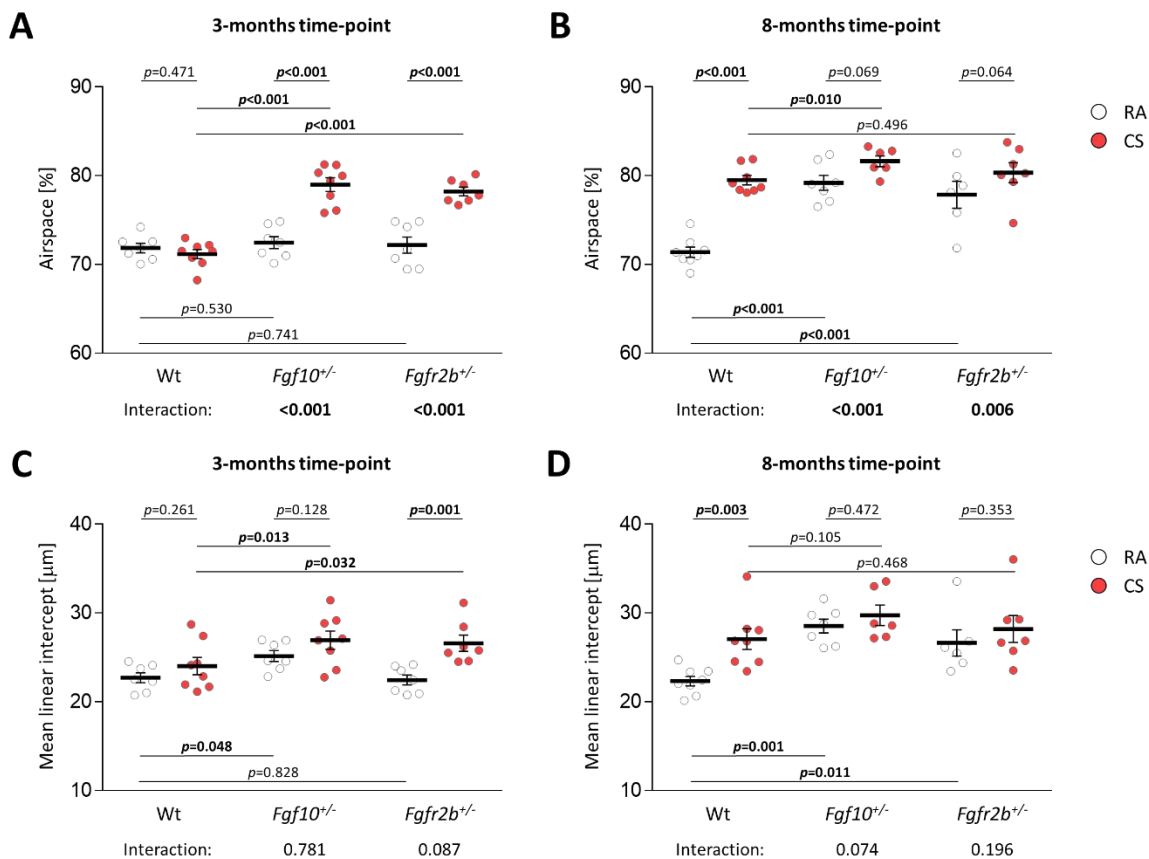


Figure 25. Histological examination of the lung parenchyma in RA- and CS-exposed Wt mice and mice with impaired FGF10 signalling. Alveolar morphometry software was employed to assess (A, B) airspace percentage and (C, D) mean linear intercept in H&E stained lung sections of Wt, *Fgf10*^{+/-}, and *Fgfr2b*^{+/-} animals after (A, C) 3 or (B, D) 8 months of room air (RA) or cigarette smoke (CS) exposure. Each dot represents a measurement from one experimental animal. The mean value for each group is represented by a horizontal line +/- standard error of the mean (SEM). Statistical analysis – Unpaired Two-Way ANOVA; p values for each comparison and interaction are noted in the graphs.

Interestingly, at the 3-months time-point, CS-exposed *Fgf10*^{+/-} and *Fgfr2b*^{+/-} mice, but not Wt littermates, had significantly increased increased airspace percentage (Figure 25A) and MLI (Figure 25C) and air-to-tissue volume ratio (Figure 26A) compared to corresponding controls. Such results indicate higher susceptibility and early emphysema development in animals with impaired FGF10 signalling.

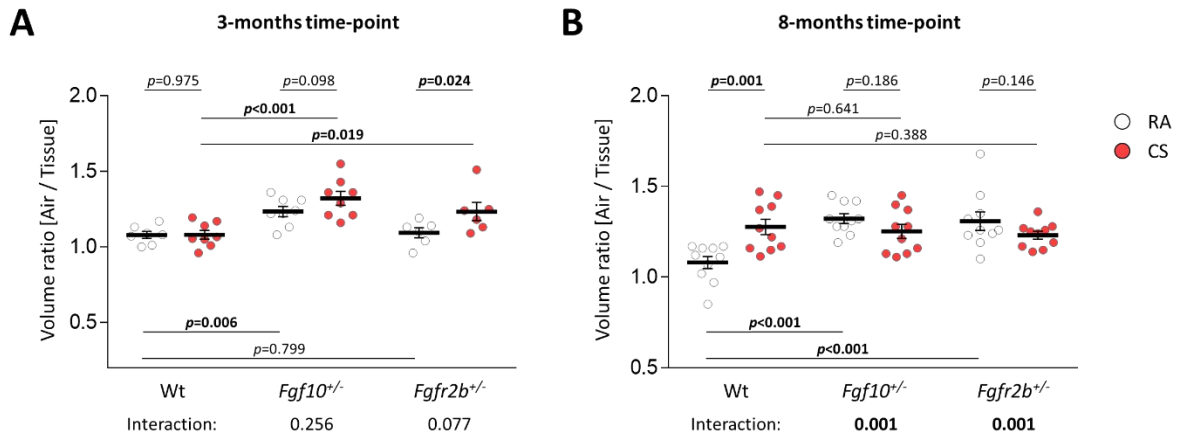


Figure 26. μ CT examination of the lung structure in RA- and CS-exposed Wt mice and mice with impaired FGF10 signalling. Air to tissue volume ratio was assessed *in vivo* by microcomputed tomography (μ CT) in *Wt*, *Fgf10*^{+/-}, and *Fgfr2b*^{+/-} animals after (A) 3 or (B) 8 months of room air (RA) or cigarette smoke (CS) exposure. Each dot represents a measurement from one experimental animal. The mean value for each group is represented by a horizontal line +/- standard error of the mean (SEM). Statistical analysis – Unpaired Two-Way ANOVA; p values for each comparison and interactions are noted in the graphs.

Consistently with previously published results, only after 8 months of CS exposure, Wt mice developed enlarged airspace (Figure 25B), increased MLI (Figure 25D) and increased air-to-tissue volume ratio (Figure 26B). Astonishingly, at the 8-months time-point, RA-exposed *Fgf10*^{+/-} and *Fgfr2b*^{+/-} mice developed spontaneous emphysema, characterised by significantly increased airspace percentage (Figure 25B), MLI (Figure 25D) and air to tissue volume ratio (Figure 26B) compared to the respective RA-exposed Wt controls. These parameters in transgenic mice remained unchanged upon 8 months of CS exposure (Figure 25B, 25D, 26B). These findings were further verified using design-based stereology, where alveoli density was determined (Figure 27). The alveoli number was calculated by relating the density of alveoli to the measured lung volume.

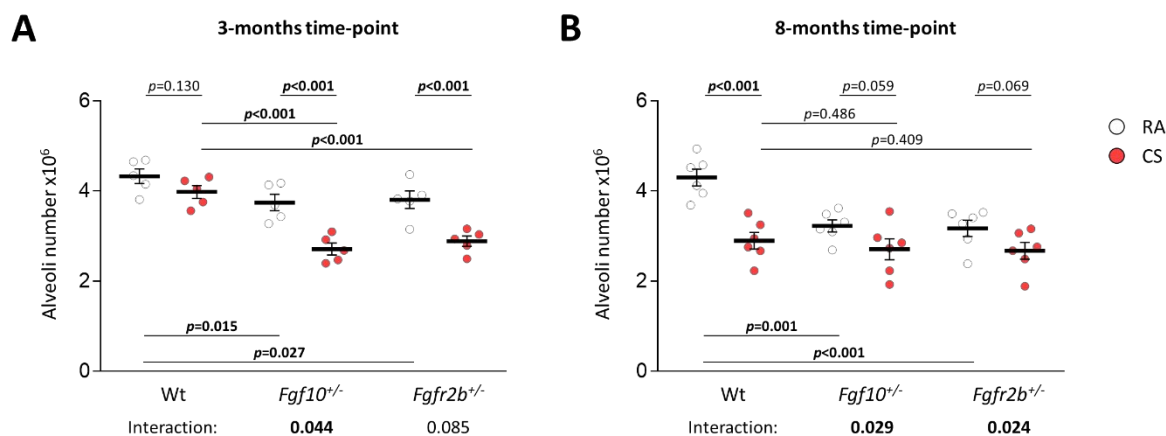


Figure 27. Alveoli number in RA- and CS-exposed Wt mice and mice with impaired FGF10 signalling. The number of alveoli in the left lung lobe of Wt, *Fgf10*^{+/-}, and *Fgfr2b*^{+/-} animals after **(A)** 3 or **(B)** 8 months of RA or CS exposure was determined using design-based stereology. Each dot represents a measurement from one experimental animal. The mean value for each group is represented by a horizontal line +/- standard error of the mean (SEM). Statistical analysis – Unpaired Two-Way ANOVA; p values for each comparison and interactions are noted in the graphs.

In contrast to the Wt animals, which developed emphysema after 8 months of CS exposure, designed-based stereology confirmed that CS-exposed transgenic mice had decreased alveoli number already after 3 months of CS exposure (**Figure 27A**). In addition, I observed a slight decrease in alveoli number in RA-exposed *Fgf10*^{+/-} and *Fgfr2b*^{+/-} compared to the corresponding Wt controls (**Figure 27A**).

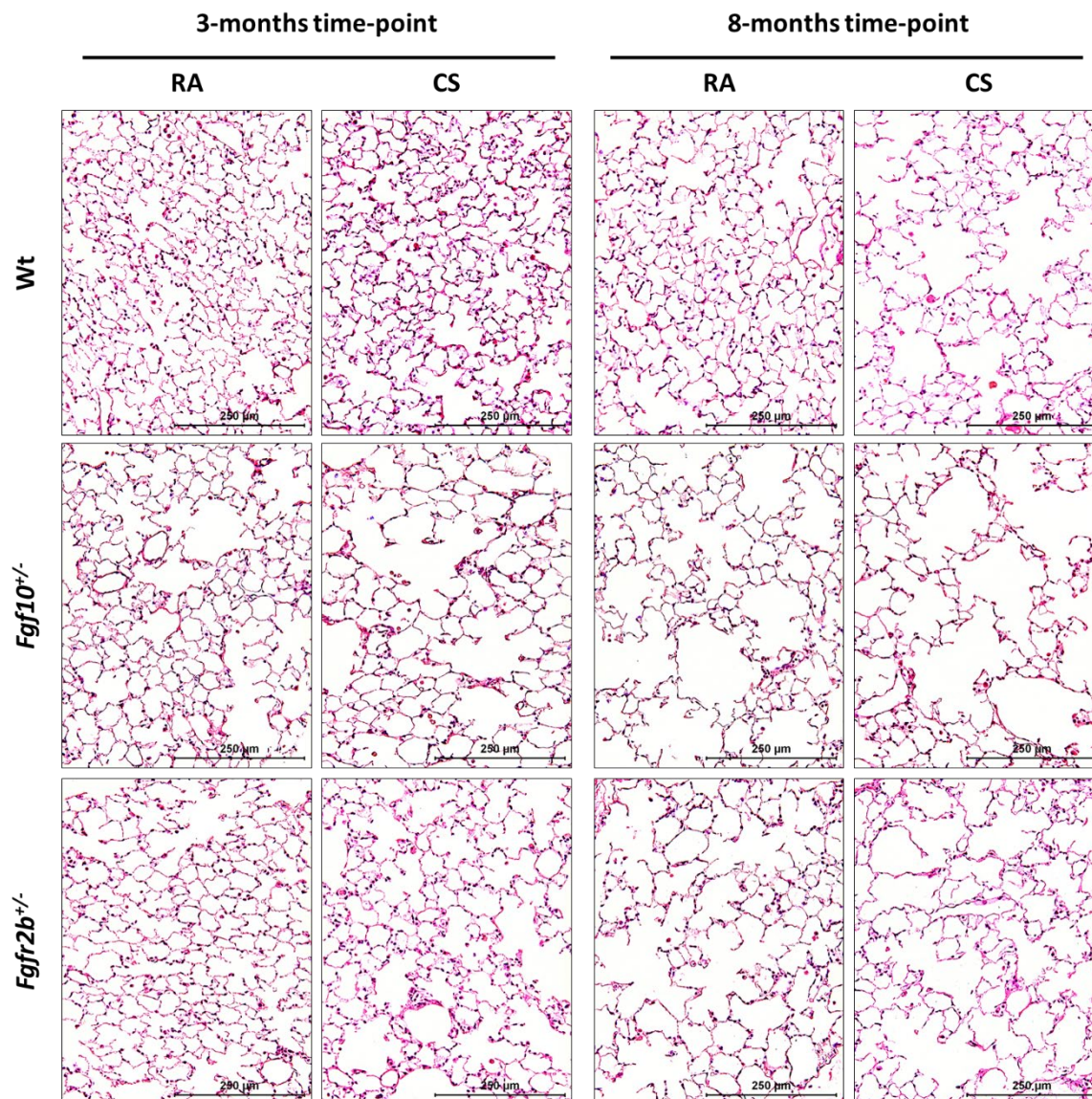


Figure 28. Representative images showing the lung structure in RA- and CS-exposed Wt mice and mice with impaired FGF10 signalling. Lung parenchyma in Wt (up), *Fgf10*^{-/-} (middle) or *Fgfr2b*^{+/-} (low) mice after 3 (left) and 8 (right) months of cigarette smoke (CS) exposure. Corresponding age-matched mice exposed to room air (RA) were used as corresponding controls. H&E staining (blue-nuclei, red-cytoplasm); 200x magnification; scale bar: 250 μm.

At the 8-month time-point, RA-exposed *Fgf10*^{-/-} and *Fgfr2b*^{+/-} mice had considerably lower alveoli number compared to the corresponding Wt controls (**Figure 27B**). Hence, the alveoli number in these groups was in the range of CS-exposed Wt mice. Long-term CS exposure did not result in a significant further decrease in alveoli number in the transgenic animals (**Figure**

27B). Representative images of H&E stained lung sections depicting the distal lung parenchyma in experimental mice after 3 or 8 months of RA and CS exposure are shown in **Figure 28**.

To characterise the severity of emphysema, I performed *in vivo* lung function test and measured lung compliance (**Figure 29**), overall respiratory system resistance (**Figure 30A, 30B**), Newtonian (airway) resistance (**Figure 30C, 30D**) and tissue damping (**Figure 31A, 31B**). *Fgfr2b*^{+/-}, but not *Fgf10*^{+/-}, mice exhibited an increase in static lung compliance already after 3 months of CS exposure, compared to the corresponding controls (**Figure 29A**). As expected, only long-term CS exposure for 8 months led to a significant increase in lung compliance in Wt mice (**Figure 29B**). At the 8-months time-point, RA-exposed *Fgfr2b*^{+/-} mice had significantly increased lung compliance, when compared to corresponding Wt controls. Lung compliance in these animals was not further increased with CS exposure (**Figure 29B**).

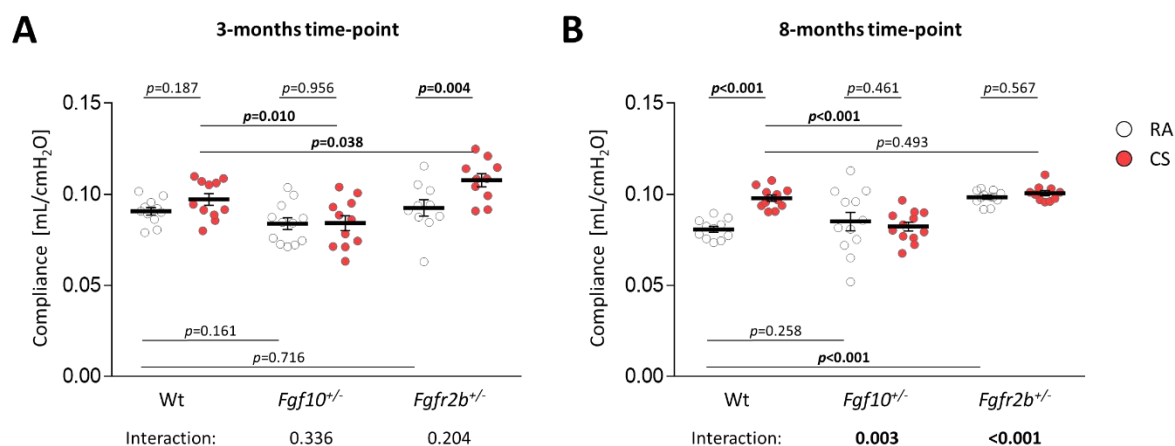


Figure 29. *In vivo* lung compliance in RA- and CS-exposed Wt mice and mice with impaired FGF10 signalling. Static lung compliance was measured by *in vivo* lung function test in Wt, *Fgf10*^{+/-}, and *Fgfr2b*^{+/-} animals after CS exposure for **(A)** 3 or **(B)** 8 months. Corresponding age-matched mice exposed to room air (RA) were used as controls. The mean value for each group is represented by a horizontal line +/- standard error of the mean (SEM). Statistical analysis – Unpaired Two-Way ANOVA; p values for each comparison and interactions are noted in the graphs.

Interestingly, lung compliance in *Fgf10*^{+/-} mice remained unchanged upon 3 or 8 months of CS exposure (**Figure 29**). Lung compliance in these animals was also not affected by ageing (**Figure 29**). Correspondingly, CS-exposed *Fgf10*^{+/-}, at 3- and 8-months time-points, had significantly

decreased lung compliance compared to the corresponding CS-exposed Wt littermates (**Figure 29**). Namely, the lung compliance results obtained from *Fgf10*^{+/-} mice did not correspond to the histologically quantified emphysema.

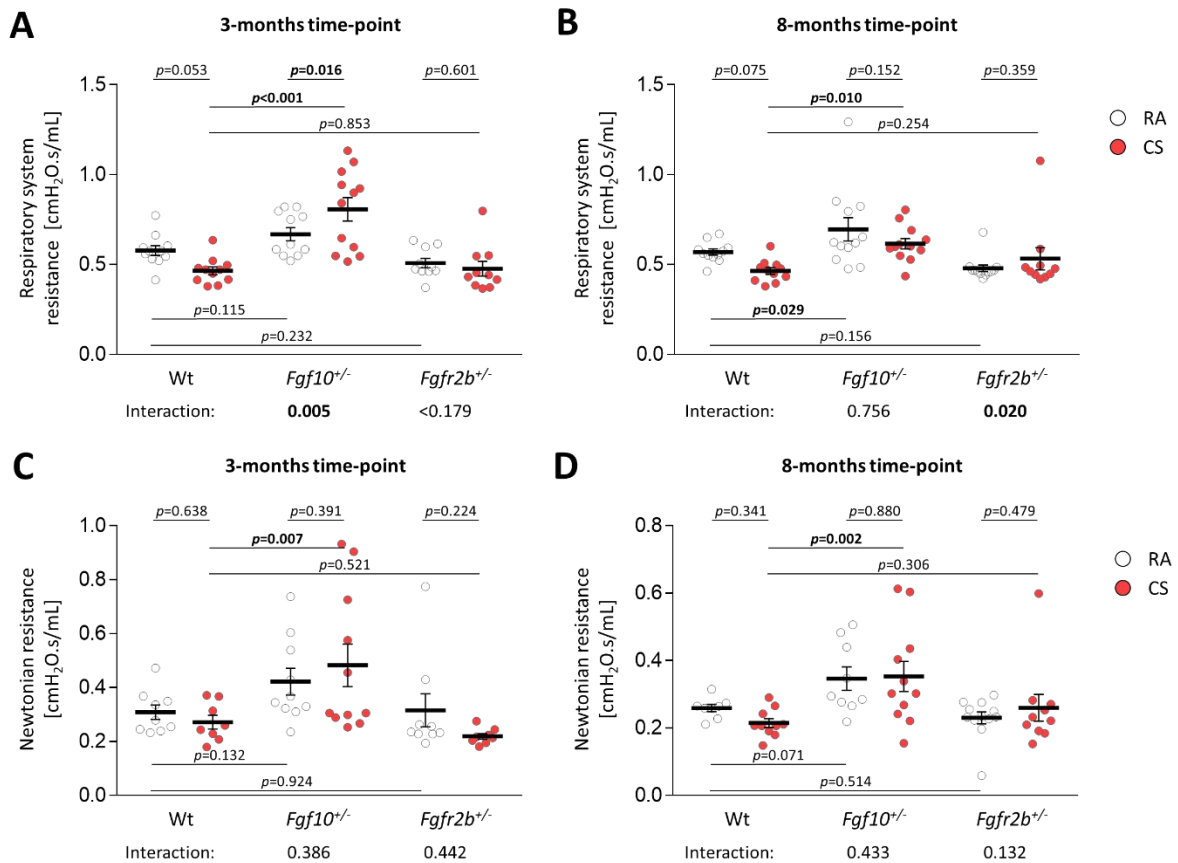


Figure 30. Respiratory resistance in Wt mice and mice with impaired FGF10 signalling. (A, B) Overall respiratory system resistance and **(C, D)** conducting airway (Newtonian) resistance measured by *in vivo* lung function test in Wt, *Fgf10*^{+/-}, and *Fgfr2b*^{+/-} animals after room air (RA) or cigarette smoke (CS) exposure for (A, C) 3 or (B, D) 8 months. Corresponding age-matched mice exposed to room air (RA) were used as corresponding controls. The mean value for each group is represented by a horizontal line +/- standard error of the mean (SEM). The mean value for each group is represented by a horizontal line +/- standard error of the mean (SEM). Statistical analysis – Unpaired Two-Way ANOVA; p values for each comparison and interactions are noted in the graphs.

To identify the cause of the observed discrepancy in the lung compliance data in *Fgf10*^{+/-} mice, I extensively analysed other parameters measured by lung function test. *Fgf10*^{+/-} mice, after 3 or 8 months of CS exposure, indeed exhibited significantly increased overall respiratory system

resistance (RRS) compared to corresponding Wt controls (**Figure 30A, 30B**). Overall respiratory system resistance could be increased due to increased airway and/or tissue resistance.

Newtonian resistance, a resistance component related to the conductive airways, was significantly increased in CS-exposed *Fgf10^{+/-}* mice at 3- and 8-months time-points, compared to the corresponding CS-exposed Wt controls (**Figure 30C, 30D**). This could suggest airflow limitation in these animals. RRS and Newtonian resistance were not affected in CS-exposed Wt mice (**Figure 30**). Furthermore, RRS and Newtonian resistance remained unchanged in *Fgfr2b^{+/-}* mice (**Figure 30**). Tissue damping, as a measure of distal tissue stiffness, was also significantly increased in CS-exposed *Fgf10^{+/-}* mice at 3- and 8-months time-points, compared to the corresponding Wt controls (**Figure 31A, 31B**). Since tissue damping corresponds to the stiffness of the distal lung parenchyma, I investigated the collagen deposition in alveolar septal walls in *Fgf10^{+/-}* mice. Even though I did not observe any typical signs of lung fibrosis, picosirius red staining revealed increased collagen deposition in the septa of 8 months CS-exposed Wt mice (**Figure 31C, 31D**). *Fgf10^{+/-}* mice had more collagen in RA conditions which increased further with CS exposure (**Figure 31C, 31D**). While collagen in CS-exposed Wt animals appeared organised in short fibres, in *Fgf10^{+/-}* mouse lungs, collagen filaments seemed interconnected and spread through septal walls (**Figure 31C**), which could be responsible for increased tissue damping and RRS.

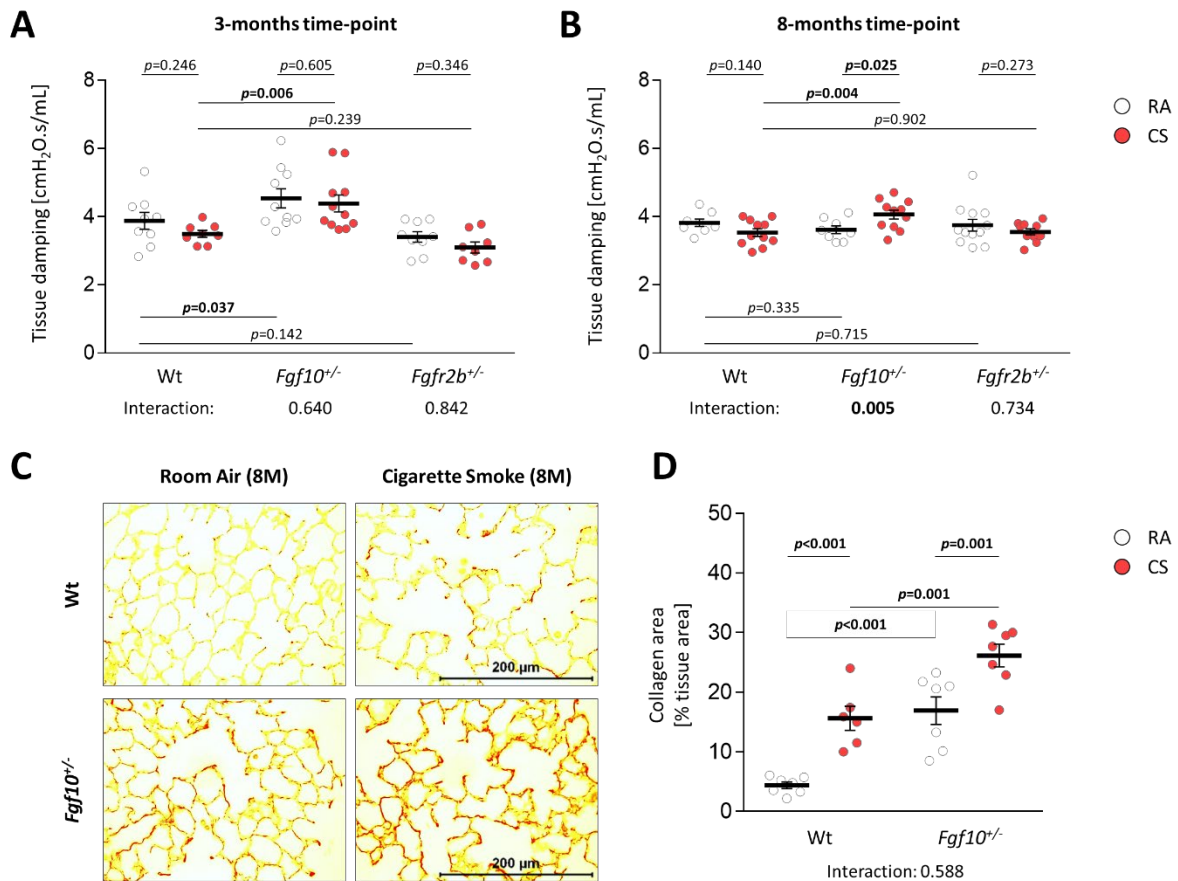


Figure 31. Alterations in the distal lung parenchyma in RA- and CS-exposed mice with impaired FGF10 signalling. Stiffness of the distal lung parenchyma – (A, B) tissue damping was measured in Wt, *Fgf10*^{+/-}, and *Fgfr2b*^{+/-} animals after room air (RA) or cigarette smoke (CS) exposure for (A) 3 or (B) 8 months using *in vivo* lung function test. (C) Representative images of picosirious red staining used to visualise collagen in lung parenchyma from Wt and *Fgf10*^{+/-} mice after 8 months of CS exposure. Corresponding age-matched mice, which were exposed to RA, were used as controls. (D) Collagen stained area (red) was quantified and standardized to the total stained area of alveolar septal walls (stained yellow). 400x magnification; scale bar: 200 μ m. The mean value for each group is represented by a horizontal line +/- standard error of the mean (SEM). Statistical analysis – Unpaired Two-Way ANOVA; p values for each comparison and interactions are noted in the graphs.

3.1.3 CS-induced PH in mice with impaired FGF10 signalling

Early in the adult life of *Fgf10*^{+/-} and *Fgfr2b*^{+/-} mice, before simplification of the distal lung parenchyma, I could observe signs of pulmonary vascular pruning (Figure 32).

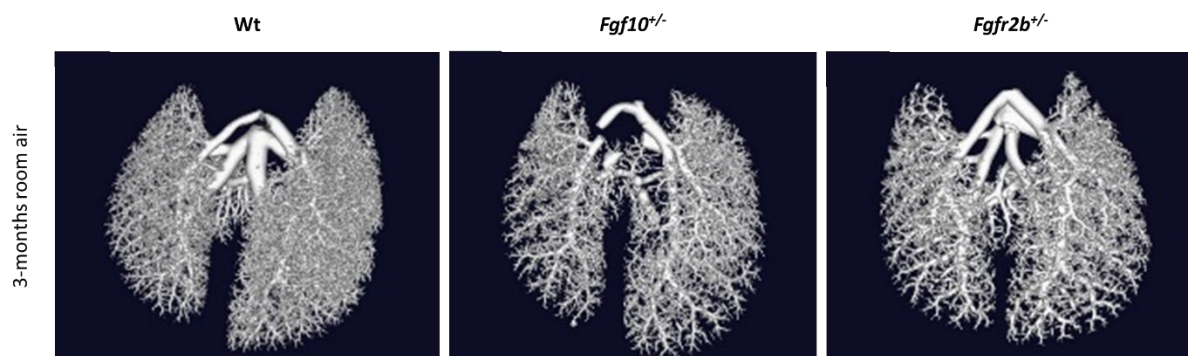


Figure 32. Pulmonary vascular tree in RA-exposed Wt mice and mice with impaired FGF10 signalling. Lungs were perfused with radio-opaque Microfil®, and the vascular tree was visualised *ex vivo* in formalin-fixed lungs using high-resolution μ CT imaging. Pulmonary vasculature is shown in lungs from RA-exposed Wt, *Fgf10*^{+/-} and *Fgfr2b*^{+/-} animals at the 3-months time-point.

Microfil® perfusion revealed the decreased density of distal pulmonary vessels of *Fgf10*^{+/-} and *Fgfr2b*^{+/-} mouse lungs at the 3-months time-point (**Figure 32**). All mice, transgenic and Wt, reacted with a similar increase in RVSP after 3 months of CS exposure (**Figure 33A**). As PH in such a model develops earlier than emphysema, already after 3 months of CS exposure, my data did not reveal if *Fgf10*^{+/-} and *Fgfr2b*^{+/-} mice are more susceptible to develop CS-induced PH as it was the case with emphysema. However, *Fgfr2b*^{+/-} mice already had slightly elevated RVSP in RA condition (**Figure 33A**).

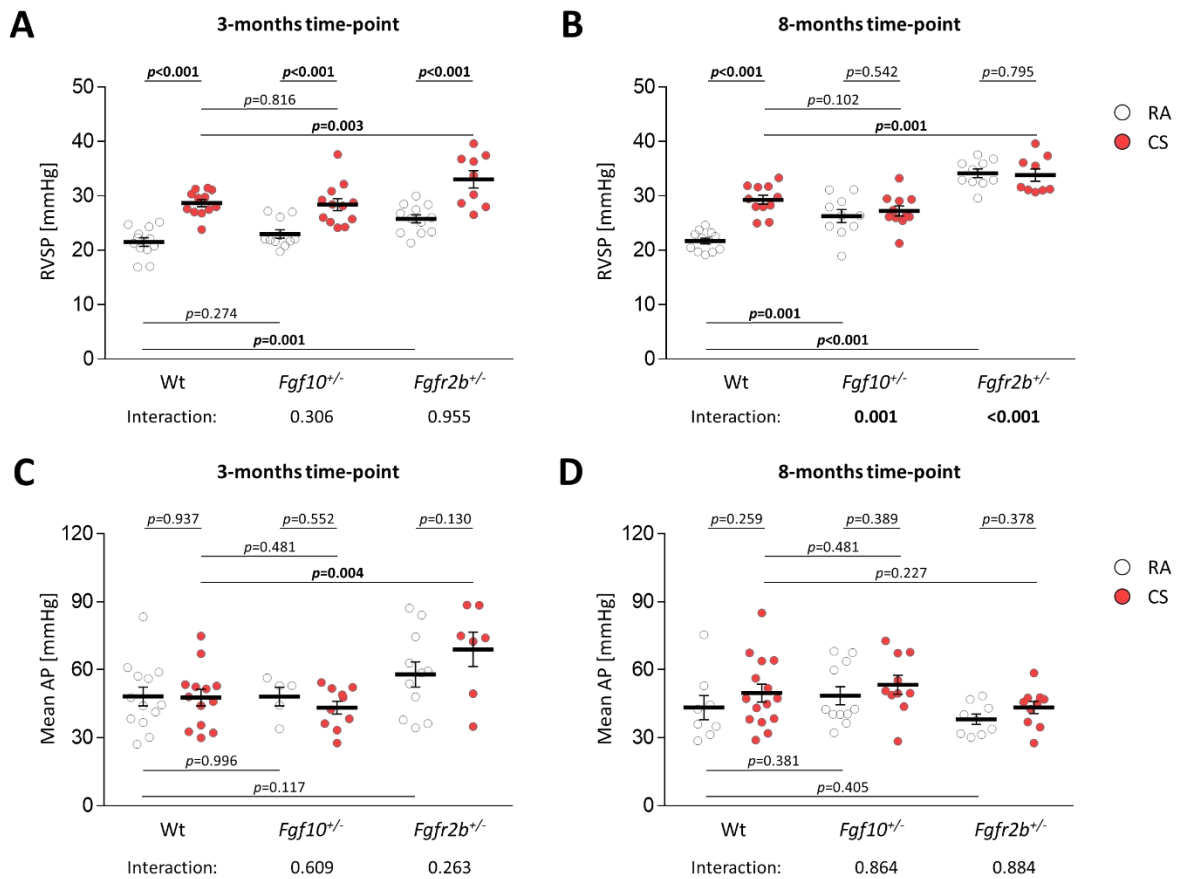


Figure 33. Pulmonary hypertension in CS-exposed mice with impaired FGF10 signalling. Hemodynamic measurements of (A, B) right ventricular systolic pressure (RVSP) and (C, D) systemic mean arterial pressure (AP) in Wt, *Fgf10*^{+/-}, and *Fgfr2b*^{+/-} animals after room air (RA) or cigarette smoke (CS) exposure for (A, C) 3 or (B, D) 8 months. The mean value for each group is represented by a horizontal line +/- standard error of the mean (SEM). Statistical analysis – Unpaired Two-Way ANOVA; p values for each comparison and interactions are noted in the graphs.

Furthermore, at the 8-months time-point, *Fgf10*^{+/-} and *Fgfr2b*^{+/-} mice had significantly increased RVSP in RA conditions. RVSP in these animals was not further increasing upon CS exposure (Figure 33A). I could observe that RA-and CS-exposed *Fgfr2b*^{+/-} mice have higher RVSP at the 8-months time-point compared to the corresponding Wt controls (Figure 33B). Interestingly, this was not the case in *Fgf10*^{+/-} mice. Mean systemic arterial pressure principally remained unchanged between groups (Figure 33), with a mild elevation in *Fgfr2b*^{+/-} mice after

3 months of CS exposure (**Figure 33C**). No differences in mean AP could be observed between the groups in the 8-months time-point (**Figure 33D**).

Tricuspid annular plane systolic excursion (TAPSE), measured by non-invasive echocardiography, is a parameter to estimate right heart function. It is often used as a prognostic parameter in human PH patients and PH animal models (Guazzi *et al.* 2013; Zhu *et al.* 2019; Seimetz *et al.* 2020). TAPSE was significantly decreased in CS-exposed Wt mice, compared to RA-exposed controls (**Figure 34A, 34B**). At the 3-months time-point, *Fgf10^{+/-}* and *Fgfr2b^{+/-}* mice had significantly lower TAPSE already in RA conditions compared to the corresponding Wt controls (**Figure 34A**). TAPSE further decreased upon 3 months of CS exposure in both transgenic animal lines (**Figure 34A**). At the 8-months time-point, TAPSE was decreased in *Fgf10^{+/-}* and *Fgfr2b^{+/-}* mice in RA conditions, compared to corresponding Wt controls (**Figure 34B**). This age-related decrease in TAPSE followed the trend observed in hemodynamic measurements and did not further worsen in transgenic animals that were long-term exposed to CS (**Figure 34B**).

Heart ratio, also referred to as Fulton's index, was measured as a ratio in weight between right ventricle (RV) and left ventricle together with the septum (LV+S; **Figure 34C, 34D**). In Wt animals, mild RV hypertrophy occurred upon CS exposure already at the 3-months time-point (**Figure 34C**) and was more pronounced after long-term CS exposure (**Figure 34D**). In line with the hemodynamic measurements, *Fgfr2b^{+/-}* mice also had more pronounced RV hypertrophy than *Fgf10^{+/-}* and Wt mice (**Figure 34C, 34D**). In *Fgf10^{+/-}* and *Fgfr2b^{+/-}* mice, RV hypertrophy increased gradually with ageing regardless of the CS exposure (**Figure 34C, 34D**).

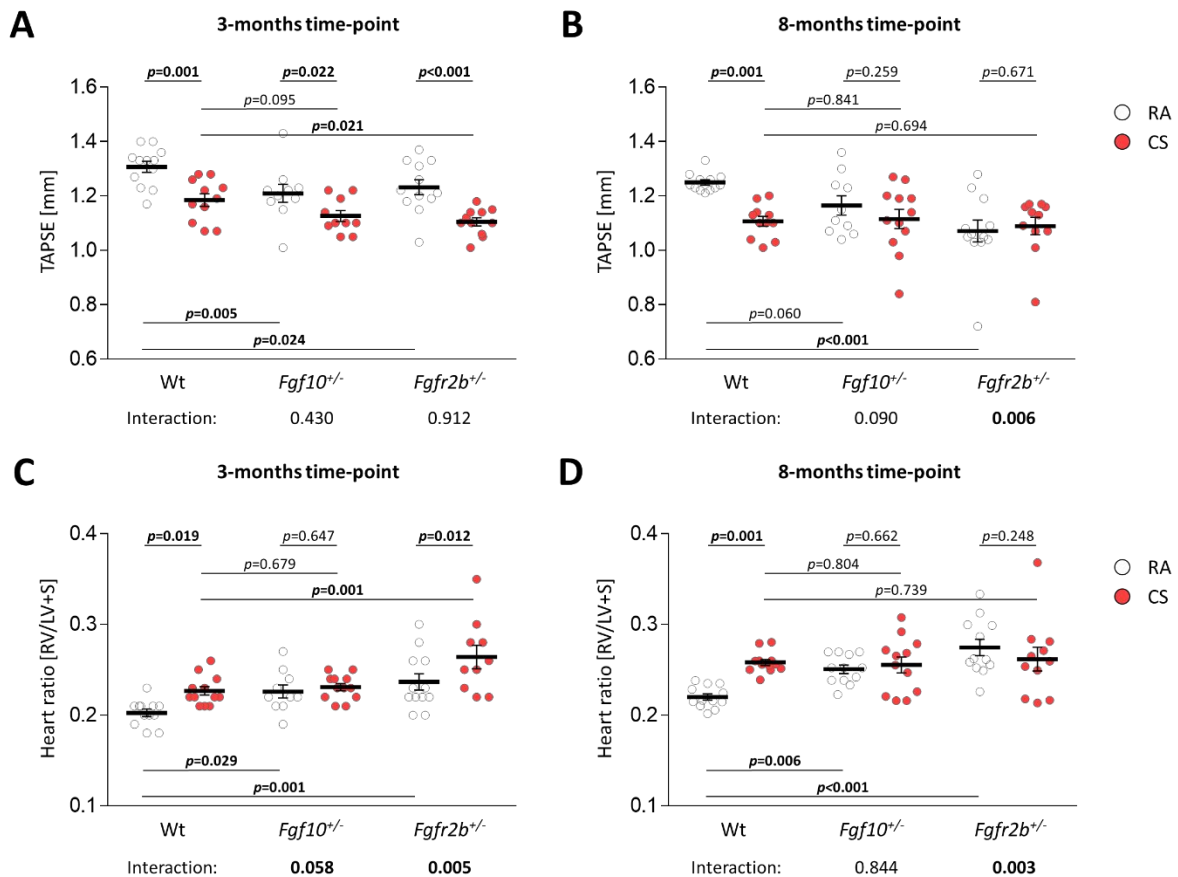


Figure 34. Right heart alterations in CS-exposed mice with impaired FGF10 signalling. (A, B) Tricuspid annular plane systolic excursion (TAPSE) measured by non-invasive echocardiography in Wt, *Fgf10*^{+/-}, and *Fgfr2b*^{+/-} animals after room air (RA) or cigarette smoke (CS) exposure for (A) 3 or (B) 8 months. **(C, D)** Right ventricular wall hypertrophy in experimental animals shown as a weight ratio between the right ventricle (RV) and left ventricle with the septum (RV+S) in RA- or CS-exposed experimental animals at the (C) 3- or (D) 8-months time-point. The mean value for each group is represented by a horizontal line +/- standard error of the mean (SEM). Statistical analysis – Unpaired Two-Way ANOVA; p values for each comparison and interactions are noted in the graphs.

3.1.4 COPD traits in mice with impaired FGF10 signalling

In contrast to the human material, FGF10 expression was significantly decreased in the lung homogenates from Wt mice after 8 months of CS exposure, compared to the RA-exposed controls (**Figure 35**). Even at the advanced age, FGF10 haploinsufficient mice had lower FGF10 expression on the protein level in the lung, compared to Wt littermates (**Figure 35**). FGF10

expression in lung homogenates was consistently decreased on, both, the mRNA (**Figure 35A**) and protein levels (**Figure 35B, 35C**). Interestingly, in *Fgf10*^{+/-} transgenic animals, FGF10 expression was not further decreased upon CS exposure. This corresponds with the other measurements where I could not observe the disease worsening in transgenic mice upon 8 months of CS-exposure.

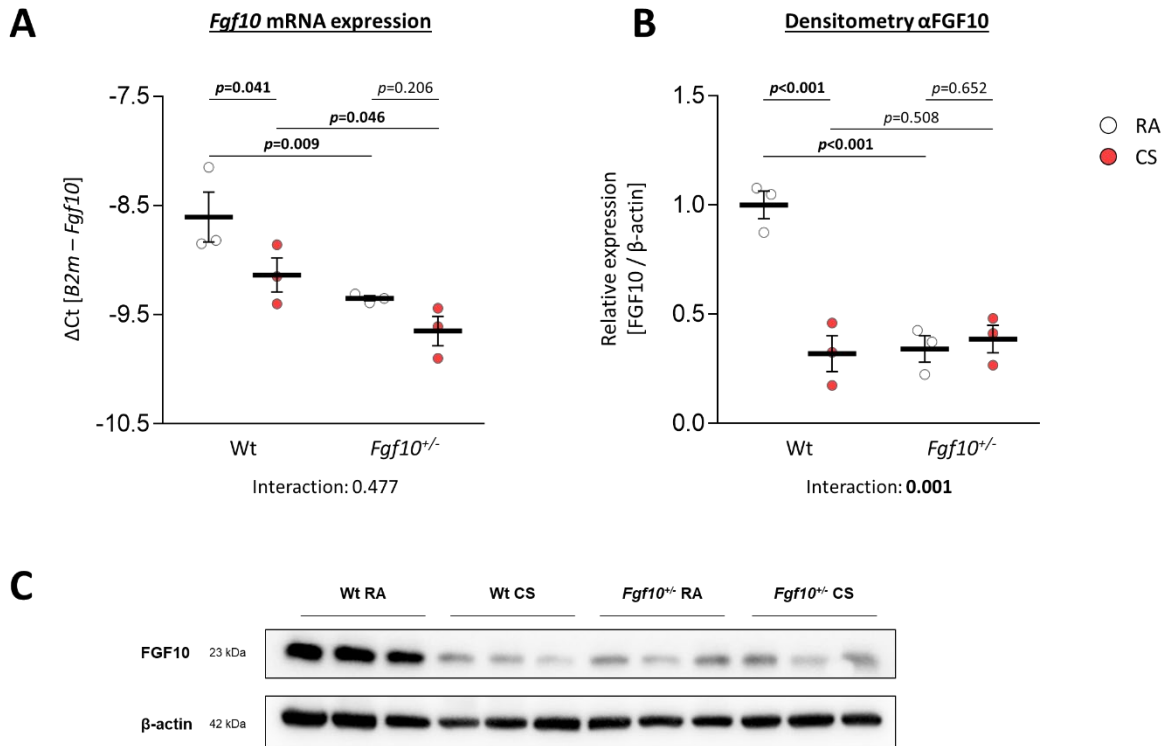


Figure 35. FGF10 expression in lung homogenate from Wt and *Fgf10*^{+/-} animals after 8 months of RA or CS exposure. FGF10 expression analysed by **(A)** RT-qPCR and **(B)** Western blot. **(C)** Representative blots showing FGF10 and β -actin in lung homogenates from experimental animals. Protein expression in Western blot was quantified by band densitometry and standardized to β -actin; relative expression was calculated by standardizing each value to the mean value of the donor control group. The mean value for each group is represented by a horizontal line +/- standard error of the mean (SEM). Statistical analysis – Unpaired Two-Way ANOVA; *p* values for each comparison and interactions are noted in the graphs.

As mentioned before, 3-nitrotyrosine formation is one of the well-described features in COPD patients and in the CS-exposed animal model. Therefore, using enzyme-linked immunoassay

(ELISA) and nitrated bovine serum albumin as standard, I measured 3-nitrotyrosine levels in lung homogenates of my experimental mice. *Fgf10*^{+/-} mice had slightly increased 3-nitrotyrosine level in their lungs already at the 3-months time-point, compared to the Wt littermates (**Figure 36A**). This occurred in, both, RA and CS exposure conditions (**Figure 36A**).

At the 8-months time-point, 3-nitrotyrosine in RA-exposed *Fgf10*^{+/-} mouse lungs was significantly increased compared to the Wt controls (**Figure 36B**). The 3-nitrotyrosine level in RA-exposed *Fgf10*^{+/-} mice was as high as in CS-exposed Wt littermates and did not further increase with CS exposure (**Figure 36B**).

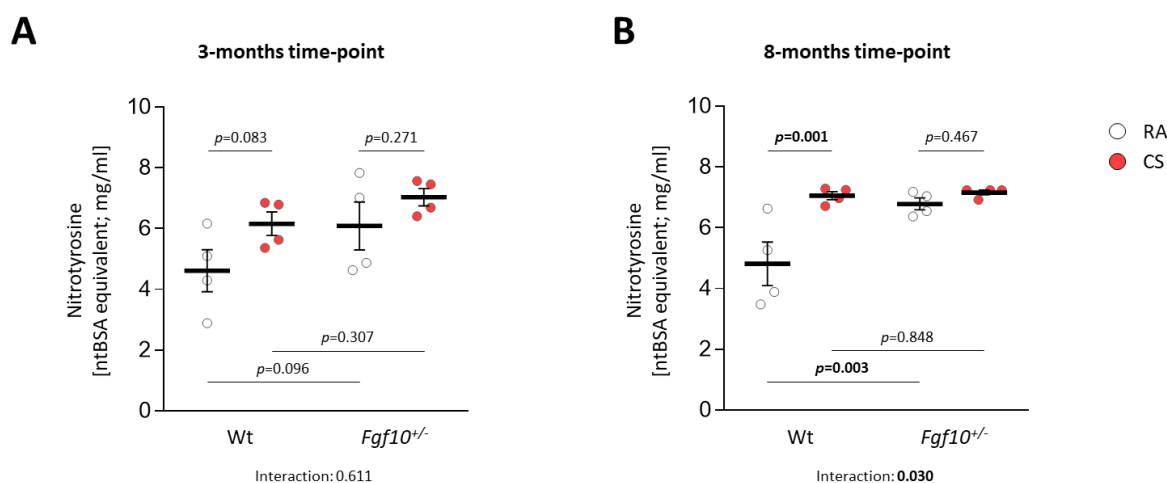


Figure 36. 3-nitrotyrosine quantification in lung homogenates from Wt and *Fgf10*^{+/-} mice. 3-nitrotyrosine was assessed using an enzyme-linked immunoassay (ELISA) kit in lung homogenates from Wt and *Fgf10*^{+/-} animals after **(A)** 3 or **(B)** 8 months of room air (RA) or cigarette smoke (CS) exposure. 3-nitrotyrosine is shown as equivalent to the concentration of nitrated bovine serum albumin (ntBSA) used as standard. The mean value for each group is represented by a horizontal line +/- standard error of the mean (SEM). Statistical analysis – Unpaired Two-Way ANOVA; p values for each comparison and interactions are noted in the graphs.

Apoptosis in lungs from my experimental animals was assessed *in vivo* using fluorescence molecular tomography (FMT) and Annexin-Vivo™ 750 fluorescent probe. Such probe binds to the accessible phosphatidylserine, which is only in apoptotic cells present on the outer layer of the cell membrane. At the 3-months time-point, all CS-exposed animals (Wt, *Fgf10*^{+/-}, and

Fgfr2b^{+/-}) had a significantly higher Annexin-Vivo™ 750 fluorescent probe signal in the lungs compared to the corresponding RA-exposed control animals (**Figure 37A**). In RA and CS conditions, *Fgfr2b*^{+/-} mice had a significantly higher fluorescence signal at the 3-months time-point when compared to the corresponding Wt control animals (**Figure 37A**).

At the 8-months time-point, CS-exposed Wt and *Fgf10*^{+/-} mice had a higher Annexin V signal compared to corresponding RA-exposed controls (**Figure 37B**). Of interest, RA- and CS-exposed *Fgf10*^{+/-} and *Fgfr2b*^{+/-} mice had significantly higher Annexin-Vivo™ 750 fluorescent probe signals in the lung compared to corresponding Wt control mice (**Figure 37B**). At the 8-months time-point, CS-exposed *Fgfr2b*^{+/-} animals had a significantly lower Annexin V fluorescent signal when compared to the CS-exposed Wt controls (**Figure 37B**). This could be due to already developed severe pulmonary emphysema in CS-exposed *Fgfr2b*^{+/-} animals.

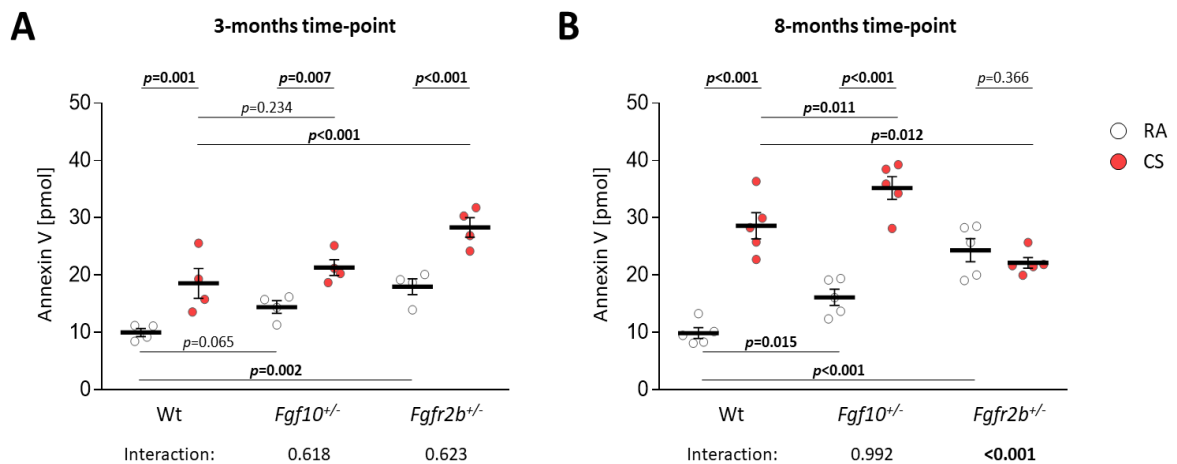


Figure 37. Apoptosis in lungs from CS-exposed mice with impaired FGF10 signalling measured by FMT-CT. Apoptosis was assessed in mouse lungs from Wt, *Fgf10*^{+/-}, and *Fgfr2b*^{+/-} animals after (A) 3 or (B) 8 months of room air (RA) or cigarette smoke (CS) exposure. Measurements were done *in vivo* using fluorescence molecular tomography (FMT) and Annexin-Vivo™ 750 fluorescent probe that binds to the phosphatidylserine on the outer layer of the cell membrane of the apoptotic cells. The scans were merged with corresponding computed tomography images and only the fluorescent signal from the lung area was taken for the calculations. The mean value for each group is represented by a horizontal line +/- standard error of the mean (SEM). Statistical analysis – Unpaired Two-Way ANOVA; p values for each comparison and interactions are noted in the graphs.

I further isolated alveolar epithelial type II (ATII) cells from unexposed Wt animals and examined apoptosis and cell viability upon CSE treatment. Apoptosis in ATII cells was visualised by incubation with fluorescence labelled Annexin V and measured using an IncuCyte® live-cell imager. CSE-induced apoptosis of ATII cells, shown as Annexin V stained area, standardized to the cell confluence, was significantly lower when cells were pre-treated with FGF10 compared to the control cells without FGF10 pre-treatment (**Figure 38A**). CSE treatment decreased cell viability in ATII cells, as measured using an AlamarBlue™ cell viability reagent (**Figure 38B**). Cells pre-treated with FGF10 had preserved cell viability upon CSE treatment, compared to the CS-treated control cells without FGF10 pre-treatment (**Figure 38B**).

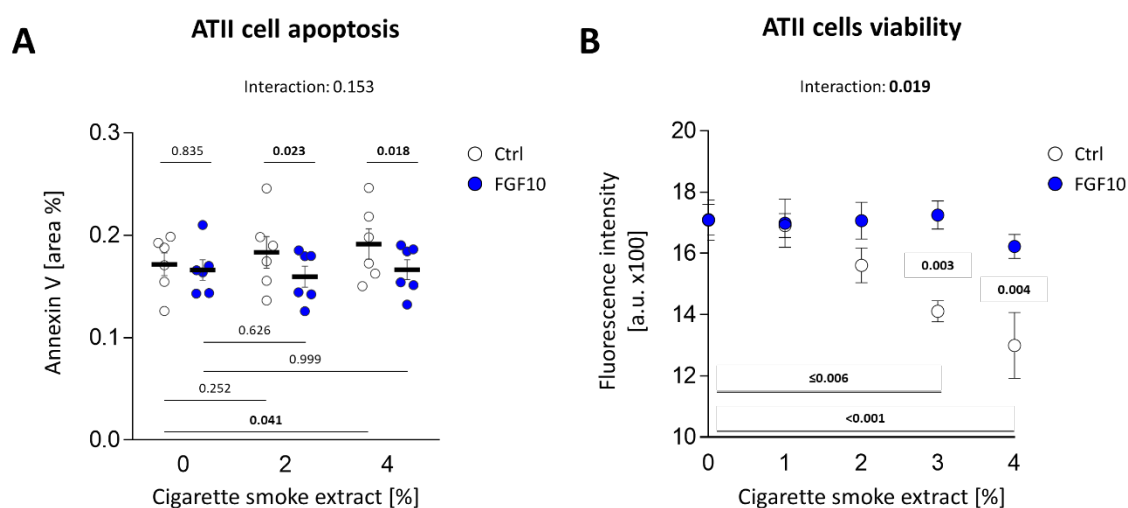


Figure 38. CSE-induced ATII cell apoptosis and decrease in cell viability. (A) Apoptosis was measured using an IncuCyte® live-cell imager and shown as the area of fluorescence labelled Annexin V staining, standardized to the cell confluence, visualised in phase contrast in primary culture of alveolar type 2 (ATII) cells isolated from Wt mice and *in vitro* treated with 250ng/ml FGF10 and/or cigarette smoke extract (CSE). (B) Cell viability was measured using an AlamarBlue™ cell viability assay. The mean value for each group is represented by a (A) horizontal line or (B) a dot +/- standard error of the mean (SEM). Statistical analysis – Paired Two-Way ANOVA with Sidak’s multiple comparisons corrections; p values for each comparison and interactions are noted in the graphs.

MMP activity was measured *in vivo*, using FMT with the MMPsense 750 fluorescent activatable sensor technology (FAST) probe. The MMPsense 750 FAST probe produces a fluorescent signal

upon cleavage by MMPs. The MMPsense 750 FAST probe can be cleaved by MMP 2, 3, 7, 9, 12, and 13. MMP activity in Wt mouse lungs increased after 3 months of CS exposure (**Figure 39A**). RA-exposed *Fgf10^{+/-}* and *Fgfr2b^{+/-}* mice had significantly higher MMP activity compared to RA-exposed Wt controls (**Figure 39A**). In the case of CS-exposed *Fgfr2b^{+/-}* mice, MMP activity was significantly increased compared to the CS-exposed Wt animals (**Figure 39A**).

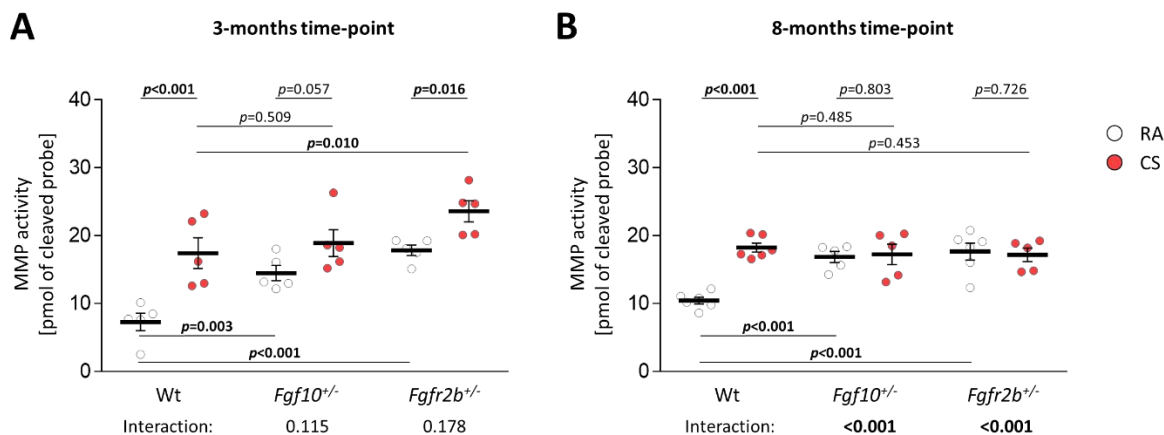


Figure 39. MMP activity in lungs from CS-exposed mice with impaired FGF10 signalling measured by FMT-CT. MMP activity was assessed in mouse lungs from Wt, *Fgf10^{+/-}*, and *Fgfr2b^{+/-}* animals after (A) 3 or (B) 8 months of room air (RA) or cigarette smoke (CS) exposure. Measurements were done *in vivo* using fluorescent molecular tomography (FMT) with the MMPsense 750 fluorescent activatable sensor technology (FAST) probe for MMP activity. Such probe emits a fluorescent signal when cleaved by MMP 2, 3, 7, 9, 12, or 13. The scans were merged with corresponding computed tomography images, and only the fluorescent signal from the lung area was taken for the calculation. The mean value for each group is represented by a horizontal line +/- standard error of the mean (SEM). Statistical analysis – Unpaired Two-Way ANOVA; p values for each comparison and interactions are noted in the graphs.

At the 8-months time-point, MMP activity was significantly increased in CS-exposed Wt animals compared to corresponding RA-exposed controls (**Figure 39B**). *Fgf10^{+/-}* and *Fgfr2b^{+/-}* animals exhibited significantly increased MMP activity in lungs in RA conditions (**Figure 39B**). However, in transgenic animals, CS exposure did not lead to a further increase in MMP activity (**Figure 39B**).

3.1.5 Gene expression regulation during emphysema and PH development in CS-exposed wild-type (Wt) mice and in FGF10-haploinsufficient mice

To decipher the underlying mechanisms of the disease development, I analysed gene expression profiles of Wt and *Fgf10*^{+/-} animals at a 3-month time-point. As different gene regulation patterns were observed between alveolar septa and the pulmonary vasculature, I therefore subjected Tissue-Tek® O.C.T.™ embedded and cryopreserved lungs from my experimental animals to laser-assisted microdissection and separately collected RNA from alveolar septa and pulmonary vessels. In the following, I show 3 types of gene expression analysis: 1) heat maps where changes in all CS-regulated genes are shown for all analysed groups; 2) Venn diagrams and comet plots focusing on the genes that are commonly regulated between different experimental groups and 3) functional protein association network analysis where only regulated genes that align on similar signalling pathway appear.

In the heat maps (**Figure 40**) are shown all genes that are regulated upon CS exposure in alveolar septa ($-\log p \geq 1.3$ for the Wt CS vs Wt RA comparison; **Figure 40A**) and in the pulmonary vasculature ($-\log p \geq 2$ for the Wt CS vs Wt RA comparison; **Figure 40B**). The clusters were formed based on the direction of the LFC in all three analysed comparisons. In the alveolar septa, I observed that most of the CS-regulated genes were also strongly regulated in RA-exposed *Fgf10*^{+/-} animals (**Figure 40A**). Of interest, the vast majority of these genes, in both comparisons, were regulated in the same direction (**Figure 40A**). Moreover, most of the genes were not further changed in *Fgf10*^{+/-} animals upon CS exposure (**Figure 40A**).

In the pulmonary vasculature, I could observe a similar situation like in septa (**Figure 40B**). Most of the CS-regulated genes were also regulated in the same direction in *Fgf10*^{+/-} animals (**Figure 40B**). However, in the pulmonary vasculature, I could observe some genes being regulated in *Fgf10*^{+/-} animals upon CS exposure (**Figure 40B**). This suggests that animals deficient in FGF10 have a slightly altered reaction to CS exposure in the pulmonary vascular compartment compared to Wt littermates.

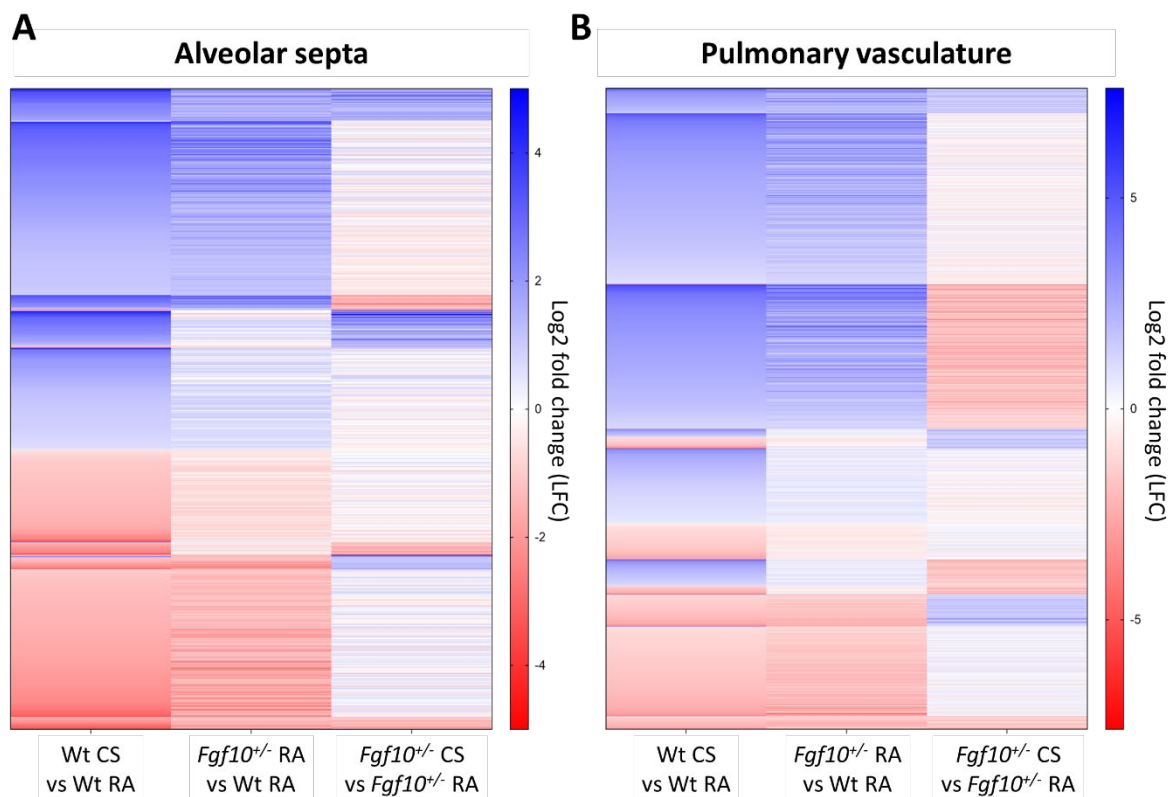


Figure 40. Heat maps showing all CS-regulated genes during the development of emphysema and PH. Heat maps are showing all genes that are regulated in Wt animals upon 3 months of cigarette smoke (CS) exposure, compared to the room air (RA)-exposed control Wt mice in **(A)** alveolar septa ($\log p \geq 1,3$ for the Wt CS vs Wt RA) and **(B)** the pulmonary vasculature ($\log p \geq 2$ for the Wt CS vs Wt RA). Gene expression regulation of the CS-regulated genes in Wt mice is also shown for *Fgf10*^{+/-} RA vs Wt RA and *Fgf10*^{+/-} CS vs *Fgf10*^{+/-} RA. Blue: upregulation, logarithmic fold change (LFC) ≥ 0 ; Red: downregulation, LFC ≤ 0 . Colour gradient indicates intensity of the expression change as noted on the left side of the corresponding heat map.

Further, I focused on the genes that are commonly regulated in Wt animals upon CS exposure and in FGF10 haploinsufficient animals (**Figure 41A, 41B**). In the alveolar septa, I found 263 genes (**Figure 41A**) and in pulmonary vessels 289 genes (**Figure 41B**) that are commonly regulated between Wt CS and *Fgf10*^{+/-} RA, compared to the WT RA control group. Moreover, in both compartments, these genes were regulated in the same direction (**Figure 41C, 41D**). Interestingly, in *Fgf10*^{+/-} animals, the vast majority of these commonly regulated genes were not further affected by CS exposure (**Figure 41A, 41B**).

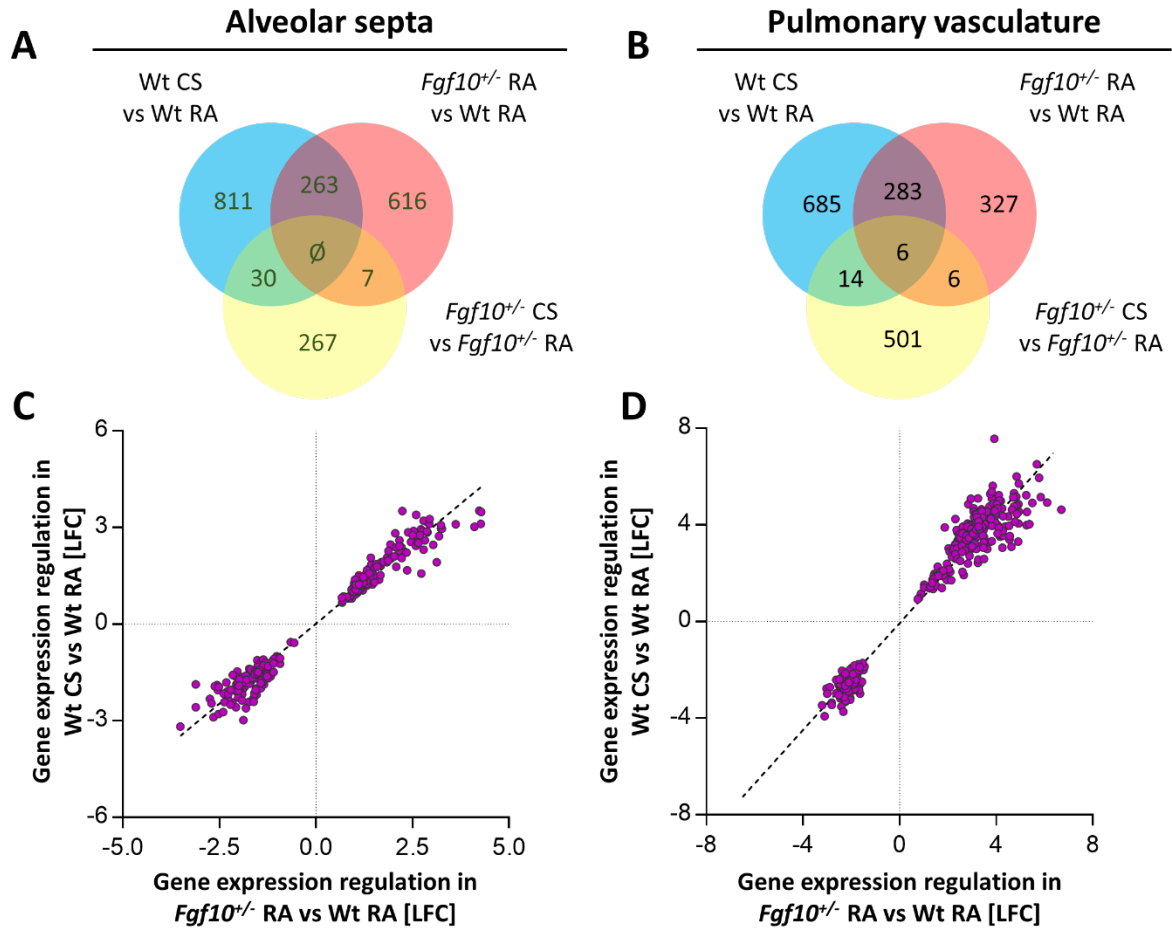


Figure 41. CS- and FGF10 haploinsufficiency-related gene expression pattern during emphysema and PH development. Venn diagrams were used to show the number of dysregulated genes in **(A)** alveolar septa ($\log p \geq 1.3$) and **(B)** the pulmonary vasculature ($\log p \geq 2$) at the 3-months time-point. The overlap region shows genes that are in common between the compared groups. Genes commonly regulated between Wt CS vs Wt RA and *Fgf10*^{+/-} RA vs Wt RA were further investigated in comet plots. Comet plots show the common genes in **(C)** alveolar septa and **(D)** the pulmonary vasculature with the direction of gene expression changes. Between the two compared groups of genes, positive correlation (black dashed line) implies the similar direction of the log fold changes (LFC).

In order to identify pathways and test if the regulated genes align in specific signalling pathways, I performed a functional protein association network analysis (STRING-DB database) (Hu *et al.* 2018; Szklarczyk *et al.* 2019). Interestingly, the targets were somewhat scattered into several clusters, comprising a few targets each, and thus, I could not find enrichment in any specific signalling pathway (**Figure 42**). It seems that FGF10 deficiency and CS exposure trigger many targets rather than one well-described signalling pathway. However, I could identify a

cluster of genes that encode for participants in Wnt signalling in the alveolar septa (**Figure 42A**). This cluster included Wnt family member 5A (Wnt5a) and receptor tyrosine kinase-like orphan receptor 1 (Ror1) (**Figure 42A**). In the pulmonary vasculature I found a cluster that is related to a network of tyrosine kinase signalling (**Figure 42B**).

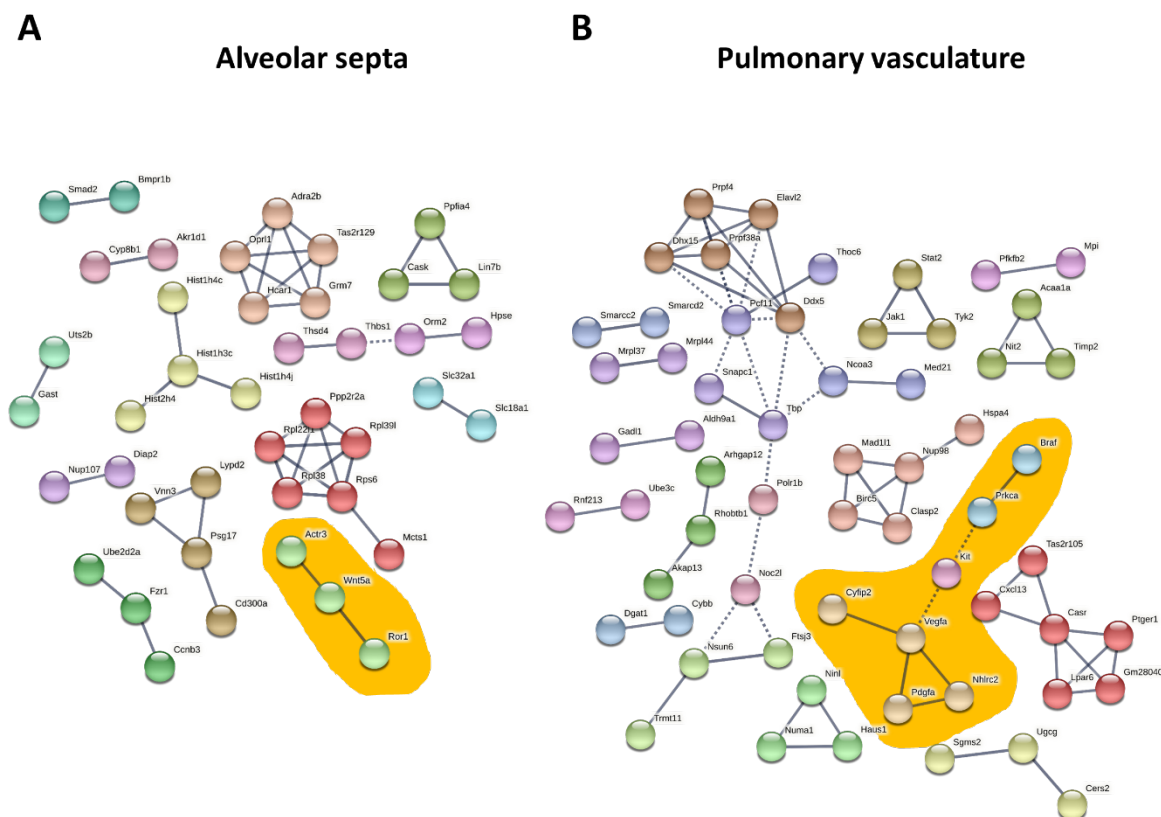


Figure 42. Functional protein association networks of CS- and FGF10 haploinsufficiency-regulated genes during emphysema and PH development. Genes that were commonly regulated between cigarette smoke (CS)- versus room air (RA)-exposed Wt mice (Wt CS vs Wt RA) and *Fgf10*^{+/-} RA vs Wt RA in **(A)** alveolar septa ($\log p \geq 1,3$ for both comparisons) and **(B)** pulmonary vasculature ($\log p \geq 2$ for both comparisons) at the 3-months time-point were analysed using functional protein association networks (STRING-DB database). Abbreviations: Wnt5a – Wnt Family Member 5A; Ror1 – receptor tyrosine kinase-like orphan receptor 1; Actr3 – actin related protein 3; Braf – serine/threonine-protein kinase B rapidly accelerated fibrosarcoma; Prkca – protein kinase C alpha; Kit – tyrosine kinase receptor KIT; Vegfa – vascular endothelial growth factor A; Cyfip2 – cytoplasmic FMR1 interacting protein 2; Nhlrc2 – NHL repeat containing 2; Pdgfa – platelet derived growth factor subunit alpha; Smad2 – SMAD family member 2; Bmpr1b – bone morphogenetic protein receptor type 1B; Cyp8b1 – cytochrome P450 family 8 subfamily B member 1; Akr1d1 – aldo-keto reductase family 1 member D1; Uts2b – urotensin 2B; Gast – gastrin; Hist – histone; Adra2b – adrenoceptor alpha 2B; Opr1 – opioid related nociceptin receptor 1; Hcar1 –

hydroxycarboxylic acid receptor 1; Tas2r129 – taste receptor type 2 member 129; Grm7 – glutamate metabotropic receptor 7; Ppfia4 – PTPRF interacting protein alpha 4; Cask – calcium/calmodulin dependent serine protein kinase; Lin7b – lin-7 homolog B, crumbs cell polarity complex component; Thsd4 – thrombospondin type 1 domain containing 4; Thbs1 – thrombospondin 1; Orm2 – orosomucoid 2; Hpse – heparanase; Slc – solute carrier; Rp – ribosomal proteins; Ppp2r2a – serine/threonine-protein phosphatase 2A 55 kDa regulatory subunit B alpha isoform; Mcts1 – malignant T-cell amplified sequence 1; Nup107 – nucleoporin 107; Diap2 – diaphanous related formin 2; Vnn3 – vanin 3; Lypd2 – LY6/PLAUR domain containing 2; Psg17 – pregnancy-specific glycoprotein; Cd300a – cluster of differentiation 300A; Ube2d2a – ubiquitin-conjugating enzyme E2D 2A; Fyr1 – RUN and FYVE domain containing 1; Ccnb3 – cyclin B3; Prpf – U4/U6 small nuclear ribonucleoprotein; Dhx – DEAH-box helicases; Elavl2 – ELAV like RNA binding protein 2; Thoc6 – THO complex 6; Pcf11 - PCF11 cleavage and polyadenylation factor subunit; Smarcb1 – SWI/SNF related, matrix associated, actin dependent regulator of chromatin; Mrpl1 – 39S ribosomal protein L1; Gad1 – glutamate decarboxylase like 1; Aldh9a1 – aldehyde dehydrogenase 9 family member A1; Rnf213 – ring finger protein 213; Ube3c – ubiquitin protein ligase E3C; Arhgap12 – Rho GTPase activating protein 12; Rhobtb1 – Rho related BTB domain containing 1; Akap13 – A-kinase anchor protein 13; Dgat1 – diacylglycerol O-acyltransferase 1; Snapc1 - small nuclear RNA activating complex polypeptide 1; Tbp – TATA-box binding protein; Nco3 - nuclear receptor coactivator 3; Med21 – mediator complex subunit 21; Cybb – cytochrome B-245 beta chain; Polr1b – RNA polymerase I subunit B; Noc2l – NOC2 like nucleolar associated transcriptional repressor; Nsun6 – NOP2/Sun RNA methyltransferase 6; Ftsj3 – ftsJ RNA 2'-O-methyltransferase 3; Trmt11 – TRNA methyltransferase 11 homolog; Stat2 – signal transducer and activator of transcription 2; Jak1 – janus kinase 1; Tyk2 – tyrosine kinase 2; Pfkfb2 – 6-phosphofructo-2-kinase/fructose-2,6-biphosphatase 2; Mpi – mannose phosphate isomerase; Acaa1a – acetyl-CoA acyltransferase 1; Nit2 – nitrilase family member 2; Timp2 – TIMP metalloproteinase inhibitor 2; Ninl – ninein like; Numa1 – nuclear mitotic apparatus protein 1; Haus1 – HAUS augmin like complex subunit 1; Mad11l1 – mitotic arrest deficient 1 like 1; Birc5 – baculoviral IAP repeat containing 5; Clasp2 – cytoplasmic linker associated protein 2; Nup98 – nucleoporin 98 and 96 precursor; Hspa4 – heat shock protein family A (Hsp70) member 4; Sgms2 – sphingomyelin synthase 2; Ugcg – UDP-glucose ceramide glucosyltransferase; Cers2 – ceramide synthase 2; Tas2r105 – taste receptor type 2 member 105; Cxcl13 – C-X-C motif chemokine ligand 13; Casr – calcium-sensing receptor; Lpar6 – lysophosphatidic acid receptor 6; Ptger1 – prostaglandin E receptor 1; Gm28040 – KISS1 isoform E.

Following the hints from the functional protein association network analysis and the literature, I focused on β -catenin as the downstream target of the canonical Wnt pathway (Kneidinger *et al.* 2011; De Langhe *et al.* 2005; Baarsma *et al.* 2017; Hu *et al.* 2020). I indeed found decreased levels of β -catenin in the lung homogenates from Wt mice that were exposed to CS for 3 (Figure 43A, 43C) or 8 months (Figure 43B, 43D). Levels of β -catenin were also significantly

decreased in lung homogenates from RA-exposed *Fgf10*^{+/-} mice at both time-points, compared to the corresponding RA-exposed Wt controls (**Figure 43**).

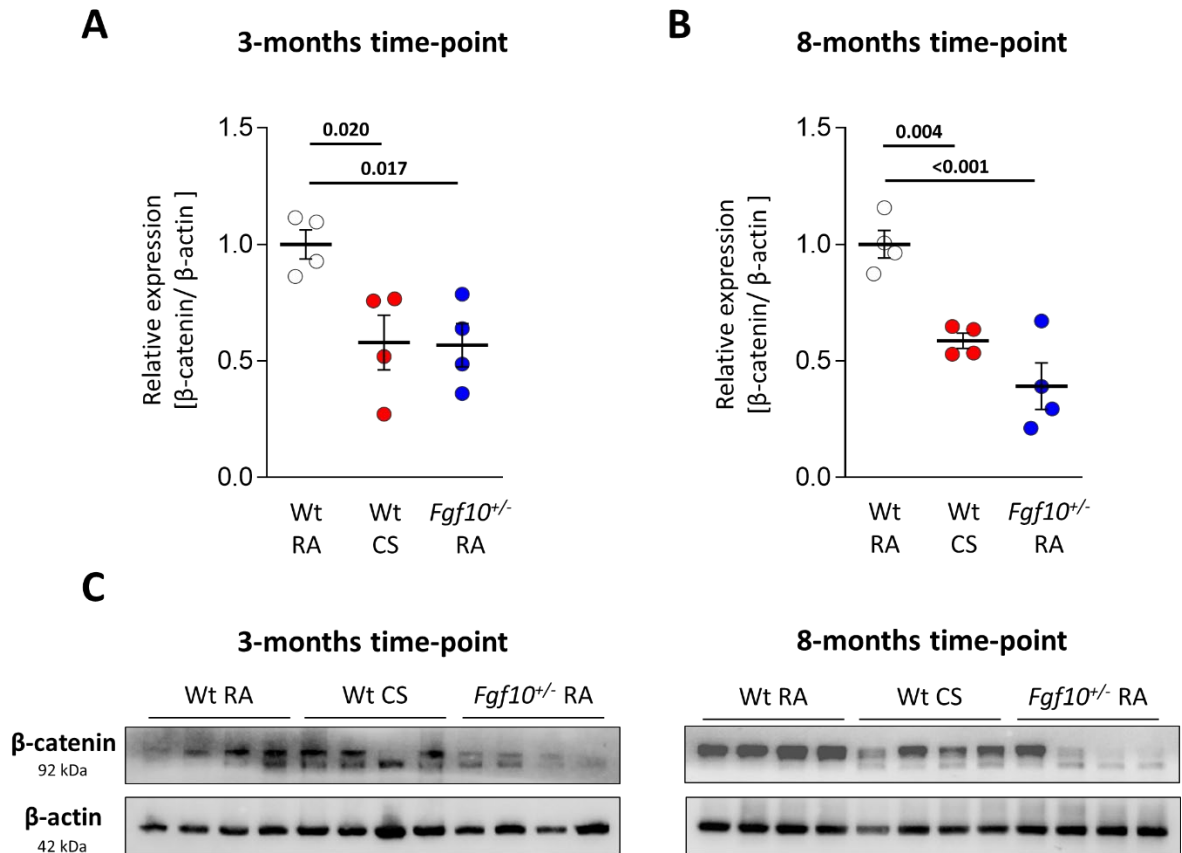


Figure 43. β-catenin expression in lung homogenates from CS-exposed or FGF10 haploinsufficient animals. Western blot quantification of β-catenin expression in lung homogenates from cigarette smoke (CS)-exposed Wt mice and room air (RA)-exposed Wt and *Fgf10*^{+/-} mice at the **(A)** 3- and **(B)** 8-months time-points. **(C)** Representative blots used for the quantification. The mean value for each group is represented by a horizontal line +/- standard error of the mean (SEM). Protein expression in Western blot was quantified by band densitometry and standardized to β-actin; relative expression was calculated by standardizing each value to the mean value of the Wt RA control group. Statistical analysis – Unpaired One-Way ANOVA with Dunnett’s multiple comparisons corrections; p value for each comparison is noted above.

In the pulmonary vasculature, I could pinpoint a cluster of genes that encode for several tyrosine kinases and growth factors. This cluster includes serine/threonine-protein kinase B rapidly accelerated fibrosarcoma (Braf), protein kinase C alpha (Prkca), tyrosine-protein kinase

receptor KIT, vascular endothelial growth factor A (Vegfa) and platelet derived growth factor subunit A (Pdgfa) (**Figure 43B**).

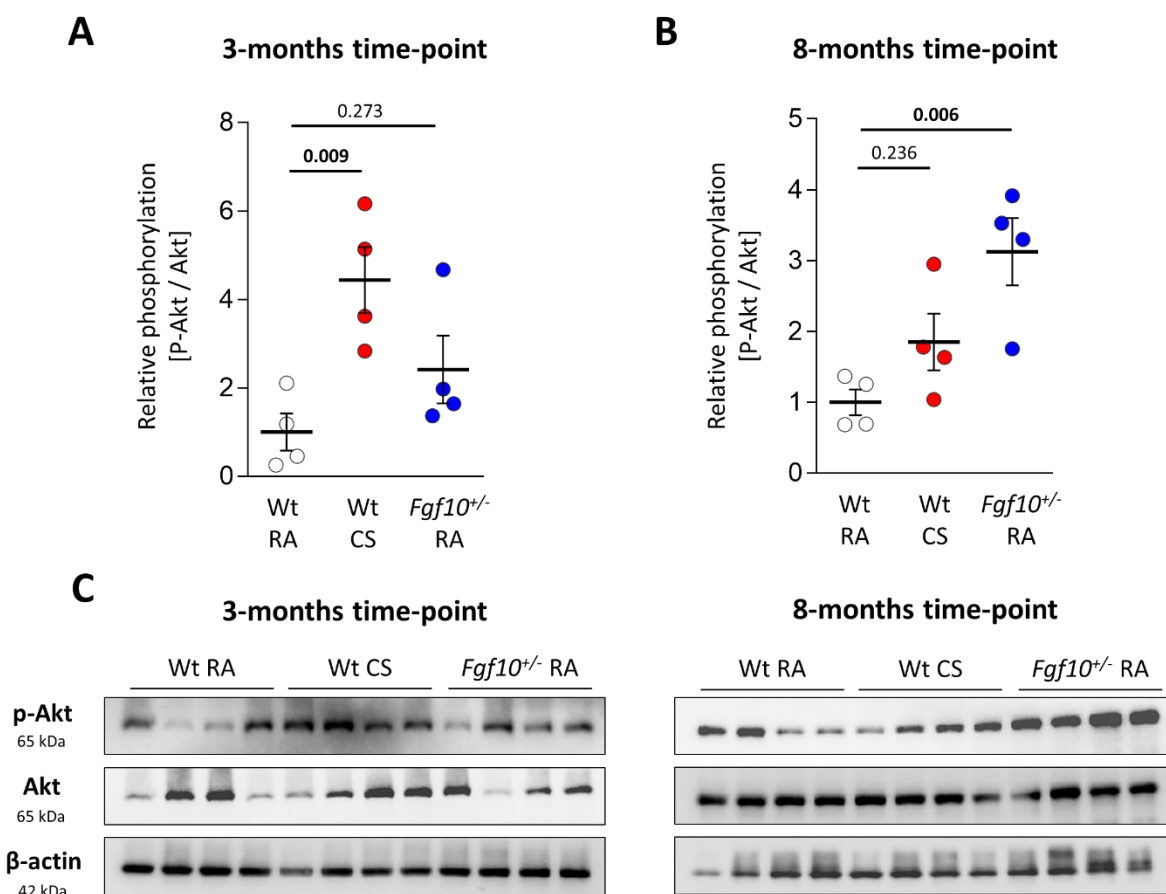


Figure 44. Phosphorylation of Akt in lung homogenates from CS-exposed or FGF10 deficient animals. Western blot quantification of p-Akt (phosphorylation at serine 473) and total Akt in lung homogenates from cigarette smoke (CS)-exposed Wt mice and room air (RA)-exposed Wt and *Fgf10*^{+/-} mice at **(A)** 3- and **(B)** 8-month time-points. **(C)** Representative blots. The mean value for each group is represented by a horizontal line +/- standard error of the mean (SEM). Quantification shows the p-Akt/Akt ratio in the experimental mouse lungs; relative phosphorylation was calculated by standardizing each value to the mean value of the Wt RA control group; β -actin was used as a loading control. Statistical analysis – Unpaired One-Way ANOVA with Dunnett’s multiple comparisons corrections; p value for each comparison is noted above.

After a literature search, I focused on Akt phosphorylation as a common downstream phosphorylation target of the tyrosine kinase cluster (Bozinovski *et al.* 2006; Tang *et al.* 2015). At the 3-months time-point, I found significantly increased Akt phosphorylation in the lung homogenate from CS-exposed Wt mice, compared to the RA controls (**Figure 44A, 44C**). Akt

phosphorylation was also significantly increased in the lung homogenates from *Fgf10^{+/-}* animals at the 8-month time-point, compared to the RA-exposed Wt controls (**Figure 44B, 44C**).

3.1.6 The effect of doxycycline on CS-induced emphysema and PH

Before investigating the effect of doxycycline-mediated FGF10 overexpression, I tested if doxycycline alone, given at the specific regimen, could influence CS-induced emphysema and PH. I used transgenic animals that expressed rtTA under ROSA26 promoter but without *Tet(O)* sequence. These animals were exposed to RA or CS for 8 months. CS exposure was then discontinued and animals were fed with doxycycline-containing food for additional 3 months in RA conditions.

Animals that were exposed to CS had significantly increased lung compliance (**Figure 45A**). Long-term doxycycline administration did not affect *in vivo* lung compliance in the treated animals, compared to the untreated controls (**Figure 45A**). Further histological examination of H&E stained lung sections from experimental animals did not reveal any apparent effect of long-term doxycycline treatment (**Figure 45B-D**). Namely, animals that were exposed to CS had significantly increased MLI (**Figure 45B**) and decreased alveoli number (**Figure 45C**) compared to the RA-exposed control mice. Of importance, doxycycline treatment had no effect on emphysema parameters such as MLI (**Figure 45B**) or the number of alveoli (**Figure 45C**).

Consistently with the previous results, animals had significantly increased RVSP after 8 months of CS exposure despite the subsequent re-exposure to RA for additional 3 months (**Figure 46A**). Doxycycline treatment had no effect on RVSP (**Figure 46A**), mean arterial pressure (AP, **Figure 46B**), TAPSE (**Figure 46C**) and RV hypertrophy (**Figure 46D**) in RA- or CS-exposed mice.

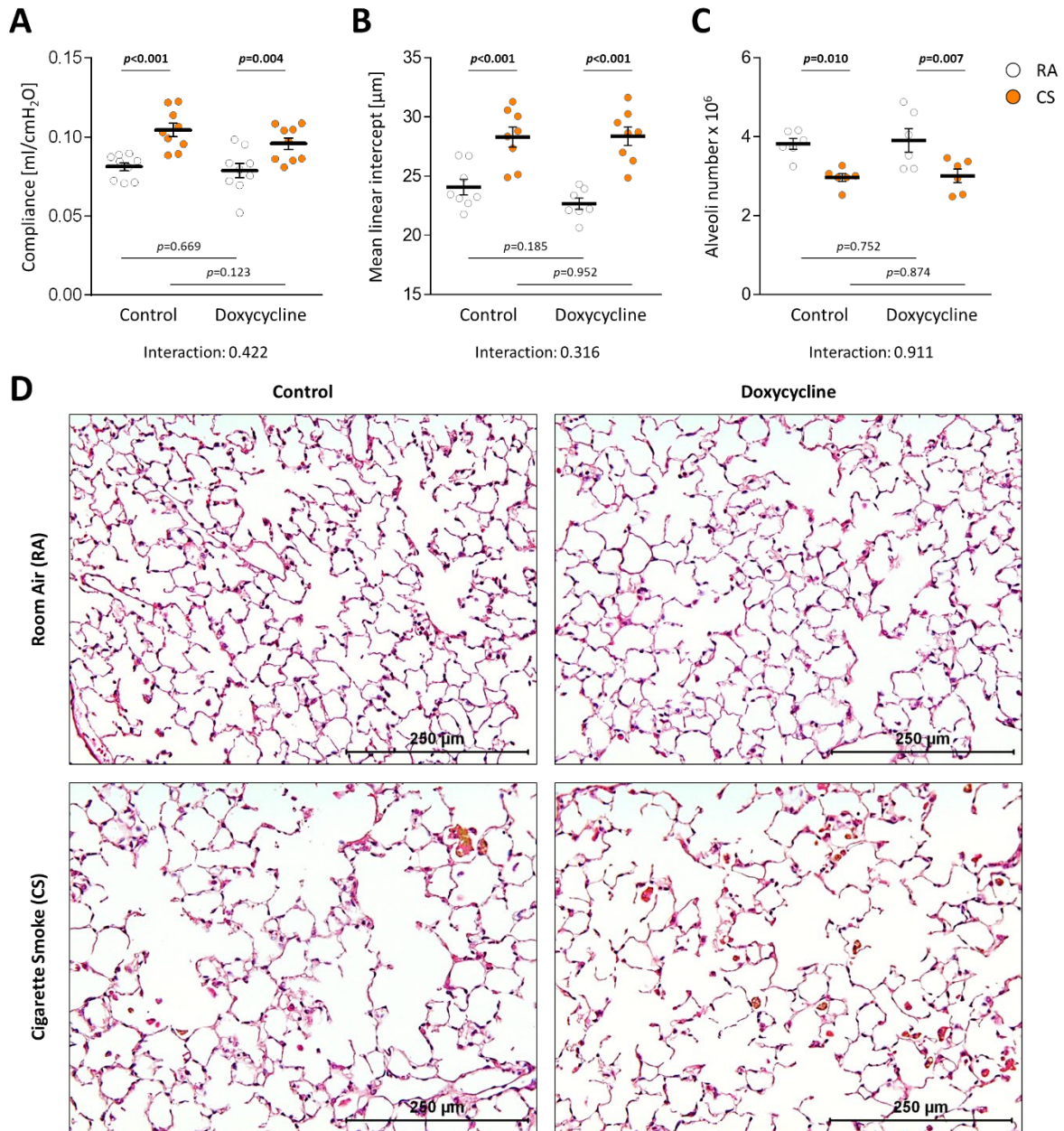


Figure 45. The sole effect of doxycycline on CS-induced emphysema. (A) Static compliance was measured by *in vivo* lung function test. **(B)** Mean linear intercept was quantified using alveolar morphometry in H&E stained lung sections from experimental mice. **(C)** The number of alveoli in the left lung lobe was determined using design-based stereology. **(D)** Representative images showing lung parenchyma in experimental animals. H&E staining (blue-nuclei, red-cytoplasm); 200x magnification; scale bar: 250 μm . Mice were exposed to cigarette smoke (CS) or room air (RA) for 8 months and treated with doxycycline-containing food for additional 3 months in RA conditions. The mean value for each group is represented by a horizontal line +/- standard error of the mean (SEM). Statistical analysis – Unpaired Two-Way ANOVA; p values for each comparison and interactions are noted in the graphs.

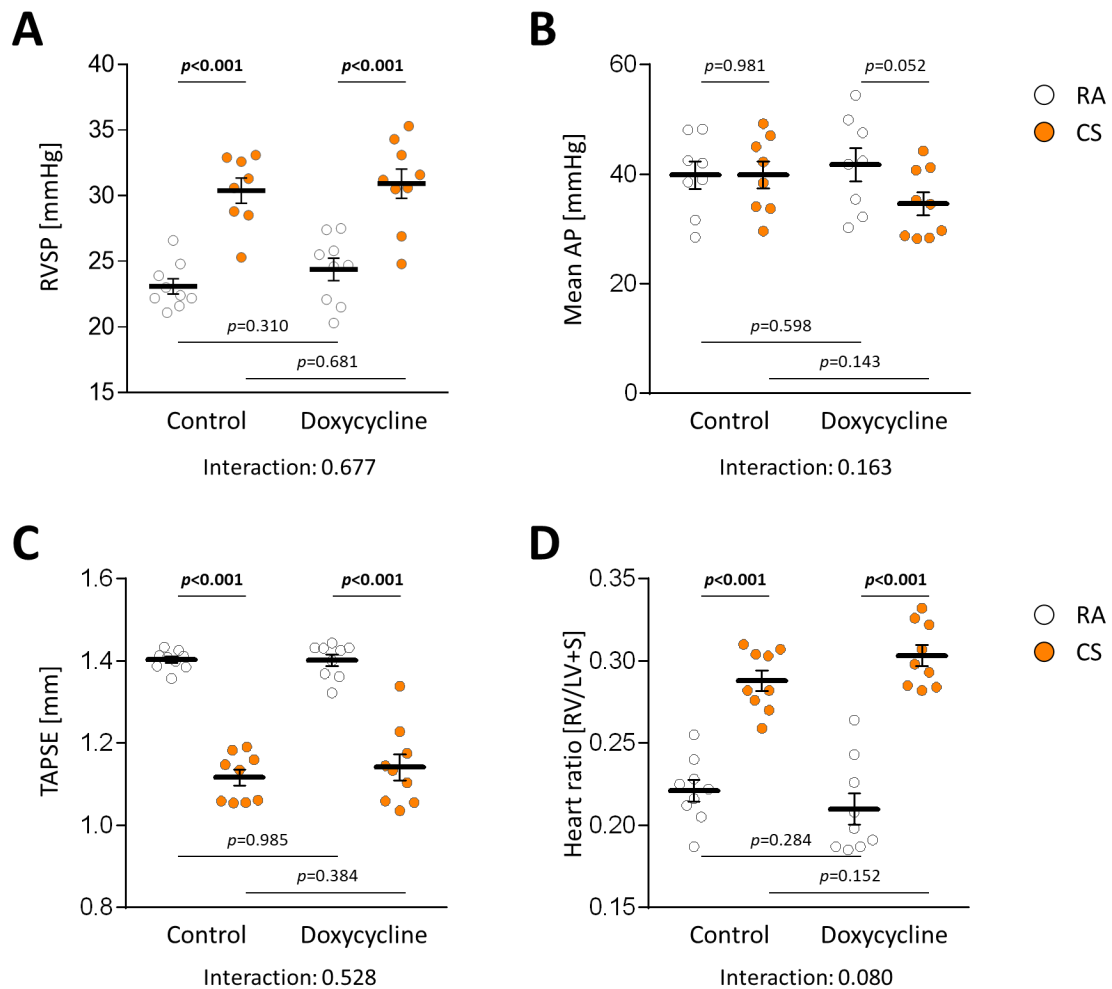


Figure 46. The sole effect of doxycycline on CS-induced PH. Hemodynamic measurements of **(A)** right ventricular systolic pressure (RVSP) and **(B)** systemic mean arterial pressure (AP) in mice that were exposed to CS for 8 months and subsequently treated with doxycycline for additional 3 months. **(C)** Tricuspid annular plane systolic excursion measured by non-invasive echocardiography. Right ventricular wall hypertrophy in experimental animals shown as **(D)** weight ratio between right ventricle (RV) and left ventricle with septum (LV+S). The mean value for each group is represented by a horizontal line +/- standard error of the mean (SEM). Statistical analysis – Unpaired Two-Way ANOVA; p values for each comparison and interactions are noted in the graphs.

3.1.7 The effect of FGF10 overexpression on CS-induced emphysema and PH

To investigate the effect of FGF10 overexpression on established CE-induced emphysema and PH in mice, the animals that contain the rtTA sequence under the *Rosa26* promoter and the

Fgf10 gene with inducible *Tet(O)* in the promoter sequence were exposed to CS for 8 months. After CS exposure was discontinued, animals were fed with doxycycline-containing food in a specific regimen to induce FGF10 overexpression (Gupte *et al.* 2009; Redelsperger *et al.* 2016; Hadzic *et al.* 2021). Namely, I fed the animals with doxycycline-containing chow for 7 days, followed by 7 days of regular, doxycycline-free chow feeding. This weekly scheme of doxycycline feeding I repeated during the entire treatment period for all time points. Such a feeding regime allowed the animals to ingest high dosages of doxycycline with minimizing common side effects of long-term antibiotic treatment. Parameters indicating emphysema and PH were measured and animals were sacrificed at 1-, 5- and 12 weeks time-points as depicted earlier in **Figure 10**.

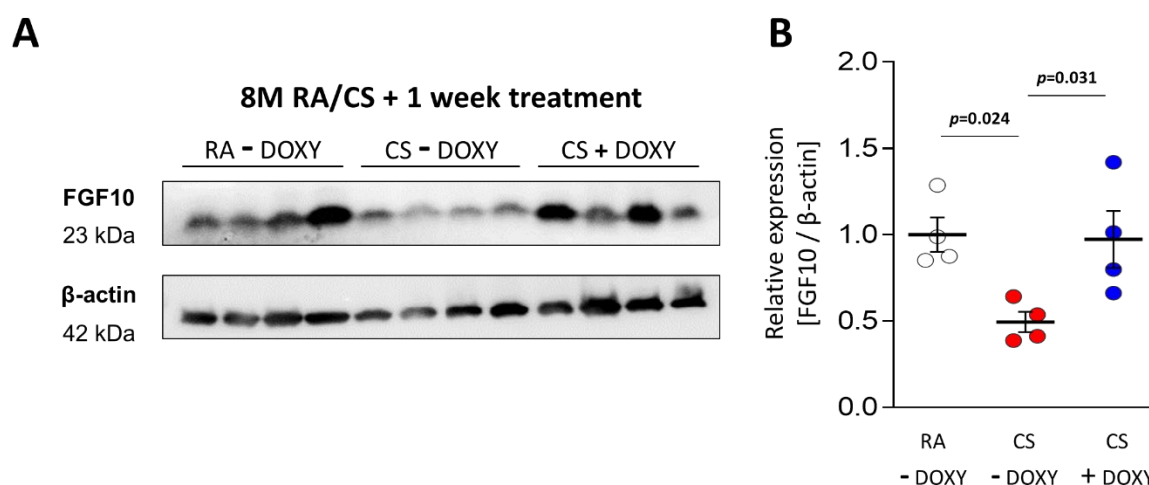


Figure 47. Confirmation of FGF10 overexpression. (A) Western blot representative membrane images and (B) quantification of FGF10 expression in lung homogenates from experimental animals after 8 months of room air (RA) or cigarette smoke (CS) exposure, with or without subsequent doxycycline feeding for 1 week (CS + Doxy). The mean value for each group is represented by a horizontal line +/- standard error of the mean (SEM). Protein expression in Western blot was quantified by band densitometry analysis and standardized to β -actin; relative expression was calculated by standardizing each value to the mean value of the room air (RA) -exposed control group. Statistical analysis – Unpaired One-Way ANOVA with Dunnett’s multiple comparisons corrections; p value for each comparison is noted above.

Furthermore, I confirmed FGF10 overexpression in lung homogenates from experimental animals at the earliest time-point – after 1 week of doxycycline feeding (**Figure 47**). Consistently with the results shown earlier (**Figure 35**), CS-exposed mice after 8 months had significantly decreased FGF10 expression in the lung homogenate, compared to the corresponding RA-exposed controls (**Figure 47**). Doxycycline feeding resulted in a significant increase of FGF10 expression in doxycycline-treated mice compared to the untreated CS-exposed animals (**Figure 47**).

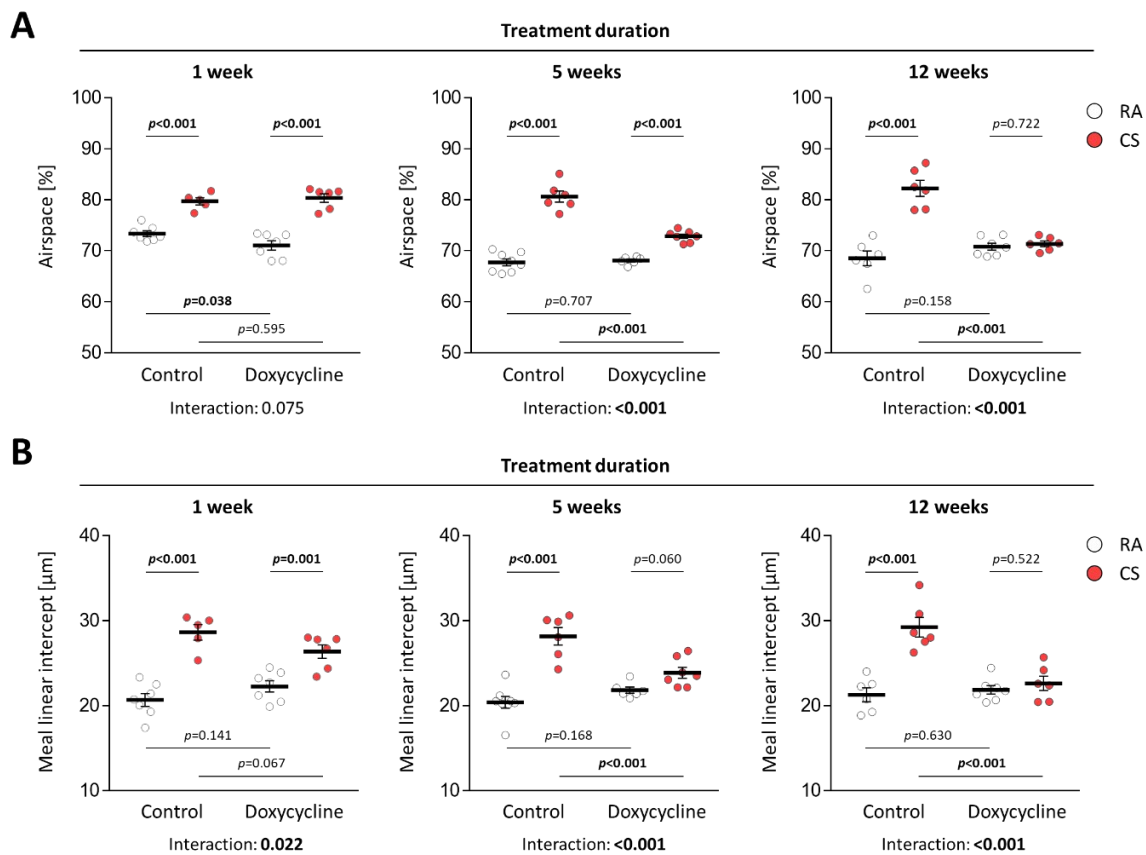


Figure 48. Airspace percentage and mean linear intercept quantified in mouse lungs after 8 months of CS exposure and subsequent FGF10 overexpression. Alveolar morphometry was employed to quantify **(A)** airspace percentage and **(B)** mean linear intercept in mouse lungs after 1, 5 or 12 weeks of doxycycline-induced FGF10 overexpression. Age-matched animals exposed to room air (RA) or cigarette smoke (CS) and fed with regular chow were used as controls. The mean value for each group is represented by a horizontal line +/- standard error of the mean (SEM). Statistical analysis – Unpaired Two-Way ANOVA; p values for each comparison and interactions are noted in the graphs.

Here I confirmed that long-term CS exposure for 8 months leads to the development of irreversible emphysema (**Figure 48, 49**). Emphysema remained even after discontinuation of CS exposure, as shown by an increase in airspace percentage (**Figure 48A**) and MLI (**Figure 48B, 49**). According to these two parameters, enlarged airspace in the untreated control animals remained stable up to 12 weeks after CS cessation (**Figure 48, 49**).

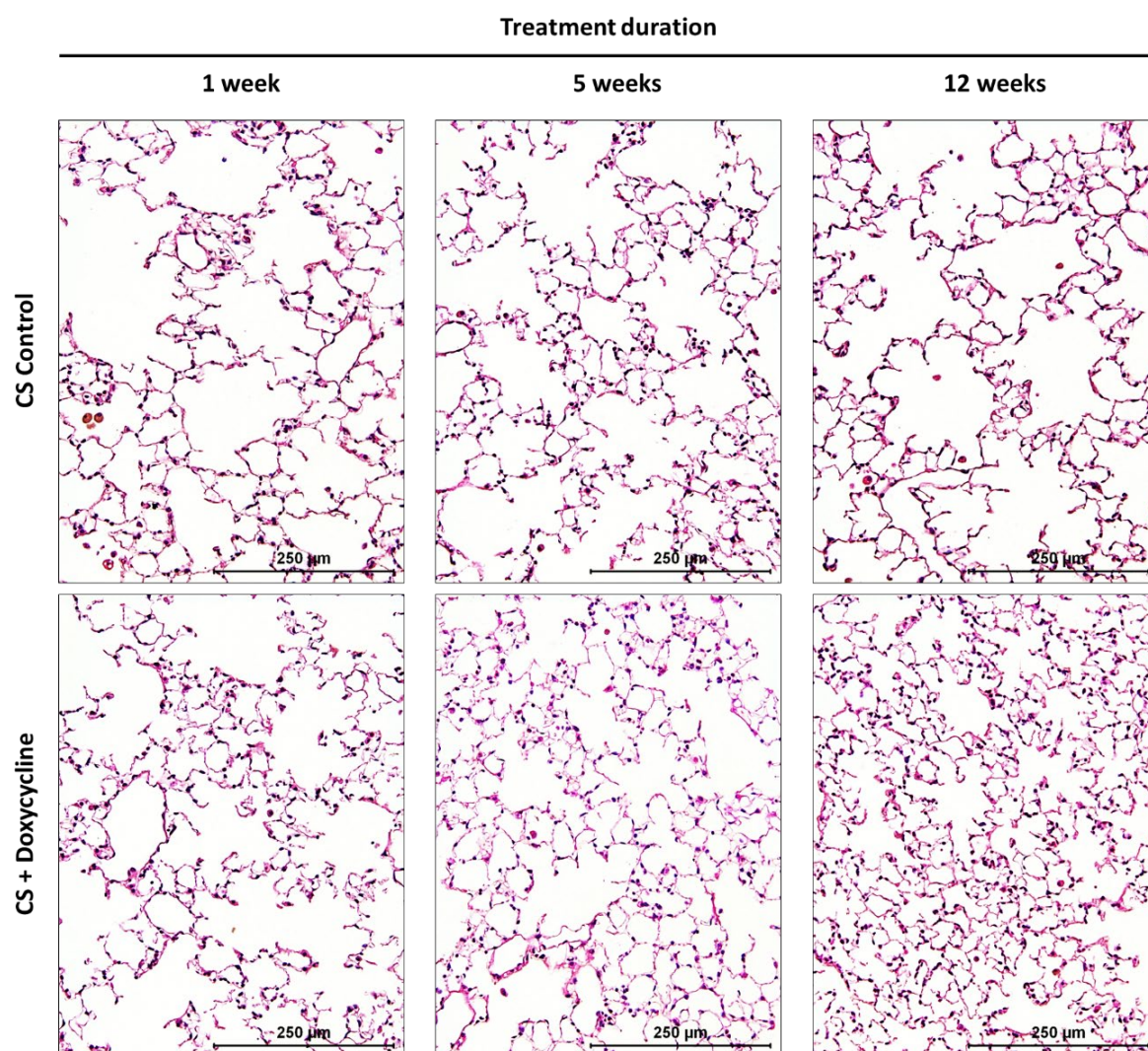


Figure 49. Representative images showing lung parenchyma in mice after 8 months of CS exposure with subsequent FGF10 overexpression. Upper row: CS-exposed untreated control mouse lungs; Bottom row: Lungs from CS-exposed mice after 1, 5 or 12 weeks of doxycycline-induced FGF10 overexpression. H&E staining (blue-nuclei, red-cytoplasm); 200x magnification; scale bar: 250 μm.

FGF10 overexpression in RA-exposed mice did not affect the structure of the distal lung parenchyma (**Figure 48**). Treatment with FGF10 overexpression for 1 week did not have any effect on lung parenchyma of 8-months CS-exposed mice, according to airspace percentage (**Figure 48A**) or MLI (**Figure 48B, 49**) data. However, 5 weeks of FGF10 overexpression resulted in a significant decrease of airspace percentage (**Figure 48A**) and MLI (**Figure 48B, 49**) in lungs from doxycycline-fed CS-exposed mice, compared to the untreated 8-months CS-exposed control mice. In animals that were treated for 12 weeks, airspace percentage (**Figure 48A**) and MLI (**Figure 48B**) were significantly decreased and in a range of healthy RA-exposed control mice (**Figure 48, 49**).

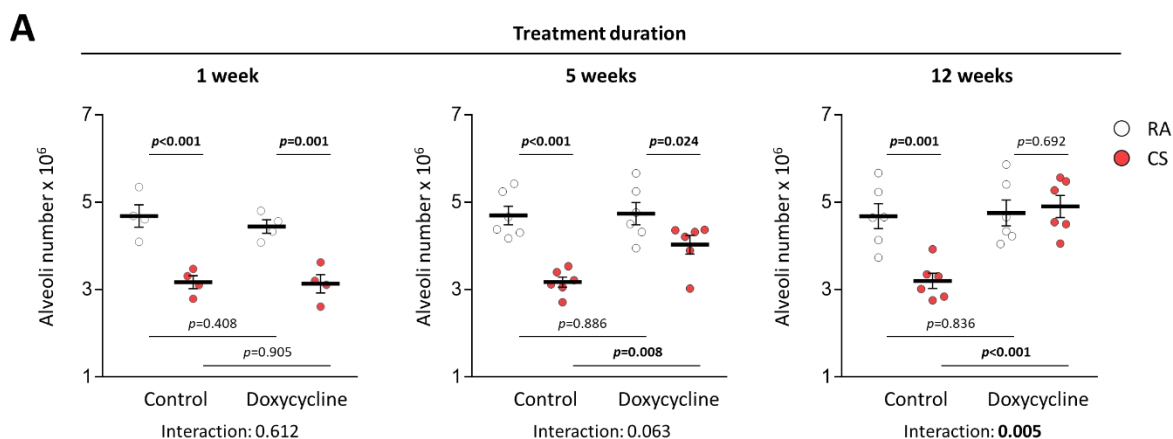


Figure 50. Alveoli number in left lung lobes from mice after CS exposure and subsequent FGF10 overexpression treatment. Number of alveoli in the left lung lobe was determined using design-based stereology. Mice were exposed to cigarette smoke (CS) or room air (RA) for 8 months and treated with doxycycline-induced FGF10 overexpression for 1, 5 or 12 weeks. The mean value for each group is represented by a horizontal line +/- standard error of the mean (SEM). Statistical analysis – Unpaired Two-Way ANOVA; p values for each comparison and interactions are noted in the graphs.

Using design-based stereology, the alveoli number was estimated, as described earlier. Alveoli number results obtained from my experimental animals were consistent with the alveolar morphometry data. Parenchymal simplification in CS-exposed mouse lungs was observed as a significant decrease in alveoli number (**Figure 50**). FGF10 overexpression for 5 weeks partially

reversed CS-induced alveoli destruction (**Figure 50**). Henceforth, 12 weeks of treatment was sufficient to restore the alveolar number in CS-exposed mouse lungs (**Figure 50**).

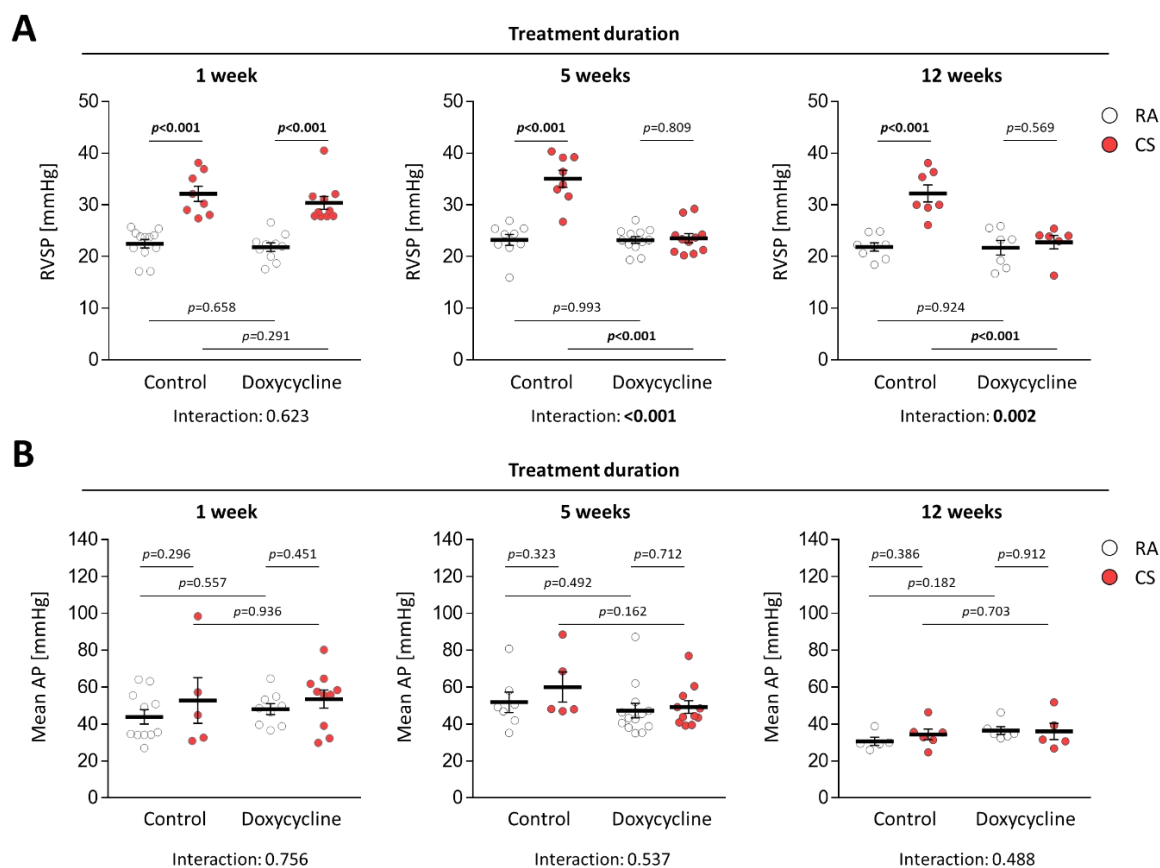


Figure 51. The effect of FGF10 overexpression on CS-induced pulmonary hypertension. Hemodynamic measurements of **(A)** right ventricular systolic pressure (RVSP) and **(B)** mean systemic arterial pressure (AP) in mice after 8 months of CS exposure and 1, 5 or 12 weeks of doxycycline-induced FGF10 overexpression treatment. The mean value for each group is represented by a horizontal line +/- standard error of the mean (SEM). Statistical analysis – Unpaired Two-Way ANOVA; p values for each comparison and interactions are noted in the graphs.

In line with the data shown earlier, hemodynamic measurements revealed significantly increased RVSP in untreated CS-exposed mice compared to the corresponding RA-exposed controls (**Figure 51A**). FGF10 overexpression for 1 week did not affect RVSP in experimental animals (**Figure 51A**). Correspondingly to the effects on emphysema, 5 weeks of FGF10 overexpression already was sufficient to completely reverse CS-induced increase in RVSP

(Figure 51A). Mean systemic arterial pressure remained unchanged between experimental groups in all time points (Figure 51B).

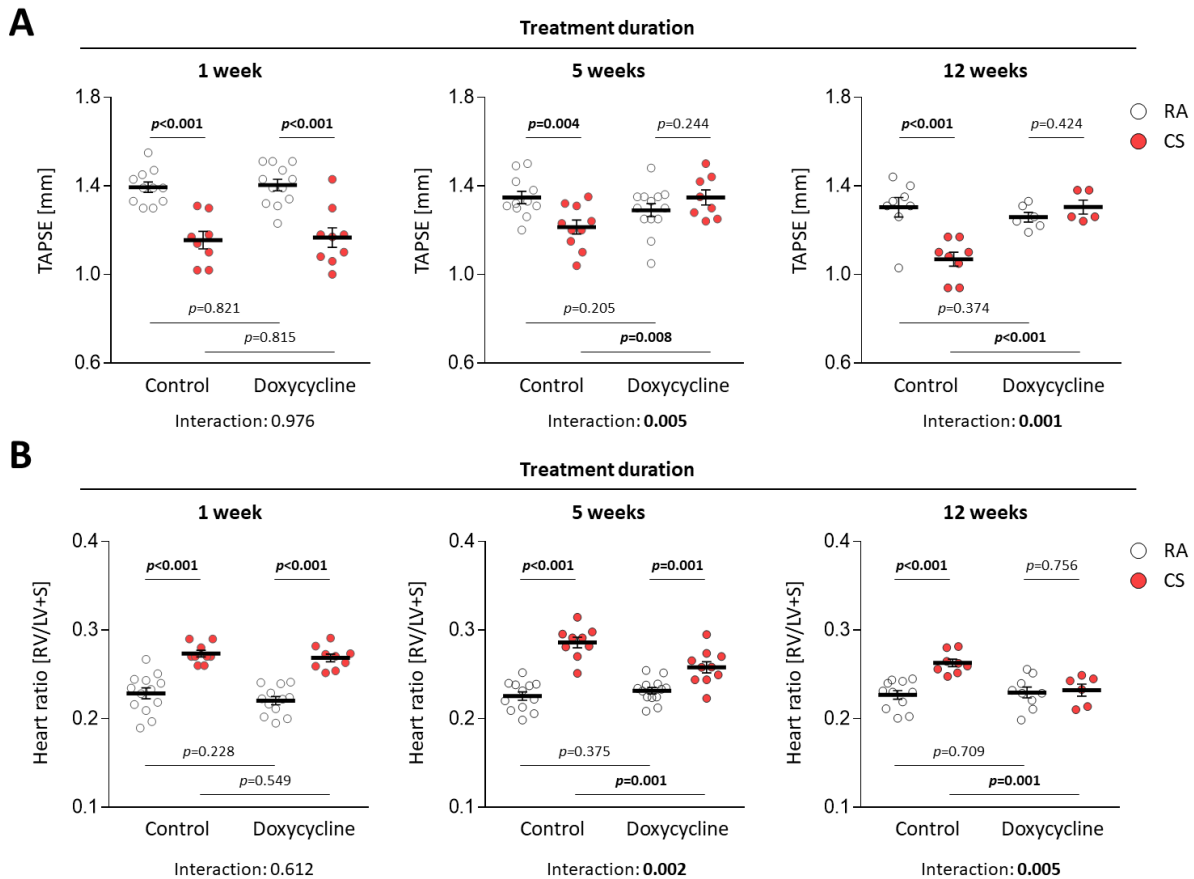


Figure 52. The effect of FGF10 overexpression on CS-induced right heart alterations. (A) Tricuspid annular plane systolic excursion (TAPSE) measured by non-invasive echocardiography in mice after 1, 5 and 12 weeks of FGF10 overexpression. **(B)** Right ventricular (RV) weight was measured and standardized to the weight of the left ventricle with the septum (LV+S). The mean value for each group is represented by a horizontal line +/- standard error of the mean (SEM). Statistical analysis – Unpaired Two-Way ANOVA; p values for each comparison and interactions are noted in the graphs.

Furthermore, FGF10 overexpression reversed the CS-induced remodelling of RV and RV function (Figure 52). FGF10 overexpression for 5 or 12 weeks restored TAPSE to the range of healthy mice (Figure 52A). After 5 weeks, FGF10 overexpression led to a significant decrease in RV mass compared to corresponding untreated CS-exposed controls (Figure 52B). However, RV mass at this time-point was still increased compared to the RA-exposed mice (Figure 52B).

After 12 weeks of treatment, Fulton's index in the treated animals was in the range of healthy mice (**Figure 52B**).

3.1.8 Signalling pathways underlying emphysema and PH reversal upon FGF10 overexpression

Genes involved in the FGF10-mediated reversal of CS-induced emphysema and PH were analysed at the earliest time-point – day 7 of FGF10 overexpression after 8 months of CS exposure.

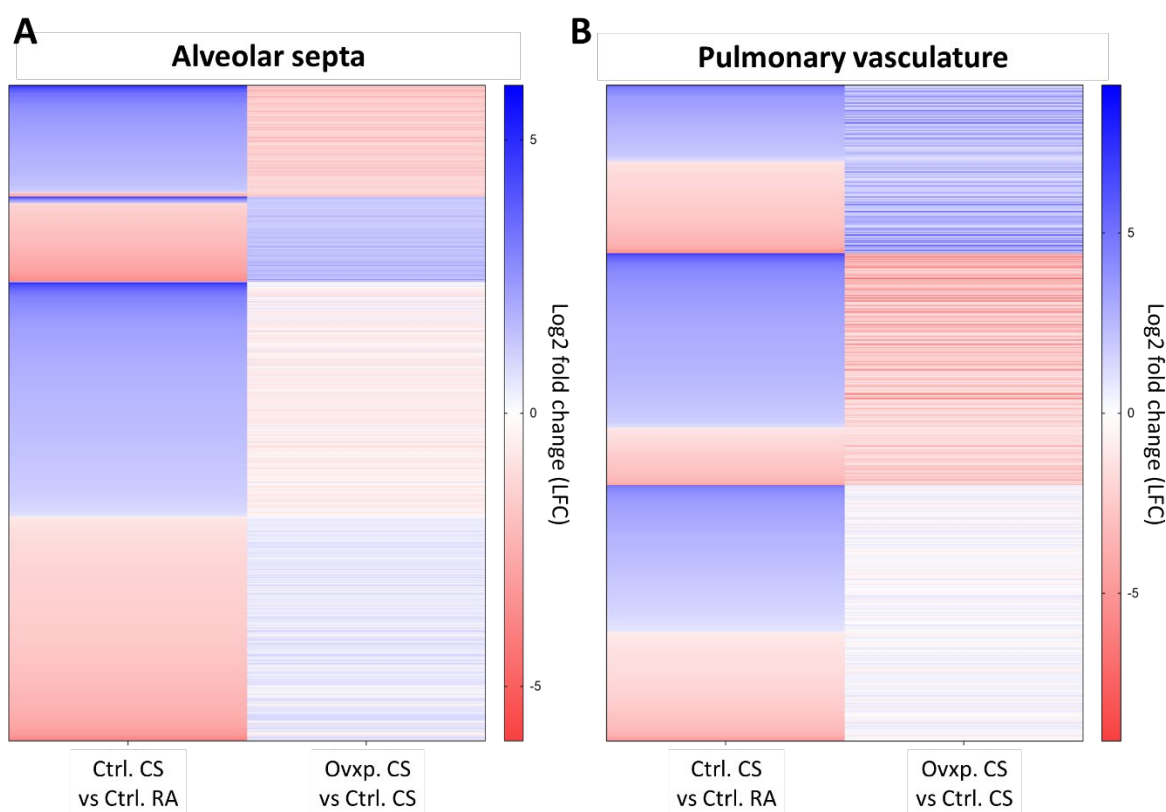


Figure 53. Heat maps showing all CS-regulated genes in untreated animals. Heat maps are showing all the genes that are regulated in untreated mice upon cigarette smoke (CS) exposure compared to room air (RA) controls ($-\log p \geq 1.3$ for the Ctrl. CS vs Ctrl. RA comparison) in **(A)** alveolar septa or **(B)** pulmonary vasculature. Gene expression regulation of the CS-regulated genes in untreated mice is also shown for FGF10 overexpressing (Ovxp.) after CS versus control CS mice (Ovxp. CS vs Ctrl. CS). Blue: upregulation, logarithmic fold change (LFC) ≥ 0 ; Red: downregulation, LFC ≤ 0 . Colour gradient indicates intensity of the expression change as indicated on the left side of the corresponding heat map.

Similarly as before, gene expression analysis was performed separately for the alveolar septal wall compartment and the pulmonary vasculature. Every gene that had $-\log p \geq 1.3$ for the given comparison was considered as regulated. In the heat maps (**Figure 53**) all the genes are shown that are regulated upon CS exposure ($\log p \geq 1.3$ for the Ctrl. CS vs Ctrl. RA comparison) in alveolar septa (**Figure 53A**) and in the pulmonary vasculature (**Figure 53B**). The clusters were formed based on the direction of the LFC, considering the direction of change in both groups.

In the alveolar septal compartment, I observed that approximately one-third of the genes had strong regulation in both comparisons (**Figure 53A**). Of interest, the vast majority of these genes are regulated in the opposite direction with FGF10 overexpression compared to CS exposure (**Figure 53A**). The rest of the CS-regulated genes in alveolar septa had very subtle LFC change with FGF10 overexpression at this early time-point (**Figure 53A**).

In contrast to the alveolar septa, in pulmonary vessels, a mixed pattern of LFC direction between the analysed comparisons was detected (**Figure 53B**). Some of the genes regulated in both analysed groups were regulated in the same, whereas the others were regulated in the opposite direction (**Figure 53B**). However, I could observe that more than half of the CS-regulated genes were regulated by FGF10 overexpression in the opposite direction (**Figure 53B**).

Further, I focused on the genes that are commonly regulated with CS exposure ($\log p \geq 1.3$ for the Ctrl. CS vs Ctrl. RA comparison) and upon FGF10 overexpression upon CS exposure ($\log p \geq 1.3$ for the Ctrl. CS vs Ovxp. CS comparison) (**Figure 54**). In the alveolar septal wall compartment, I found 209 genes that were affected by both CS exposure and subsequent FGF10 overexpression (**Figure 54A**). The vast majority of these genes were inversely regulated upon FGF10 overexpression, compared to the CS exposure (**Figure 54C**). Of interest, the most prominent genes, upregulated upon CS exposure and downregulated with FGF10 overexpression, are protease cathepsin K (Ctsk) and apoptosis inducer Bcl-2-Related Ovarian Killer (Bok) (**Figure 54C**). I also found endothelial Nos3 decreased in alveolar septa upon CS exposure and upregulated with FGF10 overexpression (**Figure 54C**).

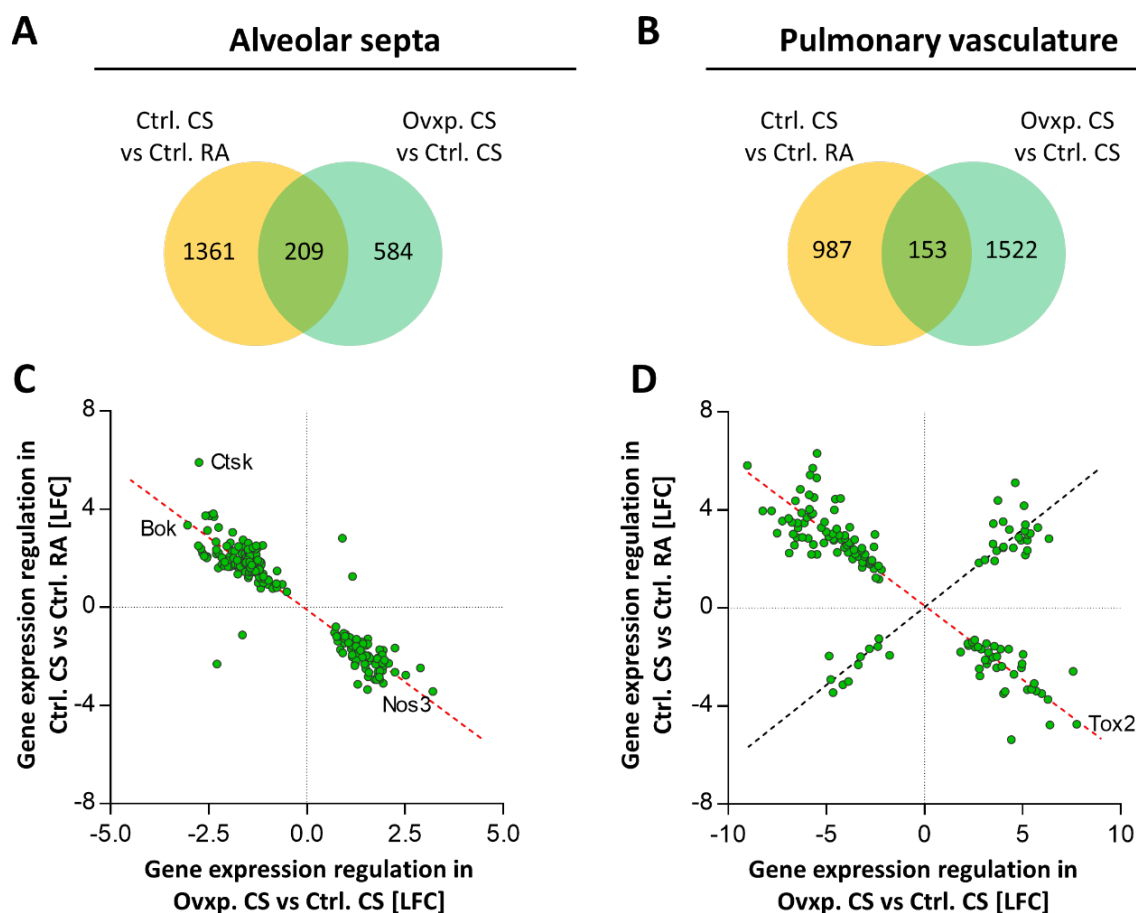


Figure 54. CS- and FGF10 overexpression-related gene expression pattern during reversion of emphysema and PH. Venn diagrams were used to show the number of dysregulated genes ($-\log p \geq 1.30$) in **(A)** alveolar septa and **(B)** the pulmonary vasculature during therapeutic intervention at the 1-week time-point. The overlap region show genes that were commonly regulated between cigarette smoke (CS)- versus room air (RA)-exposed Wt mice (Ctrl. CS vs Ctrl. RA) and FGF10 overexpressing (Ovxp.) after CS versus control CS mice (Ovxp. CS vs Ctrl. CS). These common genes are further investigated in comet plots for **(C)** alveolar septa and **(D)** pulmonary vessels. Comet plots show the direction of gene expression changes; between the two compared groups of genes, positive (black dashed line) or negative correlation (red dashed line) implies the similar or opposite direction of log fold changes (LFC), respectively. Ctsk – Cathepsin K; Bok – BCL2 Family Apoptosis Regulator BOK; Nos3 – nitric oxide synthase 3 (endothelial form); Tox2 – TOX High Mobility Group Box Family Member 2.

In the pulmonary vasculature, 153 genes were commonly regulated between the two analysed groups **(Figure 54B)**. Hereby, using comet plots, I could clearly distinguish two “populations”

of genes (**Figure 54D**). One group of genes was regulated in the same direction by CS exposure and FGF10 overexpression, as indicated by the black dashed line (**Figure 54D**). This is not surprising, taking into account that CS exposure also can upregulate FGF10 expression in the pulmonary vascular compartment. The other group of genes was inversely regulated by FGF10 expression compared to the effect of CS exposure, as indicated by the red dashed line (**Figure 54D**). These genes could be involved in the reverse remodelling process and the resolution of CS-induced PH. Among the most prominently regulated genes, not many could be connected with the vasculature and pulmonary hypertension phenotype. However, I found transcription factor TOX High Mobility Group Box Family Member 2 (Tox2) that could be of interest for the mechanism of PH reversion. Tox2 was most prominently downregulated in pulmonary vasculature upon CS exposure and markedly upregulated with FGF10 overexpression (**Figure 54D**).

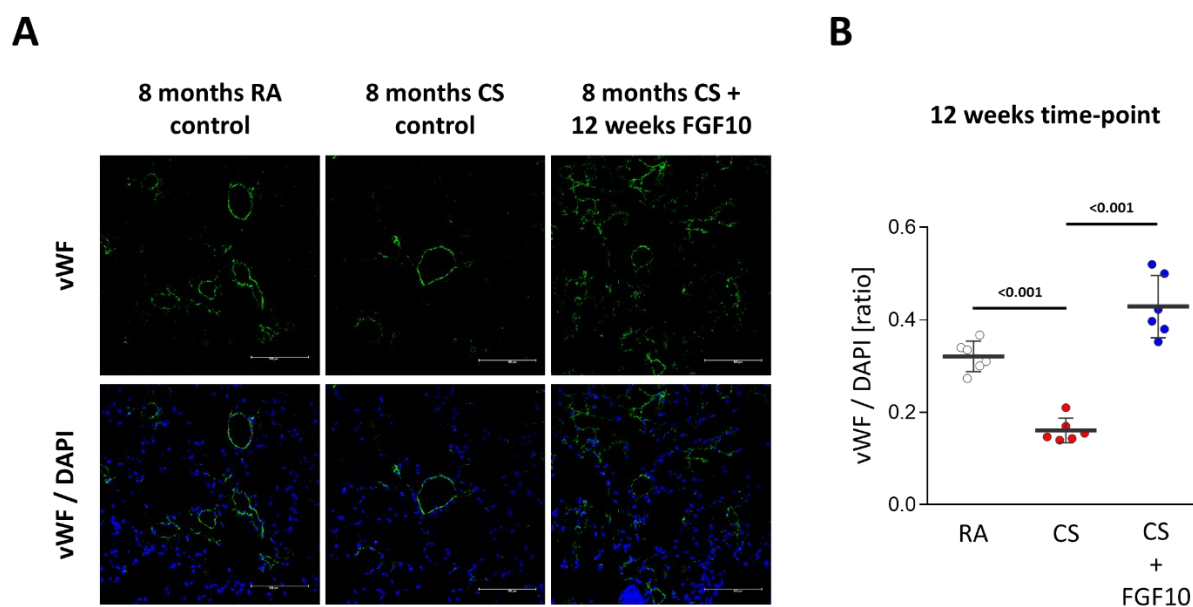


Figure 55. Endothelial cells in mouse lungs after CS-induced emphysema and PH, and subsequent doxycycline-induced FGF10 overexpression for 12 weeks. (A) Immunofluorescence staining and **(B)** fluorescence intensity quantification of von Willebrand factor (vWF) / DAPI in lungs from cigarette smoke (CS)-treated mice with or without doxycycline-induced FGF10 overexpression for 12 weeks. Statistical analysis – Unpaired One-Way ANOVA with Dunnett’s multiple comparisons corrections; p value for each comparison is noted above.

In the alveolar septa, I observed that nitric oxide synthase 3 (*Nos3*), an isoform that is typically expressed in the endothelial cells (Fish *et al.* 2006), was among the most prominently regulated genes, downregulated upon CS exposure and upregulated with FGF10 (**Figure 54C**).

This suggests that the endothelium in alveolar septa could be affected by CS exposure and by FGF10 overexpression. Therefore, I performed immunofluorescence staining for von Willebrand factor (vWF), a marker protein of endothelial cells, in lung sections from experimental animals at the 12-weeks time-point (**Figure 55**). Fluorescence intensity was analysed using confocal microscopy (**Figure 55**). In the lung sections of CS-exposed mice, I observed significantly decreased vWF signal compared to RA-exposed controls. CS-induced decrease in vWF signal was reversed with FGF10 overexpression (Figure 55B).

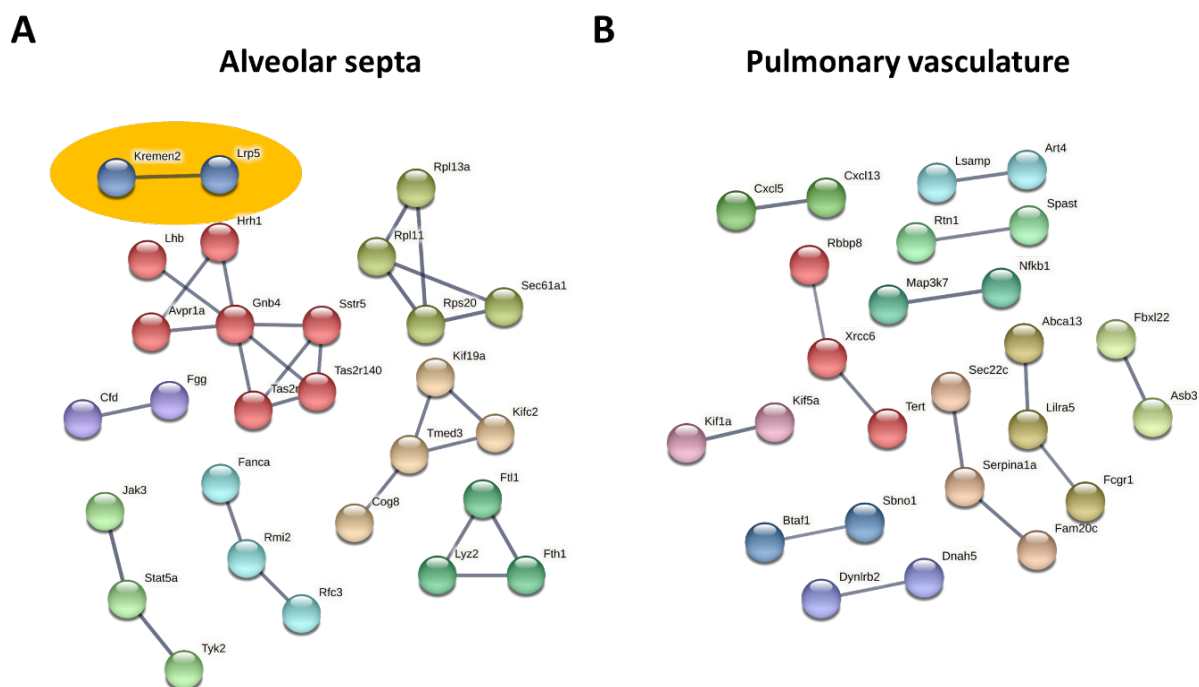


Figure 56. Functional protein association networks of CS- and FGF10 overexpression-regulated genes during reversion of emphysema and PH. Genes that were commonly regulated between cigarette smoke (CS)- versus room air (RA)-exposed Wt mice (Ctrl. CS vs Ctrl. RA) and FGF10 overexpressing after CS versus control CS mice (Ovxp. CS vs Ctrl. CS) in **(A)** alveolar septa ($-\log p \geq 1.3$ for both comparisons) and **(B)** pulmonary vasculature ($-\log p \geq 1.3$ for both comparisons) at 1-week time-point were analysed using functional protein association networks (STRING-DB database). Abbreviations: Kremen2 – kringle containing transmembrane protein 2; Lrp5 – LDL receptor related protein 5; Lhb – luteinizing hormone subunit beta; Hrhh1 – histamine receptor H1; Gnb4 – G protein subunit beta 4; Avpr1a –

arginine vasopressin receptor 1A; Sstr5 – somatostatin receptor 5; Tas2r – taste 2 receptor member 38; Cfb – complement factor B; Fgg – fibrinogen gamma chain; Jak3 – janus kinase 3; Stat5a – signal transducer and activator of transcription 5A; Tyk2 – tyrosine kinase 2; Fanca – FA complementation group A; Rmi2 – RecQ mediated genome instability 2; Rfc3 – replication factor C subunit 3; Rpl – ribosomal protein L; Rps20 – ribosomal protein S20; Kif19a – kinesin family member 19a; Kifc2 – kinesin family member C2; Sec61a1 – SEC61 translocon subunit alpha 1; Tmed3 – transmembrane P24 trafficking protein 3; Cog8 – component of oligomeric golgi complex 8; Ftl1 – ferritin light chain; Lyz2 – lysozyme 2; Cxcl – C-X-C motif chemokine ligand; Lsamp – limbic system associated membrane protein; Art4 – ADP-ribosyltransferase 4; Rtn1 – reticulon 1; Spast – spastin; Map3k7 – mitogen-activated protein kinase kinase kinase 7; Nfkb1 – nuclear factor kappa B subunit 1; Rbbp8 – RB binding protein 8, endonuclease; Xrcc6 – X-ray repair cross complementing 6; Tert – telomerase reverse transcriptase; Kif5a – kinesin family member 5a; Kif1a – kinesin family member 1a; Btaf1 – B-TFIID TATA-box binding protein associated factor 1; Sbn1 – strawberry notch homolog 1; Dynlrb2 – dynein light chain roadblock-type 2; Dnah5 – dynein axonemal heavy chain 5; Sec22c – SEC22 homolog C, vesicle trafficking protein; Serpina1a – serpin family A member 1; Fam20c – FAM20C Golgi associated secretory pathway kinase; Abca13 – ATP binding cassette subfamily A member 13; Lila5 – leukocyte immunoglobulin like receptor A5; Fcgr1 – Fc gamma receptor 1a; Fbxl22 – F-box and leucine rich repeat protein 22; Asb3 – ankyrin repeat and SOCS box containing 3.

Using a functional protein association network (STRING-DB database), I analysed the potential connection between the commonly regulated genes (Szkarczyk *et al.* 2019) (**Figure 56**). However, the analysed genes do not appear to align to one signalling pathway but are rather scattered between several not necessarily related signalling pathways (**Figure 56**). This was the case in alveolar septa (**Figure 56A**) as well as in pulmonary vasculature (**Figure 56B**). Between clusters in alveolar septa, I observed kringle containing transmembrane protein 2 (Kremen2) and low-density lipoprotein receptor-related protein 2 (Lrp2) that are connected to the Wnt signalling (Mao *et al.* 2003; Rey *et al.* 2010; Kaiser *et al.* 2019; Schulze *et al.* 2010).

3.1.9 Effect of the *in vitro* FGF10 treatment on human COPD PCLS

Furthermore, as described earlier, I prepared precision cut lung slices (PCLS) from the lungs of 6 COPD patients with end-stage emphysema that underwent lung transplantation. In order to determine if also COPD lungs could still respond to FGF10, I treated the PCLS with recombinant human FGF10 (rhFGF10) *in vitro* (**Figure 57**). A nucleotide analogue bromodeoxyuridine (BrdU)

was added in the cell culture medium together with the FGF10 treatment so I could track the newly proliferating cells.

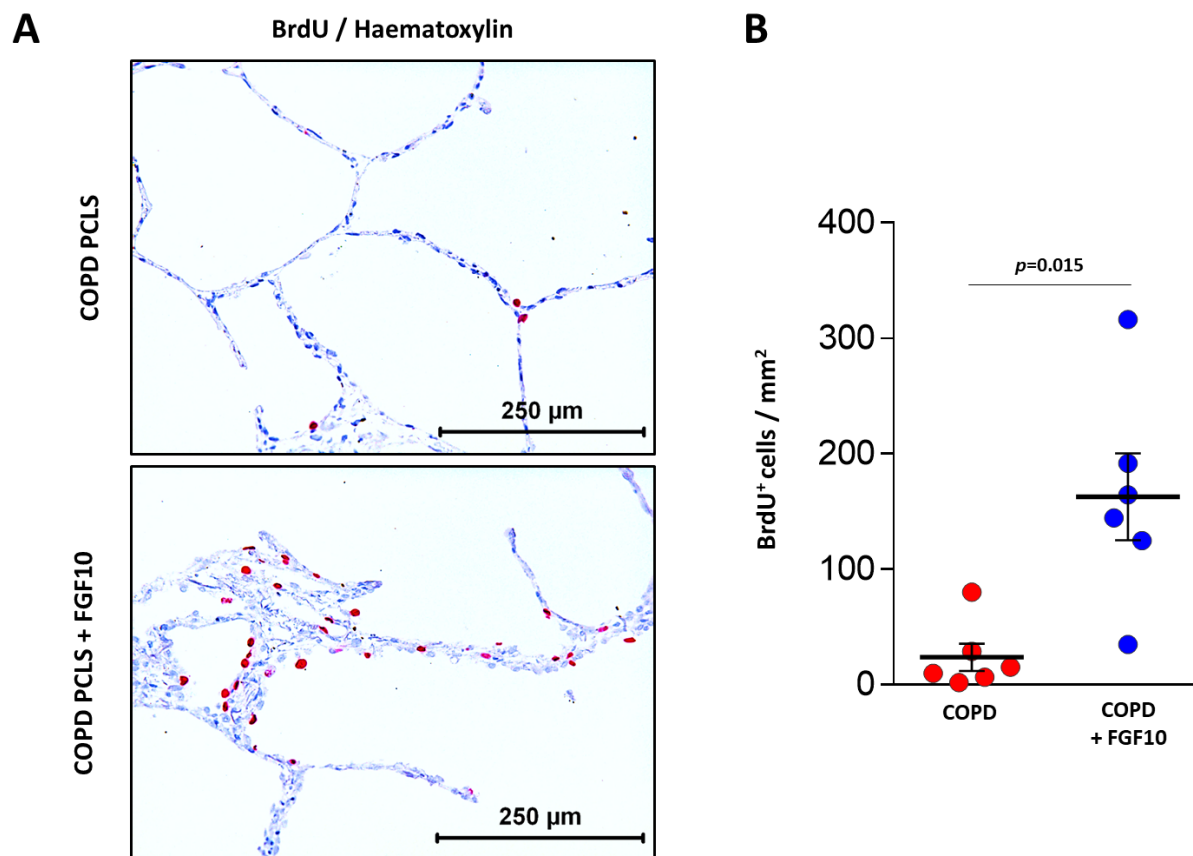


Figure 57. FGF10 treatment of precision-cut lung slices (PCLS) from patients with COPD. PCLS were prepared from COPD patients and treatment with FGF10 was performed *in vitro*, in the presence of bromodeoxyuridine (BrdU). **(A)** Representative images showing IHC staining of BrdU⁺ cells – red; blue – haematoxylin; 200x magnification; Scale bar: 250 μ m. **(B)** Proliferation was measured by counting cells that incorporated BrdU. The number of BrdU⁺ cells was standardized to the tissue area. Statistical analysis – Paired t-test was applied; p value for the comparison is given.

The number of BrdU positive (BrdU⁺) cells in COPD lungs was determined by IHC staining. COPD PCLS treated with rhFGF10 had a significantly increased number of BrdU⁺ cells compared to the corresponding untreated PCLS (**Figure 57A, 57B**). Of interest, proliferating cells upon FGF10 treatment were mainly localised in the alveolar septal walls and to a lesser extent in the

tunica intima of large vessels (**Figure 57A**). Not many proliferating cells could be observed in large bronchi or in the *tunica media* of large, clearly visible pulmonary vessels (**Figure 57A**).

3.1.10 FGF10 overexpression after elastase-induced emphysema and PH

Further, I investigated the effect of FGF10 overexpression in a more severe emphysema model – a mouse model of elastase-induced pulmonary emphysema. Single intratracheal application of elastase was used to induce severe emphysema in mice that is similar to the end-stage emphysema observed in advanced COPD. After only single administration, apparent deterioration of the lung structure is visible macroscopically (**Figure 13**). *In vivo* lung function measurements revealed a significantly increased lung compliance in animals that received elastase compared to the saline-treated controls (**Figure 58**).

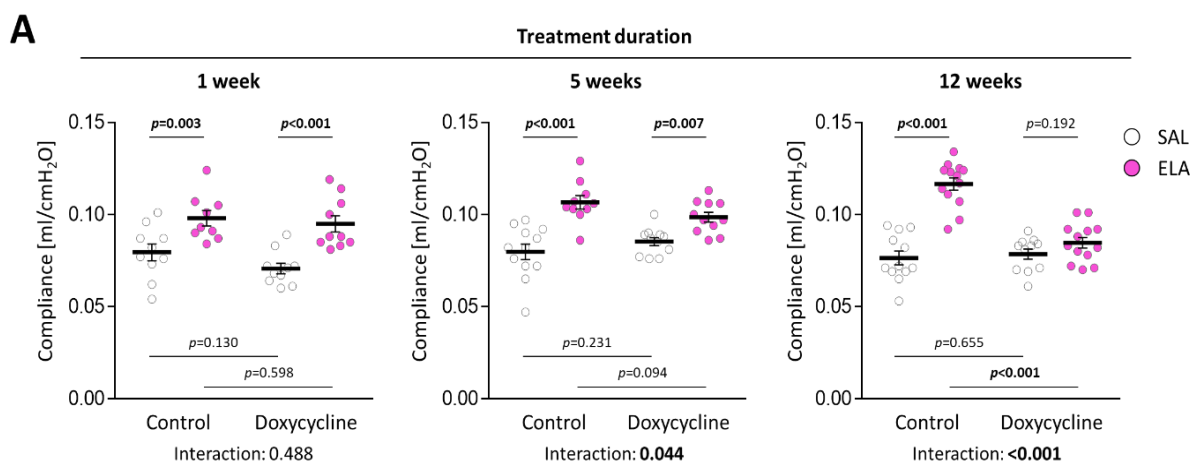


Figure 58. Lung compliance in mice after elastase-induced pulmonary emphysema and subsequent FGF10 overexpression treatment. Static compliance was measured by an *in vivo* lung function test in mice after elastase-induced lung injury and subsequent doxycycline-induced FGF10 overexpression for 1, 5 or 12 weeks. Elastase (ELA) or saline (SAL) solution was applied intratracheally using a Microsprayer® aerosoliser and feeding with doxycycline-containing chow started 4 weeks later. Control animals were fed with regular chow. The mean value for each group is represented by a horizontal line +/- standard error of the mean (SEM). Statistical analysis – Unpaired Two-Way ANOVA; p values for each comparison and interactions are noted in the graphs.

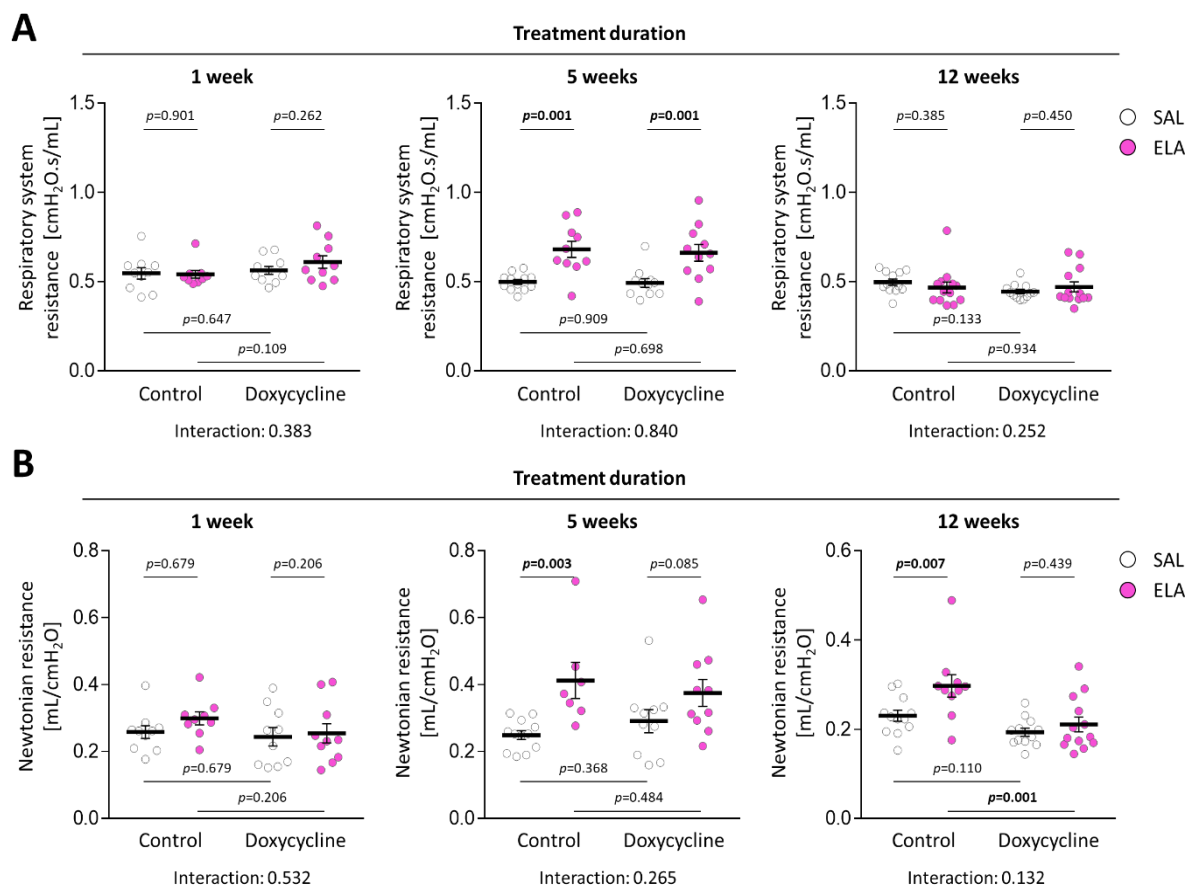


Figure 59. Respiratory resistance in mice after elastase-induced pulmonary emphysema and subsequent FGF10 overexpression treatment. (A) Overall respiratory system resistance and **(B)** conducting airway (Newtonian) resistance measured by an *in vivo* lung function test in mice after elastase-induced lung injury and subsequent doxycycline-induced FGF10 overexpression for 1, 5 or 12 weeks. Elastase (ELA) or saline (SAL) solution was applied intratracheally using Microsprayer® aerosoliser and feeding with doxycycline-containing chow started 4 weeks later. Control animals were fed with regular chow. The mean value for each group is represented by a horizontal line +/- standard error of the mean (SEM). Statistical analysis – Unpaired Two-Way ANOVA; p values for each comparison and interactions are noted in the graphs.

Doxycycline-induced FGF10 overexpression for 1 week did not cause significant changes in lung compliance when compared to untreated elastase controls (**Figure 58**). At the 5-weeks time-point, I could observe mild amelioration of increased lung compliance in FGF10 overexpression treated compared to untreated mice that received elastase – seen as a significant interaction

between elastase and FGF10 overexpression (**Figure 58**). However, after 12 weeks of doxycycline feeding, the elastase-induced increase in lung compliance was almost completely reversed in FGF10-treated mice compared to the untreated controls (**Figure 58**).

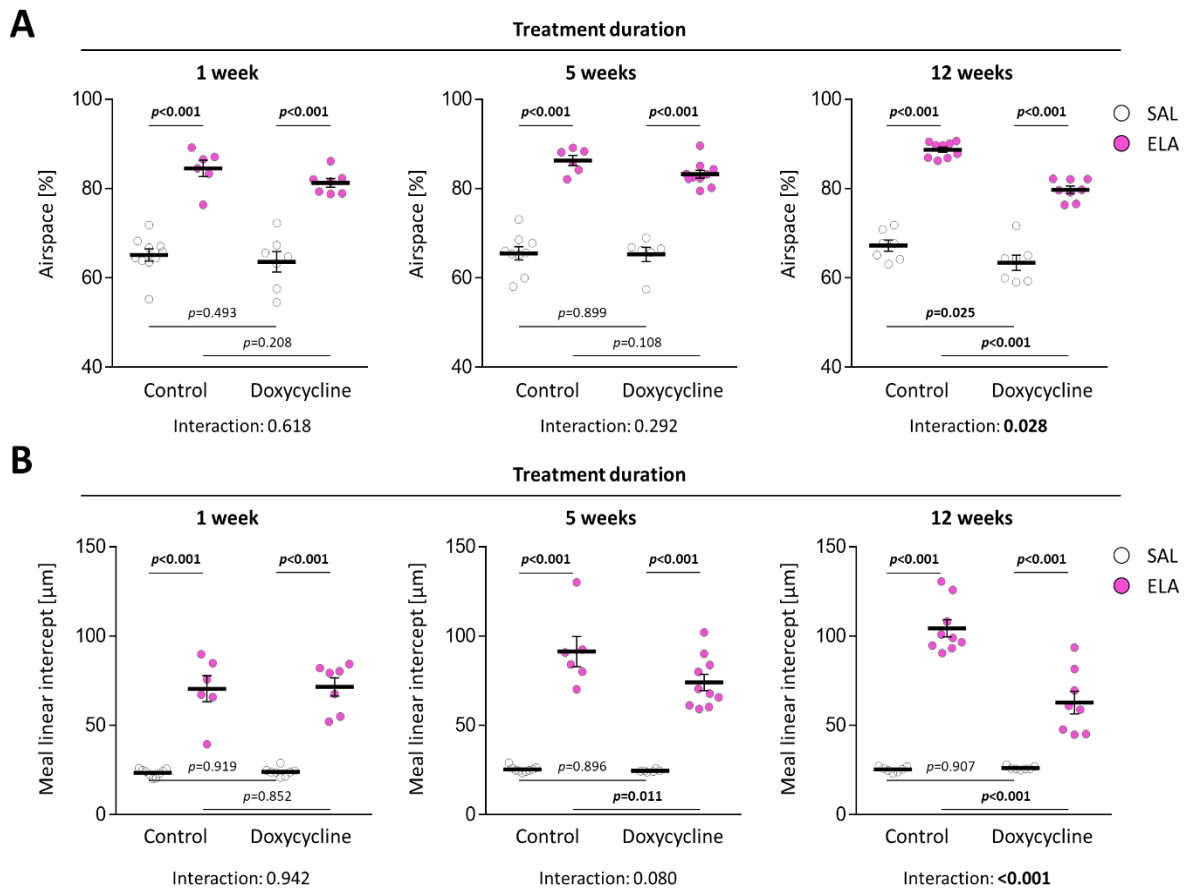


Figure 60. Lung parenchyma destruction in mouse lungs after elastase-induced emphysema and subsequent FGF10 overexpression treatment. Alveolar morphometric quantification of **(A)** airspace percentage and **(B)** mean linear intercept after elastase-induced lung injury and 1, 5 or 12 weeks of doxycycline-induced FGF10 overexpression treatment. Elastase (ELA) or saline (SAL) solution was applied intratracheally using Microsprayer® aerosoliser and feeding with doxycycline-containing chow started 4 weeks later. Control animals were fed with regular chow. The mean value for each group is represented by a horizontal line +/- standard error of the mean (SEM). Statistical analysis – Unpaired Two-Way ANOVA; p values for each comparison and interactions are noted in the graphs.

Furthermore, I analysed other parameters, measured by *in vivo* lung function tests, that are related to airflow limitation (**Figure 59**). Despite the lung parenchymal destruction in mice that received elastase, I observed a significant increase in overall respiratory system resistance at the 5-weeks time-point (**Figure 59A**). This effect was, however, not evident at the later time-point (**Figure 59A**).

Newtonian (airway) resistance was significantly increased at 5- and 12-weeks time-points in mice that received elastase compared to saline-treated controls (**Figure 59B**). Elastase-induced increase in Newtonian resistance was ameliorated in mice upon 12 weeks of doxycycline-induced FGF10 overexpression (**Figure 59B**). In saline-treated control animals, *in vivo* lung function tests did not reveal any changes in overall respiratory system resistance (**Figure 59A**) or Newtonian (airway) resistance (**Figure 59B**) upon FGF10 overexpression.

Elastase-induced destruction of the distal lung parenchyma was also quantified histologically in H&E-stained lung sections. I observed a significant increase in airspace percentage (**Figure 60A**) and in MLI (**Figure 60B**) in elastase-treated control mice. Consistently with the lung compliance measurements, only 12 weeks of doxycycline-induced FGF10 overexpression treatment significantly decreased the airspace percentage compared to the corresponding untreated elastase controls (**Figure 60A**). However, in the lungs of mice that were fed with doxycycline, MLI was significantly decreased already after 5 weeks, compared to the elastase control animals (**Figure 60B**). Further improvement in MLI was observed at the 12-week time-point (**Figure 60B**). Representative images of the changes in the lung parenchymal structure in treated and control mice that received elastase are shown in **Figure 61**. When compared to the CS-exposure animal model, elastase-induced pulmonary emphysema seems to worsen over time. This is seen as a time-dependent increase in measured emphysema parameters (lung compliance, airspace % and MLI) between saline- and elastase-treated control mice (**Figure 58, 60, 61**). This is most obvious when looking at the gradual increase in lung compliance (**Figure 58**) or MLI (**Figure 60B**). However, the reversion of the measured parameters upon the treatment in most of the animals is more remarkable than before the treatment started.

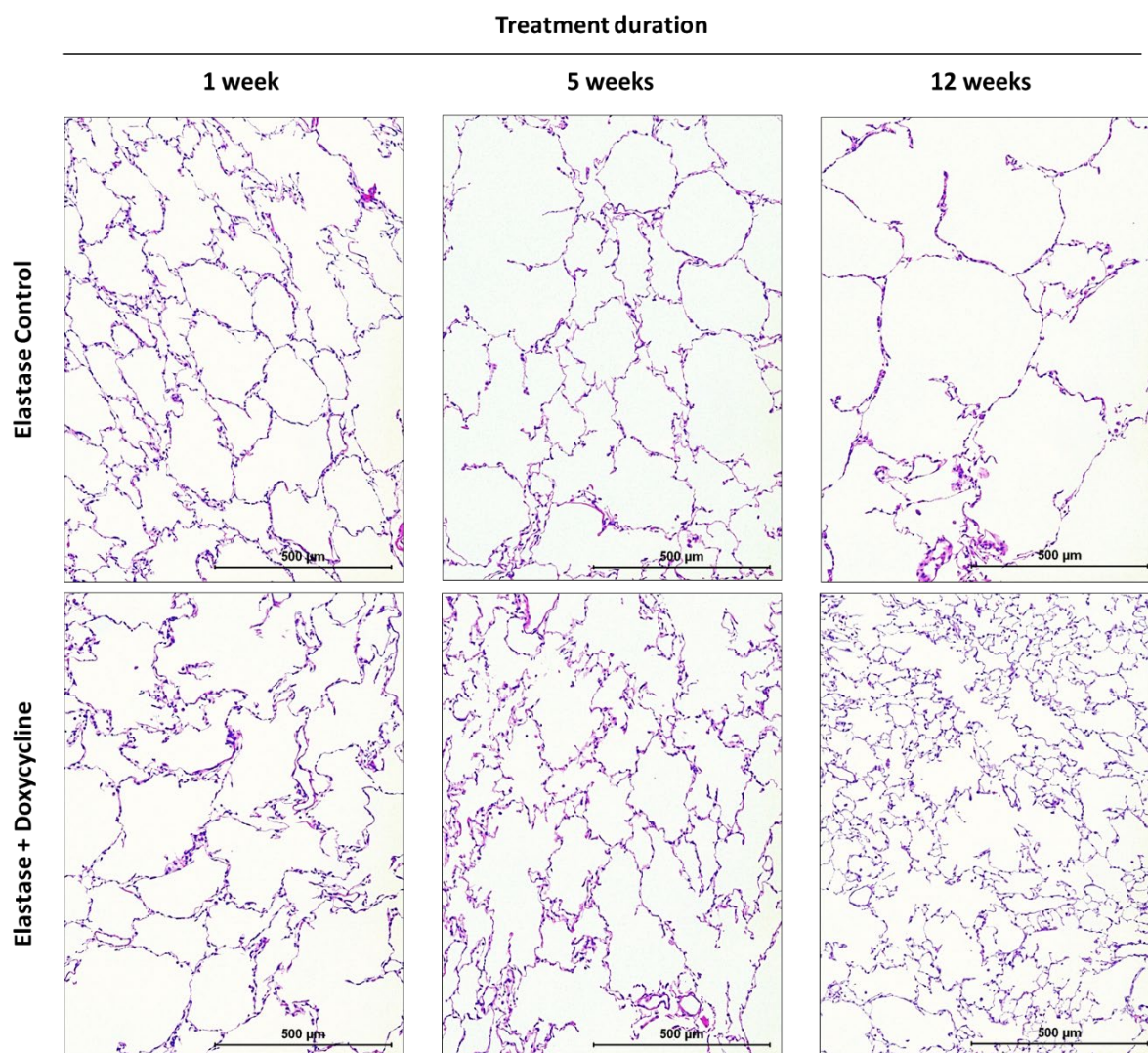


Figure 61. Representative images showing lung parenchyma after elastase-induced emphysema with or without subsequent doxycycline-induced FGF10 overexpression treatment. Upper row: Lung parenchyma in untreated control mice after elastase-induced emphysema at 1, 5 and 12 weeks time-points; Bottom row: injured lungs after 1, 5 and 12 weeks of doxycycline-induced FGF10 overexpression treatment. H&E staining (blue-nuclei, red-cytoplasm); 100x magnification; scale bar: 500 µm.

Hemodynamic measurements revealed a significant increase in RVSP in untreated control mice that received elastase (**Figure 62A**). The increase in RVSP seems to be most prominent at the 12-weeks time-point (**Figure 62A**). Doxycycline-induced FGF10 overexpression for 1 week did not affect RVSP (**Figure 62A**). However, 5 weeks of FGF10 overexpression was already

sufficient to completely reverse the elastase-induced increase in RVSP (**Figure 62A**). At the 12-week time-point, RVSP in treated animals remained at the level of healthy mice (**Figure 62A**). Mean systemic AP remained unchanged between the experimental groups at all time-points, regardless of the elastase instillation or FGF10 overexpression (**Figure 62B**).

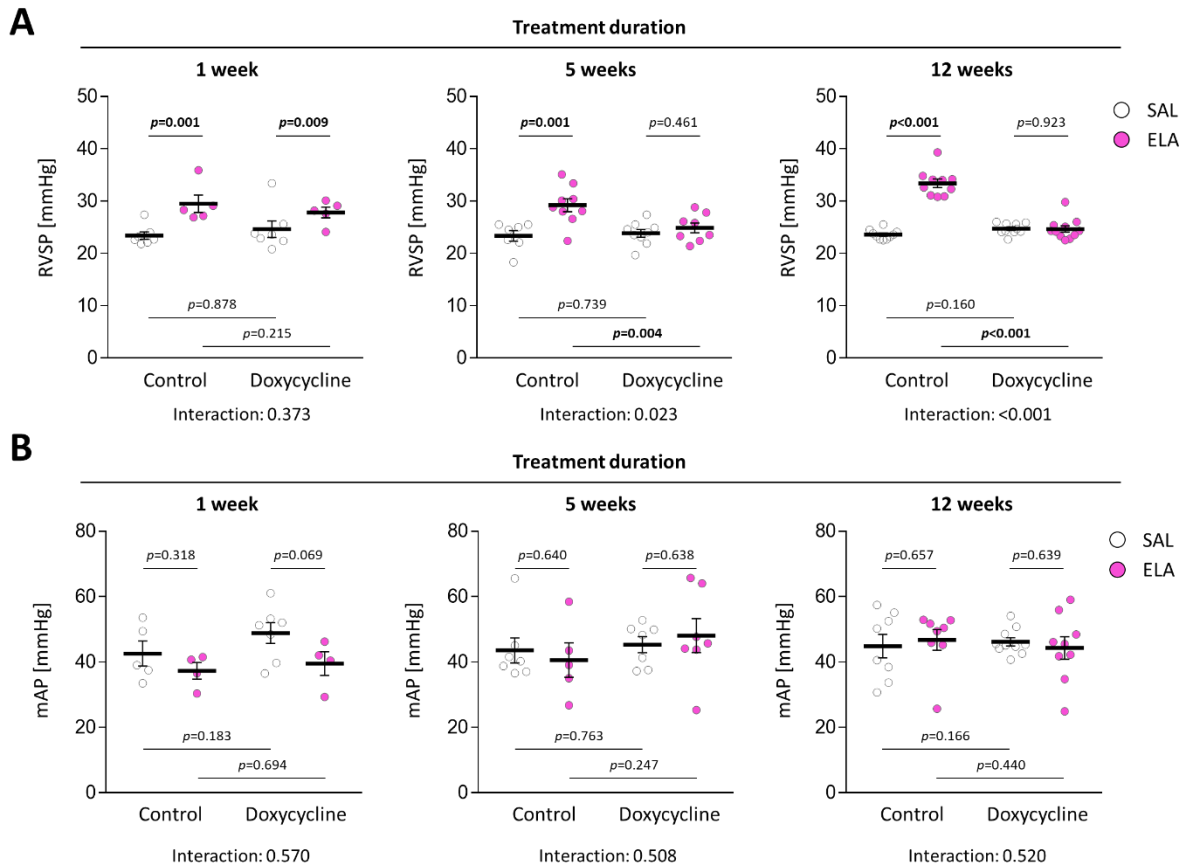


Figure 62. Hemodynamic measurements obtained in mice after elastase-induced pulmonary emphysema and PH, and subsequent FGF10 overexpression treatment. Hemodynamic measurements of (A) right ventricular systolic pressure (RVSP) and (B) mean systemic arterial pressure (AP) in mice after elastase-induced lung injury and 1, 5 or 12 weeks of doxycycline-induced FGF10 overexpression treatment. Elastase (ELA) or saline (SAL) solution was applied intratracheally using Microsprayer® aerosoliser and feeding with doxycycline-containing chow started 4 weeks later. Control animals were fed with regular chow. The mean value for each group is represented by a horizontal line +/- standard error of the mean (SEM). Statistical analysis – Unpaired Two-Way ANOVA; p values for each comparison and interactions are noted in the graphs.

TAPSE, measured by non-invasive echocardiography, was significantly decreased in elastase-treated mice, compared to corresponding saline controls in all time-points (**Figure 63A**). FGF10 overexpression significantly reversed the decrease of TAPSE in elastase treated mice already after 5 weeks of treatment (**Figure 63A**).

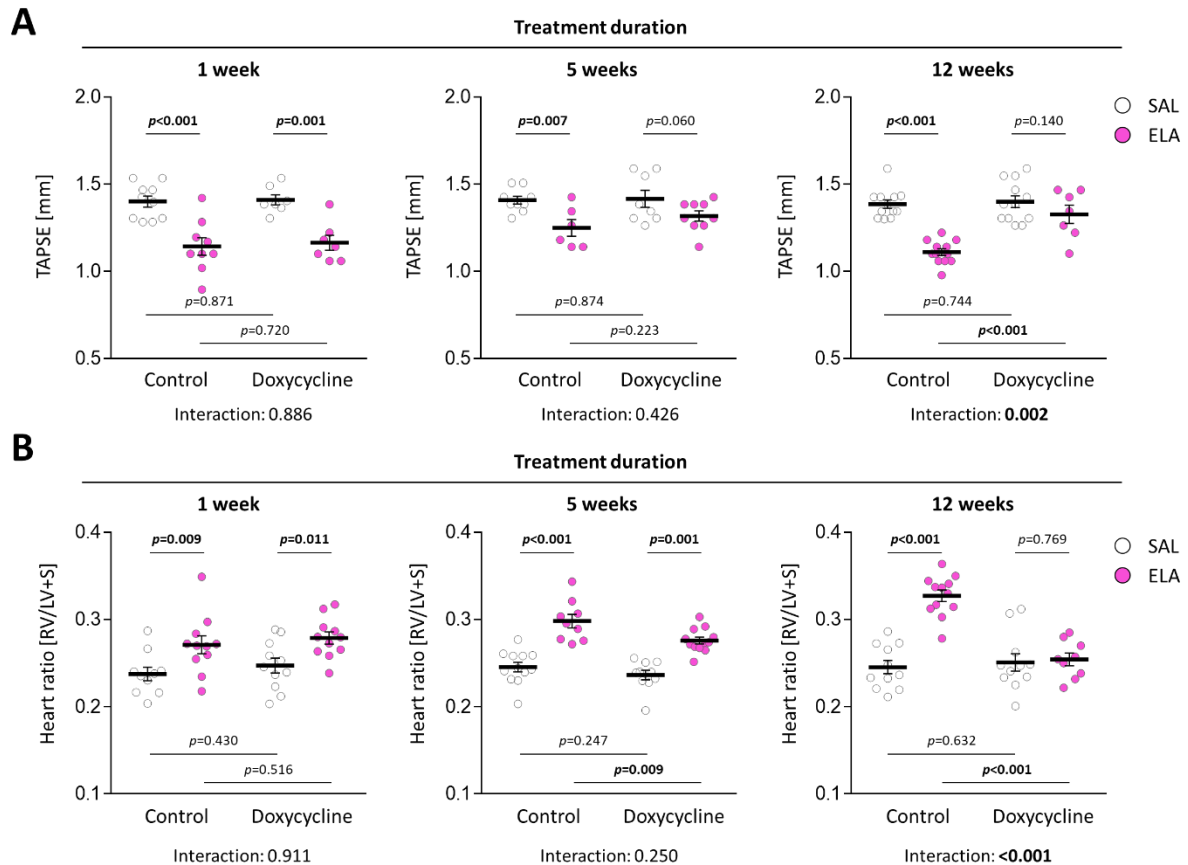


Figure 63. Right heart alterations in mice after elastase-induced pulmonary emphysema and PH, and subsequent FGF10 overexpression treatment. (A) Tricuspid annular plane systolic excursion (TAPSE) measured by non-invasive echocardiography in mice after elastase-induced emphysema and 1, 5 or 12 weeks of doxycycline-induced FGF10 overexpression. **(B)** Right ventricular wall hypertrophy in experimental animals shown as the weight ratio between right ventricle (RV) and left ventricle with septum (LV+S). Elastase (ELA) or saline (SAL) solution was applied intratracheally using Microsprayer® aerosoliser and feeding with doxycycline-containing chow started 4 weeks later. Control animals were fed with regular chow. The mean value for each group is represented by a horizontal line +/- standard error of the mean (SEM). Statistical analysis – Unpaired Two-Way ANOVA; p values for each comparison and interactions are noted in the graphs.

Heart ratio (Fulton's index) measurements revealed an increase in RV mass in mice that received elastase compared to the corresponding saline controls (**Figure 63B**). After 5 weeks, FGF10 overexpression led to a significant decrease in RV mass compared to corresponding untreated CS-exposed controls (**Figure 63B**). Despite the reverse remodelling caused by FGF10 overexpression, RV mass in 5 weeks treated elastase mice was still increased compared to the corresponding saline control mice (**Figure 63B**). After 12 weeks of FGF10 overexpression treatment, Fulton's index in treated elastase animals was in the range of healthy mice (**Figure 63B**).

Furthermore, the Microfil® perfusion experiment revealed an increased vascular density in lungs from doxycycline-treated mice at the 12-weeks time-point, compared to the corresponding untreated elastase controls (**Figure 64A**). This suggests that the pulmonary vascular component is also affected by FGF10 overexpression. Furthermore, lung sections from experimental animals at the 12-weeks time-point were subjected to immunofluorescence staining for von Willebrand factor (vWF) and analysed using confocal microscopy (**Figure 64B, 64C**). In the lung sections from doxycycline-fed animals that overexpressed FGF10, I observed a stronger vWF signal than in the untreated elastase-treated controls (**Figure 64B, 64C**).

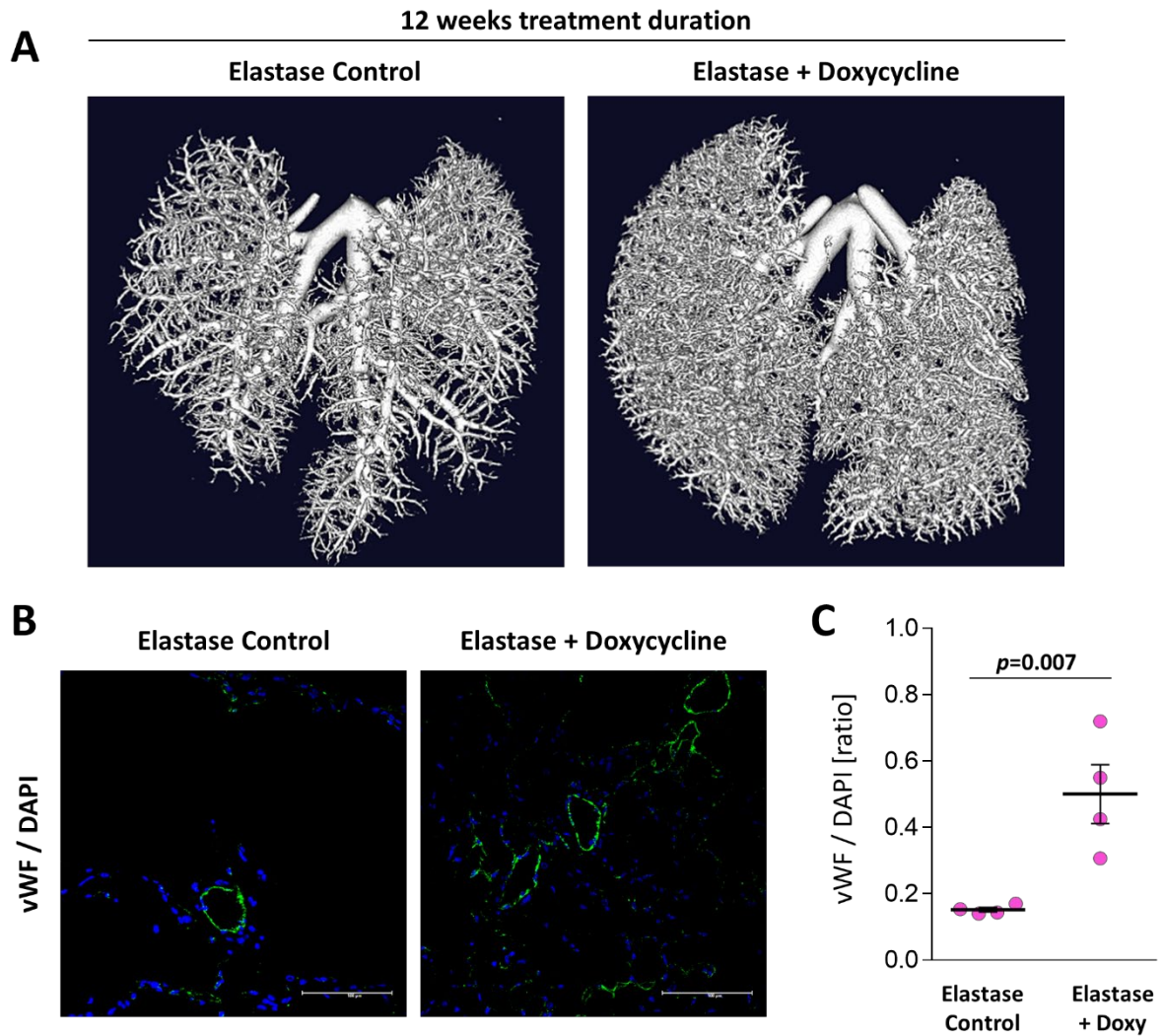


Figure 64. Pulmonary vasculature after elastase-induced emphysema and PH, and subsequent doxycycline-induced FGF10 overexpression for 12 weeks. (A) Microfil® perfused vascular tree, visualised *ex vivo* using micro-computed tomography (μ CT). Left: untreated control lungs showing the effect of elastase instillation on the pulmonary vasculature; Right: lungs after elastase instillation and doxycycline-induced FGF10 overexpression treatment for 12 weeks. **(B)** Immunofluorescence staining and **(C)** fluorescence intensity quantification of von Willebrand factor (vWF) / DAPI in lungs from elastase-treated mice with or without doxycycline-induced FGF10 overexpression for 12 weeks. Statistical analysis – Unpaired t-test; p value for each comparison is noted above.

4 Discussion

COPD is a common and still incurable lung disease. It is a complex disease comprising a wide variety of cellular and molecular alterations, including oxidative/nitrosative stress, augmented inflammation, increased proteolysis, senescence and aberrant lung repair (Gouveia *et al.* 2020; Kojonazarov *et al.* 2019; Yildirim *et al.* 2010; Houssaini *et al.* 2018; Kruk *et al.* 2021; Seimetz *et al.* 2020; Seimetz *et al.* 2011; Seimetz *et al.* 2015). Emerging literature reports dysregulation of developmental pathways in COPD, suggesting the importance of homeostatic mechanisms for maintaining lung structure integrity in adult life (Gouveia *et al.* 2020; Kruk *et al.* 2021; Kojonazarov *et al.* 2019; Yildirim *et al.* 2010). According to this concept, COPD is a disease of impaired lung repair and homeostasis. Previously, Seimetz *et al.* showed that iNOS inhibition via L-NIL treatment leads to lung parenchyma repair and reversed remodelling of the pulmonary vasculature in CS-exposed mice (Seimetz *et al.* 2011). Among several investigated targets in these animals, *Fgf10* expression was increased in the pulmonary vasculature, decreased in alveolar septa and remained unchanged in bronchi of CS-exposed mice (Seimetz *et al.* 2011). *Fgf10* expression was significantly increased upon L-NIL treatment in the pulmonary vasculature and alveolar septa (Seimetz *et al.* 2011). In bronchi from L-NIL-treated animals, *Fgf10* expression remained unchanged (Seimetz *et al.* 2011). These results indicate that *Fgf10* mRNA expression in alveolar septa and pulmonary vessels positively correlates with L-NIL-mediated reversion of CS-induced emphysema and PH in mice.

FGF10 is crucial during lung development, orchestrating branching morphogenesis (Bellusci *et al.* 1997). Additionally, *FGF10* haploinsufficiency in humans has been linked with impaired lung function, and single nuclear polymorphisms in the region of the *FGF10* locus were identified in COPD patients (Jackson *et al.* 2018; Smith *et al.* 2018; Klar *et al.* 2011). FGF10 binds predominantly to the receptor isoform FGFR2b, which is crucial for AT2 cell maintenance (Yuan *et al.* 2019). Furthermore, FGF10 promotes wound healing and prevents oxidant- as well as stretch-induced DNA damage in alveolar epithelial cells (Gupte *et al.* 2009). FGF10 overexpression, during the inflammatory or fibrotic phase of bleomycin-induced lung injury, reduced the extent of pulmonary fibrosis (Gupte *et al.* 2009; Yuan *et al.* 2019).

Therefore, I investigated the connection between RNS/ROS stress and FGF10 signalling in the context of COPD. Furthermore, I examined the effect of FGF10 signalling during the development of CS-induced emphysema and PH; and the possible therapeutic effects of FGF10 overexpression upon CS- or elastase-induced emphysema and PH in mice.

4.1 FGF10 signalling is impaired in lungs of CS-exposed mice and COPD patients

I investigated the FGF signalling in human material – lungs from healthy donors, smokers without and with COPD. *FGF1* and *FGF2* were downregulated on mRNA level in lungs of smokers with and without COPD. FGF1 and FGF2 are very potent FGF ligands that bind to all FGF receptors and their isoforms (MacKenzie, Korfei, *et al.* 2015; Zhang *et al.* 2006; Ornitz *et al.* 2015; Ornitz *et al.* 1996). Both FGF1 and FGF2 are often found upregulated in lung fibrosis and cancer (MacKenzie, Korfei, *et al.* 2015; Li, Wei, *et al.* 2015; El Agha, Seeger, *et al.* 2017; Manousakidi *et al.* 2018; Berger *et al.* 1999). Therefore, this effect might be due to the selection of lung tissue from human subjects that do not suffer from malignant diseases. However, this downregulation in lungs from smokers with and without COPD may suggest a general impairment of FGF signalling. The expression of FGF receptors and their isoforms in lung homogenate remained unchanged, which suggests no compensatory effects.

On the protein level, FGF10 expression was decreased in the lung homogenate from smokers without COPD, compared to healthy donors. Conversely, no difference in FGF10 expression could be observed between lungs of donors and smokers with COPD. This could be due to substantial parenchymal alterations occurring during COPD development that could influence the composition of the lung homogenate – the overall amount of alveolar septa decreases, while vessel wall thickness increases due to emphysema and PH development, respectively. These alterations result in different septa/vessel contributions in the lung homogenate. Due to before mentioned differential regulation in pulmonary vessels and alveolar septa, this might influence the overall FGF10 quantity in the bulk lung homogenate. Similarly, the expression of FGFR2 in lung homogenate remained unchanged.

In order to exclude the influence of emphysema (alveolar septal wall loss) and vascular remodelling (thickening of the vessel wall), FGF10 expression was evaluated histologically in human lung sections from healthy donors, smokers without and with COPD. The FGF10 stained area was always standardized to the total alveolar septa or vessel wall area. In alveolar septa, FGF10 expression was decreased in smokers without COPD, and to a greater extent, in lungs from smokers with COPD. In pulmonary vessels, FGF10 was upregulated in COPD lungs. FGF10 was mainly expressed in the tunica media of the larger vessels. These findings are indeed consistent with the data from the mouse model of chronic CS exposure. FGF10 is a paracrine or autocrine factor with a limited diffusion capacity secreted mainly by mesenchymal cells – fibroblasts and smooth muscle cells (Bellusci *et al.* 1997).

Foremost, I investigated the FGF10 expression *in vitro* in interstitial fibroblasts isolated from lungs explanted from patients with end-stage COPD and lung transplantation donors. I could observe decreased FGF10 expression in fibroblasts isolated from COPD lungs. These results suggest that FGF10 expression remained impaired even after *in vitro* cell propagation. Alterations in cell signalling in lung fibroblasts isolated from COPD patients that remain despite the *in vitro* propagation have been reported in the literature (Togo *et al.* 2008; Holz *et al.* 2004; Dagouassat *et al.* 2013). It is tempting to speculate that such a phenomenon could occur due to conserved epigenetic gene regulation. Also, the fibroblast population in the lung is heterogeneous (Ushakumary *et al.* 2021; Rajasekar *et al.* 2021), so the difference in FGF10 expression could be due to a shift in fibroblast cell phenotype. However, such persistent downregulation of FGF10 expression in the absence of initial stimuli could underlay emphysema progression in COPD patients who stopped smoking. Thus, CS induced the decrease in FGF10 expression in lung fibroblasts, which could affect lung epithelial and endothelial cells through its receptor FGFR2b.

Furthermore, in donor fibroblasts, FGF10 expression was decreased upon *in vitro* treatment with CSE or the peroxynitrite donor SIN-1 (**Figure 65**). Inhibition of iNOS with L-NIL could prevent from the CS-induced decrease in FGF10 expression in interstitial lung fibroblasts, which is consistent with the data from the previously mentioned animal study (**Figure 65**).

Taken together, these data suggest that FGF10 could be a “victim” of increased nitrosative and oxidative stress that is described to play an essential role in the pathology of COPD (Gouveia *et al.* 2020; Seimetz *et al.* 2020; Seimetz *et al.* 2011). iNOS is a crucial source of NO in animal models of CS-induced emphysema and in human COPD (Seimetz *et al.* 2011). Recently, NOXO1 was identified as the primary regulator of superoxide production in COPD. NOXO1 can potentiate the superoxide-generating activity of non-phagocytic NADPH oxidases (NOX1 and NOX3) and plays an essential role in CS-induced emphysema and PH (Boukhenouna *et al.* 2018; Seimetz *et al.* 2020; Brandes *et al.* 2014; Schröder *et al.* 2017). ROS can directly interfere with FGF10 signalling. Namely, ROS was shown to inhibit signalling downstream of FGFR2b (Gozali *et al.* 2016), and ROS can induce ligand-independent FGFR2b internalization and lysosomal degradation, thereby inhibiting FGFR2b signalling (Belleudi *et al.* 2006).

In a diffusion-limited reaction between NO and superoxide, peroxynitrite is formed (Wink *et al.* 1998). Peroxynitrite preferably attacks tyrosine residues in proteins when 3-nitrotyrosine is formed (Jin *et al.* 2011; Barnes 2019; Ichinose *et al.* 2000; Osoata *et al.* 2009). 3-nitrotyrosine levels have been linked to COPD severity in patients (Szabo *et al.* 2007; Kharitonov *et al.* 2003). Moreover, in COPD, 3-nitrotyrosine formation is not only an indicator of increased nitrosative and oxidative stress but can also, above a certain threshold, alter cell signalling and cause senescence or cell death (Jin *et al.* 2011; Barnes 2019; Ichinose *et al.* 2000; Osoata *et al.* 2009; Barnes 2014). Furthermore, 3-nitrotyrosine can trigger innate and adaptive immune responses (Ahsan 2013; Ahmad *et al.* 2019). It is yet unknown if FGF10 could be a direct protein target of peroxynitrite.

However, 3-nitrotyrosine is known to interfere with the activity of transcriptional factors (Llovera *et al.* 2001; Ng *et al.* 2013; ter Horst *et al.* 2018). In this regard, using the hypothesis-driven approach, I identified SP1 as a transcription factor that could be responsible for FGF10 downregulation upon RNS/ROS stress in interstitial lung fibroblasts (**Figure 65**). SP1 was reported downstream of NF- κ B activation, leading to decreased FGF10 expression (Benjamin *et al.* 2010). Increased NF- κ B activation was shown in human COPD lungs and in experimental COPD models (Schuliga 2015; Di Stefano *et al.* 2002; Yu *et al.* 2018; Rajendrasozhan *et al.* 2010) (references). Thus, the ability of NF- κ B to disrupt regular Sp-1-mediated expression of FGF10

may represent a link between RNS/ROS, inflammation and FGF10 in COPD. In line with my findings, another study identified SP1 as a common node in emphysema and lung cancer development (Kelly *et al.* 2014). However, I cannot exclude the contribution of other transcription factors that may be responsible for impaired FGF10 signalling in COPD interstitial lung fibroblasts. More research is needed to pinpoint the exact mechanism of FGF10 downregulation in the condition of increased RNS/ROS stress.

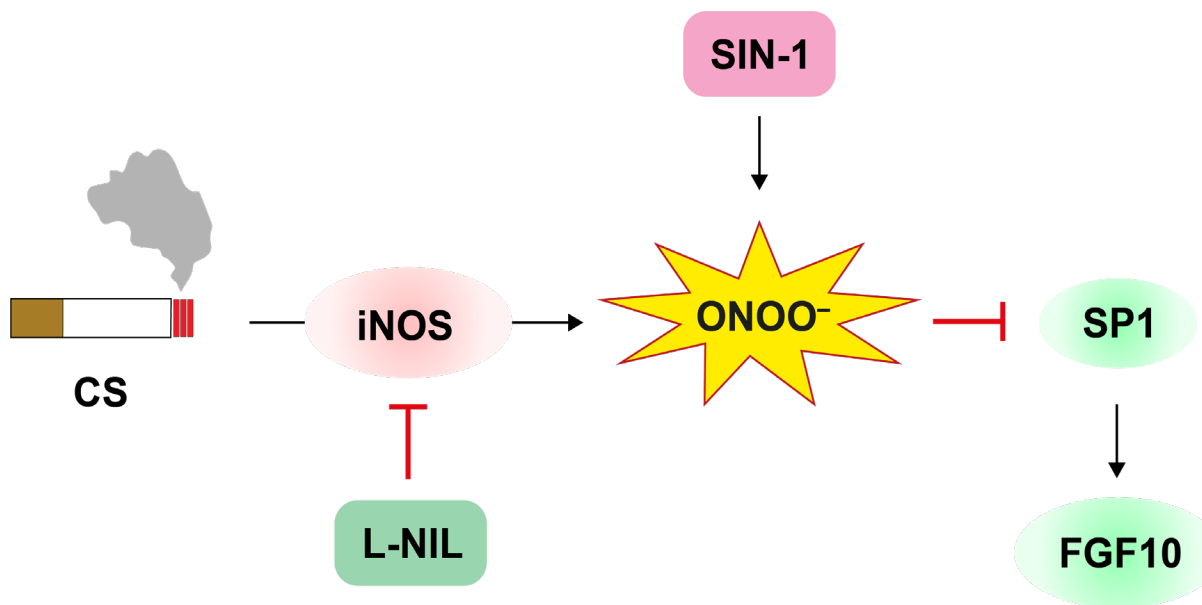


Figure 65. Cigarette smoke through peroxynitrite stress leads to decreased FGF10 expression in interstitial lung fibroblasts. Cigarette smoke (CS) exposure causes peroxynitrite stress via the upregulation of inducible nitric oxide synthase (iNOS). Increased peroxynitrite stress (either upon CS exposure or directly derived from the ONOO⁻ donor – SIN-1) leads to FGF10 downregulation, possibly through inhibition of specificity factor 1 (SP1) transcriptional activity.

In isolated donor PASCs, FGF10 expression was increased upon *in vitro* treatment with CSE. These data could confirm the observations made in FGF10-stained lung sections from COPD patients and CS-exposed mice. Interestingly, in the lung sections of smokers without COPD, FGF10 expression in the pulmonary vasculature was not affected. This suggests that FGF10 upregulation in PASCs might require a more potent injury stimulus, as observed in the pathology of COPD. In isolated cells, fibroblasts indeed reacted to CSE at lower concentrations compared to the PASCs. The cellular mechanisms underlying the increase of FGF10 in

PASMCs, as well as the effects of this increased FGF expression on PASMCs, were not the focus of the current study. However, it could be possible that the same transcriptional factor that led to a decrease in FGF10 expression in lung fibroblast evoked its increased expression in PASMCs.

FGF10 acts only in a paracrine or autocrine fashion to trigger downstream signalling in target cells (Itoh *et al.* 2014; Yuan *et al.* 2018; Bellusci *et al.* 1997; Watson *et al.* 2018). For that reason, I suggest that increased FGF10 expression in PASMCs could affect only cells in close proximity. This would primarily include endothelial cells and perivascular fibroblasts in muscularized vessels. Furthermore, I cannot exclude that an increased expression of FGF10 in pulmonary vessels could contribute to the development of pulmonary vasculature remodelling. Correspondingly, it is reported that FGF10 is upregulated in smooth muscle cells upon other types of lung injury (El Agha *et al.* 2018; El Agha *et al.* 2016; Yuan *et al.* 2018; Volckaert *et al.* 2011). Along this line, data obtained from PH patients show increased FGF10 expression in pulmonary vessels in diseased lungs compared to corresponding healthy donors (El Agha *et al.* 2018; El Agha *et al.* 2016). However, increased FGF10 expression negatively correlated with the mean pulmonary arterial pressure. This suggests a favourable effect of FGF signalling in PH (El Agha *et al.* 2018; El Agha *et al.* 2016). Thus, the role of increased FGF10 expression in the development of CS-induced PH is unclear and should be addressed in the future.

4.2 Mice with impaired FGF10 signalling spontaneously develop emphysema and PH

In order to decipher the role of FGF10 signalling in the development of COPD, I used transgenic animals with impaired FGF10 signalling and employed a mouse model of CS-induced emphysema and PH. Since homozygous *Fgf10* deletion is lethal due to complete lung angiogenesis (Ohuchi *et al.* 2000; Jones *et al.* 2021; Sekine *et al.* 1999; De Moerlooze *et al.* 2000), in this experiment, I used *Fgf10* and *Fgfr2b* heterozygous (*Fgf10*^{+/-} and *Fgfr2b*^{+/-}) mice. Littermate mice with both functional copies of *Fgf10* and *Fgfr2b* were used as Wt controls. As previously reported, 3 months of CS exposure in mice is sufficient to induce significant alterations in the pulmonary vasculature, while 8 months is needed for emphysema

development (Pichl *et al.* 2019; Seimetz *et al.* 2020; Seimetz *et al.* 2011; Gredic *et al.* 2021). *Fgf10^{+/-}* and *Fgfr2b^{+/-}* mice, compared to Wt littermates, developed emphysema much earlier – after only 3 months of CS exposure. Moreover, at the 8-month time-point, CS-exposed Wt and, importantly, RA-exposed *Fgf10^{+/-}* and *Fgfr2b^{+/-}* mice developed spontaneous emphysema (**Figure 66**). *Fgf10^{+/-}*, but not *Fgfr2b^{+/-}* mice had already signs of lung architectural simplification without CS exposure at the 3-months time-point. This could be due to impaired lung development and bronchopulmonary dysplasia (BPD)-like phenotype that has been reported in *Fgf10^{+/-}* mice (Chao *et al.* 2017; Bellusci *et al.* 1997; Chao *et al.* 2019). Despite the baseline difference, the difference in airspace enlargement upon 3 months of CS exposure in *Fgf10^{+/-}* mice is still greater than in control Wt animals. Furthermore, when compared to the severe emphysema that these animals develop with ageing, the baseline differences look negligible. However, I cannot exclude that the BPD-like phenotype in *Fgf10^{+/-}* mice might contribute to the increased susceptibility towards CS-induced emphysema. Evidence from human patients suggest that disrupted lung development may contribute to the early onset of COPD (Filippone *et al.* 2010; McGrath-Morrow *et al.* 2019), which supports my findings. Furthermore, *Fgfr2b^{+/-}* mice that have no visible structural baseline defects were also more prone to develop CS-induced emphysema and develop emphysema spontaneously.

Moreover, lung function tests revealed increased overall respiratory system resistance only in *Fgf10^{+/-}* mice. In contrast, resistance was not altered in WT mice after 8 months of CS exposure. Airway and tissue components both contributed to the increased respiratory system resistance in *Fgf10^{+/-}* mice. This suggests that FGF10 haploinsufficient mice also have signs of airway disease, independently of CS exposure which may resemble features of COPD in human patients (Saetta *et al.* 2000). I found that *Fgf10^{+/-}* mice had changes in the alveolar wall extracellular matrix, characterised by a pronounced collagen network without any signs of pulmonary fibrosis that can explain *in vivo* lung function results. Similar extracellular matrix alterations were also reported in the lungs of COPD patients (Annoni *et al.* 2012). Despite marked downregulation of FGF10 in CS-exposed Wt animals, collagen accumulation in alveolar septa in these animals was less pronounced compared to *Fgf10^{+/-}* mice. Furthermore, such phenomena could be observed only in *Fgf10^{+/-}* but not in *Fgfr2b^{+/-}* mice. This could be again

due to impaired lung development or due to FGF10 signalling through other receptor isoforms. FGF10 can also bind to the FGFR1b isoform, and signalling mediated through this receptor is not affected in FGFR2b haploinsufficient animals (Ornitz *et al.* 2015; Ornitz *et al.* 1996; Zhang *et al.* 2006). FGF10 signalling stimulation was shown to contribute to fibrosis resolution in the bleomycin mouse model (MacKenzie, Henneke, *et al.* 2015; Gupte *et al.* 2009).

In RA-exposed *Fgf10^{+/-}* and *Fgfr2b^{+/-}* mice, I observed lower vessel density prior to the emphysema development. As FGF10 is known to stimulate angiogenesis (Jones *et al.* 2021; Hubert *et al.* 2018), impaired FGF10 signalling can promote loss of pulmonary vessels – vascular pruning (**Figure 66**). FGF10 treatment *in vitro* stimulates endothelial cells to form capillary-like structures (Liu *et al.* 2017). Interestingly, vascular pruning is described in smokers' lungs, and it is one of the causes of PH development in COPD patients (Diaz *et al.* 2018). Consequently, both transgenic animal strains developed spontaneous PH at the 8-months time-point. The increase in RVSP was consistent with the heart function data obtained by echocardiography (decreased TAPSE) and RV hypertrophy. Even though FGF10 signalling is also important in the heart, my data suggest that pulmonary vascular alterations precede functional and structural changes in the RV (Vega-Hernández *et al.* 2011; Rochais *et al.* 2014; Hubert *et al.* 2018). Also, mice with impaired FGF10 signalling have a similar degree of RV remodelling like Wt mice exposed to CS for 8 months. Furthermore, these results support the hypothesis that FGF10 signalling in the pulmonary vasculature plays an important protective role rather than contributing to pulmonary vascular remodelling, as the downregulation of FGF10 leads to spontaneous PH. In addition, overexpression of FGF10 cured CS-induced as well as elastase-induced PH. However, it is possible that FGF10 plays two opposite roles: in small vessels (capillaries) promoting endothelial growth and angiogenesis and in big vessels stimulating PASM C proliferation. Activation of FGF receptors in endothelial cells of the pulmonary vasculature was suggested to protect against hypoxia-induced PH (Woo *et al.* 2021). I could observe a slight increase in systemic arterial pressure in *Fgfr2b^{+/-}* mice. This suggests that the FGFR2b could be important in the systemic circulation, which could contribute to higher RVSP values in these animals.

Interestingly, none of the parameters indicating emphysema and PH worsened in the transgenic animals upon long-term CS exposure, suggesting that emphysema and PH induced by CS exposure and impaired FGF10 signalling may share a similar mechanism (**Figure 66**). Hence, FGF10 expression was decreased in the lung homogenate from CS-exposed Wt mice and at the same level as in *Fgf10^{+/-}* mice. Moreover, in *Fgf10^{+/-}* mice, FGF10 expression was not further decreased upon CS exposure what could explain the lack of further disease worsening. Taken together, my data suggest that FGF10 downregulation is an essential pathway triggering CS-induced emphysema and PH development (**Figure 66**).

4.3 Signalling pathways of FGF10 and CS-induced emphysema and PH development

As described above, protease/antiprotease dysbalance and cell death are hallmarks of COPD. *In vivo* FMT-CT measurements revealed increased apoptosis and MMP activity in lungs from CS-exposed Wt animals as well as in RA-exposed *Fgf10^{+/-}* and *Fgfr2b^{+/-}* mice at the 3- and 8-month time-points. These results suggest that impaired FGF10 signalling and CS exposure have a similar effect on apoptosis and MMP activity in the lungs of experimental animals. Hence, *in vitro* experiments showed that treatment with recombinant FGF10 protected from CSE-induced apoptosis of AII cells. Furthermore, MMPs play an important role in COPD and hypertension, including PH (Antonio *et al.* 2014; de Jager *et al.* 2017; Churg *et al.* 2007; Hadzic *et al.* 2021; Pichl *et al.* 2019; Li *et al.* 2020). In one of the previous studies performed in mice, the reversal of CS-induced emphysema and PH by riociguat treatment was associated with decreased MMP activity and expression (Pichl *et al.* 2019). Increased MMP-2 activity was also shown in the lungs and sputum of COPD patients (Churg *et al.* 2012). MMP-2 has been described to contribute to vascular dysfunction in systemic circulation (de Jager *et al.* 2017). Furthermore, MMP-9 was upregulated in COPD patients and negatively correlated with FEV1 (Churg *et al.* 2012) and was associated with spontaneous pneumothorax and a worse prognosis (Li *et al.* 2020).

In addition, at the 8-month time-point, 3-nitrotyrosine levels in RA-exposed *Fgf10^{+/-}* mouse lungs were as high as in CS-exposed Wt littermates and did not further increase upon CS

exposure. My results indicate that impaired FGF10 signalling might be not only a “victim” of peroxynitrite but could also, in turn, contribute to the peroxynitrite formation. In ischemia-reperfusion animal models, FGF10 treatment exhibited a protective role against ROS-mediated injury (Tan *et al.* 2020; Li, Zhu, *et al.* 2021b; Li, Yang, *et al.* 2015). Furthermore, FGF10 promoted survival and inhibited apoptosis of neurons in an oxygen-glucose deprivation model. In such a model, FGF10-induced protection relied mainly on the induction of HO-1 expression (Li, Yang, *et al.* 2015). Also, FGF10 could induce a broad antioxidant response in Schwann cells, thereby enhancing peripheral nerve regeneration (Dong *et al.* 2019). This suggests that FGF10 signalling can stimulate endogenous antioxidant defence in various cell types. Lack of FGF10 could thus hamper the antioxidant defence, which would result in increased RNS/ROS stress and subsequent 3-nitrotyrosine formation. However, more research is needed to delineate the molecular mechanism and cells responsible for this possible positive feedback loop.

To decipher the underlying mechanisms of the emphysema and PH development upon CS-exposure and FGF10 haploinsufficiency, I analysed gene expression profiles in Wt and *Fgf10*^{+/-} animals at the 3-months time-point. As a different gene regulation pattern was observed between the lung parenchyma and vasculature, I therefore subjected lungs from my experimental animals to LMD and separately collected RNA from alveolar septa and pulmonary vessels. In the septa, I found 263 genes and in pulmonary vessels, 289 genes commonly regulated between Wt CS and *Fgf10*^{+/-} RA. Interestingly, in both compartments, these genes were regulated in the same direction and, to a great extent, not further changed upon CS exposure in *Fgf10*^{+/-} mice. The most prominently regulated genes identified in comet plots are not yet well described in COPD or lung pathologies. More research is needed to decipher the potential involvement/contribution of these genes in the pathology of CS-induced emphysema and PH.

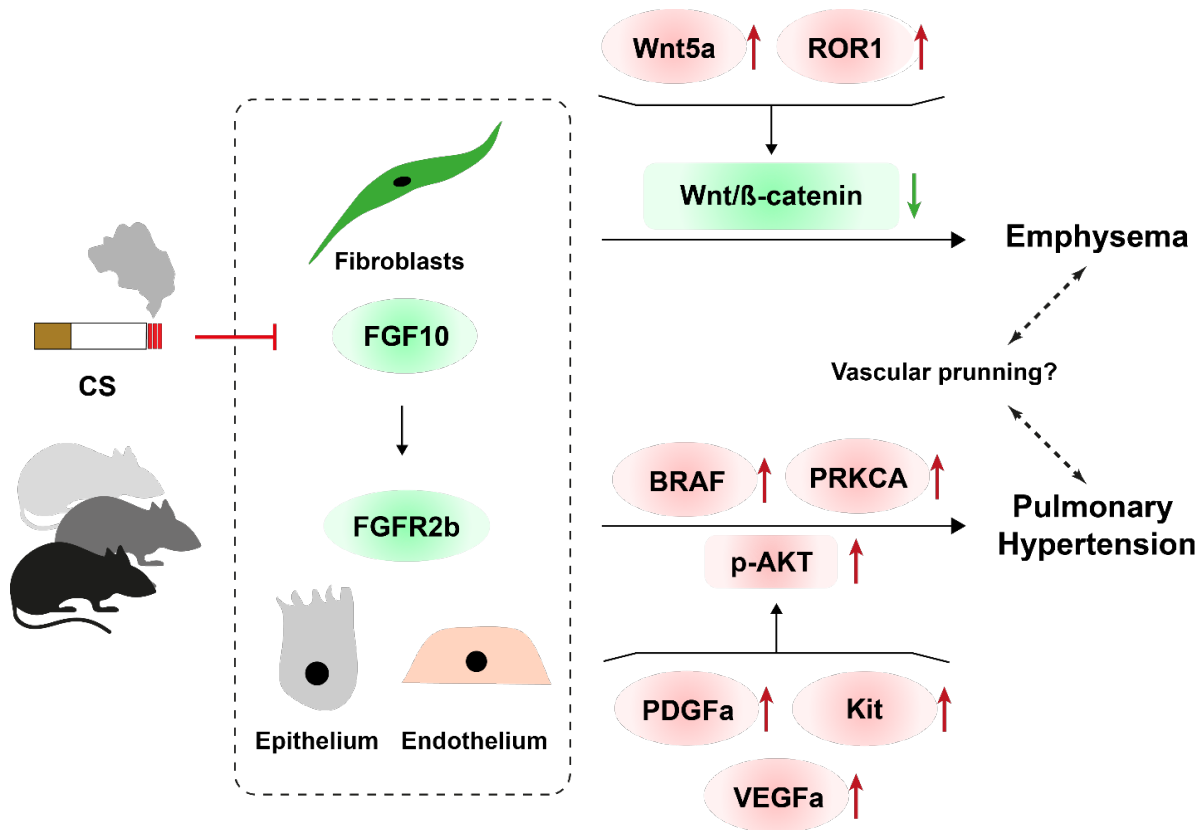


Figure 66. Cigarette smoke leads to emphysema and PH development through inhibition of FGF10 signalling. Cigarette smoke (CS) leads to FGF10 downregulation in interstitial lung fibroblasts, affecting downstream signalling through FGFR2b, expressed on epithelial and endothelial cells. Impaired FGF10 or FGFR2b signalling leads to the development of emphysema and PH in experimental mice. A common node for emphysema development in CS-exposed Wt mice and mice with impaired FGF10 signalling could be weakened canonical Wnt/ β -catenin signalling. Wnt Family Member 5A (Wnt5a) and receptor tyrosine kinase-like orphan receptor 1 (ROR1) were found dysregulated in both animal models. Vascular pruning could be a potential connection between emphysema and PH in my experimental mice. Pulmonary hypertension development could be caused by increased phosphorylation of Akt strain transforming (Akt). In these animals, Akt phosphorylation could be affected by serine/threonine-protein kinase B rapidly accelerated fibrosarcoma (BRAF), protein kinase C alpha (PRKCA), tyrosine kinase receptor KIT, vascular endothelial growth factor A (VEGFA) and the platelet-derived growth factor subunit A (PDGFA).

In order to identify pathways and test if the regulated genes align in specific signalling pathways, I performed a functional protein association network analysis (STRING-DB database) (Szklarczyk *et al.* 2019). Interestingly, the targets were somewhat scattered in several clusters, comprising a few targets each and thus, I could not find enrichment in any specific signalling

pathway. Therefore, it seemed that FGF10 deficiency and CS exposure trigger many targets rather than a few well-described signalling pathways. However, using such analysis, I could identify clusters related to canonical Wnt signalling in alveolar septa and tyrosine kinases in the pulmonary vessels (**Figure 66**). On the one hand, Wnt pathway is described in emphysema animal models and human COPD (Hu *et al.* 2020; Baarsma *et al.* 2017; Kneidinger *et al.* 2011; Wang *et al.* 2011; Conlon *et al.* 2020). On the other hand, such a pathway is clearly interconnected with FGF10 (Choe *et al.* 2006; Volckaert *et al.* 2015; Cohen *et al.* 2007; Tang *et al.* 2019; Kruk *et al.* 2021).

I could further confirm decreased levels of β -catenin and increased Akt phosphorylation in lung homogenates from RA-exposed *Fgf10*^{+/-} and CS-exposed Wt mice (**Figure 66**). The WNT/ β -catenin pathway is important for lung development and homeostasis, and it was suggested as a mechanism of lung repair in COPD (Hu *et al.* 2020; Baarsma *et al.* 2017; Kneidinger *et al.* 2011; Wang *et al.* 2011; Conlon *et al.* 2020). Wnt5a and ROR1 are well-known to activate the non-canonical Wnt pathway (Karvonen *et al.* 2019; Green *et al.* 2014; Zhang *et al.* 2018). Silencing of ROR1 was reported to augment the signalling mediated via Wnt3a and subsequently activate the canonical Wnt/ β -catenin pathway (Zhang *et al.* 2018).

Increased Akt phosphorylation could be connected with the vascular remodelling (Tang *et al.* 2015), senescence (Houssaini *et al.* 2018) and inflammation described in COPD patients (Bozinovski *et al.* 2006). In the pulmonary vasculature of my experimental animals, I could connect KIT, VEGFA and PDGFA with increased Akt phosphorylation (**Figure 66**). Upon binding to appropriate receptors, VEGFA and PDGFA are well-known inducers of AKT phosphorylation (**Figure 66**) (Hiley *et al.* 2012; Trinh *et al.* 2009; Sun *et al.* 2019; Yu *et al.* 2015). Inhibition of signalling through PDGF receptors by imatinib is known to reverse vascular remodelling and PH (Schermuly *et al.* 2005; Andrae *et al.* 2008). Furthermore, BRAF can induce cell growth, survival and proliferation independently of AKT phosphorylation (Hugen *et al.* 2015). PRKCA was already described to promote proliferation of PSMCs upon smoke exposure (Xiang *et al.* 2010) (**Figure 66**). In an asthma animal model, PRKCA was associated with increased proliferation of airway smooth muscle cells (Qiao *et al.* 2008).

Taken together, more research is needed to delineate the cellular and molecular signalling leading to emphysema and PH development upon CS exposure or due to impaired FGF10 signalling. Furthermore, the contribution of each individual target should be evaluated.

4.4 Doxycycline alone does not affect CS-induced emphysema and PH

As L-NIL treatment restored the lung structure after CS exposure and significantly upregulated FGF10 in the alveolar septa and the pulmonary vasculature, I hypothesised that FGF10 upregulation could contribute, if not mediate, the repair process after CS-induced emphysema and PH. Therefore, I wanted to test if restored FGF10 signalling could drive lung repair and reverse remodelling of the pulmonary vasculature after 8 months of CS exposure. However, FGF10 is a relatively unstable protein and thus is not suitable for treatment *in vivo* (Buchtova *et al.* 2015). Furthermore, it would be challenging to deliver such growth factors beyond the innate immunity defences in the lung. Thus, in the current study, a transgenic animal model with tetracycline-controlled transcriptional regulation as a genetic tool of reversible transcriptional activation (Tet-On system) was implemented. In Tet-On systems, under a specific promoter, cells transcribe the reverse tetracycline transactivator (rtTA). In the presence of doxycycline, rtTA binds to the Tet(O) operator sequence, which is inserted in a promoter region of the desired gene initiating gene transcription (Kistner *et al.* 1996; Hadzic *et al.* 2021).

Doxycycline is a broad-spectrum antibiotic belonging to the tetracycline family used to treat respiratory infections and exacerbations in patients suffering from COPD or cystic fibrosis (Xu *et al.* 2017; Dalvi *et al.* 2011; Rempe *et al.* 2007). In transgenic animal models, doxycycline is frequently administered to modulate gene expression via a Tet-On/Tet-Off system. Despite possible interferences with the experimental setups, the direct effects of doxycycline independent of the Tet-On/Tet-Off system are not well described. Hence, results from such experiments are often difficult to interpret. Doxycycline was shown to inhibit MMP activity via direct binding to the zinc ion domain in the catalytic centre of the enzyme (Castro *et al.* 2011). Beneficial effects of doxycycline, mainly through MMP inhibition, have been reported in

several preclinical studies (Dalvi *et al.* 2011; Castro *et al.* 2011; Cerisano *et al.* 2014; Lindeman *et al.* 2009; Baxter *et al.* 2002; Abdul-Hussien *et al.* 2009; Antonio *et al.* 2014; Nascimento *et al.* 2018; Shi *et al.* 2009; Griffin *et al.* 2005; Spaulding *et al.* 2018; Zhu *et al.* 2015; Wang, Zhang, *et al.* 2018; Errami *et al.* 2008; Wang *et al.* 2014; Parasaram *et al.* 2016; Zhang *et al.* 2019; Kistner *et al.* 1996; Gossen *et al.* 1992; Gossen *et al.* 1995; Xu *et al.* 2017; Singh *et al.* 2019; Hadzic *et al.* 2021).

Furthermore, doxycycline is suggested to have antioxidant and anti-inflammatory properties that might be independent of MMP inhibition (Singh *et al.* 2019; Hadzic *et al.* 2021). Thus, doxycycline might have a direct curative effect in a mouse model of CS-induced emphysema and PH. Therefore, I assessed the effect of long-term doxycycline treatment on established emphysema and PH in a mouse model of chronic exposure to CS. To answer this question, I used a mouse line expressing rtTA under the general *Rosa26* promoter without inserted Tet(O) operator sequence. In this study, I started with the doxycycline treatment after successfully established CS-induced emphysema and PH.

According to the *in vivo* lung function and histological data, long-term doxycycline treatment had no effects on emphysema and PH, induced in mice by exposure to CS for 8 months. It has been suggested that doxycycline might have a direct beneficial effect in rat models of PH (Shi *et al.* 2009). Data from the mouse model of CS-induced PH indicated that long-term doxycycline treatment did not influence RVSP or heart parameters. The discrepancy between my data and studies where beneficial effects of doxycycline treatment were observed on emphysema/PH could be due to the fact that in the current study, I used a mouse model where emphysema/PH was already established by CS exposure for 8 months. Thus, when emphysema is already developed, doxycycline-mediated MMPs inhibition is insufficient for lung regeneration. Accordingly, short-term doxycycline treatment in COPD patients had no effect on the lung function parameters (Dalvi *et al.* 2011) but could decrease MMPs activity and improve antioxidant defence (Singh *et al.* 2019; Hadzic *et al.* 2021). However, I cannot rule out that higher doses of doxycycline, which were not used in the current study, might have beneficial effects against CS-induced emphysema/PH.

Taken together, I could conclude that doxycycline treatment at a low dose and in the specific administration regimen as used in my studies is suitable to control Tet-On/Tet-Off systems in animal models such as CS-induced lung emphysema and PH without an effect on emphysema and PH per se.

4.5 FGF10 overexpression reverses CS-induced emphysema and PH

After confirming that doxycycline alone does not affect established CS-induced emphysema and PH, I exposed *ROSA26_rtTA TetO_Fgf10* mice to CS. After 8 months of CS exposure, animals were fed with doxycycline-containing chow in the previously described regimen (Gupte *et al.* 2009; Redelsperger *et al.* 2016; Hadzic *et al.* 2021), for up to 12 weeks. With such a feeding regimen, I could keep the FGF10 upregulated while avoiding the side effects of long-term antibiotic administration. In this model, I confirmed that 1 week of doxycycline feeding was sufficient to reverse CS-induced FGF10 downregulation. For the longer time-points (5 and 12 weeks), I fed mice with doxycycline-containing chow for 1 week, followed by 1 week of doxycycline-free chow feeding. This weekly scheme of doxycycline feeding I repeated during the entire treatment period as described earlier (Gupte *et al.* 2009; Hadzic *et al.* 2021).

In the CS-exposed animals without treatment, emphysema remained stable up to 3 months after CS cessation. This is consistent with previously published data (Hadzic *et al.* 2021; Pichl *et al.* 2019; Seimetz *et al.* 2011). Histological examination of the lungs from the experimental animals revealed that 5 weeks of FGF10 overexpression could already induce significant improvement in the lung structure. At the 12-weeks time-point, emphysema was reversed to the level of healthy mice. Similarly, stimulation of the FGF10 signalling was beneficial in several animal disease models (Yuan *et al.* 2018; Yuan *et al.* 2019; El Agha *et al.* 2016; El Agha *et al.* 2017; Gupte *et al.* 2009; Tong *et al.* 2016; Li *et al.* 2021b)

As previously reported (Hadzic *et al.* 2021; Pichl *et al.* 2019), my experiments again revealed increased RVSP, decreased TAPSE and RV wall hypertrophy in CS-exposed animals up to 3 months after CS cessation. This confirms a stable PH phenotype in my transgenic animals after

CS exposure is discontinued, as it was previously reported for other mouse lines (Hadzic *et al.* 2021; Pichl *et al.* 2019; Seimetz *et al.* 2011). FGF10 overexpression for 5 weeks was sufficient to completely reverse the CS-induced increase in RVSP and improve RV function, whereas 12 weeks were needed to resolve RV hypertrophy. Hence, in this model, FGF10-mediated reversion of PH phenotype preceded the repair of lung parenchyma. However, it is still not clear if cellular and molecular alterations in the pulmonary vasculature (PH reversion) contributed to the repair in alveolar septa. Importantly, FGF10 overexpression in the RA control groups did not affect any of the measured parameters indicating PH. Therefore, FGF10 could have a beneficial effect on alveolar septal wall repair in COPD without promoting pro-PH vascular remodelling.

It is still debatable if lungs from COPD patients retain as high regenerative capacity as mouse lungs upon long-term CS exposure (Gouveia *et al.* 2020; Ahsan 2013; Shapiro 2000; Wright *et al.* 2008; Tanner *et al.* 2020). Therefore, I prepared precision-cut lung slices (PCLS) from human COPD lungs and cultured them *in vitro* with or without recombinant human FGF10. PCLS treated with FGF10 had a significantly increased number of proliferating cells. Most proliferating cells were located in the alveolar septal walls, whereas no proliferating cells were found in the tunica media of the pulmonary vasculature. Very few proliferating cells were observed in the large bronchi. This suggests that human COPD lungs still have the reparative capacity and respond to FGF10 stimulation.

Genes involved in FGF10-mediated reversal of CS-induced emphysema and PH were analysed at day 7 of FGF10 overexpression after 8 months of CS exposure. At this earliest time-point, I could analyse the genes that are directly affected by reconstituted FGF10 expression. Both FGF10 overexpression and CS exposure trigger a wide variety of genes that belong to diverse signalling pathways. During the disease development, I showed that impaired FGF10 signalling and CS exposure indeed share a certain portion of regulated genes. Therefore, hereby I focused on the genes that were commonly regulated between CS exposure and FGF10 overexpression upon CS exposure. However, with such analysis, I excluded the potential FGF10 effect that is independent of the CS exposure.

In the septal wall compartment, the vast majority of these shared genes were inversely regulated upon FGF10 overexpression. Among the most prominently regulated genes, upregulated with CS exposure and downregulated upon FGF10 overexpression, I found Bok and Cathepsin K (Ctsk). These two genes, even though not yet described in the pathogenesis of COPD I suggest could contribute to emphysema development, based on literature reports: Cathepsin K is a potent cysteine protease described so far mainly in the context of bone resorption (Dai *et al.* 2020; Garnero *et al.* 1998). However, there are indications that cathepsin K is also important in the cardiovascular and respiratory systems (Dai *et al.* 2020). In the lung, cathepsin K is expressed in the airway and alveolar epithelial cells and in alveolar macrophages (Dai *et al.* 2020; Bühling *et al.* 1999; Bühling *et al.* 2001). Of interest, cathepsin K knockout mice develop worse lung fibrosis upon bleomycin-induced lung injury (Bühling *et al.* 2004). Such reports indicate that cathepsin K has an essential role in ECM remodelling in the lung and could be implicated in the pathogenesis of emphysema (**Figure 67**). Bok is a member of the B-cell lymphoma 2 (Bcl-2) family and can directly trigger apoptosis by mitochondrial outer membrane permeabilisation and subsequent cytochrome c release in the cytoplasm (Naim *et al.* 2020; Carpio *et al.* 2015; Llambi *et al.* 2016). Bok is described as an apoptosis inducer in response to endoplasmic reticulum (ER) stress (Carpio *et al.* 2015). Increased ER stress is indeed described in the pathology of COPD (Chen *et al.* 2018; Delbrel *et al.* 2020; Zhang *et al.* 2020). FGF10 ameliorated CS-increased Bok expression that could impact apoptosis in alveolar septa and emphysema in my experimental model (**Figure 67**). Furthermore, I found prominent regulation of *Nos3*, an endothelial NOS isoform (Fish *et al.* 2006), in alveolar septa upon CS exposure and FGF10 overexpression. This and vWF staining in lung sections from experimental mice may suggest recovery of the capillary network upon FGF10 stimulation, which is in line with the data shown before.

Similarly, like during the disease development, using functional protein association networks, I could identify a cluster of genes encoding for proteins involved in Wnt signalling. The cluster includes *Kremen2* and *Lrp5*. *Kremen2* modulates canonical Wnt signalling in an indirect manner by binding to the Wnt antagonist – Dickkopf 1 (Li *et al.* 2010; Mao *et al.* 2003; Schulze *et al.* 2010; Ellwanger *et al.* 2008). *Lrp5* and *Lrp6* are well-known co-receptors for canonical

Wnt ligands and are indispensable for Wnt signal transduction (Ren *et al.* 2021; Kang *et al.* 2015; MacDonald *et al.* 2012). Such results indicate that FGF10-mediated stimulation of the canonical Wnt pathway could promote alveolar wall regeneration, as depicted in **Figure 67**.

In the pulmonary vasculature, commonly regulated genes could be divided into two groups. One group of genes was regulated in the same direction by CS exposure and FGF10 overexpression. This is not surprising, taking into account that CS exposure also upregulates FGF10 in the pulmonary vascular compartment. These genes could be thus a direct downstream effect of FGF10 in, e.g. adjacent fibroblasts or endothelial cells. Considering the locally increased FGF10 expression, such results suggest that PH development in my mouse model requires the participation of other, not necessarily adjacent, cell types. The other group of genes was inversely regulated by FGF10 expression compared to the effect of CS exposure. These genes could be involved in the reverse remodelling process and the resolution of CS-induced PH. Among the most prominently regulated genes in this group, I found TOX2 that might be of interest in PH reversal, as depicted in **Figure 67**. TOX2 is a transcription factor described to play an important role in immune cells (Xu *et al.* 2019; Seo *et al.* 2019). Of interest here, SNP in the *TOX2* gene was associated with increased diastolic blood pressure in the systemic circulation (Basson *et al.* 2014). However, the role of TOX2 in the vasculature is still unknown.

4.6 FGF10 overexpression ameliorates elastase-induced emphysema and PH

Elastase-induced pulmonary emphysema is a mouse model of end-stage COPD, characterised by a rapid onset of severe emphysema caused by enzymatic digestion of elastic fibres in the lung (Antunes *et al.* 2011; Fysikopoulos *et al.* 2020). Unlike the mouse model of long-term CS-exposure, which covers most of the features observed in COPD patients, the elastase model mimics only the downstream mechanisms leading to septal wall destruction (Limjunyawong *et al.* 2015; Wright *et al.* 2008; Lüthje *et al.* 2009). However, this model is similar to genetic α 1-antitrypsin deficiency, which is observed in a portion of COPD in patients (Henaoui *et al.* 2016; Laurell *et al.* 2013; Limjunyawong *et al.* 2015). Furthermore, elastase-induced emphysema, in

my mouse model, is accompanied by PH and RV wall hypertrophy (Fysikopoulos *et al.* 2020). The PH features in such a model also include remodelling of the pulmonary vasculature (Fysikopoulos *et al.* 2020) as well as on vascular pruning, occurring due to significant loss of the lung parenchyma. Previously Fysikopoulos *et al.* (Fysikopoulos *et al.* 2020) showed that pharmacological iNOS inhibition could ameliorate elastase-induced pulmonary emphysema and PH. Similarly, like in the CS model, iNOS inhibition decreased 3-nitrotyrosine formation upon elastase application (Fysikopoulos *et al.* 2020).

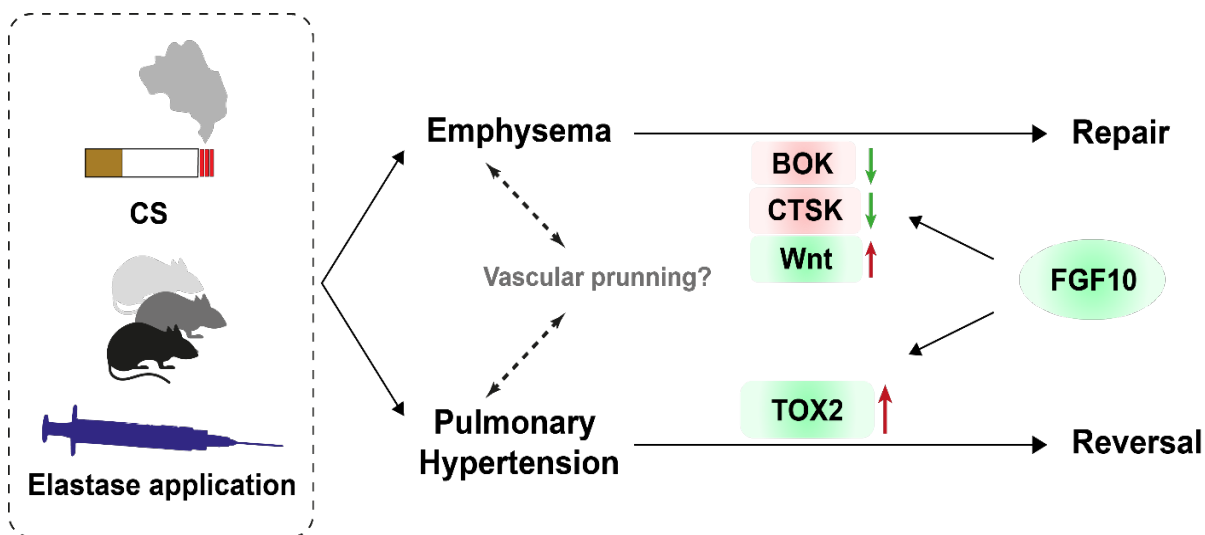


Figure 66. FGF10 overexpression reverses cigarette smoke- and elastase-induced emphysema and PH. Chronic exposure to cigarette smoke (CS) or single intratracheal instillation of elastase led to the development of emphysema and PH in experimental mice. FGF10 overexpression reversed CS-induced increase in cathepsin K (CSTK) and Bcl-2-related ovarian killer (BOK) expression in alveolar septa. Cluster analysis revealed restoration of canonical Wnt/ β -catenin signalling in alveolar septa of CS-exposed mice upon FGF10 overexpression. The effect of FGF10 overexpression in reversing vascular pruning is evident in the elastase model. TOX high mobility group box family member 2 (TOX2) could be a transcription factor responsible for FGF10-mediated reversion of CS-induced PH.

Treatment with palifermin (DeltaN23-KGF; truncated FGF7) was also beneficial upon elastase-induced emphysema (Yildirim *et al.* 2010). Furthermore, activating the canonical Wnt/ β -catenin pathway ameliorated elastase-induced emphysema in mice (Kneidinger *et al.* 2011). On the other hand, non-canonical Wnt-5A-mediated signalling was shown to impair lung repair

resulting in worsened elastase-induced lung injury (Baarsma *et al.* 2017). These reports align with the findings obtained from the CS animal model described in this thesis. Here I assessed the effect of FGF10 on elastase-induced pulmonary emphysema and PH.

In the context of emphysema, FGF10 overexpression resulted in a significant repair of the distal lung parenchyma shown by decreased lung compliance, airspace and MLI, compared to the corresponding age-matched elastase-treated controls. The casting of the pulmonary vasculature and von Willebrand staining suggested an increased vessel density after 12 weeks of FGF10 overexpression. Such data support the hypothesis that FGF10 can promote angiogenesis upon lung injury. Hence, FGF10 overexpression after elastase-induced injury completely reversed increased RVSP, RV hypertrophy and decreased TAPSE.

In my experiments, control animals that were treated with elastase exhibited progressive emphysema and PH. Such findings were reported in the literature and seem to depend on the choice of enzyme, animal strain and/or application method (Limjunyawong *et al.* 2015; Wright *et al.* 2008; Fysikopoulos *et al.* 2020). Similarly, emphysema is also progressive in some portion of COPD patients despite smoking cessation (Suki *et al.* 2003). The progressive nature of emphysema seems not to rely solely on protease-anti-protease dysbalance in the elastase model nor in COPD patients (Suki *et al.* 2003; Limjunyawong *et al.* 2015; Hamakawa *et al.* 2011). However, in my setup, FGF10 overexpression not only attenuated the disease progression but also reversed the parameters indicating emphysema and PH to a greater extent than before the treatment started.

Furthermore, lung function tests revealed increased respiratory system resistance in elastase-treated animals. The observed resistance seems to rely on the Newtonian (airway) resistance that suggests airflow limitation (Lorx *et al.* 2009; McGovern *et al.* 2013; Pillow *et al.* 2005) in this end-stage disease model. Indeed, disruption of elastic fibres, affected by elastase, was not only linked with the impaired alveolar repair but also with altered airway biomechanics enhancing airway contractility (Van Dijk *et al.* 2017; Gouveia *et al.* 2020). Of interest, FGF10 overexpression did not increase airway resistance as one might expect from growth factor treatment. On the contrary, FGF10 could ameliorate elastase-induced airway obstruction. This

suggests that FGF10 treatment might have a beneficial effect against airway remodelling in COPD.

5 Conclusions

Fibroblast growth factor 10 (FGF10) expression was decreased in alveolar septa and increased in the pulmonary vasculature in chronic obstructive pulmonary disease (COPD) lungs. In isolated interstitial fibroblasts of lungs explanted from COPD patients, FGF10 was downregulated what could be a consequence of augmented nitrosative and oxidative stress. Impaired FGF10 signalling could thus be a possible link between increased nitrosative and oxidative stress and dysregulated developmental pathways in COPD.

Mice with impaired FGF10 signalling are more prone to develop cigarette smoke (CS)-induced emphysema and developed emphysema and pulmonary hypertension (PH) spontaneously with ageing. Impaired FGF10 signalling leads to not only similar pathological phenotype but also triggers similar cellular and molecular mechanisms like CS exposure. It appears that both CS exposure and FGF10 insufficiency also share several pathways that might contribute to the development of emphysema and PH. In the described animal model, I could pinpoint β -catenin and Akt signalling pathways to be regulated during emphysema and PH development, respectively. However, more research is needed to decipher if the lack of FGF10 leads directly to lung injury or if simply the repair process is impaired and homeostasis jeopardised.

FGF10 overexpression successfully reversed established and usually irreversible CS- and elastase-induced emphysema and PH. It remains unclear which or if the same cell types react to the FGF10 stimulation, leading to the reversion of emphysema and PH in both models. In the context of CS-induced emphysema, it seems that increased FGF10 expression in the muscularized pulmonary vessels is not sufficient to maintain the lung architecture in the distal lung parenchyma. The contribution of FGF10 coming from the pulmonary vessels should be studied further in the context of COPD. Also, the possibility of FGF10 contributing to the proliferation of vascular smooth muscle cells in different disease stages cannot be excluded yet. Furthermore, I found pronounced vascular pruning in mice with impaired FGF10 signalling, whereas improvement could be observed upon FGF10 overexpression in the elastase model.

Therefore, FGF10-mediated reversion of emphysema and PH in CS and elastase animal models could also rely on the stimulation of endothelial cells promoting angiogenesis.

Taken together, boosting FGF10 signalling could be a novel mechanism and treatment concept for lung emphysema and PH in COPD if my findings from the lung hold true in the context of the human disease. This is at least supported by the data from the analysis of the FGF10 pathway in human lung samples, including FGF10 treatment of human precision cut lung slices (PCLS). However, more research is needed regarding adequate application procedures, safety and targeted FGF10 delivery or cell-specific FGF10 pathway stimulation in humans.

6 Summary

Chronic obstructive pulmonary disease (COPD) is a severe medical disorder characterised by chronic bronchitis and septal wall destruction (emphysema). Furthermore, COPD patients often suffer from at least mild pulmonary hypertension (PH) due to remodelling of the pulmonary vasculature. The main pathological driver is the inhalation of noxious particulate matter or gasses mainly coming from cigarette smoking but also from other sources such as air pollution. Several underlying mechanisms have been identified to drive disease development and progression. Such mechanisms involve protease/anti-protease disbalance, excessive nitrosative and oxidative stress and an augmented inflammatory response. Furthermore, recent studies support the idea that many developmental pathways are dysregulated in COPD, leading to impaired or even aberrant lung repair later in life. Despite the substantial efforts invested in the research and development of novel therapeutic approaches, COPD still remains an incurable and poorly treatable disease.

In previous studies, fibroblast growth factor (FGF) 10 was suggested as a potential target involved in the reversion of cigarette smoke (CS)-induced emphysema and PH upon therapeutic inhibition of inducible nitric oxide synthase (iNOS) in mice. FGF10 is essential for lung morphogenesis, and it has been shown to control the survival and proliferation of alveolar epithelial progenitor cells during lung development. Moreover, it is suggested that impaired FGF10 signalling in patients is linked with higher susceptibility to develop COPD. However, a cause-effect relationship between *FGF10* expression and COPD development, the underlying molecular mechanism, and interference with FGF10 signalling as possible therapy are not investigated yet.

To address this issue, I analysed FGF-related signalling in human lung samples from healthy donors, smokers without and with COPD. Additionally, I performed hemodynamic and lung function measurements in *Fgf10^{+/-}* and *Fgfr2b^{+/-}* (FGF receptor 2b) mice after chronic exposure to CS and evaluated indicators of pulmonary vascular remodelling and emphysema histologically. In order to explore the potential of a therapeutic application, I overexpressed

FGF10 in mice after elastase- or CS-induced lung injury. Furthermore, gene expression patterns during development and FGF10-mediated reversion of CS-induced emphysema and PH in mouse lungs were studied in dissected alveolar septa and pulmonary vasculature using microarray technology.

I found decreased FGF10 expression in alveolar septa of the lungs explanted from smokers with and without COPD and in the lung homogenate of mice exposed to CS. I could pinpoint the decrease of FGF10 expression in interstitial lung fibroblasts isolated from COPD lungs. Such effects were also mimicked in healthy donor lung fibroblasts when *in vitro* exposed to CS extract or nitrosative/oxidative stress.

Fgf10 and *Fgfr2b* haploinsufficient mice were more prone to develop CS-induced emphysema and PH. Moreover, animals with impaired FGF10 signalling developed spontaneous emphysema and PH and other typical pathomechanistic features that generally arise in response to CS exposure. These include 3-nitrotyrosine formation, increased matrix metalloproteinase (MMP) activity, apoptosis and various transcriptomic alterations. My data suggest that weakened β -catenin signalling and increased phosphorylation of Akt strain transforming (Akt) could underlay emphysema and PH development, respectively, in CS-exposed Wt mice and mice with impaired FGF10 signalling. Of interest, FGF10 overexpression could successfully reverse established elastase- and CS-induced lung injury in mice.

Taken together, my data demonstrate that FGF10 signalling is crucial for adult lung homeostasis. Moreover, FGF10 signalling could be an integral part of the pathomechanism that leads to CS-induced emphysema and PH. Application of recombinant FGF10 or stimulation of the downstream signalling cascade thus might represent a novel therapeutic strategy for treating lung emphysema and PH in COPD.

7 Zusammenfassung

Die chronisch obstruktive Lungenerkrankung (COPD) ist eine schwere Krankheit, die durch chronische Bronchitis und Zerstörung der Septumwand (Emphysem) gekennzeichnet ist. Darüber hinaus leiden COPD-Patienten häufig an zumindest milder pulmonaler Hypertonie (PH) aufgrund eines Umbaus der Lungengefäße. Der wichtigste pathologische Auslöser ist die Inhalation schädlicher Partikel oder Gase, die hauptsächlich vom Zigarettenrauchen, aber auch aus anderen Quellen wie der Luftverschmutzung stammen. Es wurden mehrere zugrundeliegende Mechanismen identifiziert, die die Entwicklung und das Fortschreiten der Krankheit vorantreiben. Zu diesen Mechanismen gehören ein Ungleichgewicht zwischen Proteasen und Antiproteasen, übermäßiger nitrosativer und oxidativer Stress sowie eine verstärkte Entzündungsreaktion. Darüber hinaus stützen neuere Studien die Idee, dass viele Entwicklungswege bei COPD dysreguliert sind, was zu einer gestörten oder sogar abnormen Lungenreparatur im späteren Leben führt. Trotz der erheblichen Mühen, die in die Erforschung und Entwicklung neuer therapeutischer Ansätze investiert werden, ist COPD nach wie vor eine unheilbare und schlecht behandelbare Krankheit.

Bereits in vorausgehenden Studien wurde der Fibroblasten-Wachstumsfaktor (fibroblast growth factor, FGF) 10 als potenzielles Zielmolekül identifiziert, welches an der Umkehrung des durch Zigarettenrauch (cigarette smoke, CS) induzierten Emphysems und der PH, durch Hemmung der induzierbaren Stickstoffmonoxid-Synthase (inducible nitric oxide synthase, iNOS) in Mäusen, beteiligt sein könnte. FGF10 ist für die Morphogenese der Lunge entscheidend und steuert nachweislich das Überleben und die Vermehrung von Vorläuferzellen des Alveolarepithels während der Lungenentwicklung. Außerdem wird vermutet, dass eine gestörte FGF10-Signalübertragung bei Patienten zu einer höheren Wahrscheinlichkeit für die Entwicklung einer COPD führt. Die Ursache-Wirkungs-Beziehung zwischen FGF10-Expression und COPD-Entwicklung, der zugrundeliegende molekulare Mechanismus und die Beeinflussung der FGF10-Signalübertragung als mögliche Therapie sind jedoch bisher nicht untersucht.

Um diese Fragen zu klären, habe ich in der vorliegenden Arbeit FGF-bezogene Signalwege in menschlichen Lungenproben von gesunden Spendern sowie Rauchern ohne und mit COPD untersucht. Darüber hinaus habe ich hämodynamische und Lungenfunktionsmessungen in *Fgf10^{+/-}*- und *Fgfr2b^{+/-}* (FGF-Rezeptor 2b)-Mäusen nach chronischer CS-Exposition durchgeführt und histologische Indikatoren für den Lungengefäßumbau und das Emphysem untersucht. Um eine mögliche therapeutische Anwendung zu erforschen, habe ich FGF10 in Mäusen nach Elastase- oder CS-induzierter Lungenschädigung überexprimiert. Darüber hinaus wurden die Genexpressionsmuster während der Entwicklung und der FGF10-vermittelten Revertierung des CS-induzierten Emphysems und der PH in Mäuselungen in seziierten Alveolarsepten und Lungengefäßen mit Hilfe von Microarray-Technologie untersucht.

Meine Untersuchungen konnten eine verminderte FGF10-Expression in den Alveolarsepten der Lungen von Rauchern mit und ohne COPD sowie im Lungenhomogenat von Mäusen, die CS ausgesetzt waren, aufdecken. Weiterhin konnte ich eine Abnahme der FGF10-Expression in interstitiellen Lungenfibroblasten, die aus COPD-Lungen isoliert wurden, feststellen. Diese Effekte konnten in gesunden Spender-Lungenfibroblasten nachgeahmt werden, indem *sie in vitro* CS-Extrakt oder nitrosativem/oxidativem Stress ausgesetzt wurden.

Fgf10- und *Fgfr2b*-haploinsuffiziente Mäuse waren anfälliger für die Entwicklung eines CS-induzierten Emphysems und einer PH. Darüber hinaus entwickelten Tiere mit beeinträchtigter FGF10-Signalgebung ein spontanes Emphysem und eine PH sowie andere typische pathomechanistische Merkmale, die im Allgemeinen als Reaktion auf CS-Exposition auftreten. Dazu gehören die Bildung von 3-Nitrotyrosin, erhöhte Matrix-Metalloproteinase (MMP)-Aktivität, Apoptose und verschiedene Veränderungen des Transkriptoms. Meine Daten deuten darauf hin, dass eine abgeschwächte β -Catenin-Signalgebung und eine erhöhte Phosphorylierung von Akt (Akt strain transforming) der Entwicklung eines Emphysems bzw. einer PH in CS-exponierten Wt-Mäusen und Mäusen mit beeinträchtigter FGF10-Signalgebung zugrunde liegen könnten. Interessanterweise konnte die Überexpression von FGF10 eine bereits bestehende Elastase- und CS-induzierte Lungenschädigung in Mäusen erfolgreich umkehren.

Insgesamt zeigen meine Daten, dass die FGF10-Signalübertragung für die Homöostase der Lunge von Erwachsenen entscheidend ist. Darüber hinaus könnte die FGF10-Signalübertragung ein wesentlicher Bestandteil des Pathomechanismus sein, der zu CS-induziertem Emphysem und PH führt. Die Anwendung von rekombinantem FGF10 oder die Stimulierung der FGF10-nachgeschalteten Signalkaskade könnte daher eine neue therapeutische Strategie zur Behandlung des Lungenemphysems und PH in der COPD darstellen.

8 Index of figures

Figure 1	Airway branching and cross-sectional area in adult human lung.
Figure 2	Airway wall of small bronchi in healthy and COPD lungs.
Figure 3	Alveolar septal wall in healthy and COPD lungs.
Figure 4	Augmented inflammatory response in COPD.
Figure 5	Cellular and molecular pathways in COPD.
Figure 6	Schematic drawing of FGFR structure.
Figure 7	FGF receptor activation and downstream signalling.
Figure 8	Schematic drawing of the experimental design and hypothesis.
Figure 9	Experimental design for the loss-of-function setup.
Figure 10	Experimental design for therapeutic approach after CS-induced emphysema and PH.
Figure 11	Experimental design for therapeutic approach after elastase-induced emphysema and PH.
Figure 12	Mouse model of long-term cigarette smoke exposure.
Figure 13	Mouse model of elastase-induced pulmonary emphysema.
Figure 14	Human precision cut lung slices (PCLS) preparation.
Figure 15	FGF10 expression in lungs from RA- or CS-exposed mice treated with placebo or L-NIL.

Figure 16	mRNA expression of FGF ligands in lung homogenates from healthy donors, smokers without and with COPD.
Figure 17	mRNA expression of FGF receptor isoforms in lung homogenates from healthy donors, smokers with and without COPD.
Figure 18	FGF10 and FGFR2 protein expression in lung homogenates from healthy donors, smokers without and with COPD.
Figure 19	Representative images showing FGF10 and FGFR2 IHC staining in human lungs from healthy donors, smokers without and with COPD.
Figure 20	Differential expression of FGF10 and FGFR2 in alveolar septal wall and in pulmonary vessels of healthy donors, smokers without and with COPD.
Figure 21	FGF10 expression in CSE-treated donor interstitial lung fibroblasts and PSMCs.
Figure 22	FGF10 expression in interstitial lung fibroblasts isolated from donor and COPD lungs.
Figure 23	FGF10 expression in interstitial lung fibroblasts upon peroxynitrite stress.
Figure 24	Expression of transcription factor SP1 in interstitial fibroblasts isolated from donor and COPD lungs.
Figure 25	Histological examination of the lung parenchyma in RA- and CS-exposed Wt mice and mice with impaired FGF10 signalling.
Figure 26	μ CT examination of the lung structure in RA- and CS-exposed Wt mice and mice with impaired FGF10 signalling.
Figure 27	Alveoli number in mice RA- and CS-exposed Wt mice and mice with impaired FGF10 signalling.
Figure 28	Representative images showing the lung structure in RA- and CS-exposed Wt mice and mice with impaired FGF10 signalling.

Figure 29	<i>In vivo</i> lung compliance in RA- and CS-exposed Wt mice and mice with impaired FGF10 signalling.
Figure 30	Respiratory resistance in Wt mice and mice with impaired FGF10 signalling.
Figure 31	Alterations in the distal lung parenchyma in RA- and CS-exposed mice with impaired FGF10 signalling.
Figure 32	Pulmonary vasculature tree in RA-exposed Wt mice and mice with impaired FGF10 signalling.
Figure 33	Pulmonary hypertension in CS-exposed mice with impaired FGF10 signalling.
Figure 34	Right heart alterations in CS-exposed mice with impaired FGF10 signalling.
Figure 35	FGF10 expression in lung homogenate from Wt and <i>Fgf10</i> ^{+/-} animals after 8 months of RA or CS exposure.
Figure 36	3-nitrotyrosine quantification in lung homogenates from Wt and <i>Fgf10</i> ^{+/-} mice.
Figure 37	Apoptosis in lungs from CS-exposed mice with impaired FGF10 signalling measured by FMT-CT.
Figure 38	CSE-induced AT II cell apoptosis and decrease in cell viability.
Figure 39	MMP activity in lungs from CS-exposed mice with impaired FGF10 signalling measured by FMT-CT.
Figure 40	Heat maps showing all CS-regulated genes during the development of emphysema and PH.
Figure 41	CS- and FGF10 haploinsufficiency-related gene expression pattern during emphysema and PH development.

Figure 42	Functional protein association networks of CS- and FGF10 haploinsufficiency-regulated genes during emphysema and PH development.
Figure 43	β -catenin expression in lung homogenates from CS-exposed or FGF10 haploinsufficient animals.
Figure 44	Phosphorylation of Akt in lung homogenates from CS-exposed or FGF10 deficient animals.
Figure 45	The sole effect of doxycycline on CS-induced emphysema.
Figure 46	The sole effect of doxycycline on CS-induced PH.
Figure 47	Confirmation of FGF10 overexpression.
Figure 48	Airspace percentage and mean linear intercept quantified in mouse lungs after 8 months of CS exposure and subsequent FGF10 overexpression.
Figure 49	Representative images showing lung parenchyma in mice after 8 months of CS exposure with subsequent FGF10 overexpression.
Figure 50	Alveoli number in left lung lobe from mice after CS exposure and subsequent FGF10 overexpression treatment.
Figure 51	The effect of FGF10 overexpression on CS-induced pulmonary hypertension.
Figure 52	The effect of FGF10 overexpression on CS-induced right heart alterations.
Figure 53	Heat maps showing all CS-regulated genes in untreated animals.
Figure 54	CS- and FGF10 overexpression-related gene expression pattern during reversion of emphysema and PH.
Figure 55	Endothelial cells in mouse lungs after CS-induced emphysema and PH, and subsequent doxycycline-induced FGF10 overexpression for 12 weeks.

Figure 56	Functional protein association networks of CS- and FGF10 overexpression-regulated genes during reversion of emphysema and PH.
Figure 57	FGF10 treatment of precision-cut lung slices (PCLS) from patients with COPD.
Figure 58	Lung compliance in mice after elastase-induced pulmonary emphysema and subsequent FGF10 overexpression treatment.
Figure 59	Respiratory resistance in mice after elastase-induced pulmonary emphysema and subsequent FGF10 overexpression treatment.
Figure 60	Lung parenchyma destruction in mouse lungs after elastase-induced emphysema and subsequent FGF10 overexpression treatment.
Figure 61	Representative images showing lung parenchyma after elastase-induced emphysema with or without subsequent doxycycline-induced FGF10 overexpression treatment.
Figure 62	Hemodynamic measurement obtained in mice after elastase-induced pulmonary emphysema and PH and subsequent FGF10 overexpression treatment.
Figure 63	Right heart alterations in mice after elastase-induced pulmonary emphysema and PH and subsequent FGF10 overexpression treatment.
Figure 64	Pulmonary vasculature after elastase-induced emphysema and PH and subsequent doxycycline-induced FGF10 overexpression for 12 weeks.
Figure 65	Cigarette smoke through peroxynitrite stress leads to decreased FGF10 expression in interstitial lung fibroblasts.
Figure 66	Cigarette smoke leads to emphysema and PH development through inhibition of FGF10 signalling.
Figure 67	FGF10 overexpression reverses cigarette smoke- and elastase-induced emphysema and PH.

9 Index of tables

Table 1	Airway branching in the human respiratory system from the conductive towards the respiratory zone.
Table 2	COPD classification based on airflow limitation severity in patients.
Table 3	FGF subfamilies and their receptor specificity.
Table 4	Ethical approvals for animal experiments approved by Regierungspräsidium Gießen.
Table 5	Experimental groups for the loss-of-function experimental setup.
Table 6	Experimental groups for therapeutic approach after CS-induced emphysema and PH.
Table 7	Experimental groups for therapeutic approach after elastase-induced emphysema and PH.
Table 8	Deparaffinization and rehydration protocol performed on paraffin cut tissue sections.
Table 9	Haematoxylin & eosin (H&E) staining protocol.
Table 10	Wiegert's elastin staining protocol.
Table 11	Picosirius red staining protocol.
Table 12	Sample preparation for reverse transcription – cDNA synthesis.
Table 13	Thermal reaction for reverse transcription – cDNA synthesis.
Table 14	Sample preparation for quantitative polymerase chain reaction (qPCR).

Table 15 Thermal reaction program for quantitative polymerase chain reaction (qPCR).

Table 16 Sample preparation for sodium dodecyl-sulphate polyacrylamide gel electrophoresis (SDS-PAGE).

10 Declaration

I declare that I have completed this thesis on my own, without unauthorized outside help and only with the assistance acknowledged therein. I have correctly acknowledged and referenced all the passages which are derived literally or analogously from published or unpublished work and all information that relates to verbal communications. I have the principles of good scientific practice such as these in the “Statute of Justus Liebig University Giessen to ensure good scientific practice” in my work and in my thesis.

Stefan Hadzic

Parts of the results presented in this thesis were already published as a part of the manuscript entitled “The effect of long-term doxycycline treatment in a mouse model of cigarette smoke-induced emphysema and pulmonary hypertension” (DOI: 10.1152/ajplung.00048.2021).

Parts of this thesis share the same topic with a previously published review article entitled “Lung epithelium damage in COPD - An unstoppable pathological event?” (DOI: 10.1016/j.cellsig.2020.109540) written in part by the same author, which may lead to the general resemblance in style.

11 References

- Abdul-Hussien, H., Hanemaaijer, R., Verheijen, J. H., van Bockel, J. H., Geelkerken, R. H., & Lindeman, J. H. (2009). Doxycycline therapy for abdominal aneurysm: Improved proteolytic balance through reduced neutrophil content. *Journal of Vascular Surgery*, *49*(3), 741-749. doi:10.1016/j.jvs.2008.09.055
- Adnot, S., Amsellem, V., Boyer, L., Marcos, E., Saker, M., Houssaini, A., Kebe, K., Dagouassat, M., Lipskaia, L., & Boczkowski, J. (2015). Telomere Dysfunction and Cell Senescence in Chronic Lung Diseases: Therapeutic Potential. *Pharmacology and Therapeutics*, *153*, 125-134. doi:10.1016/j.pharmthera.2015.06.007
- Ahmad, R., Hussain, A., & Ahsan, H. (2019). Peroxynitrite: cellular pathology and implications in autoimmunity. *Journal of Immunoassay and Immunochemistry*, *40*(2), 123-138. doi:10.1080/15321819.2019.1583109
- Ahmadvand, N., Khosravi, F., Lingampally, A., Wasnick, R., Vazquez-Armendariz, I., Carraro, G., Heiner, M., Rivetti, S., Lv, Y., Wilhelm, J., Gunther, A., Herold, S., Al Alam, D., Chen, C., Minoo, P., Zhang, J. S., & Bellusci, S. (2021). Identification of a novel subset of alveolar type 2 cells enriched in PD-L1 and expanded following pneumonectomy. *European Respiratory Journal*. doi:10.1183/13993003.04168-2020
- Ahsan, H. (2013). 3-Nitrotyrosine: A biomarker of nitrogen free radical species modified proteins in systemic autoimmunogenic conditions. *Human Immunology*, *74*(10), 1392-1399. doi:10.1016/j.humimm.2013.06.009
- Alving, K., Fornhem, C., & Lundberg, J. M. (1993). Pulmonary effects of endogenous and exogenous nitric oxide in the pig: relation to cigarette smoke inhalation. *British Journal of Pharmacology*, *110*(2), 739-746. doi:10.1111/j.1476-5381.1993.tb13874.x
- Ambasta, R. K., Kumar, P., Griendling, K. K., Schmidt, H. H., Busse, R., & Brandes, R. P. (2004). Direct interaction of the novel Nox proteins with p22phox is required for the formation of a functionally active NADPH oxidase. *Journal of Biological Chemistry*, *279*(44), 45935-45941. doi:10.1074/jbc.M406486200
- Andrae, J., Gallini, R., & Betsholtz, C. (2008). Role of platelet-derived growth factors in physiology and medicine. *Genes and Development*, *22*(10), 1276-1312. doi:10.1101/gad.1653708
- Antonio, R. C., Ceron, C. S., Rizzi, E., Coelho, E. B., Tanus-Santos, J. E., & Gerlach, R. F. (2014). Antioxidant effect of doxycycline decreases MMP activity and blood pressure in SHR. *Molecular and Cellular Biochemistry*, *386*(1-2), 99-105. doi:10.1007/s11010-013-1848-7
- Antunes, M. A., & Rocco, P. R. (2011). Elastase-induced pulmonary emphysema: insights from experimental models. *Anais da Academia Brasileira de Ciencias*, *83*(4), 1385-1396. doi:10.1590/s0001-37652011005000039

-
- Baarsma, H. A., Skronska-Wasek, W., Mutze, K., Ciolek, F., Wagner, D. E., John-Schuster, G., Heinzelmann, K., Günther, A., Bracke, K. R., Dagouassat, M., Boczkowski, J., Brusselle, G. G., Smits, R., Eickelberg, O., Yildirim, A. Ö., & Königshoff, M. (2017). Noncanonical WNT-5A signaling impairs endogenous lung repair in COPD. *The Journal of experimental medicine*, *214*(1), 143-163. doi:10.1084/jem.20160675
- Baile, E. M. (1996). The anatomy and physiology of the bronchial circulation. *Journal of Aerosol Medicine*, *9*(1), 1-6. doi:10.1089/jam.1996.9.1
- Baker, C. L., Zou, K. H., & Su, J. (2013). Risk assessment of readmissions following an initial COPD-related hospitalization. *International Journal of Chronic Obstructive Pulmonary Disease*, *8*, 551-559. doi:10.2147/copd.S51507
- Barkauskas, C. E., Cronce, M. J., Rackley, C. R., Bowie, E. J., Keene, D. R., Stripp, B. R., Randell, S. H., Noble, P. W., & Hogan, B. L. (2013). Type 2 alveolar cells are stem cells in adult lung. *Journal of Clinical Investigation*, *123*(7), 3025-3036. doi:10.1172/jci68782
- Barnes, P. J. (2007). Unexpected failure of anti-tumor necrosis factor therapy in chronic obstructive pulmonary disease. *American journal of respiratory and critical care medicine*, *175*(9), 866-867. doi:10.1164/rccm.200702-253ED
- Barnes, P. J. (2009). Histone deacetylase-2 and airway disease. *Therapeutic Advances in Respiratory Disease*, *3*(5), 235-243. doi:10.1177/1753465809348648
- Barnes, P. J. (2014). Cellular and molecular mechanisms of chronic obstructive pulmonary disease. *Clinics in Chest Medicine*, *35*(1), 71-86. doi:10.1016/j.ccm.2013.10.004
- Barnes, P. J. (2016). Inflammatory mechanisms in patients with chronic obstructive pulmonary disease. *The Journal of Allergy and Clinical Immunology*, *138*(1), 16-27. doi:10.1016/j.jaci.2016.05.011
- Barnes, P. J. (2017). Senescence in COPD and Its Comorbidities. *Annual Review of Physiology*, *79*, 517-539. doi:10.1146/annurev-physiol-022516-034314
- Barnes, P. J. (2019). Nitrosative stress in patients with asthma-chronic obstructive pulmonary disease overlap. *The Journal of Allergy and Clinical Immunology*, *144*(4), 928-930. doi:10.1016/j.jaci.2019.07.040
- Barnes, P. J., Burney, P. G. J., Silverman, E. K., Celli, B. R., Vestbo, J., Wedzicha, J. A., & Wouters, E. F. M. (2015). Chronic obstructive pulmonary disease. *Nature Reviews Disease Primers*, *1*(1), 15076. doi:10.1038/nrdp.2015.76
- Barnes, P. J., & Hansel, T. T. (2004). Prospects for new drugs for chronic obstructive pulmonary disease. *Lancet*, *364*(9438), 985-996. doi:10.1016/s0140-6736(04)17025-6
- Basrai, H. S., Christie, K. J., Turbic, A., Bye, N., & Turnley, A. M. (2016). Suppressor of Cytokine Signaling-2 (SOCS2) Regulates the Microglial Response and Improves Functional Outcome after Traumatic Brain Injury in Mice. *PLoS One*, *11*(4), e0153418. doi:10.1371/journal.pone.0153418
- Basson, J., Sung, Y. J., Schwander, K., Kume, R., Simino, J., de las Fuentes, L., & Rao, D. (2014). Gene-education interactions identify novel blood pressure loci in the Framingham

- Heart Study. *American Journal of Hypertension*, 27(3), 431-444. doi:10.1093/ajh/hpt283
- Bates, J. H. T. (2009). *Lung mechanics : an inverse modeling approach*. Cambridge, UK; New York: Cambridge University Press. doi:10.1017/CBO9780511627156
- Baxter, B. T., Pearce, W. H., Waltke, E. A., Littooy, F. N., Hallett, J. W., Jr., Kent, K. C., Upchurch, G. R., Jr., Chaikof, E. L., Mills, J. L., Fleckten, B., Longo, G. M., Lee, J. K., & Thompson, R. W. (2002). Prolonged administration of doxycycline in patients with small asymptomatic abdominal aortic aneurysms: report of a prospective (Phase II) multicenter study. *Journal of Vascular Surgery*, 36(1), 1-12. doi:10.1067/mva.2002.125018
- Behnke, R. H., Blount, S. G., Bristow, J. D., Carrieri, V., Pierce, J. A., Sasahara, A., Soffer, A., & Greenspan, R. (1970). Primary prevention of pulmonary heart disease. *Journal of Osteopathic Medicine*, 69(11), 1139-1146. PMID: 5202395
- Belleudi, F., Leone, L., Aimati, L., Stirparo, M. G., Cardinali, G., Marchese, C., Frati, L., Picardo, M., & Torrisi, M. R. (2006). Endocytic pathways and biological effects induced by UVB-dependent or ligand-dependent activation of the keratinocyte growth factor receptor. *The FASEB Journal*, 20(2), 395-397. doi:10.1096/fj.05-3934fje
- Bellusci, S., Grindley, J., Emoto, H., Itoh, N., & Hogan, B. L. (1997). Fibroblast growth factor 10 (FGF10) and branching morphogenesis in the embryonic mouse lung. *Development*, 124(23), 4867-4878. doi: 10.1242/dev.124.23.4867
- Benderradji, H., Kraiem, S., Courty, E., Eddarkaoui, S., Bourouh, C., Faivre, E., Rolland, L., Caron, E., Besegher, M., Oger, F., Boschetti, T., Carvalho, K., Thiroux, B., Gauvrit, T., Nicolas, E., Gomez-Murcia, V., Bogdanova, A., Bongiovanni, A., Muhr-Tailleux, A., Lancel, S., Bantubungi, K., Sergeant, N., Annicotte, J. S., Buée, L., Vieau, D., Blum, D., & Buée-Scherrer, V. (2022). Impaired Glucose Homeostasis in a Tau Knock-In Mouse Model. *Frontiers in Molecular Neuroscience*, 15, 841892. doi:10.3389/fnmol.2022.841892
- Benjamin, J. T., Carver, B. J., Plosa, E. J., Yamamoto, Y., Miller, J. D., Liu, J.-H., van der Meer, R., Blackwell, T. S., & Prince, L. S. (2010). NF- κ B Activation Limits Airway Branching through Inhibition of Sp1-Mediated Fibroblast Growth Factor-10 Expression. *The Journal of Immunology*, 185(8), 4896-4903. doi:10.4049/jimmunol.1001857
- Berger, W., Setinek, U., Mohr, T., Kindas-Mügge, I., Vetterlein, M., Dekan, G., Eckersberger, F., Caldas, C., & Micksche, M. (1999). Evidence for a role of FGF-2 and FGF receptors in the proliferation of non-small cell lung cancer cells. *International Journal of Cancer*, 83(3), 415-423. doi:10.1002/(sici)1097-0215(19991029)83:3<415::aid-ijc19>3.0.co;2-y
- Berry, C. E., & Wise, R. A. (2010). Mortality in COPD: causes, risk factors, and prevention. *COPD: Journal of Chronic Obstructive Pulmonary Disease*, 7(5), 375-382. doi:10.3109/15412555.2010.510160
- Black, P. N., Ching, P. S., Beaumont, B., Ranasinghe, S., Taylor, G., & Merrilees, M. J. (2008). Changes in elastic fibres in the small airways and alveoli in COPD. *European Respiratory Journal*, 31(5), 998-1004. doi:10.1183/09031936.00017207

- Boucher, M., Henry, C., Khadangi, F., Dufour-Mailhot, A., Tremblay-Pitre, S., Fereydoonzad, L., Brunet, D., Robichaud, A., & Bossé, Y. (2021). Effects of airway smooth muscle contraction and inflammation on lung tissue compliance. *The American Journal of Physiology-Lung Cellular and Molecular Physiology* 322: L294–L304. doi:10.1152/ajplung.00384.2021
- Boucherat, O., Morissette, M. C., Provencher, S., Bonnet, S., & Maltais, F. (2016). Bridging Lung Development with Chronic Obstructive Pulmonary Disease. Relevance of Developmental Pathways in Chronic Obstructive Pulmonary Disease Pathogenesis. *American journal of respiratory and critical care medicine*, 193(4), 362-375. doi:10.1164/rccm.201508-1518PP
- Boukhenouna, S., Wilson, M. A., Bahmed, K., & Kosmider, B. (2018). Reactive Oxygen Species in Chronic Obstructive Pulmonary Disease. *Oxidative Medicine and Cellular Longevity*, 2018, 5730395. doi:10.1155/2018/5730395
- Bozinovski, S., Vlahos, R., Hansen, M., Liu, K., & Anderson, G. P. (2006). Akt in the pathogenesis of COPD. *International Journal of Chronic Obstructive Pulmonary Disease*, 1(1), 31-38. doi:10.2147/copd.2006.1.1.31
- Bracke, K. R., D'Hulst A, I., Maes, T., Moerloose, K. B., Demedts, I. K., Lebecque, S., Joos, G. F., & Brusselle, G. G. (2006). Cigarette smoke-induced pulmonary inflammation and emphysema are attenuated in CCR6-deficient mice. *Journal of Immunology*, 177(7), 4350-4359. doi:10.4049/jimmunol.177.7.4350
- Brandes, R. P., Weissmann, N., & Schröder, K. (2014). Nox family NADPH oxidases: Molecular mechanisms of activation. *Free Radical Biology and Medicine*, 76, 208-226. doi:10.1016/j.freeradbiomed.2014.07.046
- Brindicci, C., Ito, K., Torre, O., Barnes, P. J., & Kharitonov, S. A. (2009). Effects of aminoguanidine, an inhibitor of inducible nitric oxide synthase, on nitric oxide production and its metabolites in healthy control subjects, healthy smokers, and COPD patients. *Chest*, 135(2), 353-367. doi:10.1378/chest.08-0964
- Brode, S. K., Ling, S. C., & Chapman, K. R. (2012). Alpha-1 antitrypsin deficiency: a commonly overlooked cause of lung disease. *CMAJ : Canadian Medical Association journal = journal de l'Association medicale canadienne*, 184(12), 1365-1371. doi:10.1503/cmaj.111749
- Buchtova, M., Chaloupkova, R., Zakrzewska, M., Vesela, I., Cela, P., Barathova, J., Gudernova, I., Zajickova, R., Trantirek, L., Martin, J., Kostas, M., Otlewski, J., Damborsky, J., Kozubik, A., Wiedlocha, A., & Krejci, P. (2015). Instability restricts signaling of multiple fibroblast growth factors. *Cellular and Molecular Life Sciences*, 72(12), 2445-2459. doi:10.1007/s00018-015-1856-8
- Bühling, F., Gerber, A., Häckel, C., Krüger, S., Köhnlein, T., Brömme, D., Reinhold, D., Ansoerge, S., & Welte, T. (1999). Expression of cathepsin K in lung epithelial cells. *American Journal of Respiratory Cell and Molecular Biology*, 20(4), 612-619. doi:10.1165/ajrcmb.20.4.3405

- Bühling, F., Reisenauer, A., Gerber, A., Krüger, S., Weber, E., Brömme, D., Roessner, A., Ansorge, S., Welte, T., & Röcken, C. (2001). Cathepsin K--a marker of macrophage differentiation? *The Journal of Pathology*, *195*(3), 375-382. doi:10.1002/path.959
- Bühling, F., Röcken, C., Brasch, F., Hartig, R., Yasuda, Y., Saftig, P., Brömme, D., & Welte, T. (2004). Pivotal role of cathepsin K in lung fibrosis. *The American Journal of Pathology*, *164*(6), 2203-2216. doi:10.1016/s0002-9440(10)63777-7
- Bunel, V., Guyard, A., Dauriat, G., Danel, C., Montani, D., Gauvain, C., Thabut, G., Humbert, M., Castier, Y., Dorfmüller, P., & Mal, H. (2019). Pulmonary Arterial Histologic Lesions in Patients With COPD With Severe Pulmonary Hypertension. *Chest*, *156*(1), 33-44. doi:10.1016/j.chest.2019.02.333
- Caffa, I., Spagnolo, V., Vernieri, C., Valdemarin, F., Becherini, P., Wei, M., Brandhorst, S., Zucal, C., Driehuis, E., Ferrando, L., Piacente, F., Tagliafico, A., Cilli, M., Mastracci, L., Vellone, V. G., Piazza, S., Cremonini, A. L., Gradaschi, R., Mantero, C., Passalacqua, M., Ballestrero, A., Zoppoli, G., Cea, M., Arrighi, A., Odetti, P., Monacelli, F., Salvadori, G., Cortellino, S., Clevers, H., De Braud, F., Sukkar, S. G., Provenzani, A., Longo, V. D., & Nencioni, A. (2020). Fasting-mimicking diet and hormone therapy induce breast cancer regression. *Nature*, *583*(7817), 620-624. doi:10.1038/s41586-020-2502-7
- Campreciós, G., Ruat, M., Anton, A., Suárez-Herrera, N., Montironi, C., Martínez, C., Jiménez, N., Lafoz, E., García-Calderó, H., Vilaseca, M., Magaz, M., Coll, M., Graupera, I., Friedman, S. L., García-Pagán, J. C., & Hernández-Gea, V. (2021). Spermidine Supplementation Protects the Liver Endothelium from Liver Damage in Mice. *Nutrients*, *13*(11). doi:10.3390/nu13113700
- Carpio, M. A., Michaud, M., Zhou, W., Fisher, J. K., Walensky, L. D., & Katz, S. G. (2015). BCL-2 family member BOK promotes apoptosis in response to endoplasmic reticulum stress. *Proceedings of the National Academy of Sciences*, *112*(23), 7201-7206. doi:10.1073/pnas.1421063112
- Castaldi, P. J., Cho, M. H., San Jose Estepar, R., McDonald, M. L., Laird, N., Beaty, T. H., Washko, G., Crapo, J. D., & Silverman, E. K. (2014). Genome-wide association identifies regulatory Loci associated with distinct local histogram emphysema patterns. *American journal of respiratory and critical care medicine*, *190*(4), 399-409. doi:10.1164/rccm.201403-0569OC
- Castets, P., Rion, N., Théodore, M., Falcetta, D., Lin, S., Reischl, M., Wild, F., Guérard, L., Eickhorst, C., Brockhoff, M., Guridi, M., Ibebunjo, C., Cruz, J., Sinnreich, M., Rudolf, R., Glass, D. J., & Rüegg, M. A. (2019). mTORC1 and PKB/Akt control the muscle response to denervation by regulating autophagy and HDAC4. *Nature Communications*, *10*(1), 3187. doi:10.1038/s41467-019-11227-4
- Castro, M. M., Tanus-Santos, J. E., & Gerlach, R. F. (2011). Matrix metalloproteinases: Targets for doxycycline to prevent the vascular alterations of hypertension. *Pharmacological Research*, *64*(6), 567-572. doi:10.1016/j.phrs.2011.04.002

- Cerisano, G., Buonamici, P., Valenti, R., Sciagra, R., Raspanti, S., Santini, A., Carrabba, N., Dovellini, E. V., Romito, R., Pupi, A., Colonna, P., & Antoniucci, D. (2014). Early short-term doxycycline therapy in patients with acute myocardial infarction and left ventricular dysfunction to prevent the ominous progression to adverse remodelling: the TIPTOP trial. *European Heart Journal*, *35*(3), 184-191. doi:10.1093/eurheartj/eh420
- Chao, C. M., Moiseenko, A., Kosanovic, D., Rivetti, S., El Agha, E., Wilhelm, J., Kampschulte, M., Yahya, F., Ehrhardt, H., Zimmer, K. P., Barreto, G., Rizvanov, A. A., Schermuly, R. T., Reiss, I., Morty, R. E., Rottier, R. J., Bellusci, S., & Zhang, J. S. (2019). Impact of Fgf10 deficiency on pulmonary vasculature formation in a mouse model of bronchopulmonary dysplasia. *Human Molecular Genetics*, *28*(9), 1429-1444. doi:10.1093/hmg/ddy439
- Chao, C. M., Yahya, F., Moiseenko, A., Tiozzo, C., Shrestha, A., Ahmadvand, N., El Agha, E., Quantius, J., Dilai, S., Kheirollahi, V., Jones, M., Wilhem, J., Carraro, G., Ehrhardt, H., Zimmer, K. P., Barreto, G., Ahlbrecht, K., Morty, R. E., Herold, S., Abellar, R. G., Seeger, W., Schermuly, R., Zhang, J. S., Minoo, P., & Bellusci, S. (2017). Fgf10 deficiency is causative for lethality in a mouse model of bronchopulmonary dysplasia. *The Journal of Pathology*, *241*(1), 91-103. doi:10.1002/path.4834
- Chaouat, A., Naeije, R., & Weitzenblum, E. (2008). Pulmonary hypertension in COPD. *European Respiratory Journal*, *32*(5), 1371-1385. doi:10.1183/09031936.00015608
- Chelladurai, P., Seeger, W., & Pullamsetti, S. S. (2012). Matrix metalloproteinases and their inhibitors in pulmonary hypertension. *European Respiratory Journal*, *40*(3), 766-782. doi:10.1183/09031936.00209911
- Chen, A. C.-H., Burr, L., & McGuckin, M. A. (2018). Oxidative and endoplasmic reticulum stress in respiratory disease. *Clinical and Translational Immunology*, *7*(6), e1019. doi:https://doi.org/10.1002/cti2.1019
- Chen, Q., Ren, D., Wu, J., Yu, H., Chen, X., Wang, J., Zhang, Y., Liu, M., & Wang, T. (2021). Shenyan Kangfu tablet alleviates diabetic kidney disease through attenuating inflammation and modulating the gut microbiota. *Journal of Natural Medicine*, *75*(1), 84-98. doi:10.1007/s11418-020-01452-3
- Chen, X. L., Cai, Y. H., Liu, Q., Pan, L. L., Shi, S. L., Liu, X. L., Chen, Y., Li, J. G., Wang, J., Li, Y., Li, X. F., & Wang, S. Y. (2018). ETS1 and SP1 drive DHX15 expression in acute lymphoblastic leukaemia. *Journal of Cellular and Molecular Medicine*, *22*(5), 2612-2621. doi:10.1111/jcmm.13525
- Choe, A., Veltmaat, J. M., Sala, F. G., DelMoral, P., DeLanghe, S., Stein, J., Ford, H., Warburton, D., Bellusci, S., & Wang, K. S. (2006). FGF10 induces activation of canonical WNT signaling in the developing mouse liver. *Journal of Surgical Research*, *130*(2), 161-162. doi:10.1016/j.jss.2005.11.006
- Chung, H. Y., Sung, B., Jung, K. J., Zou, Y., & Yu, B. P. (2006). The molecular inflammatory process in aging. *Antioxid Redox Signal*, *8*(3-4), 572-581. doi:10.1089/ars.2006.8.572

-
- Churg, A., Cosio, M., & Wright, J. L. (2008). Mechanisms of cigarette smoke-induced COPD: insights from animal models. *The American Journal of Physiology-Lung Cellular and Molecular Physiology*, *294*(4), L612-631. doi:10.1152/ajplung.00390.2007
- Churg, A., Sin, D. D., & Wright, J. L. (2011). Everything prevents emphysema: are animal models of cigarette smoke-induced chronic obstructive pulmonary disease any use? *American Journal of Respiratory Cell and Molecular Biology*, *45*(6), 1111-1115. doi:10.1165/rcmb.2011-0087PS
- Churg, A., Wang, R., Wang, X., Onnervik, P. O., Thim, K., & Wright, J. L. (2007). Effect of an MMP-9/MMP-12 inhibitor on smoke-induced emphysema and airway remodelling in guinea pigs. *Thorax*, *62*(8), 706-713. doi:10.1136/thx.2006.068353
- Churg, A., Wang, R. D., Tai, H., Wang, X., Xie, C., & Wright, J. L. (2004). Tumor necrosis factor-alpha drives 70% of cigarette smoke-induced emphysema in the mouse. *American Journal of Respiratory and Critical Care Medicine*, *170*(5), 492-498. doi:10.1164/rccm.200404-511OC
- Churg, A., Wang, R. D., Xie, C., & Wright, J. L. (2003). alpha-1-Antitrypsin ameliorates cigarette smoke-induced emphysema in the mouse. *American journal of respiratory and critical care medicine*, *168*(2), 199-207. doi:10.1164/rccm.200302-203OC
- Churg, A., Wang, X., Wang, R. D., Meixner, S. C., Pryzdial, E. L., & Wright, J. L. (2007). Alpha1-antitrypsin suppresses TNF-alpha and MMP-12 production by cigarette smoke-stimulated macrophages. *American Journal of Respiratory Cell and Molecular Biology*, *37*(2), 144-151. doi:10.1165/rcmb.2006-0345OC
- Churg, A., & Wright, J. L. (2005). Proteases and emphysema. *Current Opinion in Pulmonary Medicine*, *11*(2), 153-159. doi: 10.1097/01.mcp.0000149592.51761.e3.
- Churg, A., Zay, K., Shay, S., Xie, C., Shapiro, S. D., Hendricks, R., & Wright, J. L. (2002). Acute cigarette smoke-induced connective tissue breakdown requires both neutrophils and macrophage metalloelastase in mice. *American Journal of Respiratory Cell and Molecular Biology*, *27*(3), 368-374. doi:10.1165/rcmb.4791
- Churg, A., Zhou, S., Wang, X., Wang, R., & Wright, J. L. (2009). The role of interleukin-1beta in murine cigarette smoke-induced emphysema and small airway remodeling. *American Journal of Respiratory Cell and Molecular Biology*, *40*(4), 482-490. doi:10.1165/rcmb.2008-0038OC
- Churg, A., Zhou, S., & Wright, J. L. (2012). Series "matrix metalloproteinases in lung health and disease": Matrix metalloproteinases in COPD. *European Respiratory Journal*, *39*(1), 197-209. doi:10.1183/09031936.00121611
- Cohen, A. J., Brauer, M., Burnett, R., Anderson, H. R., Frostad, J., Estep, K., Balakrishnan, K., Brunekreef, B., Dandona, L., Dandona, R., Feigin, V., Freedman, G., Hubbell, B., Jobling, A., Kan, H., Knibbs, L., Liu, Y., Martin, R., Morawska, L., Pope, C. A., 3rd, Shin, H., Straif, K., Shaddick, G., Thomas, M., van Dingenen, R., van Donkelaar, A., Vos, T., Murray, C. J. L., & Forouzanfar, M. H. (2017). Estimates and 25-year trends of the global burden of disease attributable to ambient air pollution: an analysis of data from the Global

- Burden of Diseases Study 2015. *Lancet*, 389(10082), 1907-1918. doi:10.1016/s0140-6736(17)30505-6
- Cohen, E., Wang, Z., Lepore, J., Lu, M., Taketo, M., Epstein, D., & Morrissey, E. (2007). Wnt/beta-catenin signaling promotes expansion of Isl-1-positive cardiac progenitor cells through regulation of FGF signaling. *Journal of Clinical Investigation*, 117, 1794-1804. doi:10.1172/JCI31731
- Collum, S. D., Amione-Guerra, J., Cruz-Solbes, A. S., DiFrancesco, A., Hernandez, A. M., Hanmandlu, A., Youker, K., Guha, A., & Karmouty-Quintana, H. (2017). Pulmonary Hypertension Associated with Idiopathic Pulmonary Fibrosis: Current and Future Perspectives. *Canadian respiratory journal*, 2017, 1430350-1430350. doi:10.1155/2017/1430350
- Conlon, T. M., John-Schuster, G., Heide, D., Pfister, D., Lehmann, M., Hu, Y., Ertüz, Z., Lopez, M. A., Ansari, M., Strunz, M., Mayr, C., Angelidis, I., Ciminieri, C., Costa, R., Kohlhepp, M. S., Guillot, A., Günes, G., Jeridi, A., Funk, M. C., Beroshvili, G., Prokosch, S., Hetzer, J., Verleden, S. E., Alsafadi, H., Lindner, M., Burgstaller, G., Becker, L., Irmeler, M., Dudek, M., Janzen, J., Goffin, E., Gosens, R., Knolle, P., Pirotte, B., Stoeger, T., Beckers, J., Wagner, D., Singh, I., Theis, F. J., de Angelis, M. H., O'Connor, T., Tacke, F., Boutros, M., Dejardin, E., Eickelberg, O., Schiller, H. B., Königshoff, M., Heikenwalder, M., & Yildirim, A. Ö. (2020). Inhibition of LT β R signalling activates WNT-induced regeneration in lung. *Nature*, 588(7836), 151-156. doi:10.1038/s41586-020-2882-8
- Cowan, K. N., Heilbut, A., Humpl, T., Lam, C., Ito, S., & Rabinovitch, M. (2000). Complete reversal of fatal pulmonary hypertension in rats by a serine elastase inhibitor. *Nature Medicine*, 6(6), 698-702. doi:10.1038/76282
- Cruz, F. F., Antunes, M. A., Abreu, S. C., Fujisaki, L. C., Silva, J. D., Xisto, D. G., Maron-Gutierrez, T., Ornellas, D. S., Sá, V. K., Rocha, N. N., Capelozzi, V. L., Morales, M. M., & Rocco, P. R. (2012). Protective effects of bone marrow mononuclear cell therapy on lung and heart in an elastase-induced emphysema model. *Respiratory Physiology and Neurobiology*, 182(1), 26-36. doi:10.1016/j.resp.2012.01.002
- Cukic, V. (2013). The Most Common Detected Bacteria in Sputum of Patients with the Acute Exacerbation of COPD. *Materia Socio-Medica*, 25(4), 226-229. doi:10.5455/msm.2013.25.226-229
- Dagouassat, M., Gagliolo, J. M., Chrusciel, S., Bourin, M. C., Duprez, C., Caramelle, P., Boyer, L., Hue, S., Stern, J. B., Validire, P., Longrois, D., Norel, X., Dubois-Randé, J. L., Le Gouvello, S., Adnot, S., & Boczkowski, J. (2013). The cyclooxygenase-2-prostaglandin E2 pathway maintains senescence of chronic obstructive pulmonary disease fibroblasts. *American journal of respiratory and critical care medicine*, 187(7), 703-714. doi:10.1164/rccm.201208-1361OC
- Dai, R., Wu, Z., Chu, H. Y., Lu, J., Lyu, A., Liu, J., & Zhang, G. (2020). Cathepsin K: The Action in and Beyond Bone. *Frontiers in Cell and Developmental Biology*, 8(433). doi:10.3389/fcell.2020.00433

- Dalvi, P. S., Singh, A., Trivedi, H. R., Ghanchi, F. D., Parmar, D. M., & Mistry, S. D. (2011). Effect of doxycycline in patients of moderate to severe chronic obstructive pulmonary disease with stable symptoms. *Annals of thoracic medicine*, *6*(4), 221-226. doi:10.4103/1817-1737.84777
- Davies, J. R., Herrmann, A., Russell, W., Svitacheva, N., Wickstrom, C., & Carlstedt, I. (2002). Respiratory tract mucins: structure and expression patterns. *Novartis Foundation Symposia*, *248*, 76-88; discussion 88-93, 277-282. doi:10.1111/his.14251
- Davis, I. C., Zhu, S., Sampson, J. B., Crow, J. P., & Matalon, S. (2002). Inhibition of human surfactant protein A function by oxidation intermediates of nitrite. *Free Radical Biology and Medicine*, *33*(12), 1703-1713. doi:10.1016/S0891-5849(02)01170-X
- De Giacomo, T., Rendina, E. A., Venuta, F., Moretti, M., Mercadante, E., Mohsen, I., Filice, M. J., & Coloni, G. F. (2002). Bullectomy is comparable to lung volume reduction in patients with end-stage emphysema. *European Journal of Cardio-Thoracic Surgery*, *22*(3), 357-362. doi:10.1016/s1010-7940(02)00351-2
- de Jager, S. C. A., & Hoefer, I. E. (2017). Beyond the matrix: MMP2 as critical regulator of inflammation-mediated vascular dysfunction. *Cardiovascular Research*, *113*(14), 1705-1707. doi:10.1093/cvr/cvx202
- De Langhe, S. P., Sala, F. G., Del Moral, P.-M., Fairbanks, T. J., Yamada, K. M., Warburton, D., Burns, R. C., & Bellusci, S. (2005). Dickkopf-1 (DKK1) reveals that fibronectin is a major target of Wnt signaling in branching morphogenesis of the mouse embryonic lung. *Developmental Biology*, *277*(2), 316-331. doi:10.1016/j.ydbio.2004.09.023
- De Moerlooze, L., Spencer-Dene, B., Revest, J. M., Hajihosseini, M., Rosewell, I., & Dickson, C. (2000). An important role for the IIIb isoform of fibroblast growth factor receptor 2 (FGFR2) in mesenchymal-epithelial signalling during mouse organogenesis. *Development*, *127*(3), 483-492. doi:10.1242/dev.127.3.483
- De Rose, V., Molloy, K., Gohy, S., Pilette, C., & Greene, C. M. (2018). Airway Epithelium Dysfunction in Cystic Fibrosis and COPD. *Mediators of Inflammation*, *2018*, 1309746. doi:10.1155/2018/1309746
- Decramer, M., & Janssens, W. (2013). Chronic obstructive pulmonary disease and comorbidities. *The Lancet Respiratory Medicine*, *1*(1), 73-83. doi:10.1016/s2213-2600(12)70060-7
- Delbrel, E., Fenwick, P. S., Wrench, C., Baker, J. R., Donnelly, L. E., & Barnes, P. J. (2020). Endoplasmic reticulum stress implication in fibroblast senescence in COPD. *ERJ Open Research*, *6*(suppl 5), 97. doi:10.1183/23120541.Lsc-2020.97
- Di Stefano, A., Caramori, G., Oates, T., Capelli, A., Lusuardi, M., Gnemmi, I., Ioli, F., Chung, K. F., Donner, C. F., Barnes, P. J., & Adcock, I. M. (2002). Increased expression of nuclear factor- κ B in bronchial biopsies from smokers and patients with COPD. *European Respiratory Journal*, *20*(3), 556-563. doi:10.1183/09031936.02.00272002

- Diaz, A. A., Maselli, D. J., Rahaghi, F., Come, C. E., Yen, A., Maclean, E. S., Okajima, Y., Martinez, C. H., Yamashiro, T., Lynch, D. A., Wang, W., Kinney, G. L., Washko, G. R., & San José Estépar, R. (2018). Pulmonary vascular pruning in smokers with bronchiectasis. *ERJ Open Research*, 4(4), 00044-02018. doi:10.1183/23120541.00044-2018
- Dionne, C. A., Crumley, G., Bellot, F., Kaplow, J. M., Searfoss, G., Ruta, M., Burgess, W. H., Jaye, M., & Schlessinger, J. (1990). Cloning and expression of two distinct high-affinity receptors cross-reacting with acidic and basic fibroblast growth factors. *The EMBO journal*, 9(9), 2685-2692. PMID: 1697263
- Dong, L., Li, R., Li, D., Wang, B., Lu, Y., Li, P., Yu, F., Jin, Y., Ni, X., Wu, Y., Yang, S., Lv, G., Li, X., Xiao, J., & Wang, J. (2019). FGF10 Enhances Peripheral Nerve Regeneration via the Preactivation of the PI3K/Akt Signaling-Mediated Antioxidant Response. *Frontiers in Pharmacology*, 10(1224). doi:10.3389/fphar.2019.01224
- Dummler, B., Tschopp, O., Hynx, D., Yang, Z. Z., Dirnhofer, S., & Hemmings, B. A. (2006). Life with a single isoform of Akt: mice lacking Akt2 and Akt3 are viable but display impaired glucose homeostasis and growth deficiencies. *Molecular and Cellular Biology*, 26(21), 8042-8051. doi:10.1128/mcb.00722-06
- Eidelman, D., Saetta, M. P., Ghezzi, H., Wang, N. S., Hoidal, J. R., King, M., & Cosio, M. G. (1990). Cellularity of the alveolar walls in smokers and its relation to alveolar destruction. Functional implications. *The American Review of Respiratory Disease*, 141(6), 1547-1552. doi:10.1164/ajrccm/141.6.1547
- El Agha, E., Kosanovic, D., Schermuly, R. T., & Bellusci, S. (2016). Role of fibroblast growth factors in organ regeneration and repair. *Seminars in Cell and Developmental Biology*, 53, 76-84. doi:10.1016/j.semcd.2015.10.009
- El Agha, E., Moiseenko, A., Kheirollahi, V., De Langhe, S., Crnkovic, S., Kwapiszewska, G., Szibor, M., Kosanovic, D., Schwind, F., Schermuly, R. T., Henneke, I., MacKenzie, B., Quantius, J., Herold, S., Ntokou, A., Ahlbrecht, K., Braun, T., Morty, R. E., Günther, A., Seeger, W., & Bellusci, S. (2017). Two-Way Conversion between Lipogenic and Myogenic Fibroblastic Phenotypes Marks the Progression and Resolution of Lung Fibrosis. *Cell stem cell*. 20(2):261-273.e3. doi:10.1016/j.stem.2016.10.004
- El Agha, E., Schwind, F., Ruppert, C., Gunther, A., Bellusci, S., Schermuly, R. T., & Kosanovic, D. (2018). Is the fibroblast growth factor signaling pathway a victim of receptor tyrosine kinase inhibition in pulmonary parenchymal and vascular remodeling? *The American Journal of Physiology-Lung Cellular and Molecular Physiology*, 315(2), L248-L252. doi:10.1152/ajplung.00140.2018
- El Agha, E., Seeger, W., & Bellusci, S. (2017). Therapeutic and pathological roles of fibroblast growth factors in pulmonary diseases. *Developmental Dynamics*, 246(4), 235-244. doi:https://doi.org/10.1002/dvdy.24468
- El Zein, R. M., Soria, A. H., Golib Dzib, J. F., Rickard, A. J., Fernandes-Rosa, F. L., Samson-Couterie, B., Giscos-Douriez, I., Rocha, A., Poglitsch, M., Gomez-Sanchez, C. E., Amar, L., Ghyselinck, N. B., Benecke, A., Zennaro, M. C., & Boulkroun, S. (2019). Retinoic acid

- receptor α as a novel contributor to adrenal cortex structure and function through interactions with Wnt and Vegfa signalling. *Scientific Reports*, 9(1), 14677. doi:10.1038/s41598-019-50988-2
- Ellwanger, K., Saito, H., Clément-Lacroix, P., Maltry, N., Niedermeyer, J., Lee, W. K., Baron, R., Rawadi, G., Westphal, H., & Niehrs, C. (2008). Targeted Disruption of the Wnt Regulator Kremen Induces Limb Defects and High Bone Density. *Molecular and Cellular Biology*, 28(15), 4875-4882. doi:doi:10.1128/MCB.00222-08
- Emoto, H., Tagashira, S., Mattei, M.-G., Yamasaki, M., Hashimoto, G., Katsumata, T., Negoro, T., Nakatsuka, M., Birnbaum, D., Coulier, F., & Itoh, N. (1997). Structure and Expression of Human Fibroblast Growth Factor-10. *The Journal of biological chemistry*, 272, 23191-23194. doi:10.1074/jbc.272.37.23191
- Errami, M., Galindo, C. L., Tassa, A. T., DiMaio, J. M., Hill, J. A., & Garner, H. R. (2008). Doxycycline Attenuates Isoproterenol- and Transverse Aortic Banding-Induced Cardiac Hypertrophy in Mice. *Journal of Pharmacology and Experimental Therapeutics*, 324(3), 1196-1203. doi:10.1124/jpet.107.133975
- Estépar, R. S., Kinney, G. L., Black-Shinn, J. L., Bowler, R. P., Kindlmann, G. L., Ross, J. C., Kikinis, R., Han, M. K., Come, C. E., Diaz, A. A., Cho, M. H., Hersh, C. P., Schroeder, J. D., Reilly, J. J., Lynch, D. A., Crapo, J. D., Wells, J. M., Dransfield, M. T., Hokanson, J. E., & Washko, G. R. (2013). Computed tomographic measures of pulmonary vascular morphology in smokers and their clinical implications. *American journal of respiratory and critical care medicine*, 188(2), 231-239. doi:10.1164/rccm.201301-0162OC
- Euler, U. S. v., & Liljestrand, G. (1946). Observations on the Pulmonary Arterial Blood Pressure in the Cat. *Acta Physiologica Scandinavica*, 12(4), 301-320. doi: 10.1111/j.1748-1716.1946.tb00389.x
- Evans, M. D., & Pryor, W. A. (1994). Cigarette smoking, emphysema, and damage to alpha 1-proteinase inhibitor. *American Journal of Physiology*, 266(6 Pt 1), L593-611. doi:10.1152/ajplung.1994.266.6.L593
- Fabbri, L. M., Calverley, P. M. A., Izquierdo-Alonso, J. L., Bundschuh, D. S., Brose, M., Martinez, F. J., & Rabe, K. F. (2009). Roflumilast in moderate-to-severe chronic obstructive pulmonary disease treated with longacting bronchodilators: two randomised clinical trials. *The Lancet*, 374(9691), 695-703. doi:https://doi.org/10.1016/S0140-6736(09)61252-6
- Faiz, A., Heijink, I. H., Vermeulen, C. J., Guryev, V., van den Berge, M., Nawijn, M. C., & Pouwels, S. D. (2018). Cigarette smoke exposure decreases CFLAR expression in the bronchial epithelium, augmenting susceptibility for lung epithelial cell death and DAMP release. *Sci Rep*, 8(1), 12426. doi:10.1038/s41598-018-30602-7
- Ferrer, E., Peinado, V. I., Díez, M., Carrasco, J. L., Musri, M. M., Martínez, A., Rodríguez-Roisin, R., & Barberà, J. A. (2009). Effects of cigarette smoke on endothelial function of pulmonary arteries in the guinea pig. *Respiratory Research*, 10(1), 76. doi:10.1186/1465-9921-10-76

- Filippone, M., Carraro, S., & Baraldi, E. (2010). From BPD to COPD? The hypothesis is intriguing but we lack lung pathology data in humans. *European Respiratory Journal*, *35*(6), 1419-1420. doi:10.1183/09031936.00013310
- Finkelstein, R., Fraser, R. S., Ghezzi, H., & Cosio, M. G. (1995). Alveolar inflammation and its relation to emphysema in smokers. *American journal of respiratory and critical care medicine*, *152*(5 Pt 1), 1666-1672. doi:10.1164/ajrccm.152.5.7582312
- Fischer, C., Seki, T., Lim, S., Nakamura, M., Andersson, P., Yang, Y., Honek, J., Wang, Y., Gao, Y., Chen, F., Samani, N. J., Zhang, J., Miyake, M., Oyadomari, S., Yasue, A., Li, X., Zhang, Y., Liu, Y., & Cao, Y. (2017). A miR-327–FGF10–FGFR2-mediated autocrine signaling mechanism controls white fat browning. *Nature Communications*, *8*(1), 2079. doi:10.1038/s41467-017-02158-z
- Fish, J. E., & Marsden, P. A. (2006). Endothelial nitric oxide synthase: insight into cell-specific gene regulation in the vascular endothelium. *Cellular and Molecular Life Sciences*, *63*(2), 144-162. doi:10.1007/s00018-005-5421-8
- Foronjy, R., & D'Armiento, J. (2006). The Effect of Cigarette Smoke-derived Oxidants on the Inflammatory Response of the Lung. *Clinical and Applied Immunology Reviews*, *6*(1), 53-72. doi:10.1016/j.cair.2006.04.002
- Francavilla, C., Rigbolt, K. T., Emdal, K. B., Carraro, G., Vernet, E., Bekker-Jensen, D. B., Streicher, W., Wikström, M., Sundström, M., Bellusci, S., Cavallaro, U., Blagoev, B., & Olsen, J. V. (2013). Functional proteomics defines the molecular switch underlying FGF receptor trafficking and cellular outputs. *Molecular Cell*, *51*(6), 707-722. doi:10.1016/j.molcel.2013.08.002
- Fredenburgh, L. E., Perrella, M. A., & Mitsialis, S. A. (2007). The role of heme oxygenase-1 in pulmonary disease. *American Journal of Respiratory Cell and Molecular Biology*, *36*(2), 158-165. doi:10.1165/rcmb.2006-0331TR
- Fukuzaki, S., Garrido, A. C., Righetti, R. F., Santos, T. M., Camargo, L. N., Aristoteles, L. R. C. R. B., Souza, F. C. R., Saraiva-Romanholo, B. M., Leick, E. A., Prado, C. M., Martins, M. A., & Tiberio, I. F. L. C. (2018). Anti - IL17 treatment control responses in lung injury induced by elastase. *European Respiratory Journal*, *52*, PA4286. doi:10.1183/13993003.congress-2018.PA4286
- Fysikopoulos, A., Seimetz, M., Hadzic, S., Knoepp, F., Wu, C. Y., Malkmus, K., Wilhelm, J., Pichl, A., Bednorz, M., Tadele Roxlau, E., Ghofrani, H. A., Sommer, N., Gierhardt, M., Schermuly, R. T., Seeger, W., Grimminger, F., Weissmann, N., & Kraut, S. (2020). Amelioration of elastase-induced lung emphysema and reversal of pulmonary hypertension by pharmacological iNOS inhibition in mice. *British Journal of Pharmacology*. doi:10.1111/bph.15057
- Garnero, P., Borel, O., Byrjalsen, I., Ferreras, M., Drake, F. H., McQueney, M. S., Foged, N. T., Delmas, P. D., & Delaissé, J. M. (1998). The collagenolytic activity of cathepsin K is unique among mammalian proteinases. *Journal of Biological Chemistry*, *273*(48), 32347-32352. doi:10.1074/jbc.273.48.32347

- Ghorani, V., Boskabady, M. H., Khazdair, M. R., & Kianmeher, M. (2017). Experimental animal models for COPD: a methodological review. *Tobacco induced diseases, 15*, 25-25. doi:10.1186/s12971-017-0130-2
- Ghosh, M., Miller, Y. E., Nakachi, I., Kwon, J. B., Barón, A. E., Brantley, A. E., Merrick, D. T., Franklin, W. A., Keith, R. L., & Vandivier, R. W. (2018). Exhaustion of Airway Basal Progenitor Cells in Early and Established Chronic Obstructive Pulmonary Disease. *American journal of respiratory and critical care medicine, 197*(7), 885-896. doi:10.1164/rccm.201704-0667OC
- Giangreco, A., Reynolds, S. D., & Stripp, B. R. (2002). Terminal bronchioles harbor a unique airway stem cell population that localizes to the bronchoalveolar duct junction. *The American Journal of Pathology, 161*(1), 173-182. doi:10.1016/s0002-9440(10)64169-7
- Glynos, C., Toumpanakis, D., Loverdos, K., Karavana, V., Zhou, Z., Magkou, C., Dettoraki, M., Perlikos, F., Pavlidou, A., Kotsikoris, V., Topouzis, S., Theocharis, S. E., Brouckaert, P., Giannis, A., Papapetropoulos, A., & Vassilakopoulos, T. (2015). Guanylyl cyclase activation reverses resistive breathing-induced lung injury and inflammation. *American Journal of Respiratory Cell and Molecular Biology, 52*(6), 762-771. doi:10.1165/rcmb.2014-0092OC
- Gossen, M., & Bujard, H. (1992). Tight control of gene expression in mammalian cells by tetracycline-responsive promoters. *Proceedings of the National Academy of Sciences, 89*(12), 5547-5551. doi:10.1073/pnas.89.12.5547
- Gossen, M., Freundlieb, S., Bender, G., Müller, G., Hillen, W., & Bujard, H. (1995). Transcriptional activation by tetracyclines in mammalian cells. *Science, 268*(5218), 1766-1769. doi:10.1126/science.7792603
- Gouveia, L., Kraut, S., Hadzic, S., Vazquez-Liébanas, E., Kojonazarov, B., Wu, C. Y., Veith, C., He, L., Mermelekas, G., Schermuly, R. T., Weissmann, N., Betsholtz, C., & Andrae, J. (2020). Lung developmental arrest caused by PDGF-A deletion: consequences for the adult mouse lung. *The American Journal of Physiology-Lung Cellular and Molecular Physiology, 318*(4), L831-L843. doi:10.1152/ajplung.00295.2019
- Gozali, M. V., Yi, F., Zhang, J.-a., Liu, J., Wu, H.-j., Xu, Y., Luo, D., & Zhou, B.-r. (2016). Photodynamic therapy inhibit Fibroblast Growth Factor-10 induced keratinocyte differentiation and proliferation through ROS in Fibroblast Growth Factor Receptor-2b pathway. *Scientific Reports, 6*(1), 27402. doi:10.1038/srep27402
- Graham, B. L., Brusasco, V., Burgos, F., Cooper, B. G., Jensen, R., Kendrick, A., MacIntyre, N. R., Thompson, B. R., & Wanger, J. (2017). Executive Summary: 2017 ERS/ATS standards for single-breath carbon monoxide uptake in the lung. *European Respiratory Journal, 49*(1). doi:10.1183/13993003.E0016-2016
- Gredic, M., Blanco, I., Kovacs, G., Helyes, Z., Ferdinandy, P., Olschewski, H., Barbera, J. A., & Weissmann, N. (2020). Pulmonary hypertension in chronic obstructive pulmonary disease. *British Journal of Pharmacology*. doi:10.1111/bph.14979

-
- Gredic, M., Wu, C.-Y., Hadzic, S., Pak, O., Savai, R., Kojonazarov, B., Doswada, S., Weiss, A., Weigert, A., Guenther, A., Brandes, R. P., Schermuly, R. T., Grimminger, F., Seeger, W., Sommer, N., Kraut, S., & Weissmann, N. (2021). Myeloid cell-specific deletion of inducible nitric oxide synthase protects against smoke-induced pulmonary hypertension in mice. *European Respiratory Journal*, 2101153. doi:10.1183/13993003.01153-2021
- Green, C. E., & Turner, A. M. (2017). The role of the endothelium in asthma and chronic obstructive pulmonary disease (COPD). *Respiratory Research*, 18(1), 20-20. doi:10.1186/s12931-017-0505-1
- Green, J., Nusse, R., & van Amerongen, R. (2014). The role of Ryk and Ror receptor tyrosine kinases in Wnt signal transduction. *Cold Spring Harbor perspectives in biology*, 6(2), a009175. doi:10.1101/cshperspect.a009175
- Griffin, M. O., Jinno, M., Miles, L. A., & Villarreal, F. J. (2005). Reduction of myocardial infarct size by doxycycline: a role for plasmin inhibition. *Molecular and Cellular Biochemistry*, 270(1-2), 1-11. doi:10.1007/s11010-005-2540-3
- Grinstein, M., Dingwall, H. L., O'Connor, L. D., Zou, K., Capellini, T. D., & Galloway, J. L. (2019). A distinct transition from cell growth to physiological homeostasis in the tendon. *eLife*, 8, e48689. doi:10.7554/eLife.48689
- Grippi, M. A., Elias, J. A., Fishman, J. A., Kotloff, R. M., Pack, A. I., & Senior, R. M. (2015). Part 4 - Obstructive Lung Diseases. In *Fishman's Pulmonary Diseases and Disorders, 5th edition*. New York, NY: McGraw-Hill Education. ISBN:9780071796729
- Groneberg, D. A., & Chung, K. F. (2004). Models of chronic obstructive pulmonary disease. *Respiratory Research*, 5(1), 18. doi:10.1186/1465-9921-5-18
- Guazzi, M., Cahalin, L. P., & Arena, R. (2013). Cardiopulmonary exercise testing as a diagnostic tool for the detection of left-sided pulmonary hypertension in heart failure. *Journal of Cardiac Failure*, 19(7), 461-467. doi:10.1016/j.cardfail.2013.05.005
- Gupte, V. V., Ramasamy, S. K., Reddy, R., Lee, J., Weinreb, P. H., Violette, S. M., Guenther, A., Warburton, D., Driscoll, B., Minoo, P., & Bellusci, S. (2009). Overexpression of fibroblast growth factor-10 during both inflammatory and fibrotic phases attenuates bleomycin-induced pulmonary fibrosis in mice. *American journal of respiratory and critical care medicine*, 180(5), 424-436. doi:10.1164/rccm.200811-1794OC
- Hadzic, S., Wu, C. Y., Gredic, M., Kojonazarov, B., Pak, O., Kraut, S., Sommer, N., Kosanovic, D., Grimminger, F., Schermuly, R. T., Seeger, W., Bellusci, S., & Weissmann, N. (2021). The effect of long-term doxycycline treatment in a mouse model of cigarette smoke-induced emphysema and pulmonary hypertension. *The American Journal of Physiology-Lung Cellular and Molecular Physiology*, 320(5), L903-L915. doi:10.1152/ajplung.00048.2021
- Hamakawa, H., Bartolák-Suki, E., Parameswaran, H., Majumdar, A., Lutchen, K. R., & Suki, B. (2011). Structure–Function Relations in an Elastase-Induced Mouse Model of

- Emphysema. *American Journal of Respiratory Cell and Molecular Biology*, 45(3), 517-524. doi:10.1165/rcmb.2010-0473OC
- Hansell, A. L., Walk, J. A., & Soriano, J. B. (2003). What do chronic obstructive pulmonary disease patients die from? A multiple cause coding analysis. *European Respiratory Journal*, 22(5), 809-814. doi:10.1183/09031936.03.00031403
- Hantos, Z., Adamicza, Á., Jánosi, T. Z., Szabari, M. V., Tolnai, J., & Suki, B. (2008). Lung volumes and respiratory mechanics in elastase-induced emphysema in mice. *Journal of Applied Physiology*, 105(6), 1864-1872. doi:10.1152/jappphysiol.90924.2008
- Harkema, J. R., Mauderly, J. L., Gregory, R. E., & Pickrell, J. A. (1984). A comparison of starvation and elastase models of emphysema in the rat. *The American Review of Respiratory Disease*, 129(4), 584-591. PMID: 6561948
- Hautamaki, R. D., Kobayashi, D. K., Senior, R. M., & Shapiro, S. D. (1997). Requirement for macrophage elastase for cigarette smoke-induced emphysema in mice. *Science*, 277(5334), 2002-2004. doi:10.1126/science.277.5334.2002.
- Hekimi, S., Lapointe, J., & Wen, Y. (2011). Taking a "good" look at free radicals in the aging process. *Trends in Cell Biology*, 21(10), 569-576. doi:10.1016/j.tcb.2011.06.008
- Henao, M. P., & Craig, T. J. (2016). Recent advances in understanding and treating COPD related to alpha1-antitrypsin deficiency. *Expert Review of Respiratory Medicine*, 10(12), 1281-1294. doi:10.1080/17476348.2016.1249851
- Hersh, C. P., Make, B. J., Lynch, D. A., Barr, R. G., Bowler, R. P., Calverley, P. M., Castaldi, P. J., Cho, M. H., Coxson, H. O., DeMeo, D. L., Foreman, M. G., Han, M. K., Harshfield, B. J., Hokanson, J. E., Lutz, S., Ramsdell, J. W., Regan, E. A., Rennard, S. I., Schroeder, J. D., Sciruba, F. C., Steiner, R. M., Tal-Singer, R., van Beek, E., Jr., Silverman, E. K., & Crapo, J. D. (2014). Non-emphysematous chronic obstructive pulmonary disease is associated with diabetes mellitus. *BMC Pulmonary Medicine*, 14, 164. doi:10.1186/1471-2466-14-164
- Hesse, E., Saito, H., Kiviranta, R., Correa, D., Yamana, K., Neff, L., Toben, D., Duda, G., Atfi, A., Geoffroy, V., Horne, W. C., & Baron, R. (2010). Zfp521 controls bone mass by HDAC3-dependent attenuation of Runx2 activity. *Journal of Cell Biology*, 191(7), 1271-1283. doi:10.1083/jcb.201009107
- Hiley, C., Chard, L., Gangeswaran, R., Tysome, J., Briat, A., Lemoine, N., & Wang, Y. (2012). Vascular Endothelial Growth Factor A Promotes Vaccinia Virus Entry into Host Cells via Activation of the Akt Pathway. *Journal of virology*, 87. doi:10.1128/JVI.00854-12
- Hill, S. M., Nesser, N. K., Johnson-Camacho, K., Jeffress, M., Johnson, A., Boniface, C., Spencer, S. E., Lu, Y., Heiser, L. M., Lawrence, Y., Pande, N. T., Korkola, J. E., Gray, J. W., Mills, G. B., Mukherjee, S., & Spellman, P. T. (2017). Context Specificity in Causal Signaling Networks Revealed by Phosphoprotein Profiling. *Cell Systems*, 4(1), 73-83. doi:10.1016/j.cels.2016.11.013

- Hind, M., & Maden, M. (2004). Retinoic acid induces alveolar regeneration in the adult mouse lung. *European Respiratory Journal*, *23*(1), 20-27. doi:10.1183/09031936.03.00119103
- Hirota, N., & Martin, J. G. (2013). Mechanisms of airway remodeling. *Chest*, *144*(3), 1026-1032. doi:10.1378/chest.12-3073
- Hoang, T.-V., Nardiello, C., Surate Solaligue, D. E., Rodríguez-Castillo, J. A., Rath, P., Mayer, K., Vadász, I., Herold, S., Ahlbrecht, K., Seeger, W., & Morty, R. E. (2018). Stereological analysis of individual lung lobes during normal and aberrant mouse lung alveolarisation. *Journal of anatomy*, *232*(3), 472-484. doi:10.1111/joa.12773
- Hoeper, M. M., Bogaard, H. J., Condliffe, R., Frantz, R., Khanna, D., Kurzyna, M., Langleben, D., Manes, A., Satoh, T., Torres, F., Wilkins, M. R., & Badesch, D. B. (2013). Definitions and diagnosis of pulmonary hypertension. *Journal of the American College of Cardiology*, *62*(25 Suppl), D42-50. doi:10.1016/j.jacc.2013.10.032
- Hoeper, M. M., & Humbert, M. (2019). The new haemodynamic definition of pulmonary hypertension: evidence prevails, finally! *European Respiratory Journal*, *53*(3), 1900038. doi:10.1183/13993003.00038-2019
- Hoesel, B., Mussbacher, M., Dikorman, B., Salzmann, M., Assinger, A., Hell, L., Thaler, J., Basílio, J., Moser, B., Resch, U., Paar, H., Mackman, N., & Schmid, J. A. (2018). Androgen receptor dampens tissue factor expression via nuclear factor- κ B and early growth response protein 1. *Journal of Thrombosis and Haemostasis*, *16*(4), 749-758. doi:10.1111/jth.13971
- Hogg, J. C., Chu, F., Utokaparch, S., Woods, R., Elliott, W. M., Buzatu, L., Cherniack, R. M., Rogers, R. M., Sciurba, F. C., Coxson, H. O., & Pare, P. D. (2004). The nature of small-airway obstruction in chronic obstructive pulmonary disease. *The New England Journal of Medicine*, *350*(26), 2645-2653. doi:10.1056/NEJMoa032158
- Hogg, N., Darley-Usmar, V. M., Wilson, M. T., & Moncada, S. (1992). Production of hydroxyl radicals from the simultaneous generation of superoxide and nitric oxide. *The Biochemical journal*, *281* (Pt 2)(Pt 2), 419-424. doi:10.1042/bj2810419
- Holz, O., Zühlke, I., Jaksztat, E., Müller, K. C., Welker, L., Nakashima, M., Diemel, K. D., Branscheid, D., Magnussen, H., & Jörres, R. A. (2004). Lung fibroblasts from patients with emphysema show a reduced proliferation rate in culture. *European Respiratory Journal*, *24*(4), 575-579. doi:10.1183/09031936.04.00143703
- Houssaini, A., Breau, M., Kebe, K., Abid, S., Marcos, E., Lipskaia, L., Rideau, D., Parpaleix, A., Huang, J., Amsellem, V., Vienney, N., Validire, P., Maitre, B., Attwe, A., Lukas, C., Vindrieux, D., Boczkowski, J., Derumeaux, G., Pende, M., Bernard, D., Meiners, S., & Adnot, S. (2018). mTOR pathway activation drives lung cell senescence and emphysema. *JCI Insight*, *3*(3). doi:10.1172/jci.insight.93203
- Houssaint, E., Blanquet, P. R., Champion-Arnaud, P., Gesnel, M. C., Torriglia, A., Courtois, Y., & Breathnach, R. (1990). Related fibroblast growth factor receptor genes exist in the human genome. *Proceedings of the National Academy of Sciences of the United States of America*, *87*(20), 8180-8184. doi:10.1073/pnas.87.20.8180

- Hovenberg, H. W., Davies, J. R., & Carlstedt, I. (1996). Different mucins are produced by the surface epithelium and the submucosa in human trachea: identification of MUC5AC as a major mucin from the goblet cells. *The Biochemical journal*, *318* (Pt 1)(Pt 1), 319-324. doi:10.1042/bj3180319
- Hsu, J. M., Xia, W., Hsu, Y. H., Chan, L. C., Yu, W. H., Cha, J. H., Chen, C. T., Liao, H. W., Kuo, C. W., Khoo, K. H., Hsu, J. L., Li, C. W., Lim, S. O., Chang, S. S., Chen, Y. C., Ren, G. X., & Hung, M. C. (2018). STT3-dependent PD-L1 accumulation on cancer stem cells promotes immune evasion. *Nature Communications*, *9*(1), 1908. doi:10.1038/s41467-018-04313-6
- Hu, D., Zhou, Z., Davidson, N. E., Huang, Y., & Wan, Y. (2012). Novel insight into KLF4 proteolytic regulation in estrogen receptor signaling and breast carcinogenesis. *Journal of Biological Chemistry*, *287*(17), 13584-13597. doi:10.1074/jbc.M112.343566
- Hu, W. P., Zeng, Y. Y., Zuo, Y. H., & Zhang, J. (2018). Identification of novel candidate genes involved in the progression of emphysema by bioinformatic methods. *International Journal of Chronic Obstructive Pulmonary Disease*, *13*, 3733-3747. doi:10.2147/copd.S183100
- Hu, Y., Ng-Blichfeldt, J.-P., Ota, C., Ciminieri, C., Ren, W., Hiemstra, P. S., Stolk, J., Gosens, R., & Königshoff, M. (2020). Wnt/ β -catenin signaling is critical for regenerative potential of distal lung epithelial progenitor cells in homeostasis and emphysema. *Stem cells (Dayton, Ohio)*, *38*(11), 1467-1478. doi:10.1002/stem.3241
- Huang, C., Chambers, D., & Matthews, G. (2015). Lung anatomy and function. In *Basic Physiology for Anaesthetists* (pp. 21-27). Cambridge: Cambridge University Press. ISBN:9781107637825
- Huang, X., Mu, X., Deng, L., Fu, A., Pu, E., Tang, T., & Kong, X. (2019). The etiologic origins for chronic obstructive pulmonary disease. *International Journal of Chronic Obstructive Pulmonary Disease*, *14*, 1139-1158. doi:10.2147/COPD.S203215
- Hubert, F., Payan, S. M., & Rochais, F. (2018). FGF10 Signaling in Heart Development, Homeostasis, Disease and Repair. *Frontiers in genetics*, *9*(599). doi:10.3389/fgene.2018.00599
- Hugen, N., Simons, M., Halilović, A., van der Post, R. S., Bogers, A. J., Marijnissen-van Zanten, M. A., de Wilt, J. H., & Nagtegaal, I. D. (2015). The molecular background of mucinous carcinoma beyond MUC2. *The Journal of Pathology: Clinical Research*, *1*(1), 3-17. doi: 10.1002/cjp2.1
- Hutchinson, D., Müller, J., McCarthy, J. E., Gun'ko, Y. K., Verma, N. K., Bi, X., Di Cristo, L., Kickham, L., Movia, D., Prina-Mello, A., & Volkov, Y. (2018). Cadmium nanoparticles citrullinate cytokeratins within lung epithelial cells: cadmium as a potential cause of citrullination in chronic obstructive pulmonary disease. *International Journal of Chronic Obstructive Pulmonary Disease*, *13*, 441-449. doi:10.2147/copd.S152028
- Ichinose, M., Sugiura, H., Yamagata, S., Koarai, A., & Shirato, K. (2000). Increase in reactive nitrogen species production in chronic obstructive pulmonary disease airways.

- American journal of respiratory and critical care medicine*, 162(2 Pt 1), 701-706. doi:10.1164/ajrccm.162.2.9908132
- Icochea, A., Cooper, B. S., & Kuhn, C. (1982). The effect of oxygen on Cor pulmonale in experimental emphysema induced by elastase or elastase and beta-aminopropionitrile in hamsters. *The American Review of Respiratory Disease*, 126(5), 792-796. doi:10.1164/arrd.1982.126.5.792
- Im, J. G., Itoh, H., & Han, M. C. (1995). CT of pulmonary tuberculosis. *Semin Ultrasound CT MR*, 16(5), 420-434. doi:10.1016/0887-2171(95)90029-2
- Irvin, C. G., & Bates, J. H. T. (2003). Measuring the lung function in the mouse: the challenge of size. *Respiratory Research*, 4(1), 1. doi:10.1186/rr199
- Ishizawa, K., Kubo, H., Yamada, M., Kobayashi, S., Numasaki, M., Ueda, S., Suzuki, T., & Sasaki, H. (2004). Bone marrow-derived cells contribute to lung regeneration after elastase-induced pulmonary emphysema. *FEBS Letters*, 556(1-3), 249-252. doi:10.1016/s0014-5793(03)01399-1
- Ito, K., & Barnes, P. J. (2009). COPD as a disease of accelerated lung aging. *Chest*, 135(1), 173-180. doi:10.1378/chest.08-1419
- Ito, K., Ito, M., Elliott, W. M., Cosio, B., Caramori, G., Kon, O. M., Barczyk, A., Hayashi, S., Adcock, I. M., Hogg, J. C., & Barnes, P. J. (2005). Decreased histone deacetylase activity in chronic obstructive pulmonary disease. *The New England Journal of Medicine*, 352(19), 1967-1976. doi:10.1056/NEJMoa041892
- Itoh, N., & Ohta, H. (2014). Fgf10: a paracrine-signaling molecule in development, disease, and regenerative medicine. *Current Molecular Medicine*, 14(4), 504-509. doi:10.2174/1566524014666140414204829
- Izvolosky, K. I., Shoykhet, D., Yang, Y., Yu, Q., Nugent, M. A., & Cardoso, W. V. (2003). Heparan sulfate-FGF10 interactions during lung morphogenesis. *Developmental Biology*, 258(1), 185-200. doi:10.1016/s0012-1606(03)00114-3
- Jackson, V. E., Latourelle, J. C., Wain, L. V., Smith, A. V., Grove, M. L., Bartz, T. M., Obeidat, M., Province, M. A., Gao, W., Qaiser, B., Porteous, D. J., Cassano, P. A., Ahluwalia, T. S., Grarup, N., Li, J., Altmaier, E., Marten, J., Harris, S. E., Manichaikul, A., Pottinger, T. D., Li-Gao, R., Lind-Thomsen, A., Mahajan, A., Lahousse, L., Imboden, M., Teumer, A., Prins, B., Lyytikainen, L. P., Eiriksdottir, G., Franceschini, N., Sitlani, C. M., Brody, J. A., Bosse, Y., Timens, W., Kraja, A., Loukola, A., Tang, W., Liu, Y., Bork-Jensen, J., Justesen, J. M., Linneberg, A., Lange, L. A., Rawal, R., Karrasch, S., Huffman, J. E., Smith, B. H., Davies, G., Burkart, K. M., Mychaleckyj, J. C., Bonten, T. N., Enroth, S., Lind, L., Brusselle, G. G., Kumar, A., Stubbe, B., Kahonen, M., Wyss, A. B., Psaty, B. M., Heckbert, S. R., Hao, K., Rantanen, T., Kritchevsky, S. B., Lohman, K., Skaaby, T., Pisinger, C., Hansen, T., Schulz, H., Polasek, O., Campbell, A., Starr, J. M., Rich, S. S., Mook-Kanamori, D. O., Johansson, A., Ingelsson, E., Uitterlinden, A. G., Weiss, S., Raitakari, O. T., Gudnason, V., North, K. E., Gharib, S. A., Sin, D. D., Taylor, K. D., O'Connor, G. T., Kaprio, J., Harris, T. B., Pederson, O., Vestergaard, H., Wilson, J. G., Strauch, K., Hayward, C., Kerr, S., Deary, I.

- J., Barr, R. G., de Mutsert, R., Gyllensten, U., Morris, A. P., Ikram, M. A., Probst-Hensch, N., Glaser, S., Zeggini, E., Lehtimäki, T., Strachan, D. P., Dupuis, J., Morrison, A. C., Hall, I. P., Tobin, M. D., & London, S. J. (2018). Meta-analysis of exome array data identifies six novel genetic loci for lung function. *Wellcome Open Research*, 3, 4. doi:10.12688/wellcomeopenres.12583.3
- Jimenez, R. V., Kuznetsova, V., Connelly, A. N., Hel, Z., & Szalai, A. J. (2019). C-Reactive Protein Promotes the Expansion of Myeloid Derived Cells With Suppressor Functions. *Frontiers in Immunology*, 10, 2183. doi:10.3389/fimmu.2019.02183.
- Jin, H., Webb-Robertson, B. J., Peterson, E. S., Tan, R., Bigelow, D. J., Scholand, M. B., Hoidal, J. R., Pounds, J. G., & Zangar, R. C. (2011). Smoking, COPD, and 3-nitrotyrosine levels of plasma proteins. *Environ Health Perspect*, 119(9), 1314-1320. doi:10.1289/ehp.1103745
- Jones, M. R., Chong, L., & Bellusci, S. (2021). Fgf10/Fgfr2b Signaling Orchestrates the Symphony of Molecular, Cellular, and Physical Processes Required for Harmonious Airway Branching Morphogenesis. *Frontiers in Cell and Developmental Biology*, 8(1746). doi:10.3389/fcell.2020.620667
- Kaiser, K., Gyllborg, D., Procházka, J., Salašová, A., Kompaníková, P., Molina, F. L., Laguna-Goya, R., Radaszkiewicz, T., Harnoš, J., Procházková, M., Potěšil, D., Barker, R. A., Casado, Á. G., Zdráhal, Z., Sedláček, R., Arenas, E., Villaescusa, J. C., & Bryja, V. (2019). WNT5A is transported via lipoprotein particles in the cerebrospinal fluid to regulate hindbrain morphogenesis. *Nature Communications*, 10(1), 1498. doi:10.1038/s41467-019-09298-4
- Kang, K. S., & Robling, A. G. (2015). New Insights into Wnt–Lrp5/6– β -Catenin Signaling in Mechanotransduction. *Frontiers in Endocrinology*, 5(246). doi:10.3389/fendo.2014.00246
- Karvonen, H., Perttilä, R., Niininen, W., Hautanen, V., Barker, H., Murumägi, A., Heckman, C. A., & Ungureanu, D. (2019). Wnt5a and ROR1 activate non-canonical Wnt signaling via RhoA in TCF3-PBX1 acute lymphoblastic leukemia and highlight new treatment strategies via Bcl-2 co-targeting. *Oncogene*, 38(17), 3288-3300. doi:10.1038/s41388-018-0670-9
- Kawahara, Y., Tuder, R. M., Taraseviciene-Stewart, L., Le Cras, T. D., Abman, S., Hirth, P. K., Waltenberger, J., & Voelkel, N. F. (2000). Inhibition of VEGF receptors causes lung cell apoptosis and emphysema. *Journal of Clinical Investigation*, 106(11), 1311-1319. doi:10.1172/jci10259
- Keen, A. N., Payne, L. A., Mehta, V., Rice, A., Simpson, L. J., Pang, K. L., Del Rio Hernandez, A., Reader, J. S., & Tzima, E. (2022). Eukaryotic initiation factor 6 regulates mechanical responses in endothelial cells. *Journal of Cell Biology*, 221(2). doi:10.1083/jcb.202005213

- Kelly, N., Radder, J., Leme, A., & Shapiro, S. (2014). Network-based approach identifies SP1 as a common node in emphysema and lung cancer. *European Respiratory Journal*, *44*, P3948. doi:erj.ersjournals.com/content/44/Suppl_58/P3948
- Kharitonov, S. A., & Barnes, P. J. (2003). Nitric oxide, nitrotyrosine, and nitric oxide modulators in asthma and chronic obstructive pulmonary disease. *Current Allergy and Asthma Reports*, *3*(2), 121-129. doi:10.1007/s11882-003-0024-7.
- Khelloufi, M.-K., Loiseau, E., Jaeger, M., Molinari, N., Chanez, P., Gras, D., & Viallat, A. (2018). Spatiotemporal organization of cilia drives multiscale mucus swirls in model human bronchial epithelium. *Scientific Reports*, *8*(1), 2447. doi:10.1038/s41598-018-20882-4
- Khush, K. K., Cherikh, W. S., Chambers, D. C., Goldfarb, S., Hayes, D., Jr., Kucheryavaya, A. Y., Levvey, B. J., Meiser, B., Rossano, J. W., & Stehlik, J. (2018). The International Thoracic Organ Transplant Registry of the International Society for Heart and Lung Transplantation: Thirty-fifth Adult Heart Transplantation Report-2018; Focus Theme: Multiorgan Transplantation. *The Journal of Heart and Lung Transplantation*, *37*(10), 1155-1168. doi:10.1016/j.healun.2018.07.022
- Kim, D., Chen, Z., Zhou, L.-F., & Huang, S.-X. (2018). Air pollutants and early origins of respiratory diseases. *Chronic diseases and translational medicine*, *4*(2), 75-94. doi:10.1016/j.cdtm.2018.03.003
- Kim, S. T., Lee, I. K., Rom, E., Sirkis, R., Park, S. H., Park, J. O., Park, Y. S., Lim, H. Y., Kang, W. K., Kim, K. M., Yayon, A., & Lee, J. (2019). Neutralizing antibody to FGFR2 can act as a selective biomarker and potential therapeutic agent for gastric cancer with FGFR2 amplification. *American Journal of Translational Research*, *11*(7), 4508-4515. ISSN:1943-8141/AJTR0096289
- Kim, W. D., Eidelman, D. H., Izquierdo, J. L., Ghezzi, H., Saetta, M. P., & Cosio, M. G. (1991). Centrilobular and panlobular emphysema in smokers. Two distinct morphologic and functional entities. *The American Review of Respiratory Disease*, *144*(6), 1385-1390. doi:10.1164/ajrccm/144.6.1385
- Kirkham, P. A., Caramori, G., Casolari, P., Papi, A. A., Edwards, M., Shamji, B., Triantaphyllopoulos, K., Hussain, F., Pinart, M., Khan, Y., Heinemann, L., Stevens, L., Yeadon, M., Barnes, P. J., Chung, K. F., & Adcock, I. M. (2011). Oxidative stress-induced antibodies to carbonyl-modified protein correlate with severity of chronic obstructive pulmonary disease. *American journal of respiratory and critical care medicine*, *184*(7), 796-802. doi:10.1164/rccm.201010-1605OC
- Kistner, A., Gossen, M., Zimmermann, F., Jerecic, J., Ullmer, C., Lübbert, H., & Bujard, H. (1996). Doxycycline-mediated quantitative and tissue-specific control of gene expression in transgenic mice. *Proceedings of the National Academy of Sciences*, *93*(20), 10933-10938. doi:10.1073/pnas.93.20.10933
- Klar, J., Blomstrand, P., Brunmark, C., Badhai, J., Hakansson, H. F., Brange, C. S., Bergendal, B., & Dahl, N. (2011). Fibroblast growth factor 10 haploinsufficiency causes chronic

- obstructive pulmonary disease. *Journal of Medical Genetics*, 48(10), 705-709. doi:10.1136/jmedgenet-2011-100166
- Klinger, J. R. (2016). Group III Pulmonary Hypertension: Pulmonary Hypertension Associated with Lung Disease: Epidemiology, Pathophysiology, and Treatments. *Clinical Cardiology*, 34(3), 413-433. doi:10.1016/j.ccl.2016.04.003
- Kneidinger, N., Yildirim, A., Callegari, J., Takenaka, S., Stein, M. M., Dumitrascu, R., Bohla, A., Bracke, K. R., Morty, R. E., Brusselle, G. G., Schermuly, R. T., Eickelberg, O., & Königshoff, M. (2011). Activation of the WNT/ β -catenin pathway attenuates experimental emphysema. *American journal of respiratory and critical care medicine*, 183(6), 723-733. doi:10.1164/rccm.200910-1560OC
- Kojonazarov, B., Hadzic, S., Ghofrani, H. A., Grimminger, F., Seeger, W., Weissmann, N., & Schermuly, R. T. (2019). Severe Emphysema in the SU5416/Hypoxia Rat Model of Pulmonary Hypertension. *American journal of respiratory and critical care medicine*, 200(4), 515-518. doi:10.1164/rccm.201902-0390LE
- Kolobaric, A., Vukojevic, K., Brekalo, S., Misković, J., Ries, M., Lasic Arapovic, L., & Soljic, V. (2021). Expression and localization of FGFR1, FGFR2 and CTGF during normal human lung development. *Acta Histochemica*, 123(5), 151719. doi:10.1016/j.acthis.2021.151719
- Koo, H. K., Vasilescu, D. M., Booth, S., Hsieh, A., Katsamenis, O. L., Fishbane, N., Elliott, W. M., Kirby, M., Lackie, P., Sinclair, I., Warner, J. A., Cooper, J. D., Coxson, H. O., Pare, P. D., Hogg, J. C., & Hackett, T. L. (2018). Small airways disease in mild and moderate chronic obstructive pulmonary disease: a cross-sectional study. *The Lancet Respiratory Medicine*, 6(8), 591-602. doi:10.1016/s2213-2600(18)30196-6
- Kornmann, M., & Korc, M. (1998). Role of fibroblast growth factors and their receptors in pancreatic cancer and chronic pancreatitis. *Pancreas* 17(2):169-75. doi:10.1097/00006676-199808000-00010.
- Kosanovic, D., Dahal, B. K., Peters, D. M., Seimetz, M., Wygrecka, M., Hoffmann, K., Antel, J., Reiss, I., Ghofrani, H. A., Weissmann, N., Grimminger, F., Seeger, W., & Schermuly, R. T. (2014). Histological characterization of mast cell chymase in patients with pulmonary hypertension and chronic obstructive pulmonary disease. *Pulmonary Circulation*, 4(1), 128-136. doi:10.1086/675642
- Koyanagi, M., Imai, S., Matsumoto, M., Iguma, Y., Kawaguchi-Sakita, N., Kotake, T., Iwamitsu, Y., Ntogwa, M., Hiraiwa, R., Nagayasu, K., Saigo, M., Ogihara, T., Yonezawa, A., Omura, T., Nakagawa, S., Nakagawa, T., & Matsubara, K. (2021). Pronociceptive Roles of Schwann Cell-Derived Galectin-3 in Taxane-Induced Peripheral Neuropathy. *Cancer Research*, 81(8), 2207-2219. doi:10.1158/0008-5472.Can-20-2799
- Kruk, D., Wisman, M., Bruin, H. G., Lodewijk, M. E., Hof, D. J., Borghuis, T., Daamen, W. F., van Kuppevelt, T. H., Timens, W., Burgess, J. K., Ten Hacken, N. H. T., & Heijink, I. H. (2021). Abnormalities in reparative function of lung-derived mesenchymal stromal cells in

- emphysema. *The American Journal of Physiology-Lung Cellular and Molecular Physiology*, 320(5), L832-L844. doi:10.1152/ajplung.00147.2020
- Lahzami, S., Bridevaux, P. O., Soccacal, P. M., Wellinger, J., Robert, J. H., Ris, H. B., & Aubert, J. D. (2010). Survival impact of lung transplantation for COPD. *European Respiratory Journal*, 36(1), 74-80. doi:10.1183/09031936.00087809
- Lambeth, J. D., Kawahara, T., & Diebold, B. (2007). Regulation of Nox and Duox enzymatic activity and expression. *Free Radical Biology and Medicine*, 43(3), 319-331. doi:10.1016/j.freeradbiomed.2007.03.028
- Lanner, F., & Rossant, J. (2010). The role of FGF/Erk signaling in pluripotent cells. *Development*, 137(20), 3351-3360. doi:10.1242/dev.050146
- Laurell, C. B., & Eriksson, S. (2013). The electrophoretic α 1-globulin pattern of serum in α 1-antitrypsin deficiency. 1963. *COPD: Journal of Chronic Obstructive Pulmonary Disease*, 10 Suppl 1, 3-8. doi:10.3109/15412555.2013.771956
- Leberl, M., Kratzer, A., & Taraseviciene-Stewart, L. (2013). Tobacco smoke induced COPD/emphysema in the animal model-are we all on the same page? *Frontiers in Physiology*, 4, 91. doi:10.3389/fphys.2013.00091
- Lee, S., Xu, G., Jay, T. R., Bhatta, S., Kim, K. W., Jung, S., Landreth, G. E., Ransohoff, R. M., & Lamb, B. T. (2014). Opposing effects of membrane-anchored CX3CL1 on amyloid and tau pathologies via the p38 MAPK pathway. *The Journal of Neuroscience*, 34(37), 12538-12546. doi:10.1523/jneurosci.0853-14.2014
- Lee, S. Y., Cho, J. H., Cho, S. S., Bae, C. S., Kim, G. Y., & Park, D. H. (2018). Establishment of a chronic obstructive pulmonary disease mouse model based on the elapsed time after LPS intranasal instillation. *Laboratory Animal Research*, 34(1), 1-10. doi:10.5625/lar.2018.34.1.1
- Li, H., Shi, K., Zhao, Y., Du, J., Hu, D., & Liu, Z. (2020). TIMP-1 and MMP-9 expressions in COPD patients complicated with spontaneous pneumothorax and their correlations with treatment outcomes. *Pakistan Journal of Medical Sciences*, 36(2), 192-197. doi:10.12669/pjms.36.2.1244
- Li, J., Li, E., Czepielewski, R. S., Chi, J., Guo, X., Han, Y. H., Wang, D., Wang, L., Hu, B., Dawes, B., Jacobs, C., Tenen, D., Lin, S. J., Lee, B., Morris, D., Tobias, A., Randolph, G. J., Cohen, P., Tsai, L., & Rosen, E. D. (2021). Neurotensin is an anti-thermogenic peptide produced by lymphatic endothelial cells. *Cell Metabolism*, 33(7), 1449-1465.e1446. doi:10.1016/j.cmet.2021.04.019
- Li, J., Wei, Z., Li, H., Dang, Q., Zhang, Z., Wang, L., Gao, W., Zhang, P., Yang, D., Liu, J., Sun, Y., & Gao, W. (2015). Clinicopathological significance of fibroblast growth factor 1 in non-small cell lung cancer. *Human Pathology*, 46(12), 1821-1828. doi:10.1016/j.humpath.2015.07.022
- Li, Q., Hu, Y., Chen, Y., Lv, Z., Wang, J., An, G., Du, X., Wang, H., Corrigan, C. J., Wang, W., & Ying, S. (2019). IL-33 induces production of autoantibody against autologous

- respiratory epithelial cells: a potential mechanism for the pathogenesis of COPD. *Immunology*, *157*(2), 137-150. doi:10.1111/imm.13054
- Li, S., Zhu, Z., Xue, M., Pan, X., Tong, G., Yi, X., Fan, J., Li, Y., Li, W., Dong, Y., Shen, E., Gong, W., Wang, X., Yu, Y., Maeng, Y. J., Li, X., Lee, K. Y., Jin, L., & Cong, W. (2021). The protective effects of fibroblast growth factor 10 against hepatic ischemia-reperfusion injury in mice. *Redox biology*, *40*, 101859-101859. doi:10.1016/j.redox.2021.101859
- Li, S., Zhu, Z., Xue, M., Pan, X., Tong, G., Yi, X., Fan, J., Li, Y., Li, W., Dong, Y., Shen, E., Gong, W., Wang, X., Yu, Y., Maeng, Y. J., Li, X., Lee, K. Y., Jin, L., & Cong, W. (2021). The protective effects of fibroblast growth factor 10 against hepatic ischemia-reperfusion injury in mice. *Redox Biology*, *40*, 101859. doi:10.1016/j.redox.2021.101859
- Li, Y.-H., Yang, L.-Y., Chen, W., Li, Y.-K., & Yuan, H.-B. (2015). Fibroblast growth factor 10 protects neuron against oxygen–glucose deprivation injury through inducing heme oxygenase-1. *Biochemical and Biophysical Research Communications*, *456*(1), 225-231. doi:10.1016/j.bbrc.2014.11.063
- Li, Y., Lu, W., King, T., Liu, C.-C., Bijur, G., & Bu, G. (2010). Dkk1 Stabilizes Wnt Co-Receptor LRP6: Implication for Wnt Ligand-Induced LRP6 Down-Regulation. *PLoS One*, *5*, e11014. doi:10.1371/journal.pone.0011014
- Liew, F. Y., Girard, J. P., & Turnquist, H. R. (2016). Interleukin-33 in health and disease. *Nature Reviews Immunology*, *16*(11), 676-689. doi:10.1038/nri.2016.95
- Limjunyawong, N., Craig, J. M., Lagassé, H. A., Scott, A. L., & Mitzner, W. (2015). Experimental progressive emphysema in BALB/cJ mice as a model for chronic alveolar destruction in humans. *The American Journal of Physiology-Lung Cellular and Molecular Physiology*, *309*(7), L662-676. doi:10.1152/ajplung.00214.2015
- Lindeman, J. H., Abdul-Hussien, H., van Bockel, J. H., Wolterbeek, R., & Kleemann, R. (2009). Clinical trial of doxycycline for matrix metalloproteinase-9 inhibition in patients with an abdominal aneurysm: doxycycline selectively depletes aortic wall neutrophils and cytotoxic T cells. *Circulation*, *119*(16), 2209-2216. doi:10.1161/circulationaha.108.806505
- Liu, F., Li, G., Deng, L., Kuang, B., & Li, X. (2017). The roles of FGF10 in vasculogenesis and angiogenesis. *28*, 1329-1332. ISSN:0970-938X
- Llambi, F., Wang, Y.-M., Victor, B., Yang, M., Schneider, D. M., Gingras, S., Parsons, M. J., Zheng, J. H., Brown, S. A., Pelletier, S., Moldoveanu, T., Chen, T., & Green, D. R. (2016). BOK Is a Non-canonical BCL-2 Family Effector of Apoptosis Regulated by ER-Associated Degradation. *Cell*, *165*(2), 421-433. doi:10.1016/j.cell.2016.02.026
- Llovera, M., Pearson, J. D., Moreno, C., & Riveros-Moreno, V. (2001). Impaired response to interferon-gamma in activated macrophages due to tyrosine nitration of STAT1 by endogenous nitric oxide. *British Journal of Pharmacology*, *132*(2), 419-426. doi:10.1038/sj.bjp.0703838

- Lomonosova, E. E., Kirsch, M., Rauen, U., & de Groot, H. (1998). The critical role of Hesperes in SIN-1 cytotoxicity, peroxyxynitrite versus hydrogen peroxide. *Free Radical Biology and Medicine*, *24*(4), 522-528. doi:10.1016/s0891-5849(97)00295-5
- Lopez-Otin, C., Blasco, M. A., Partridge, L., Serrano, M., & Kroemer, G. (2013). The hallmarks of aging. *Cell*, *153*(6), 1194-1217. doi:10.1016/j.cell.2013.05.039
- Lorx, A., Szabó, B., Hercsuth, M., Péntzes, I., & Hantos, Z. (2009). Low-frequency assessment of airway and tissue mechanics in ventilated COPD patients. *Journal of Applied Physiology*, *107*(6), 1884-1892. doi:10.1152/jappphysiol.00151.2009
- Louhelainen, N., Stark, H., Mazur, W., Ryttilä, P., Djukanovic, R., & Kinnula, V. L. (2010). Elevation of sputum matrix metalloproteinase-9 persists up to 6 months after smoking cessation: a research study. *BMC Pulmonary Medicine*, *10*, 13. doi:10.1186/1471-2466-10-13
- Lozano, R., Naghavi, M., Foreman, K., Lim, S., Shibuya, K., Aboyans, V., Abraham, J., Adair, T., Aggarwal, R., Ahn, S. Y., Alvarado, M., Anderson, H. R., Anderson, L. M., Andrews, K. G., Atkinson, C., Baddour, L. M., Barker-Collo, S., Bartels, D. H., Bell, M. L., Benjamin, E. J., Bennett, D., Bhalla, K., Bikbov, B., Bin Abdulhak, A., Birbeck, G., Blyth, F., Bolliger, I., Boufous, S., Bucello, C., Burch, M., Burney, P., Carapetis, J., Chen, H., Chou, D., Chugh, S. S., Coffeng, L. E., Colan, S. D., Colquhoun, S., Colson, K. E., Condon, J., Connor, M. D., Cooper, L. T., Corriere, M., Cortinovis, M., de Vaccaro, K. C., Couser, W., Cowie, B. C., Criqui, M. H., Cross, M., Dabhadkar, K. C., Dahodwala, N., De Leo, D., Degenhardt, L., Delossantos, A., Denenberg, J., Des Jarlais, D. C., Dharmaratne, S. D., Dorsey, E. R., Driscoll, T., Duber, H., Ebel, B., Erwin, P. J., Espindola, P., Ezzati, M., Feigin, V., Flaxman, A. D., Forouzanfar, M. H., Fowkes, F. G., Franklin, R., Fransen, M., Freeman, M. K., Gabriel, S. E., Gakidou, E., Gaspari, F., Gillum, R. F., Gonzalez-Medina, D., Halasa, Y. A., Haring, D., Harrison, J. E., Havmoeller, R., Hay, R. J., Hoen, B., Hotez, P. J., Hoy, D., Jacobsen, K. H., James, S. L., Jasrasaria, R., Jayaraman, S., Johns, N., Karthikeyan, G., Kassebaum, N., Keren, A., Khoo, J. P., Knowlton, L. M., Kobusingye, O., Koranteng, A., Krishnamurthi, R., Lipnick, M., Lipshultz, S. E., Ohno, S. L., Mabweijano, J., MacIntyre, M. F., Mallinger, L., March, L., Marks, G. B., Marks, R., Matsumori, A., Matzopoulos, R., Mayosi, B. M., McAnulty, J. H., McDermott, M. M., McGrath, J., Mensah, G. A., Merriman, T. R., Michaud, C., Miller, M., Miller, T. R., Mock, C., Mocumbi, A. O., Mokdad, A. A., Moran, A., Mulholland, K., Nair, M. N., Naldi, L., Narayan, K. M., Nasser, K., Norman, P., O'Donnell, M., Omer, S. B., Ortblad, K., Osborne, R., Ozgediz, D., Pahari, B., Pandian, J. D., Rivero, A. P., Padilla, R. P., Perez-Ruiz, F., Perico, N., Phillips, D., Pierce, K., Pope, C. A., 3rd, Porrini, E., Pourmalek, F., Raju, M., Ranganathan, D., Rehm, J. T., Rein, D. B., Remuzzi, G., Rivara, F. P., Roberts, T., De Leon, F. R., Rosenfeld, L. C., Rushton, L., Sacco, R. L., Salomon, J. A., Sampson, U., Sanman, E., Schwebel, D. C., Segui-Gomez, M., Shepard, D. S., Singh, D., Singleton, J., Sliwa, K., Smith, E., Steer, A., Taylor, J. A., Thomas, B., Tleyjeh, I. M., Towbin, J. A., Truelsen, T., Undurraga, E. A., Venketasubramanian, N., Vijayakumar, L., Vos, T., Wagner, G. R., Wang, M., Wang, W., Watt, K., Weinstock, M. A., Weintraub, R., Wilkinson, J. D., Woolf, A. D., Wulf, S., Yeh, P. H., Yip, P., Zabetian, A., Zheng, Z. J., Lopez, A. D., Murray, C. J., AlMazroa, M. A., &

- Memish, Z. A. (2012). Global and regional mortality from 235 causes of death for 20 age groups in 1990 and 2010: a systematic analysis for the Global Burden of Disease Study 2010. *Lancet*, *380*(9859), 2095-2128. doi:10.1016/s0140-6736(12)61728-0
- Lüthje, L., Raupach, T., Michels, H., Unsöld, B., Hasenfuss, G., Kögler, H., & Andreas, S. (2009). Exercise intolerance and systemic manifestations of pulmonary emphysema in a mouse model. *Respiratory Research*, *10*(1), 7. doi:10.1186/1465-9921-10-7
- Luu, M., Pautz, S., Kohl, V., Singh, R., Romero, R., Lucas, S., Hofmann, J., Raifer, H., Vachharajani, N., Carrascosa, L. C., Lamp, B., Nist, A., Stiewe, T., Shaul, Y., Adhikary, T., Zaiss, M. M., Lauth, M., Steinhoff, U., & Visekruna, A. (2019). The short-chain fatty acid pentanoate suppresses autoimmunity by modulating the metabolic-epigenetic crosstalk in lymphocytes. *Nature Communications*, *10*(1), 760. doi:10.1038/s41467-019-08711-2
- MacDonald, B. T., & He, X. (2012). Frizzled and LRP5/6 receptors for Wnt/ β -catenin signaling. *Cold Spring Harbor perspectives in biology*, *4*(12), a007880. doi:10.1101/cshperspect.a007880
- MacKenzie, B., Henneke, I., Hezel, S., Al Alam, D., El Agha, E., Chao, C. M., Quantius, J., Wilhelm, J., Jones, M., Goth, K., Li, X., Seeger, W., Königshoff, M., Herold, S., Rizvanov, A. A., Günther, A., & Bellusci, S. (2015). Attenuating endogenous Fgfr2b ligands during bleomycin-induced lung fibrosis does not compromise murine lung repair. *The American Journal of Physiology-Lung Cellular and Molecular Physiology*, *308*(10), L1014-1024. doi:10.1152/ajplung.00291.2014
- MacKenzie, B., Korfei, M., Henneke, I., Sibinska, Z., Tian, X., Hezel, S., Dilai, S., Wasnick, R., Schneider, B., Wilhelm, J., El Agha, E., Klepetko, W., Seeger, W., Schermuly, R., Günther, A., & Bellusci, S. (2015). Increased FGF1-FGFRc expression in idiopathic pulmonary fibrosis. *Respiratory Research*, *16*(1), 83. doi:10.1186/s12931-015-0242-2
- Maeno, T., Houghton, A. M., Quintero, P. A., Grumelli, S., Owen, C. A., & Shapiro, S. D. (2007). CD8+ T Cells are required for inflammation and destruction in cigarette smoke-induced emphysema in mice. *Journal of Immunology*, *178*(12), 8090-8096. doi:10.4049/jimmunol.178.12.8090
- Maestrelli, P., Saetta, M., Mapp, C. E., & Fabbri, L. M. (2001). Remodeling in response to infection and injury. Airway inflammation and hypersecretion of mucus in smoking subjects with chronic obstructive pulmonary disease. *American journal of respiratory and critical care medicine*, *164*(10 Pt 2), S76-80. doi:10.1164/ajrccm.164.supplement_2.2106067
- Manousakidi, S., Guillaume, A., Pirou, C., Bouleau, S., Mignotte, B., Renaud, F., & Le Floch, N. (2018). FGF1 induces resistance to chemotherapy in ovarian granulosa tumor cells through regulation of p53 mitochondrial localization. *Oncogenesis*, *7*(2), 18. doi:10.1038/s41389-018-0033-y
- Mao, B., & Niehrs, C. (2003). Kremen2 modulates Dickkopf2 activity during Wnt/LRP6 signaling. *Gene*, *302*(1-2), 179-183. doi:10.1016/s0378-1119(02)01106-x

-
- Martinez, F. J., & Chang, A. (2005). Surgical therapy for chronic obstructive pulmonary disease. *Seminars in Respiratory and Critical Care Medicine*, *26*(2), 167-191. doi:10.1055/s-2005-869537
- Martino, A. T., & Markusic, D. M. (2020). Immune Response Mechanisms against AAV Vectors in Animal Models. *Molecular Therapy - Methods & Clinical Development*, *17*, 198-208. doi:10.1016/j.omtm.2019.12.008
- Massaad, C. A., Washington, T. M., Pautler, R. G., & Klann, E. (2009). Overexpression of SOD-2 reduces hippocampal superoxide and prevents memory deficits in a mouse model of Alzheimer's disease. *Proceedings of the National Academy of Sciences of the United States of America*, *106*(32), 13576-13581. doi:10.1073/pnas.0902714106
- Matsuo, I., & Kimura-Yoshida, C. (2013). Extracellular modulation of Fibroblast Growth Factor signaling through heparan sulfate proteoglycans in mammalian development. *Current Opinion in Genetics and Development*, *23*(4), 399-407. doi:10.1016/j.gde.2013.02.004
- McGovern, T. K., Robichaud, A., Fereydoonzad, L., Schuessler, T. F., & Martin, J. G. (2013). Evaluation of respiratory system mechanics in mice using the forced oscillation technique. *Journal of visualized experiments : Journal of Visualized Experiments* (75), e50172-e50172. doi:10.3791/50172
- McGrath-Morrow, S. A., & Collaco, J. M. (2019). Bronchopulmonary dysplasia: what are its links to COPD? *Therapeutic Advances in Respiratory Disease*, *13*, 1753466619892492. doi:10.1177/1753466619892492
- McKendry, R. T., Spalluto, C. M., Burke, H., Nicholas, B., Cellura, D., Al-Shamkhani, A., Staples, K. J., & Wilkinson, T. M. (2016). Dysregulation of Antiviral Function of CD8(+) T Cells in the Chronic Obstructive Pulmonary Disease Lung. Role of the PD-1-PD-L1 Axis. *American journal of respiratory and critical care medicine*, *193*(6), 642-651. doi:10.1164/rccm.201504-0782OC
- Meiners, S., Eickelberg, O., & Konigshoff, M. (2015). Hallmarks of the ageing lung. *European Respiratory Journal*, *45*(3), 807-827. doi:10.1183/09031936.00186914
- Mercado, N., Ito, K., & Barnes, P. J. (2015). Accelerated ageing of the lung in COPD: new concepts. *Thorax*, *70*(5), 482-489. doi:10.1136/thoraxjnl-2014-206084
- Miravittles, M., Soler-Cataluña, J. J., Calle, M., & Soriano, J. B. (2013). Treatment of COPD by clinical phenotypes: putting old evidence into clinical practice. *European Respiratory Journal*, *41*(6), 1252-1256. doi:10.1183/09031936.00118912
- Moiseenko, A., Vazquez-Armendariz, A. I., Kheirollahi, V., Chu, X., Tata, A., Rivetti, S., Günther, S., Lebrigand, K., Herold, S., Braun, T., Mari, B., De Langhe, S., Kwapiszewska, G., Günther, A., Chen, C., Seeger, W., Tata, P. R., Zhang, J. S., Bellusci, S., & El Agha, E. (2020). Identification of a Repair-Supportive Mesenchymal Cell Population during Airway Epithelial Regeneration. *Cell Reports*, *33*(12), 108549. doi:10.1016/j.celrep.2020.108549

- Morgan, R. G., Pearn, L., Liddiard, K., Pumford, S. L., Burnett, A. K., Tonks, A., & Darley, R. L. (2013). γ -Catenin is overexpressed in acute myeloid leukemia and promotes the stabilization and nuclear localization of β -catenin. *Leukemia*, *27*(2), 336-343. doi:10.1038/leu.2012.221
- Morichika, D., Miyahara, N., Fujii, U., Taniguchi, A., Oda, N., Senoo, S., Kataoka, M., Tanimoto, M., Kakuta, H., Kiura, K., Maeda, Y., & Kanehiro, A. (2019). A retinoid X receptor partial agonist attenuates pulmonary emphysema and airway inflammation. *Respiratory Research*, *20*(1), 2-2. doi:10.1186/s12931-018-0963-0
- Murata, M., & Kawanishi, S. (2004). Oxidative DNA damage induced by nitrotyrosine, a biomarker of inflammation. *Biochemical and Biophysical Research Communications*, *316*(1), 123-128. doi:10.1016/j.bbrc.2004.02.022
- Murillo, H., Cutalo, M. J., Jones, R. P., Lane, M. J., Fleischmann, D., & Restrepo, C. S. (2012). Pulmonary circulation imaging: embryology and normal anatomy. *Seminars in Ultrasound, CT and MRI*, *33*(6), 473-484. doi:10.1053/j.sult.2012.08.001
- Naim, S., & Kaufmann, T. (2020). The Multifaceted Roles of the BCL-2 Family Member BOK. *Frontiers in Cell and Developmental Biology*, *8*(909). doi:10.3389/fcell.2020.574338
- Nakajima, M., Kawanami, O., Jin, E., Ghazizadeh, M., Honda, M., Asano, G., Horiba, K., & Ferrans, V. J. (1998). Immunohistochemical and ultrastructural studies of basal cells, Clara cells and bronchiolar cuboidal cells in normal human airways. *Pathology International*, *48*(12), 944-953. doi: 10.1111/j.1440-1827.1998.tb03865.x.
- Nascimento, R. A., Possomato-Vieira, J. S., Goncalves-Rizzi, V. H., Bonacio, G. F., Rizzi, E., & Dias-Junior, C. A. (2018). Hypertension, augmented activity of matrix metalloproteinases-2 and -9 and angiogenic imbalance in hypertensive pregnancy are attenuated by doxycycline. *European Journal of Pharmacology*, *840*, 60-69. doi:10.1016/j.ejphar.2018.10.017
- Ng-Blichfeldt, J.-P., Gosens, R., Dean, C., Griffiths, M., & Hind, M. (2019). Regenerative pharmacology for COPD: breathing new life into old lungs. *Thorax*, *74*(9), 890-897. doi:10.1136/thoraxjnl-2018-212630
- Ng, J. Y., Boelen, L., & Wong, J. W. H. (2013). Bioinformatics analysis reveals biophysical and evolutionary insights into the 3-nitrotyrosine post-translational modification in the human proteome. *Open Biology*, *3*(2), 120148. doi:doi:10.1098/rsob.120148
- Ng, P. K., Li, J., Jeong, K. J., Shao, S., Chen, H., Tsang, Y. H., Sengupta, S., Wang, Z., Bhavana, V. H., Tran, R., Soewito, S., Minussi, D. C., Moreno, D., Kong, K., Dogruluk, T., Lu, H., Gao, J., Tokheim, C., Zhou, D. C., Johnson, A. M., Zeng, J., Ip, C. K. M., Ju, Z., Wester, M., Yu, S., Li, Y., Vellano, C. P., Schultz, N., Karchin, R., Ding, L., Lu, Y., Cheung, L. W. T., Chen, K., Shaw, K. R., Meric-Bernstam, F., Scott, K. L., Yi, S., Sahni, N., Liang, H., & Mills, G. B. (2018). Systematic Functional Annotation of Somatic Mutations in Cancer. *Cancer Cell*, *33*(3), 450-462.e410. doi:10.1016/j.ccell.2018.01.021
- Niedermaier, M. S., & Matthay, R. A. (1986). Cardiovascular function in secondary pulmonary hypertension. *Heart and Lung*, *15*(4), 341-351. PMID:3522488

- Ohuchi, H., Hori, Y., Yamasaki, M., Harada, H., Sekine, K., Kato, S., & Itoh, N. (2000). FGF10 acts as a major ligand for FGF receptor 2 IIIb in mouse multi-organ development. *Biochemical and Biophysical Research Communications*, 277(3), 643-649. doi:10.1006/bbrc.2000.3721
- Oliveira, M. V., Abreu, S. C., Padilha, G. A., Rocha, N. N., Maia, L. A., Takiya, C. M., Xisto, D. G., Suki, B., Silva, P. L., & Rocco, P. R. (2016). Characterization of a Mouse Model of Emphysema Induced by Multiple Instillations of Low-Dose Elastase. *Frontiers in Physiology*, 7, 457. doi:10.3389/fphys.2016.00457
- Ono, S., Matsui, H., Noda, M., Kasuda, S., Yada, N., Yoshimoto, K., Akiyama, M., Miyata, T., Sugimoto, M., & Nishio, K. (2019). Functional regulation of von Willebrand factor ameliorates acute ischemia-reperfusion kidney injury in mice. *Scientific Reports*, 9(1), 14453. doi:10.1038/s41598-019-51013-2
- Ornitz, D. M. (2000). FGFs, heparan sulfate and FGFRs: complex interactions essential for development. *Bioessays*, 22(2), 108-112. doi:10.1002/(sici)1521-1878(200002)22:2<108::Aid-bies2>3.0.Co;2-m
- Ornitz, D. M., & Itoh, N. (2015). The Fibroblast Growth Factor signaling pathway. *Wiley interdisciplinary reviews. Developmental biology*, 4(3), 215-266. doi:10.1002/wdev.176
- Ornitz, D. M., Xu, J., Colvin, J. S., McEwen, D. G., MacArthur, C. A., Coulier, F., Gao, G., & Goldfarb, M. (1996). Receptor Specificity of the Fibroblast Growth Factor Family *. *Journal of Biological Chemistry*, 271(25), 15292-15297. doi:10.1074/jbc.271.25.15292
- Osoata, G. O., Hanazawa, T., Brindicci, C., Ito, M., Barnes, P. J., Kharitonov, S., & Ito, K. (2009). Peroxynitrite elevation in exhaled breath condensate of COPD and its inhibition by fudosteine. *Chest*, 135(6), 1513-1520. doi:10.1378/chest.08-2105
- Padilha, G. A., Henriques, I., Lopes-Pacheco, M., Abreu, S. C., Oliveira, M. V., Morales, M. M., Lima, L. M., Barreiro, E. J., Silva, P. L., Xisto, D. G., & Rocco, P. R. M. (2015). Therapeutic effects of LASSBio-596 in an elastase-induced mouse model of emphysema. *Frontiers in Physiology*, 6(267). doi:10.3389/fphys.2015.00267
- Pan, H., Deutsch, G. H., Wert, S. E., Ambalavanan, N., Ansong, C., Ardini-Poleske, M. E., Bagwell, J., Chan, C., Deutsch, G. H., Frevert, C., Gabriel, D., Hagood, J. S., Hill, C. B., Holden-Wiltse, J., Jegga, A. G., Mariani, T. J., Masci, A. M., Pan, H., Shi, W., Warburton, D., Wert, S. E., A, K., On behalf of the Ontology, S., & Consortium, N. M. A. o. L. D. P. (2019). Comprehensive anatomic ontologies for lung development: A comparison of alveolar formation and maturation within mouse and human lung. *Journal of Biomedical Semantics*, 10(1), 18. doi:10.1186/s13326-019-0209-1
- Parasaram, V., Nosoudi, N., LeClair, R. J., Binks, A., & Vyavahare, N. (2016). Targeted drug delivery to emphysematous lungs: Inhibition of MMPs by doxycycline loaded nanoparticles. *Pulmonary Pharmacology and Therapeutics*, 39, 64-73. doi:10.1016/j.pupt.2016.06.004
- Pauwels, R. A., Buist, A. S., Calverley, P. M., Jenkins, C. R., & Hurd, S. S. (2001). Global strategy for the diagnosis, management, and prevention of chronic obstructive pulmonary

- disease. NHLBI/WHO Global Initiative for Chronic Obstructive Lung Disease (GOLD) Workshop summary. *American journal of respiratory and critical care medicine*, 163(5), 1256-1276. doi:10.1164/ajrccm.163.5.2101039
- Peng, T., Frank, D. B., Kadzik, R. S., Morley, M. P., Rathi, K. S., Wang, T., Zhou, S., Cheng, L., Lu, M. M., & Morrissey, E. E. (2015). Hedgehog actively maintains adult lung quiescence and regulates repair and regeneration. *Nature*, 526(7574), 578-582. doi:10.1038/nature14984
- Perciaccante, A., Charlier, P., Negri, C., Coralli, A., Appenzeller, O., & Bianucci, R. (2018). Lessons from the Past: Some Histories of Alpha-1 Antitrypsin Deficiency Before Its Discovery. *COPD: Journal of Chronic Obstructive Pulmonary Disease*, 15(1), 1-3. doi:10.1080/15412555.2017.1421151
- Petrache, I., Natarajan, V., Zhen, L., Medler, T. R., Richter, A. T., Cho, C., Hubbard, W. C., Berdyshev, E. V., & Tuder, R. M. (2005). Ceramide upregulation causes pulmonary cell apoptosis and emphysema-like disease in mice. *Nature Medicine*, 11(5), 491-498. doi:10.1038/nm1238
- Petro, W., Hübner, C., Greschuchna, D., Maassen, W., & Konietzko, N. (1983). Bullectomy. *The Journal of Thoracic and Cardiovascular Surgery*, 31(6), 342-345. doi:10.1055/s-2007-1022015
- Pichl, A., Sommer, N., Bednorz, M., Seimetz, M., Hadzic, S., Kuhnert, S., Kraut, S., Roxlau, E. T., Kojonazarov, B., Wilhelm, J., Gredic, M., Gall, H., Tello, K., Richter, M. J., Pak, O., Petrovic, A., Hecker, M., Schermuly, R. T., Grimminger, F., Seeger, W., Ghofrani, H. A., & Weissmann, N. (2019). Riociguat for treatment of pulmonary hypertension in COPD: a translational study. *European Respiratory Journal*, 53(6). doi:10.1183/13993003.02445-2018
- Pillow, J. J., Stocks, J., Sly, P. D., & Hantos, Z. (2005). Partitioning of Airway and Parenchymal Mechanics in Unsedated Newborn Infants. *Pediatric Research*, 58(6), 1210-1215. doi:10.1203/01.pdr.0000185273.86320.13
- Pirard, L., & Marchand, E. (2018). Reassessing the BODE score as a criterion for listing COPD patients for lung transplantation. *International Journal of Chronic Obstructive Pulmonary Disease*, 13, 3963-3970. doi:10.2147/COPD.S182483
- Plopper, C. G., & Hyde, D. M. (2015). Chapter 7 - Epithelial Cells of the Bronchiole. In R. A. Parent (Ed.), *Comparative Biology of the Normal Lung (Second Edition)* (pp. 83-92). San Diego: Academic Press. ISBN: 9780124045774, 9780124047266
- Powers, C. J., McLeskey, S. W., & Wellstein, A. (2000). Fibroblast growth factors, their receptors and signaling. *Endocrine-Related Cancer*, 7(3), 165-197. doi:10.1677/erc.0.0070165
- Pretorius, D., Kahn-Krell, A. M., LaBarge, W. C., Lou, X., & Zhang, J. (2022). Engineering of thick human functional myocardium via static stretching and electrical stimulation. *iScience*, 25(3), 103824. doi:10.1016/j.isci.2022.103824

- Prince, L. S. (2018). FGF10 and Human Lung Disease Across the Life Spectrum. *Frontiers in genetics*, 9(517). doi:10.3389/fgene.2018.00517
- Qiao, L. F., Xu, Y. J., Liu, X. S., Xie, J. G., Wang, J., Du, C. L., Zhang, J., Ni, W., & Chen, S. X. (2008). Role of protein kinase C alpha and cyclin D1 in the proliferation of airway smooth muscle in asthmatic rats. *Chinese Medical Journal (Engl)*, 121(20), 2070-2076. PMID: 19080278
- Rabe, K. F. (2010). Roflumilast for the treatment of chronic obstructive pulmonary disease. *Expert Review of Respiratory Medicine*, 4(5), 543-555. doi:10.1586/ers.10.56
- Ragland, M. F., Benway, C. J., Lutz, S. M., Bowler, R. P., Hecker, J., Hokanson, J. E., Crapo, J. D., Castaldi, P. J., DeMeo, D. L., Hersh, C. P., Hobbs, B. D., Lange, C., Beaty, T. H., Cho, M. H., & Silverman, E. K. (2019). Genetic Advances in Chronic Obstructive Pulmonary Disease. Insights from COPD Gene. *American journal of respiratory and critical care medicine*, 200(6), 677-690. doi:10.1164/rccm.201808-1455SO
- Rahman, I. (2012). Pharmacological antioxidant strategies as therapeutic interventions for COPD. *Biochimica et Biophysica Acta*, 1822(5), 714-728. doi:10.1016/j.bbadis.2011.11.004
- Rajasekar, P., Patel, J., & Clifford, R. L. (2021). DNA Methylation of Fibroblast Phenotypes and Contributions to Lung Fibrosis. *Cells*, 10(8), 1977. doi:10.3390/cells10081977.
- Rajendrasozhan, S., Chung, S., Sundar, I. K., Yao, H., & Rahman, I. (2010). Targeted disruption of NF- κ B1 (p50) augments cigarette smoke-induced lung inflammation and emphysema in mice: a critical role of p50 in chromatin remodeling. *American Journal of Physiology-Lung Cellular and Molecular Physiology*, 298(2), L197-L209. doi:10.1152/ajplung.00265.2009
- Rapraeger, A. C., Krufka, A., & Olwin, B. B. (1991). Requirement of heparan sulfate for bFGF-mediated fibroblast growth and myoblast differentiation. *Science*, 252(5013), 1705-1708. doi:10.1126/science.1646484
- Rawlins, E. L., Okubo, T., Que, J., Xue, Y., Clark, C., Luo, X., & Hogan, B. L. (2008). Epithelial stem/progenitor cells in lung postnatal growth, maintenance, and repair. *Cold Spring Harbor Symposia on Quantitative Biology*, 73, 291-295. doi:10.1101/sqb.2008.73.037
- Redelsperger, I. M., Taldone, T., Riedel, E. R., Lepherd, M. L., Lipman, N. S., & Wolf, F. R. (2016). Stability of Doxycycline in Feed and Water and Minimal Effective Doses in Tetracycline-Inducible Systems. *Journal of the American Association for Laboratory Animal Science*, 55(4), 467-474. PMID: 27423155
- Rehfeld, A., Nylander, M., & Karnov, K. (2017). The Respiratory System. In A. Rehfeld, M. Nylander, & K. Karnov (Eds.), *Compendium of Histology: A Theoretical and Practical Guide* (pp. 351-377). Cham: Springer International Publishing. ISBN: 3319418718
- Rempe, S., Hayden, J. M., Robbins, R. A., & Hoyt, J. C. (2007). Tetracyclines and Pulmonary Inflammation. *Endocrine, Metabolic and Immune Disorders - Drug Targets*, 7(4), 232-236. doi:10.2174/187153007782794344

-
- Ren, Q., Chen, J., & Liu, Y. (2021). LRP5 and LRP6 in Wnt Signaling: Similarity and Divergence. *Frontiers in Cell and Developmental Biology*, 9(1167). doi:10.3389/fcell.2021.670960
- Repine, J. E., Bast, A., & Lankhorst, I. (1997). Oxidative stress in chronic obstructive pulmonary disease. Oxidative Stress Study Group. *American journal of respiratory and critical care medicine*, 156(2 Pt 1), 341-357. doi:10.1164/ajrccm.156.2.9611013
- Rey, J.-P., & Ellies, D. L. (2010). Wnt modulators in the biotech pipeline. *Developmental dynamics : an official publication of the American Association of Anatomists*, 239(1), 102-114. doi:10.1002/dvdy.22181
- Ricciardolo, F. L., Sterk, P. J., Gaston, B., & Folkerts, G. (2004). Nitric oxide in health and disease of the respiratory system. *Physiological Reviews*, 84(3), 731-765. doi:10.1152/physrev.00034.2003
- Rochais, F., Sturny, R., Chao, C.-M., Mesbah, K., Bennett, M., Mohun, T. J., Bellusci, S., & Kelly, R. G. (2014). FGF10 promotes regional foetal cardiomyocyte proliferation and adult cardiomyocyte cell-cycle re-entry. *Cardiovascular Research*, 104(3), 432-442. doi:10.1093/cvr/cvu232
- Rock, J. R., Randell, S. H., & Hogan, B. L. (2010). Airway basal stem cells: a perspective on their roles in epithelial homeostasis and remodeling. *Disease Models and Mechanisms*, 3(9-10), 545-556. doi:10.1242/dmm.006031
- Römer, C., Engel, O., Winek, K., Hochmeister, S., Zhang, T., Rojl, G., Klehmet, J., Dirnagl, U., Meisel, C., & Meisel, A. (2015). Blocking stroke-induced immunodeficiency increases CNS antigen-specific autoreactivity but does not worsen functional outcome after experimental stroke. *The Journal of Neuroscience*, 35(20), 7777-7794. doi:10.1523/jneurosci.1532-14.2015
- Saetta, M., Turato, G., Baraldo, S., Zanin, A., Braccioni, F., Mapp, C. E., Maestrelli, P., Cavallesco, G., Papi, A., & Fabbri, L. M. (2000). Goblet cell hyperplasia and epithelial inflammation in peripheral airways of smokers with both symptoms of chronic bronchitis and chronic airflow limitation. *American journal of respiratory and critical care medicine*, 161(3 Pt 1), 1016-1021. doi:10.1164/ajrccm.161.3.9907080
- Sahebjami, H., & Wirman, J. A. (1981). Emphysema-like changes in the lungs of starved rats. *The American Review of Respiratory Disease*, 124(5), 619-624. doi:10.1164/arrd.1981.124.5.619
- Santos, S., Peinado, V. I., Ramírez, J., Melgosa, T., Roca, J., Rodriguez-Roisin, R., & Barberà, J. A. (2002). Characterization of pulmonary vascular remodelling in smokers and patients with mild COPD. *European Respiratory Journal*, 19(4), 632-638. doi:10.1183/09031936.02.00245902
- Sarady, J. K., Zuckerbraun, B. S., Bilban, M., Wagner, O., Usheva, A., Liu, F., Ifedigbo, E., Zamora, R., Choi, A. M., & Otterbein, L. E. (2004). Carbon monoxide protection against endotoxic shock involves reciprocal effects on iNOS in the lung and liver. *The FASEB Journal*, 18(7), 854-856. doi:10.1096/fj.03-0643fje

- Schermuly, R. T., Dony, E., Ghofrani, H. A., Pullamsetti, S., Savai, R., Roth, M., Sydykov, A., Lai, Y. J., Weissmann, N., Seeger, W., & Grimminger, F. (2005). Reversal of experimental pulmonary hypertension by PDGF inhibition. *Journal of Clinical Investigation*, *115*(10), 2811-2821. doi:10.1172/jci24838
- Schröder, K., Weissmann, N., & Brandes, R. P. (2017). Organizers and activators: Cytosolic Nox proteins impacting on vascular function. *Free Radical Biology and Medicine*, *109*, 22-32. doi:10.1016/j.freeradbiomed.2017.03.017
- Schuliga, M. (2015). NF-kappaB Signaling in Chronic Inflammatory Airway Disease. *Biomolecules*, *5*(3), 1266-1283. doi:10.3390/biom5031266
- Schulze, J., Seitz, S., Saito, H., Schneebauer, M., Marshall, R. P., Baranowsky, A., Busse, B., Schilling, A. F., Friedrich, F. W., Albers, J., Spiro, A. S., Zustin, J., Streichert, T., Ellwanger, K., Niehrs, C., Amling, M., Baron, R., & Schinke, T. (2010). Negative Regulation of Bone Formation by the Transmembrane Wnt Antagonist Kremen-2. *PLoS One*, *5*(4), e10309. doi:10.1371/journal.pone.0010309
- Schweitzer, K. S., Johnstone, B. H., Garrison, J., Rush, N. I., Cooper, S., Traktuev, D. O., Feng, D., Adamowicz, J. J., Van Demark, M., Fisher, A. J., Kamocki, K., Brown, M. B., Presson, R. G., Jr., Broxmeyer, H. E., March, K. L., & Petrache, I. (2011). Adipose stem cell treatment in mice attenuates lung and systemic injury induced by cigarette smoking. *American journal of respiratory and critical care medicine*, *183*(2), 215-225. doi:10.1164/rccm.201001-0126OC
- Seimetz, M., Parajuli, N., Pichl, A., Bednorz, M., Ghofrani, H. A., Schermuly, R. T., Seeger, W., Grimminger, F., & Weissmann, N. (2015). Cigarette Smoke-Induced Emphysema and Pulmonary Hypertension Can Be Prevented by Phosphodiesterase 4 and 5 Inhibition in Mice. *PLoS One*, *10*(6), e0129327. doi:10.1371/journal.pone.0129327
- Seimetz, M., Parajuli, N., Pichl, A., Veit, F., Kwapiszewska, G., Weisel, F. C., Milger, K., Egemnazarov, B., Turowska, A., Fuchs, B., Nikam, S., Roth, M., Sydykov, A., Medebach, T., Klepetko, W., Jaksch, P., Dumitrascu, R., Garn, H., Voswinckel, R., Kostin, S., Seeger, W., Schermuly, R. T., Grimminger, F., Ghofrani, H. A., & Weissmann, N. (2011). Inducible NOS inhibition reverses tobacco-smoke-induced emphysema and pulmonary hypertension in mice. *Cell*, *147*(2), 293-305. doi:10.1016/j.cell.2011.08.035
- Seimetz, M., Sommer, N., Bednorz, M., Pak, O., Veith, C., Hadzic, S., Gredic, M., Parajuli, N., Kojonazarov, B., Kraut, S., Wilhelm, J., Knoepp, F., Henneke, I., Pichl, A., Kanbagli, Z. I., Scheibe, S., Fysikopoulos, A., Wu, C. Y., Klepetko, W., Jaksch, P., Eichstaedt, C., Grünig, E., Hinderhofer, K., Geiszt, M., Müller, N., Rezende, F., Buchmann, G., Wittig, I., Hecker, M., Hecker, A., Padberg, W., Dorfmueller, P., Gattenlöhner, S., Vogelmeier, C. F., Günther, A., Karnati, S., Baumgart-Vogt, E., Schermuly, R. T., Ghofrani, H. A., Seeger, W., Schröder, K., Grimminger, F., Brandes, R. P., & Weissmann, N. (2020). NADPH oxidase subunit NOXO1 is a target for emphysema treatment in COPD. *Nature Metabolism*, *2*(6), 532-546. doi:10.1038/s42255-020-0215-8

- Sekine, K., Ohuchi, H., Fujiwara, M., Yamasaki, M., Yoshizawa, T., Sato, T., Yagishita, N., Matsui, D., Koga, Y., Itoh, N., & Kato, S. (1999). Fgf10 is essential for limb and lung formation. *Nature Genetics*, *21*(1), 138-141. doi:10.1038/5096
- Seo, H., Chen, J., González-Avalos, E., Samaniego-Castruita, D., Das, A., Wang, Y. H., López-Moyado, I. F., Georges, R. O., Zhang, W., Onodera, A., Wu, C. J., Lu, L. F., Hogan, P. G., Bhandoola, A., & Rao, A. (2019). TOX and TOX2 transcription factors cooperate with NR4A transcription factors to impose CD8(+) T cell exhaustion. *Proceedings of the National Academy of Sciences of the United States of America*, *116*(25), 12410-12415. doi:10.1073/pnas.1905675116
- Seymour, P. A., Shih, H. P., Patel, N. A., Freude, K. K., Xie, R., Lim, C. J., & Sander, M. (2012). A Sox9/Fgf feed-forward loop maintains pancreatic organ identity. *Development*, *139*(18), 3363-3372. doi:10.1242/dev.078733
- Shapiro, S. D. (2000). Animal Models for COPD. *Chest*, *117*, 223S-227S. doi:10.1378/chest.117.5_suppl_1.223S
- Shapiro, S. D. (2003). Proteolysis in the lung. *European Respiratory Journal*, *44*, 30s-32s. doi:10.1183/09031936.03.00000903a.
- Shaykhiev, R. (2019). Emerging biology of persistent mucous cell hyperplasia in COPD. *Thorax*, *74*(1), 4-6. doi:10.1136/thoraxjnl-2018-212271
- Shi, K., Qiao, L. N., Liu, B., Zhao, S. S., Zhou, T. F., Wang, X. M., Wei, L., Liu, H. M., & Hua, Y. M. (2009). [Effect of doxycycline on the development of pulmonary hypertension induced by four methods in rats]. *Zhonghua Er Ke Za Zhi (Chinese Journal of Pediatrics)*, *47*(4), 260-264. doi:10.3760/cma.j.issn.0578-1310.2009.04.006.
- Shigemura, N., Okumura, M., Mizuno, S., Imanishi, Y., Nakamura, T., & Sawa, Y. (2006). Autologous transplantation of adipose tissue-derived stromal cells ameliorates pulmonary emphysema. *American Journal of Transplantation*, *6*(11), 2592-2600. doi:10.1111/j.1600-6143.2006.01522.x
- Shimbori, C., & El Agha, E. (2020). Good Things Come in 2s: Type 2 Alveolar Epithelial Cells and Fibroblast Growth Factor Receptor 2. *American Journal of Respiratory Cell and Molecular Biology*, *62*(5), 543-545. doi:10.1165/rcmb.2020-0013ED
- Shukla, S. D., Swaroop Vanka, K., Chavelier, A., Shastri, M. D., Tambuwala, M. M., Bakshi, H. A., Pabreja, K., Mahmood, M. Q., & O'Toole, R. F. (2020). Chronic respiratory diseases: An introduction and need for novel drug delivery approaches. *Targeting Chronic Inflammatory Lung Diseases Using Advanced Drug Delivery Systems*, 1-31. doi:10.1016/B978-0-12-820658-4.00001-7
- Sim, J., Cowburn, A. S., Palazon, A., Madhu, B., Tyrakis, P. A., Macías, D., Bargiela, D. M., Pietsch, S., Gralla, M., Evans, C. E., Kittipassorn, T., Chey, Y. C. J., Branco, C. M., Rundqvist, H., Peet, D. J., & Johnson, R. S. (2018). The Factor Inhibiting HIF Asparaginyl Hydroxylase Regulates Oxidative Metabolism and Accelerates Metabolic Adaptation to Hypoxia. *Cell Metabolism*, *27*(4), 898-913.e897. doi:10.1016/j.cmet.2018.02.020

- Simonneau, G., Montani, D., Celermajer, D. S., Denton, C. P., Gatzoulis, M. A., Krowka, M., Williams, P. G., & Souza, R. (2019). Haemodynamic definitions and updated clinical classification of pulmonary hypertension. *European Respiratory Journal*, *53*(1), 1801913. doi:10.1183/13993003.01913-2018
- Singh, B., Ghosh, N., Saha, D., Sarkar, S., Bhattacharyya, P., & Chaudhury, K. (2019). Effect of doxycycline in chronic obstructive pulmonary disease - An exploratory study. *Pulmonary Pharmacology and Therapeutics*, *58*, 101831. doi:10.1016/j.pupt.2019.101831
- Singh, D., Agusti, A., Anzueto, A., Barnes, P. J., Bourbeau, J., Celli, B. R., Criner, G. J., Frith, P., Halpin, D. M. G., Han, M., Lopez Varela, M. V., Martinez, F., Montes de Oca, M., Papi, A., Pavord, I. D., Roche, N., Sin, D. D., Stockley, R., Vestbo, J., Wedzicha, J. A., & Vogelmeier, C. (2019). Global Strategy for the Diagnosis, Management, and Prevention of Chronic Obstructive Lung Disease: the GOLD science committee report 2019. *European Respiratory Journal*, *53*(5). doi:10.1183/13993003.00164-2019
- Smith, B. M., Austin, J. H., Newell, J. D., Jr., D'Souza, B. M., Rozenshtein, A., Hoffman, E. A., Ahmed, F., & Barr, R. G. (2014). Pulmonary emphysema subtypes on computed tomography: the MESA COPD study. *The American Journal of Medicine*, *127*(1), 94.e97-23. doi:10.1016/j.amjmed.2013.09.020
- Smith, B. M., Traboulsi, H., Austin, J. H. M., Manichaikul, A., Hoffman, E. A., Bleeker, E. R., Cardoso, W. V., Cooper, C., Couper, D. J., Dashnaw, S. M., Guo, J., Han, M. K., Hansel, N. N., Hughes, E. W., Jacobs, D. R., Jr., Kanner, R. E., Kaufman, J. D., Kleerup, E., Lin, C. L., Liu, K., Lo Cascio, C. M., Martinez, F. J., Nguyen, J. N., Prince, M. R., Rennard, S., Rich, S. S., Simon, L., Sun, Y., Watson, K. E., Woodruff, P. G., Baglole, C. J., & Barr, R. G. (2018). Human airway branch variation and chronic obstructive pulmonary disease. *Proceedings of the National Academy of Sciences of the United States of America*, *115*(5), E974-e981. doi:10.1073/pnas.1715564115
- Snider, G. L., Kleinerman, J., Thurlbeck, W. M., & Bengali, Z. H. (1985). The Definition of Emphysema. *American Review of Respiratory Disease*, *132*(1), 182-185. doi:10.1164/arrd.1985.132.1.182
- Sommer, N., Strielkov, I., Pak, O., & Weissmann, N. (2016). Oxygen sensing and signal transduction in hypoxic pulmonary vasoconstriction. *European Respiratory Journal*, *47*(1), 288-303. doi:10.1183/13993003.00945-2015
- Spaulding, K., Takaba, K., Collins, A., Faraji, F., Wang, G., Aguayo, E., Ge, L., Saloner, D., Wallace, A. W., Baker, A. J., Lovett, D. H., & Ratcliffe, M. B. (2018). Short term doxycycline treatment induces sustained improvement in myocardial infarction border zone contractility. *PLoS One*, *13*(2), e0192720. doi:10.1371/journal.pone.0192720
- Stolk, J., Stockley, R. A., Stoel, B. C., Cooper, B. G., Piitulainen, E., Seersholm, N., Chapman, K. R., Burdon, J. G., Decramer, M., Abboud, R. T., Mannes, G. P., Wouters, E. F., Garrett, J. E., Barros-Tizon, J. C., Russi, E. W., Lomas, D. A., MacNee, W. A., & Rames, A. (2012). Randomised controlled trial for emphysema with a selective agonist of the gamma-type retinoic acid receptor. *European Respiratory Journal*, *40*(2), 306-312. doi:10.1183/09031936.00161911

- Stoller, J. K., Panos, R. J., Krachman, S., Doherty, D. E., Make, B., & Long-term Oxygen Treatment Trial Research, G. (2010). Oxygen therapy for patients with COPD: current evidence and the long-term oxygen treatment trial. *Chest*, *138*(1), 179-187. doi:10.1378/chest.09-2555
- Suarez, C. J., Dintzis, S. M., & Frevert, C. W. (2012). 9 - Respiratory. In P. M. Treuting & S. M. Dintzis (Eds.), *Comparative Anatomy and Histology* (pp. 121-134). San Diego: Academic Press. ISBN: 9780128029190
- Sugiura, H., Ichinose, M., Tomaki, M., Ogawa, H., Koarai, A., Kitamuro, T., Komaki, Y., Akita, T., Nishino, H., Okamoto, S., Akaike, T., & Hattori, T. (2004). Quantitative assessment of protein-bound tyrosine nitration in airway secretions from patients with inflammatory airway disease. *Free Radical Research*, *38*(1), 49-57. doi: 10.1080/10715760310001633817
- Suki, B., Lutchen, K. R., & Ingenito, E. P. (2003). On the Progressive Nature of Emphysema. *American journal of respiratory and critical care medicine*, *168*(5), 516-521. doi:10.1164/rccm.200208-908PP
- Sun, X., Meng, L., Qiao, W., Yang, R., Gao, Q., Peng, Y., & Bian, Z. (2019). Vascular endothelial growth factor A/Vascular endothelial growth factor receptor 2 axis promotes human dental pulp stem cell migration via the FAK/PI3K/Akt and p38 MAPK signalling pathways. *International Endodontic Journal*, *52*(12), 1691-1703. doi:doi.org/10.1111/iej.13179
- Sundaravinayagam, D., Rahjouei, A., Andreani, M., Tupiņa, D., Balasubramanian, S., Saha, T., Delgado-Benito, V., Coralluzzo, V., Daumke, O., & Di Virgilio, M. (2019). 53BP1 Supports Immunoglobulin Class Switch Recombination Independently of Its DNA Double-Strand Break End Protection Function. *Cell Reports*, *28*(6), 1389-1399.e1386. doi:10.1016/j.celrep.2019.06.035
- Suresh, K., & Shimoda, L. A. (2016). Lung Circulation. *Comprehensive Physiology*, *6*(2), 897-943. doi:10.1002/cphy.c140049
- Sussan, T. E., Rangasamy, T., Blake, D. J., Malhotra, D., El-Haddad, H., Bedja, D., Yates, M. S., Kombairaju, P., Yamamoto, M., Liby, K. T., Sporn, M. B., Gabrielson, K. L., Champion, H. C., Tuder, R. M., Kensler, T. W., & Biswal, S. (2009). Targeting Nrf2 with the triterpenoid CDDO-imidazolide attenuates cigarette smoke-induced emphysema and cardiac dysfunction in mice. *Proceedings of the National Academy of Sciences of the United States of America*, *106*(1), 250-255. doi:10.1073/pnas.0804333106
- Szabo, C., Ischiropoulos, H., & Radi, R. (2007). Peroxynitrite: biochemistry, pathophysiology and development of therapeutics. *Nature Reviews Drug Discovery*, *6*(8), 662-680. doi:10.1038/nrd2222
- Szklarczyk, D., Gable, A. L., Lyon, D., Junge, A., Wyder, S., Huerta-Cepas, J., Simonovic, M., Doncheva, N. T., Morris, J. H., Bork, P., Jensen, L. J., & Mering, C. V. (2019). STRING v11: protein-protein association networks with increased coverage, supporting functional

- discovery in genome-wide experimental datasets. *Nucleic Acids Research*, 47(D1), D607-d613. doi:10.1093/nar/gky1131
- Takahashi, S., Nakamura, H., Seki, M., Shiraiishi, Y., Yamamoto, M., Furuuchi, M., Nakajima, T., Tsujimura, S., Shirahata, T., Nakamura, M., Minematsu, N., Yamasaki, M., Tateno, H., & Ishizaka, A. (2008). Reversal of elastase-induced pulmonary emphysema and promotion of alveolar epithelial cell proliferation by simvastatin in mice. *The American Journal of Physiology-Lung Cellular and Molecular Physiology*, 294(5), L882-890. doi:10.1152/ajplung.00238.2007
- Tam, A., Hughes, M., McNagny, K. M., Obeidat, M., Hackett, T. L., Leung, J. M., Shaipanich, T., Dorscheid, D. R., Singhera, G. K., Yang, C. W. T., Paré, P. D., Hogg, J. C., Nickle, D., & Sin, D. D. (2019). Hedgehog signaling in the airway epithelium of patients with chronic obstructive pulmonary disease. *Scientific Reports*, 9(1), 3353-3353. doi:10.1038/s41598-019-40045-3
- Tan, X., Yu, L., Yang, R., Tao, Q., Xiang, L., Xiao, J., & Zhang, J.-S. (2020). Fibroblast Growth Factor 10 Attenuates Renal Damage by Regulating Endoplasmic Reticulum Stress After Ischemia–Reperfusion Injury. *Frontiers in Pharmacology*, 11(39). doi:10.3389/fphar.2020.00039
- Tang, D., He, Y., Li, W., & Li, H. (2019). Wnt/ β -catenin interacts with the FGF pathway to promote proliferation and regenerative cell proliferation in the zebrafish lateral line neuromast. *Experimental and Molecular Medicine*, 51(5), 1-16. doi:10.1038/s12276-019-0247-x
- Tang, H., Chen, J., Fraidenburg, D. R., Song, S., Sysol, J. R., Drennan, A. R., Offermanns, S., Ye, R. D., Bonini, M. G., Minshall, R. D., Garcia, J. G. N., Machado, R. F., Makino, A., & Yuan, J. X. J. (2015). Deficiency of Akt1, but not Akt2, attenuates the development of pulmonary hypertension. *American journal of physiology. Lung cellular and molecular physiology*, 308(2), L208-L220. doi:10.1152/ajplung.00242.2014
- Tanner, L., & Single, A. B. (2020). Animal Models Reflecting Chronic Obstructive Pulmonary Disease and Related Respiratory Disorders: Translating Pre-Clinical Data into Clinical Relevance. *Journal of Innate Immunity*, 12(3), 203-225. doi:10.1159/000502489
- Taylor, S., Dirir, O., Zamanian, R. T., Rabinovitch, M., & Thompson, A. A. R. (2018). The Role of Neutrophils and Neutrophil Elastase in Pulmonary Arterial Hypertension. *Frontiers in Medicine*, 5(217). doi:10.3389/fmed.2018.00217
- ter Horst, E. N., Hahn, N. E., Geerts, D., Musters, R. J. P., Paulus, W. J., van Rossum, A. C., Meischl, C., Piek, J. J., Niessen, H. W. M., & Krijnen, P. A. J. (2018). p47phox-Dependent Reactive Oxygen Species Stimulate Nuclear Translocation of the FoxO1 Transcription Factor During Metabolic Inhibition in Cardiomyoblasts. *Cell Biochemistry and Biophysics*, 76(3), 401-410. doi:10.1007/s12013-018-0847-4
- Thomson, B. R., Souma, T., Tompson, S. W., Onay, T., Kizhatil, K., Siggs, O. M., Feng, L., Whisenhunt, K. N., Yanovitch, T. L., Kalaydjieva, L., Azmanov, D. N., Finzi, S., Tanna, C. E., Hewitt, A. W., Mackey, D. A., Bradfield, Y. S., Souzeau, E., Javadiyan, S., Wiggs, J. L.,

- Pasutto, F., Liu, X., John, S. W., Craig, J. E., Jin, J., Young, T. L., & Quaggin, S. E. (2017). Angiopoietin-1 is required for Schlemm's canal development in mice and humans. *Journal of Clinical Investigation*, *127*(12), 4421-4436. doi:10.1172/jci95545
- Tiffeneau, R., & Pinelli, A. (1948). [Bronchial regulation of pulmonary ventilation]. *Journal francais de medecine et chirurgie thoraciques*, *2*(3), 221-244. PMID: 18870958
- Tilley, A. E., Harvey, B. G., Heguy, A., Hackett, N. R., Wang, R., O'Connor, T. P., & Crystal, R. G. (2009). Down-regulation of the notch pathway in human airway epithelium in association with smoking and chronic obstructive pulmonary disease. *American journal of respiratory and critical care medicine*, *179*(6), 457-466. doi:10.1164/rccm.200705-7950C
- Togo, S., Holz, O., Liu, X., Sugiura, H., Kamio, K., Wang, X., Kawasaki, S., Ahn, Y., Fredriksson, K., Skold, C. M., Mueller, K. C., Branscheid, D., Welker, L., Watz, H., Magnussen, H., & Rennard, S. I. (2008). Lung fibroblast repair functions in patients with chronic obstructive pulmonary disease are altered by multiple mechanisms. *American journal of respiratory and critical care medicine*, *178*(3), 248-260. doi:10.1164/rccm.200706-9290C
- Tong, L., Zhou, J., Rong, L., Seeley, E. J., Pan, J., Zhu, X., Liu, J., Wang, Q., Tang, X., Qu, J., Bai, C., & Song, Y. (2016). Fibroblast Growth Factor-10 (FGF-10) Mobilizes Lung-resident Mesenchymal Stem Cells and Protects Against Acute Lung Injury. *Scientific Reports*, *6*(1), 21642. doi:10.1038/srep21642
- Toumpanakis, D., Kastis, G. A., Zacharatos, P., Sigala, I., Michailidou, T., Kouvela, M., Glynos, C., Divangahi, M., Roussos, C., Theocharis, S. E., & Vassilakopoulos, T. (2010). Inspiratory resistive breathing induces acute lung injury. *American journal of respiratory and critical care medicine*, *182*(9), 1129-1136. doi:10.1164/rccm.201001-01160C
- Toumpanakis, D., Mizi, E., Vassilakopoulou, V., Dettoraki, M., Chatzianastasiou, A., Perlikos, F., Giatra, G., Moscholaki, M., Theocharis, S., & Vassilakopoulos, T. (2020). Spontaneous Breathing Through Increased Airway Resistance Augments Elastase-Induced Pulmonary Emphysema. *International Journal of Chronic Obstructive Pulmonary Disease*, *15*, 1679-1688. doi:10.2147/copd.S256750
- Trinh, X. B., Tjalma, W. A. A., Vermeulen, P. B., Van den Eynden, G., Van der Auwera, I., Van Laere, S. J., Helleman, J., Berns, E. M. J. J., Dirix, L. Y., & van Dam, P. A. (2009). The VEGF pathway and the AKT/mTOR/p70S6K1 signalling pathway in human epithelial ovarian cancer. *British Journal of Cancer*, *100*(6), 971-978. doi:10.1038/sj.bjc.6604921
- Tsoumakidou, M., Tzanakis, N., Chrysofakis, G., & Siafakas, N. M. (2005). Nitrosative stress, heme oxygenase-1 expression and airway inflammation during severe exacerbations of COPD. *Chest*, *127*(6), 1911-1918. doi:10.1378/chest.127.6.1911
- Tsuji, T., Aoshiba, K., & Nagai, A. (2006). Alveolar cell senescence in patients with pulmonary emphysema. *American journal of respiratory and critical care medicine*, *174*(8), 886-893. doi:10.1164/rccm.200509-13740C

- Uhlén, M., Fagerberg, L., Hallström, B. M., Lindskog, C., Oksvold, P., Mardinoglu, A., Sivertsson, Å., Kampf, C., Sjöstedt, E., Asplund, A., Olsson, I., Edlund, K., Lundberg, E., Navani, S., Szigartyo, C. A.-K., Odeberg, J., Djureinovic, D., Takanen, J. O., Hober, S., Alm, T., Edqvist, P.-H., Berling, H., Tegel, H., Mulder, J., Rockberg, J., Nilsson, P., Schwenk, J. M., Hamsten, M., von Feilitzen, K., Forsberg, M., Persson, L., Johansson, F., Zwahlen, M., von Heijne, G., Nielsen, J., & Pontén, F. (2015). Tissue-based map of the human proteome. *Science*, *347*(6220), 1260419. doi:10.1126/science.1260419
- Ushakumary, M. G., Riccetti, M., & Perl, A.-K. T. (2021). Resident interstitial lung fibroblasts and their role in alveolar stem cell niche development, homeostasis, injury, and regeneration. *STEM CELLS Translational Medicine*, *10*(7), 1021-1032. doi:doi.org/10.1002/sctm.20-0526
- van der Mark, S. C., Hoek, R. A. S., & Hellemons, M. E. (2020). Developments in lung transplantation over the past decade. *European Respiratory Review*, *29*(157), 190132. doi:10.1183/16000617.0132-2019
- Van Dijk, E. M., Culha, S., Menzen, M. H., Bidan, C. M., & Gosens, R. (2017). Elastase-Induced Parenchymal Disruption and Airway Hyper Responsiveness in Mouse Precision Cut Lung Slices: Toward an Ex vivo COPD Model. *Frontiers in Physiology*, *7*, 657-657. doi:10.3389/fphys.2016.00657
- Vega-Hernández, M., Kovacs, A., De Langhe, S., & Ornitz, D. M. (2011). FGF10/FGFR2b signaling is essential for cardiac fibroblast development and growth of the myocardium. *Development*, *138*(15), 3331-3340. doi:10.1242/dev.064410
- Veith, C., Vartürk-Özcan, I., Wujak, M., Hadzic, S., Wu, C. Y., Knoepp, F., Kraut, S., Petrovic, A., Gredic, M., Pak, O., Brosien, M., Heimbrodt, M., Wilhelm, J., Weisel, F. C., Malkmus, K., Schäfer, K., Gall, H., Tello, K., Kosanovic, D., Sydykov, A., Sarybaev, A., Günther, A., Brandes, R. P., Seeger, W., Grimminger, F., Ghofrani, H. A., Schermuly, R. T., Kwapiszewska, G., Sommer, N., & Weissmann, N. (2022). Secreted Protein Acidic and Rich in Cysteine, a Novel Regulator of Vascular Cell Function in Pulmonary Hypertension. *Circulation*. doi:10.1161/circulationaha.121.057001
- Verhamme, F. M., De Smet, E. G., Van Hooste, W., Delanghe, J., Verleden, S. E., Joos, G. F., Brusselle, G. G., & Bracke, K. R. (2019). Bone morphogenetic protein 6 (BMP-6) modulates lung function, pulmonary iron levels and cigarette smoke-induced inflammation. *Mucosal Immunology*, *12*(2), 340-351. doi:10.1038/s41385-018-0116-2
- Viegi, G., Scognamiglio, A., Baldacci, S., Pistelli, F., & Carrozzi, L. (2001). Epidemiology of Chronic Obstructive Pulmonary Disease (COPD). *Respiration*, *68*(1), 4-19. doi:10.1159/000050456
- Virani, A., Baltaji, S., Young, M., Dumont, T., & Cheema, T. (2021). Chronic Obstructive Pulmonary Disease: Diagnosis and GOLD Classification. *Critical Care Nursing Quarterly*, *44*(1), 9-18. doi:10.1097/cnq.0000000000000335

- Volckaert, T., & De Langhe, S. P. (2015). Wnt and FGF mediated epithelial-mesenchymal crosstalk during lung development. *Developmental dynamics : an official publication of the American Association of Anatomists*, 244(3), 342-366. doi:10.1002/dvdy.24234
- Volckaert, T., Dill, E., Campbell, A., Tiozzo, C., Majka, S., Bellusci, S., & De Langhe, S. P. (2011). Parabronchial smooth muscle constitutes an airway epithelial stem cell niche in the mouse lung after injury. *Journal of Clinical Investigation*, 121(11), 4409-4419. doi:10.1172/jci58097
- Volckaert, T., Yuan, T., Chao, C.-M., Bell, H., Sitaula, A., Szimntenings, L., El Agha, E., Chanda, D., Majka, S., Bellusci, S., Thannickal, V. J., Fässler, R., & De Langhe, S. P. (2017). Fgf10-Hippo Epithelial-Mesenchymal Crosstalk Maintains and Recruits Lung Basal Stem Cells. *Developmental Cell*, 43(1), 48-59.e45. doi:10.1016/j.devcel.2017.09.003
- Wang, C. T., Zhang, L., Wu, H. W., Wei, L., Xu, B., & Li, D. M. (2014). Doxycycline attenuates acute lung injury following cardiopulmonary bypass: involvement of matrix metalloproteinases. *International Journal of Clinical and Experimental Pathology*, 7(11), 7460-7468. ISSN:1936-2625/IJCEP0002425
- Wang, M., Aaron, C. P., Madrigano, J., Hoffman, E. A., Angelini, E., Yang, J., Laine, A., Vetterli, T. M., Kinney, P. L., Sampson, P. D., Sheppard, L. E., Szpiro, A. A., Adar, S. D., Kirwa, K., Smith, B., Lederer, D. J., Diez-Roux, A. V., Vedal, S., Kaufman, J. D., & Barr, R. G. (2019). Association Between Long-term Exposure to Ambient Air Pollution and Change in Quantitatively Assessed Emphysema and Lung Function. *JAMA*, 322(6), 546-556. doi:10.1001/jama.2019.10255
- Wang, R., Ahmed, J., Wang, G., Hassan, I., Strulovici-Barel, Y., Hackett, N. R., & Crystal, R. G. (2011). Down-regulation of the canonical Wnt β -catenin pathway in the airway epithelium of healthy smokers and smokers with COPD. *PLoS One*, 6(4), e14793-e14793. doi:10.1371/journal.pone.0014793
- Wang, W., Zhang, K., Li, X., Ma, Z., Zhang, Y., Yuan, M., Suo, Y., Liang, X., Tse, G., Goudis, C. A., Liu, T., & Li, G. (2018). Doxycycline attenuates chronic intermittent hypoxia-induced atrial fibrosis in rats. *Cardiovascular Therapeutics*, 36(3), e12321. doi:10.1111/1755-5922.12321
- Wang, Y., Liu, Z., Liu, Z., Zhao, H., Zhou, X., Cui, Y., & Han, J. (2013). Advances in research on and diagnosis and treatment of achondroplasia in China. *Intractable and rare diseases research*, 2(2), 45-50. doi:10.5582/irdr.2013.v2.2.45
- Wang, Y., Xu, J., Meng, Y., Adcock, I. M., & Yao, X. (2018). Role of inflammatory cells in airway remodeling in COPD. *International Journal of Chronic Obstructive Pulmonary Disease*, 13, 3341-3348. doi:10.2147/copd.S176122
- Watson, J., & Francavilla, C. (2018). Regulation of FGF10 Signaling in Development and Disease. *Frontiers in genetics*, 9, 500-500. doi:10.3389/fgene.2018.00500
- Weibel, E. R. (1984). *The pathway for oxygen : structure and function in the mammalian respiratory system*. Cambridge, Mass.: Harvard University Press. ISBN:9780674657908

- Weissmann, N., Akkayagil, E., Quanz, K., Schermuly, R. T., Ghofrani, H. A., Fink, L., Hänze, J., Rose, F., Seeger, W., & Grimminger, F. (2004). Basic features of hypoxic pulmonary vasoconstriction in mice. *Respiratory Physiology and Neurobiology*, *139*(2), 191-202. doi:10.1016/j.resp.2003.10.003
- Weissmann, N., Grimminger, F., Walmrath, D., & Seeger, W. (1995). Hypoxic vasoconstriction in buffer-perfused rabbit lungs. *Respiratory Physiology*, *100*(2), 159-169. doi:10.1016/0034-5687(94)00133-k
- Weissmann, N., Lobo, B., Pichl, A., Parajuli, N., Seimetz, M., Puig-Pey, R., Ferrer, E., Peinado, V. I., Dominguez-Fandos, D., Fysikopoulos, A., Stasch, J. P., Ghofrani, H. A., Coll-Bonfill, N., Frey, R., Schermuly, R. T., Garcia-Lucio, J., Blanco, I., Bednorz, M., Tura-Ceide, O., Tadele, E., Brandes, R. P., Grimminger, J., Klepetko, W., Jaksch, P., Rodriguez-Roisin, R., Seeger, W., Grimminger, F., & Barbera, J. A. (2014). Stimulation of soluble guanylate cyclase prevents cigarette smoke-induced pulmonary hypertension and emphysema. *American journal of respiratory and critical care medicine*, *189*(11), 1359-1373. doi:10.1164/rccm.201311-2037OC
- West, J. B., & Luks, A. (2016). *West's respiratory physiology : the essentials*. ISBN:149631011X
- Wink, D. A., & Mitchell, J. B. (1998). Chemical biology of nitric oxide: Insights into regulatory, cytotoxic, and cytoprotective mechanisms of nitric oxide. *Free Radical Biology and Medicine*, *25*(4-5), 434-456. doi:10.1016/s0891-5849(98)00092-6.
- Wittekindt, O. H. (2017). Tight junctions in pulmonary epithelia during lung inflammation. *Pflügers Archiv: European Journal of Physiology*, *469*(1), 135-147. doi:10.1007/s00424-016-1917-3
- Woo, K. V., Shen, I. Y., Weinheimer, C. J., Kovacs, A., Nigro, J., Lin, C. Y., Chakinala, M., Byers, D. E., & Ornitz, D. M. (2021). Endothelial FGF signaling is protective in hypoxia-induced pulmonary hypertension. *Journal of Clinical Investigation*, *131*(17). doi:10.1172/jci141467
- Wright, J. L., & Churg, A. (1991). Effect of long-term cigarette smoke exposure on pulmonary vascular structure and function in the guinea pig. *Experimental Lung Research*, *17*(6), 997-1009. doi:10.3109/01902149109064331
- Wright, J. L., Cosio, M., & Churg, A. (2008). Animal models of chronic obstructive pulmonary disease. *American Journal of Physiology-Lung Cellular and Molecular Physiology*, *295*(1), L1-L15. doi:10.1152/ajplung.90200.2008
- Wright, J. L., Farmer, S. G., & Churg, A. (2002). Synthetic serine elastase inhibitor reduces cigarette smoke-induced emphysema in guinea pigs. *American journal of respiratory and critical care medicine*, *166*(7), 954-960. doi:10.1164/rccm.200202-098OC
- Wright, J. L., Postma, D. S., Kerstjens, H. A., Timens, W., Whittaker, P., & Churg, A. (2007). Airway remodeling in the smoke exposed guinea pig model. *Inhalation Toxicology*, *19*(11), 915-923. doi:10.1080/08958370701515563

- Wu, J., Chu, X., Chen, C., & Bellusci, S. (2018). Role of Fibroblast Growth Factor 10 in Mesenchymal Cell Differentiation During Lung Development and Disease. *Frontiers in genetics, 9*, 545-545. doi:10.3389/fgene.2018.00545
- Wu, X., Chen, D., Gu, X., Su, X., Song, Y., & Shi, Y. (2014). Prevalence and risk of viral infection in patients with acute exacerbation of chronic obstructive pulmonary disease: a meta-analysis. *Molecular Biologz Reports, 41(7)*, 4743-4751. doi:10.1007/s11033-014-3345-9
- Xiang, M., Xu, Y. J., Liu, X. S., & Zeng, D. X. (2010). Cigarette smoke extract promotes human pulmonary artery smooth muscle cells proliferation through protein kinase C alpha-dependent induction of cyclin D1. *Chinese Medical Journal (Engl), 123(24)*, 3663-3670. doi:10.3760/cma.j.issn.0366-6999.2010.24.028
- Xu, K., Wang, X., Zhang, Q., Liang, A., Zhu, H., Huang, D., Li, C., & Ye, W. (2016). Sp1 downregulates proinflammatory cytokine-induced catabolic gene expression in nucleus pulposus cells. *Molecular Medicine Reports, 14(4)*, 3961-3968. doi:10.3892/mmr.2016.5730
- Xu, W., Zhao, X., Wang, X., Feng, H., Gou, M., Jin, W., Wang, X., Liu, X., & Dong, C. (2019). The Transcription Factor Tox2 Drives T Follicular Helper Cell Development via Regulating Chromatin Accessibility. *Immunity, 51(5)*, 826-839.e825. doi:10.1016/j.immuni.2019.10.006
- Xu, X., Abdalla, T., Bratcher, P. E., Jackson, P. L., Sabbatini, G., Wells, J. M., Lou, X. Y., Quinn, R., Blalock, J. E., Clancy, J. P., & Gaggar, A. (2017). Doxycycline improves clinical outcomes during cystic fibrosis exacerbations. *European Respiratorz Journal, 49(4)*. doi:10.1183/13993003.01102-2016
- Yang, Y., Riccio, P., Schotsaert, M., Mori, M., Lu, J., Lee, D. K., Garcia-Sastre, A., Xu, J., & Cardoso, W. V. (2018). Spatial-Temporal Lineage Restrictions of Embryonic p63(+) Progenitors Establish Distinct Stem Cell Pools in Adult Airways. *Developmental Cell, 44(6)*, 752-761.e754. doi:10.1016/j.devcel.2018.03.001
- Yao, H., & Rahman, I. (2011). Current concepts on oxidative/carbonyl stress, inflammation and epigenetics in pathogenesis of chronic obstructive pulmonary disease. *Toxicology and Applied Pharmacology, 254(2)*, 72-85. doi:10.1016/j.taap.2009.10.022
- Ye, F., Duvillié, B., & Scharfmann, R. (2005). Fibroblast growth factors 7 and 10 are expressed in the human embryonic pancreatic mesenchyme and promote the proliferation of embryonic pancreatic epithelial cells. *Diabetologia, 48(2)*, 277-281. doi:10.1007/s00125-004-1638-6
- Yildirim, A. O., Muyal, V., John, G., Muller, B., Seifart, C., Kasper, M., & Fehrenbach, H. (2010). Palifermin induces alveolar maintenance programs in emphysematous mice. *American journal of respiratory and critical care medicine, 181(7)*, 705-717. doi:10.1164/rccm.200804-573OC

- Yin, Y., & Ornitz, D. M. (2020). FGF9 and FGF10 activate distinct signaling pathways to direct lung epithelial specification and branching. *Science Signaling*, 13, 621. doi:10.1126/scisignal.aay4353
- Yoshida, M., Minagawa, S., Araya, J., Sakamoto, T., Hara, H., Tsubouchi, K., Hosaka, Y., Ichikawa, A., Saito, N., Kadota, T., Sato, N., Kurita, Y., Kobayashi, K., Ito, S., Utsumi, H., Wakui, H., Numata, T., Kaneko, Y., Mori, S., Asano, H., Yamashita, M., Odaka, M., Morikawa, T., Nakayama, K., Iwamoto, T., Imai, H., & Kuwano, K. (2019). Involvement of cigarette smoke-induced epithelial cell ferroptosis in COPD pathogenesis. *Nature Communications*, 10(1), 3145. doi:10.1038/s41467-019-10991-7
- Yu, D., Liu, X., Zhang, G., Ming, Z., & Wang, T. (2018). Isoliquiritigenin Inhibits Cigarette Smoke-Induced COPD by Attenuating Inflammation and Oxidative Stress via the Regulation of the Nrf2 and NF- κ B Signaling Pathways. *Frontiers in Pharmacology*, 9(1001). doi:10.3389/fphar.2018.01001
- Yu, G., Zhou, A., Xue, J., Huang, C., Zhang, X., Kang, S.-H., Chiu, W.-T., Tan, C., Xie, K., Wang, J., & Huang, S. (2015). FoxM1 promotes breast tumorigenesis by activating PDGF-A and forming a positive feedback loop with the PDGF/AKT signaling pathway. *Oncotarget*, 6. doi:10.18632/oncotarget.3596
- Yuan, T., Volckaert, T., Chanda, D., Thannickal, V. J., & De Langhe, S. P. (2018). Fgf10 Signaling in Lung Development, Homeostasis, Disease, and Repair After Injury. *Frontiers in Genetics*, 9(418). doi:10.3389/fgene.2018.00418
- Yuan, T., Volckaert, T., Redente, E. F., Hopkins, S., Klinkhammer, K., Wasnick, R., Chao, C. M., Yuan, J., Zhang, J. S., Yao, C., Majka, S., Stripp, B. R., Günther, A., Riches, D. W. H., Bellusci, S., Thannickal, V. J., & De Langhe, S. P. (2019). FGF10-FGFR2B Signaling Generates Basal Cells and Drives Alveolar Epithelial Regeneration by Bronchial Epithelial Stem Cells after Lung Injury. *Stem Cell Reports*, 12(5), 1041-1055. doi:10.1016/j.stemcr.2019.04.003
- Zepp, J. A., & Morrissey, E. E. (2019). Cellular crosstalk in the development and regeneration of the respiratory system. *Nat Rev Molecular and Cellular Biology*, 20(9), 551-566. doi:10.1038/s41580-019-0141-3
- Zhai, G., Valdes, A. M., Cherkas, L., Clement, G., Strachan, D., & Spector, T. D. (2007). The interaction of genes and smoking on forced expiratory volume: a classic twin study. *Chest*, 132(6), 1772-1777. doi:10.1378/chest.07-1438
- Zhang, F., Hu, L., Wu, Y. X., Fan, L., Liu, W. T., Wang, J., Sun, H., & Zhang, J. S. (2019). Doxycycline alleviates paraquat-induced acute lung injury by inhibiting neutrophil-derived matrix metalloproteinase 9. *International Immunopharmacology*, 72, 243-251. doi:10.1016/j.intimp.2019.04.015
- Zhang, H., Zhang, S., Ghia, E. M., Choi, M. Y., Zhang, J., Chen, L., Widhopf II, G. F., Rassenti, L. Z., & Kipps, T. J. (2018). Cirmtuzumab Inhibits Non-Canonical Wnt Signaling without Enhancing Canonical Wnt/ β -Catenin Signaling in Chronic Lymphocytic Leukemia. *Blood*, 132(Supplement 1), 2652-2652. doi:10.1182/blood-2018-99-119606

-
- Zhang, L., Luo, B., Ting, Y., He, S., Xie, L., & Sun, S. (2020). SIRT1 attenuates endoplasmic reticulum stress and apoptosis in rat models of COPD. *Growth Factors*, *38*(2), 94-104. doi:10.1080/08977194.2020.1810029
- Zhang, X., Ibrahimi, O. A., Olsen, S. K., Umemori, H., Mohammadi, M., & Ornitz, D. M. (2006). Receptor Specificity of the Fibroblast Growth Factor Family: The complete mammalian FGF family. *Journal of Biological Chemistry*, *281*(23), 15694-15700. doi:10.1074/jbc.M601252200
- Zhao, J., Lai, L., Ji, W., & Zhou, Q. (2019). Genome editing in large animals: current status and future prospects. *National Science Review*, *6*(3), 402-420. doi:10.1093/nsr/nwz013
- Zhu, H., Sun, X., Wang, D., Hu, N., & Zhang, Y. (2015). Doxycycline ameliorates aggregation of collagen and atrial natriuretic peptide in murine post-infarction heart. *European Journal of Pharmacology*, *754*, 66-72. doi:10.1016/j.ejphar.2015.02.026
- Zhu, Z., Godana, D., Li, A., Rodriguez, B., Gu, C., Tang, H., Minshall, R. D., Huang, W., & Chen, J. (2019). Echocardiographic assessment of right ventricular function in experimental pulmonary hypertension. *Pulmonary Circulation*, *9*(2), 2045894019841987. doi:10.1177/2045894019841987
- Zhu, Z., Shukla, A., Ramezani-Rad, P., Apgar, J. R., & Rickert, R. C. (2019). The AKT isoforms 1 and 2 drive B cell fate decisions during the germinal center response. *Life Science Alliance*, *2*(6), e201900506. doi:10.26508/lsa.201900506
- Zosky, G. R., Janosi, T. Z., Adamicza, Á., Bozanich, E. M., Cannizzaro, V., Larcombe, A. N., Turner, D. J., Sly, P. D., & Hantos, Z. (2008). The bimodal quasi-static and dynamic elastance of the murine lung. *Journal of Applied Physiology*, *105*(2), 685-692. doi:10.1152/jappphysiol.90328.2008
- Zou, M., BinEssa, H. A., Al-Malki, Y. H., Al-Yahya, S., Al-Alwan, M., Al-Jammaz, I., Khabar, K. S. A., Almohanna, F., Assiri, A. M., Meyer, B. F., Alzahrani, A. S., Al-Mohanna, F. A., & Shi, Y. (2021). β -Catenin Attenuation Inhibits Tumor Growth and Promotes Differentiation in a BRAFV600E-Driven Thyroid Cancer Animal Model. *Molecular Cancer Therapeutics*, *20*(9), 1603-1613. doi:10.1158/1535-7163.Mct-21-0037

12 Acknowledgements

Doctoral dissertation "Fibroblast Growth Factor 10 Reverses Cigarette Smoke- and Elastase-induced Emphysema and Pulmonary Hypertension in Mice" was done in the laboratory for Molecular Mechanisms of Emphysema, Hypoxia and Lung ageing (Professor Dr. Norbert Weißmann) at the Excellence Cluster Cardio Pulmonary Institute, Department of Internal Medicine, Justus Liebig University Giessen.

I owe the greatest gratitude to Professor Dr. Norbert Weißmann, who had shown the trust in me coming to his research group as well as support, advice and assistance during my doctoral work. Sincere gratitude for trust, selfless help, on all the advice and effort to make this work see the light of day.

To my primary supervisor, Professor Dr. Reinhard Lakes-Harlan from the Faculty of Biology and Chemistry at the Justus Liebig University, I owe a great deal of gratitude for all the advice, suggestions and insightful comments to this work.

My warmest thanks to Professor Dr. Saverio Bellusci for expert suggestions, selfless great help and professional commitment to the thesis. I am also thankful to Professor Dr. Ivan Manzini for his comments and insightful questions.

Special acknowledgements to Professor Dr. Werner Seeger, Department of Internal Medicine, Director of the Medical Clinic II, Chairmen of the German Centre for Lung Research (DZL), Director of the Department IV, Max Planck Institute for Heart and Lung Research, Bad Nauheim. Thanks to his scientific and leading skills, personal commitment to the science and pursuance to provide the best possible scientific work surrounding, I had the opportunity to develop my skills further in the best possible conditions and environment, alongside worldwide renowned scientists, with Professor Dr. Seeger at lead.

I owe a great deal of gratitude to Dr. Oleg Pak, firstly for all the friendship, but also valuable advice, understanding, expert suggestions and selfless great help. I would like to thank to Dr. Simone Kraut as well for her professional and friendly support and work.

I would like to thank the following: Dr. Michael Seimetz, Dr. Monika Brosien, Dr. Baktybek Kojonazarov, Dr. Jochen Wilhelm, Dr. Mariola Bednorz, Prof. Dr. Andreas Günther, Prof. Dr. Natascha Sommer, Prof. Dr. David Warburton, Prof. Dr. Friedrich Grimminger, Prof. Dr. Hossein A. Ghofrani, Prof. Dr. Ralph T. Schermuly, Prof. Dr. Elie El Agha, Dr. Ingrid Henneke, Dr. Thomas Sontag, Siddartha Doswada, Marouane Qsaib, Edma Loku and Lea Pellekoorne for the valuable exchange of opinions and practical assistance.

I would like to thank Karin Quanz, Kerstin Goth, Christina Pilz, Miriam Wessendorf, Dileep Bonthu, Nils Schupp and Ingrid Breitenborn-Müller for their incredible technical assistance and support, and for all the fun we have had in the last years.

I would like to thank dear friends Marija Gredić, Dr. Đuro Kosanović, Aleksandar Petrović, Elizabeta Krstić, Claudia Fernanda Garcia Castro, Dr. Claudio Nardiello, Dr. Ipek Vartürk-Özcan, Dr. Mira Y. Gökyildirim, and Cheng-Yu Wu who have been with me over the years, who have been my support and encouragement to finish what I started.

I owe great gratitude to my family, especially my parents Lidija and Nebojša, brother Nikola and sister Bojana who believe in me and who have subordinated their lives to my successes. Unconditionally, they have always been support, whether it was difficult or happy moments and without which none of this I have achieved so far would be possible.

13 Attachment

13.1 Publications

1. **Hadzic S.**, Wu C-Y., Gredic M., Pak O., Kraut S., Baktybek Kojonazarov B., Wilhelm J., Brosien M., Bednorz M., Seimetz M., Gunther A., Kosanovic D., Sommer N., Warburton D., Grimminger F., Ghofrani H. A., Schermuly R.T., Seeger W., El Agha E., Bellusci S. and Weissmann N. FGF10 reverses cigarette smoke- and elastase-induced emphysema and PH in mice.

Submitted (2022).

2. **Hadzic S.**, Wu C-Y., Gredic M., Kojonazarov B., Pak O., Kraut S., Sommer N., Kosanovic D., Grimminger F., Schermuly R. T., Seeger W., Bellusci S. and Weissmann N. The effect of long-term doxycycline treatment in a mouse model of cigarette smoke-induced emphysema and pulmonary hypertension.

American Journal of Physiology-Lung Cellular and Molecular Physiology; DOI: 10.1152/ajplung.00048.2021 (2021).

3. **Hadzic S.**, Wu C-Y., Avdeev S., Weissmann N., Schermuly R. T. and Kosanovic D. *Lung epithelium damage in COPD - An unstoppable pathological event?*

Cell Signalling; DOI: 10.1016/j.cellsig.2020.109540 (2020).

4. Kojonazarov B.*, **Hadzic S.***, Ghofrani H. A., Grimminger F., Seeger W., Weissmann N. and Schermuly R. T. *Severe Emphysema in the SU5416/Hypoxia Rat Model of Pulmonary Hypertension. *equal contribution.*

American Journal of Respiratory and Critical Care Medicine; DOI: 10.1164/rccm.201902-0390LE (2019).

5. Shahzad T., Chao C-M., **Hadzic S.**, Behnke J., Biebach L., Friebertshäuser E., Wilhelm J., Hilgendorff A., Zimmer K. P., Morty R. E., Bellusci S., and Ehrhardt H.. *TRAIL protects the immature lung from hyperoxic injury.*

Cell Death & Disease; DOI: 10.1038/s41419-022-05072-5 (2022)

6. Kuhnert S., Mansouri S., Rieger M., Savai R., Avci E., Looso M., **Hadzic S.**, Acker T., Klatt S., Wilhelm J., Fleming I., Sommer N., Weissmann N., Vogelmeier C., Bals R., Zeiher A., Dimmeler S., Seeger W. and Pullamsetti S. Association of clonal hematopoiesis of indeterminate potential with inflammatory gene expression in patients with COPD.

Cells, DOI: 10.3390/cells11132121 (2022)

7. Veith C.*, Vartürk-Özcan I.*, Wujak M., **Hadzic S.**, Wu C-Y., Knoepp F., Kraut S., Petrovic A., Gredic M., Pak O., Brosien M., Heimbrodtt M., Wilhelm J., Weisel F., Malkmus K., Schäfer K., Gall H., Tello K., Kosanovic D., Sarybaev A., Günther A.; Brandes R.P., Seeger W., Grimminger F.; Ghofrani H. A., Schermuly R. T., Kwapiszewska G., Sommer N. and Weissmann N. *Secreted protein acidic and rich in cysteine, a novel regulator of vascular cell function in pulmonary hypertension. *equal contribution.*

Circulation; DOI: 10.1161/CIRCULATIONAHA.121.057001 (2022).

8. Gredic M., Wu C.-Y., **Hadzic S.**, Pak O., Savai R., Kojonazarov B., Doswada S., Weiss A., Weigert A., Guenther A., Brandes R. P., Schermuly R. T., Grimminger F., Seeger W., Sommer N., Kraut S., and Weissmann N. (2021). Myeloid cell-specific deletion of inducible nitric oxide synthase protects against smoke-induced pulmonary hypertension in mice.

European Respiratory Journal; DOI: 10.1183/13993003.01153-2021 (2021)

9. Saraji A., Sydykov A., Schäfer K., Garcia-Castro C. F., Henneke I., Alebrahimdehkordi N., Koanovic D., **Hadzic S.**, Guenther A., Hecker M., Ghofrani H. A., Seeger W., Schermuly R. T., Weissmann N., Sommer N. and Pak O. *PINK1-mediated Mitophagy Contributes to Pulmonary Vascular Remodeling in Pulmonary Hypertension.*

American Journal of Respiratory Cell and Molecular Biology; DOI: 10.1165/rcmb.2021-0082LE (2021).

10. Qi H., Liu H., Pullamsetti S. S., Günther S., Kuenne C., Atzberger A., Sommer N., **Hadzic S.**, Günther A., Weissmann N., Zhou Y., Yuan X. and Braun T. *Epigenetic Regulation by Suv4-*

20h1 in Cardiopulmonary Progenitor Cells is Required to Prevent Pulmonary Hypertension and COPD.

Circulation; DOI: 10.1161/circulationaha.120.051680 (2021).

11. Wang F., **Hadzic S.**, Roxlau E. T., Fuehler B., Janise-Libawski A., Wimmer T., Lei B., Li S. W., Weissmann N. and Stieger K. *Retinal tissue develops an inflammatory reaction to tobacco smoke and electronic cigarette vapor in mice.*

Journal of Molecular Medicine; DOI: 10.1007/s00109-021-02108-9 (2021).

12. Fysikopoulos A., Seimetz M., **Hadzic S.**, Knoepp F., Wu C-Y., Malkmus K., Wilhelm J., Pichl A., Bednorz M., Tadele Roxlau E., Ghofrani H. A., Sommer N., Gierhardt M., Schermuly R. T., Seeger W., Grimminger F., Weissmann N. and Kraut S. *Amelioration of elastase-induced lung emphysema and reversal of pulmonary hypertension by pharmacological iNOS inhibition in mice.*

British Journal of Pharmacology; DOI: 10.1111/bph.15057 (2021).

13. Seimetz M.*, Sommer N.*, Bednorz M.*, Pak O., Veith C., **Hadzic S.**, Gredic M., Parajuli N., Kojonazarov B., Kraut S., Wilhelm J., Knoepp F., Henneke I., Pichl A., Kanbagli Z. I., Scheibe S., Fysikopoulos A., Wu C-Y., Klepetko W., Jaksch P., Eichstaedt C., Grünig E., Hinderhofer K., Geiszt M., Müller N., Rezende F., Buchmann G., Wittig I., Hecker M., Hecker A., Padberg W., Dorfmueller P., Gattenlöhner S., Vogelmeier C. F., Günther A., Karnati S., Baumgart-Vogt E., Schermuly R. T., Ghofrani H. A., Seeger W., Schröder K., Grimminger F., Brandes R. P. and Weissmann N. *NADPH oxidase subunit NOXO1 is a target for emphysema treatment in COPD. *equal contribution.*

Nature Metabolism; DOI: 10.1038/s42255-020-0215-8 (2020).

14. Gouveia L., Kraut S.*, **Hadzic S.***, Vazquez-Liébanas E., Kojonazarov B., Wu C-Y., Veith C., He L., Mermelekas G., Schermuly R. T., Weissmann N., Betsholtz C. and Andrae J. *Lung developmental arrest caused by PDGF-A deletion: consequences for the adult mouse lung. *equal contribution.*

-
- American Journal of Physiology-Lung Cellular and Molecular Physiology*; DOI: 10.1152/ajplung.00295.2019 **(2020)**.
15. Biswas S., Kojonazarov B., **Hadzic S.**, Majer M., Bajraktari G., Novoyatleva T., Ghofrani H. A., Grimminger F., Seeger W., Weissmann N., Schlossmann J. and Schermuly R. T. *IRAG1 Deficient Mice Develop PKG1 β Dependent Pulmonary Hypertension. Cells*; DOI: 10.3390/cells9102280 **(2020)**.
16. Gierhardt M., Pak O., Sydykov A., Kraut S., Schäffer J., Garcia C., Veith C., Zeidan E. M., Brosien M., Quanz K., Esfandiary A., Saraji A., **Hadzic S.**, Kojonazarov B., Wilhelm J., Ghofrani H. A., Schermuly R. T., Seeger W., Grimminger F., Herden C., Schulz R., Weissmann N., Heger J. and Sommer N. *Genetic Deletion of p66shc and/or Cyclophilin D Results in Decreased Pulmonary Vascular Tone. Cardiovascular Research*; DOI: 10.1093/cvr/cvaa310 **(2020)**.
17. Pichl A., Sommer N., Bednorz M., Seimetz M., **Hadzic S.**, Kuhnert S., Kraut S., Roxlau E. T., Kojonazarov B., Wilhelm J., Gredic M., Gall H., Tello K., Richter M. J., Pak O., Petrovic A., Hecker M., Schermuly R. T., Grimminger F., Seeger W., Ghofrani H. A. and Weissmann N. *Riociguat for treatment of pulmonary hypertension in COPD: a translational study. European Respiratory Journal*; DOI: 10.1183/13993003.02445-2018 **(2019)**.
18. Buric S. S., Podolski-Renic A., Dinic J., Stankovic T., Jovanovic M., **Hadzic S.**, Ayuso J. M., Virumbrales-Munoz M., Fernandez L. J., Ochoa I., Perez-Garcia V. M. and Pesic M. *Modulation of Antioxidant Potential with Coenzyme Q10 Suppressed Invasion of Temozolomide-Resistant Rat Glioma In Vitro and In Vivo. Oxidative Medicine and Cellular Longevity*; DOI: 10.1155/2019/3061607 **(2019)**.
19. Babic T., Dinic J., Buric S. S., **Hadzic S.**, Pesic M., Radojkovic D. and Rankov A. D. *Comparative toxicity evaluation of targeted anticancer therapeutics in embryonic zebrafish and sea urchin models. Acta Biologica Hungarica*; DOI: 10.1556/018.69.2018.4.3 **(2018)**.

20. **Hadzic S.**, Karnati S., Kosanovic D. and Seimetz M. *COPD/emphysema: cause or consequence of aging/senescence?*

PVRI Chronicle Vol 3: Issue 2 (2016).

21. Stojkovic S., Podolski-Renic A., Dinic J., Stankovic T., Bankovic J., **Hadzic S.**, Paunovic V., Isakovic A., Tanic N. and Pesic M. *Development of resistance to antiglioma agents in rat C6 cells caused collateral sensitivity to doxorubicin.*

Experimental Cell Research; DOI: 10.1016/j.yexcr.2015.05.018 (2015).

13.2 Oral presentations

2022: Impaired FGF10 signalling is involved in the development of cigarette smoke-induced emphysema and pulmonary hypertension; Giessen PH Workshop at Cardio-Pulmonary Institute / Institute for Lung Health; March 18, 2022; Online webinar.

2021: NOXO1 as a driver for development of cigarette smoke-induced emphysema and pulmonary hypertension; Macroenvironmental cues, Cardio-Pulmonary Institute (CPI) webinar series; October 19, 2021; Online webinar.

2019: Impaired FGF10 signaling in the adult lung leads to development of emphysema and pulmonary hypertension; 3rd Fibroblast Growth Factors in Development and Repair Conference; February 15 – 18, 2019; Nassau, Bahamas.

2018: Translational COPD research; Precision Medicine in COPD; September 10, 2018; Marburg, Germany.

2018: The role of FGF10 in COPD and COPD-PH; 16th Annual retreat of the International Graduate Programme Molecular Biology and Medicine of the Lung (MBML); July 4-6, 2018; Rauschholzhausen, Germany.

2017: Pulmonary hypertension in COPD animal models; 2nd PVRI Annual Symposium for Young Investigators; September 14 – 17, 2017; Wiesbaden, Germany.

2017: The role of FGF10 signalling in pathogenesis of PH in COPD; 15th Annual retreat of the International Graduate Programme Molecular Biology and Medicine of the Lung (MBML); July 12 - 14, 2017; Rauschholzhausen, Germany.

2017: The role of FGF10 signalling pathway in cigarette smoke-induced emphysema and pulmonary hypertension; 2nd Fibroblast Growth Factors in Development and Repair Conference; March 8 - 11, 2017; Cancun, Mexico.

2016: COPD: cause or consequence of aging/senescence?; 1st PVRI Annual Symposium for Young Investigators; September 9 - 12, 2016; Waldeck, Germany.

13.3 Poster presentations

2022: 10th Annual Meeting of the German Centre for Lung Research (Deutsches Zentrum für Lungenforschung – DZL); July 5 - 7, 2022; Hannover, Germany.

2022: 15th Annual World Congress of the Pulmonary Vascular Research Institute (PVRI); June 22 – 26, 2022; Athens, Greece.

2022: Retreat of the Cardio-Pulmonary Institute – CPI 2022; June 2 - 3, 2022; Bad Nauheim, Germany

2022: American Thoracic Society (ATS) International Conference 2022; May 13 - 18, 2022; San Francisco, CA, USA.

2020: 9th Annual Meeting of the German Centre for Lung Research (Deutsches Zentrum für Lungenforschung – DZL); January 23 - 24, 2020; Travemünde, Germany.

2019: Epithelial-Mesenchymal Interactions in Lung Development and Fibrosis Conference; February 17 – 20, 2019; Nassau, Bahamas.

2019: 13th PVRI Annual World Congress; January 31 – February 3, 2019; Barcelona, Spain.

2018: Fibroblast Growth Factors in Development and Disease - Gordon Research Conference; March 25 – 30, 2018; Ventura, CA, USA.

2018: 7th Annual Meeting of the German Centre for Lung Research (Deutsches Zentrum für Lungenforschung – DZL); February 8 – 9, 2018; Bad Nauheim, Germany.

2017: Symposium of the Excellence Cluster Cardio-Pulmonary System (ECCPS); June 7 – 8, 2017; Bad Nauheim, Germany.

2017: 2nd Fibroblast Growth Factors in Development and Repair Conference; March 8 - 11, 2017; Cancun, Mexico.

2017: 6th Annual Meeting of the German Centre for Lung Research (Deutsches Zentrum für Lungenforschung – DZL); January 30 – 31, 2017; Munich, Germany.

2017: 11th Annual World Congress of the Pulmonary Vascular Research Institute (PVRI); January 26 – 29, 2017; Miami, FL, USA.

2016: 14th Annual retreat of the International Graduate Programme Molecular Biology and Medicine of the Lung (MBML); July 20 – 22, 2016; Rauschholzhausen, Germany.

13.4 Awards

2022: Poster award at Retreat of the Cardio-Pulmonary Institute – CPI 2022. Poster title: Impaired FGF10 signalling is involved in the development of cigarette smoke-induced emphysema and pulmonary hypertension.

2018: Poster award at 7th DZL Annual Meeting. Poster title: Impaired FGF10 signalling in adult mice lung leads to development of emphysema and pulmonary hypertension.

2018: Travel award from the International Graduate Programme Molecular Biology and Medicine of the Lung (MBML) for successful graduation.

2017: Poster award at the Symposium of the Excellence Cluster Cardio Pulmonary System (ECCPS). Poster title: The role of FGF10 signalling in pathogenesis of cigarette smoke-induced emphysema and pulmonary hypertension.

2016: Travel award from the International Graduate Programme Molecular Biology and Medicine of the Lung (MBML) for the Second Place in the Second Student Examination.

2015: Travel award from the International Graduate Programme Molecular Biology and Medicine of the Lung (MBML) for the First Place in the First Student Examination.

2015: “Ivan Đaja” award for the best MSc thesis of the class of 2015 in the field of physiology.

13.5 Courses and workshops

2018: Stereology workshop; August 20 – 26, 2018; Institute of Anatomy, University of Bern, Switzerland.

2018: Project planning module for animal experiments; April 23 – 24, 2018; Goethe University, Frankfurt, Germany.

2015: FELASA B – Basic course for performing animal experiments with mice and rats; November 9 – 12, 2015; Berlin, Germany.

Der Lebenslauf wurde aus der elektronischen Version der Arbeit entfernt.

The curriculum vitae was removed from the electronic version of the paper.